Flutter Analysis of Stonecutters Cable-stayed Bridge Using Finite Element Model

by

Fan Feng

A thesis submitted to the Faculty of Graduate and Postdoctoral Studies in partial fulfilment of the requirements for the degree of

Master of Applied Science

In

Civil Engineering

uOttawa

Department of Civil Engineering

University of Ottawa

Ottawa, Canada

May 2015

Acknowledgements

I wish to express my sincere gratitude to all the people who helped me during the graduate study.

First and foremost, I would like to thank my supervisor Dr. Elena Dragomirescu, for her patient guidance, encouragement and teachings. I have been extremely lucky to have a supervisor who cared so much about my study.

I would like to thank Dr. Tanaka, Xi Chen, Zhida Wang, Hamid Reza Naderian and all my friends for their great help and recommendations during my research project. I would also like to thank all the professors in the Civil Engineering Department of the University of Ottawa, who taught me and let me learn an extensive engineering knowledge.

Finally, my deepest thanks go to my beloved family and my girlfriend, especially my parents for their financial and moral supports, and for always encouraging and believing in me to accomplish my academic goals.

Abstract

The current research analyzed the flutter response of the Stonecutters Cable-Stayed Bridge in Hong Kong, which has a twin deck configuration, under the effect of wind. The aerodynamic instability response of the bridge steel deck of the main span is mainly the focus of the current project.

Initially, a complete finite element bridge model was created in ABAQUS finite element software, representing all the structural elements of the Stonecutters Cable-Stayed Bridge in a lumped mass bridge model. The natural frequencies and the vibration modes were validated against the data available in the literature at first.

Secondly, the effect of the mean wind loading for wind speeds between 35 m/s and 211 m/s were determined. The vertical and horizontal displacements and the torsional angle at mid-span are indicated to determine the bridge performance under mean wind load.

Moreover the flutter instability was modeled based on Scanlan's theory and the response of the bridge model at several different locations along the main and the side span and the top of the tower, were determined for wind speeds of 35 m/s and higher, where this critical aerodynamic instability is expected to occur. In addition, the responses of the bridge under natural wind data were also determined by applying a wind speed recorded data to the bridge model.

Finally, the critical flutter wind speed and the flutter frequency were determined by Fast Fourier Transform in MATLAB program. The flutter onset wind speed was also determined.

Contents

List of Figures

List of Tables

Notation:

B, L:	Bridge deck width and bridge length, m
b:	Half width of the plane plate, the width of bridge is $B = 2b$, m
C:	Structural damping matrix
C_D, C_L, C_M:	Drag, lift and moment coefficients, respectively;
$C(k)$:	Theodorson function, which can be expressed as: $C(k)= F(k)+i\ G(k)$
C_z, C_y, C_a:	Damping constants in bending and torsion.
D:	Horizontal wind force per unit length. (Eq. 2.3), N
D:	Diameter. (Eq. 2.9), m
E^{cable}:	Actual modulus of cables, N/m^2
E_{eq}^{truss}:	Equivalent truss element modulus, N/m^2
F:	External loading on the mass, N
F_d:	Dynamic wind loading, N
F_m:	Mean wind loading, N
f:	Natural frequency, Hz
g:	Acceleration due to gravity, m/s^2
$g_b = \frac{\theta_b}{\pi} = 2\zeta_b$: $g_a = \frac{\theta_a}{\pi} = 2\zeta_a$:	Complex damping coefficients of bending and torsion.
h, p, α:	Vertical, lateral, and torsional displacements of the bridge deck, respectively. (Eq. 2.14), m
$\dot{h}, \dot{p}, \dot{\alpha}$:	Partial differentiation with respect to time t. (Eq. 2.14)
H_i^*, P_i^*, A_i^*:	Non-dimensional flutter derivatives.
I:	Moment of inertia, $kg.m^2$

$I_{xx}, I_{yy}, I_{zz}, I_{xy}, I_{yz}, I_{zx}$:	Moments of Inertia about the Mass Center, m^4
J:	Torsional rigidity, m^4
K:	Structural stiffness matrix.
$K = \omega B / \bar{U}$:	Reduced frequency.
L:	Aerodynamic lift force per unit length, N
L_x:	Horizontal projected length of the cable, m
M:	Structure mass matrix. (Eq. 2.1)
M:	Dynamic pitching moment per unit length (Eq. 2.3), $N.m$
m:	Mass per unit length, kg
$2M\omega$:	Critical damping coefficient.
N_s:	Frequency of vortex cycle shedding, Hz
R_e:	Reynold's Number.
S_t:	Strouhal number.
S_z, S_y, S_a:	Stiffness constants in bending and torsion.
$\bar{U}$:	Wind velocity, m/s
U_{cr}:	Critical wind velocity, m/s
U_d:	Design wind velocity, m/s
U/fb:	Reduced wind velocity, m/s
X , $\dot{X}$, $\ddot{X}$:	Nodal displacement, velocity and acceleration vector.
y:	Horizontal deflection, positive in wind direction, m
z:	Vertical deflection, positive upwards, m
α:	The angle of attack of the wind. (Eq. 2.6), $degree$
μ :	Viscosity.
$\mu = \frac{m}{\pi \rho b^2}$:	Mass ratio, construction to air.
ρ :	Air density, 1.225 kg/m^3 in this thesis.
ρ_c :	Cable material density, kg/m^3

σ:	Cable pre-stress, N/m^2
ω:	Natural circular frequency, *rad*
ω_b, ω_a:	Bending natural frequency and torsional natural frequency, *rad*

Chapter 1: Introduction

1.1: Introduction to bridge aerodynamics

1.1.1: A short history of bridge aerodynamics

In modern times, the strength of slender structures, such as long-span bridges, is not the only factor we need to consider when evaluating their structural integrity, but aerodynamic stability plays an increasingly important role in the structure's design. Due to its magnitude variation and direction, wind load is considered as the most uncertain factor that influences the long-span bridges' structural behavior. In the history of bridge engineering, the lack of knowledge of bridge's response under dynamic wind loads has led to a series of catastrophes [1], especially the Tacoma Bridge collapse. The First Tacoma Narrows Bridge (853 m) opened on July 1st, 1940, and dramatically collapsed under a medium wind speed of 18 m/s on November 7th of the same year. At the time of its construction (and its destruction), the bridge was the third longest suspension bridge in the world in terms of main span length, after the Golden Gate Bridge and the George Washington Bridge. The bridge's collapse had a lasting effect on science and engineering, setting the beginning of the new field of bridge aerodynamics. In many physics textbooks, the Tacoma collapse event is presented as an example of elementary forced resonance with the wind speed providing an external periodic frequency that matched the bridge's natural structural frequency, though the actual cause of failure was aeroelastic flutter [2]. Its failure also boosted research in the field of bridge aerodynamics and aeroelastic response of structures, studies which influenced the designs of the entire world's great long-span bridges built since 1940 and until present.

Because of the progress of science and technology, the span of bridges became longer and longer in order to supply the demand on artistic appearance, transportation requirements, aerodynamic performance, etc. But, longer span implies more flexible bridges, consequently, when the bridge is exposed to the dynamic wind loading, the possibility of instability phenomenon of the structure to occur will greatly increase, in other words, the safety performance of the bridge will decrease rapidly, even brings a probability of initiating the structural damage followed by a potential collapse. The factors above are the main reasons for which the aerodynamic instability problems became vital verification criteria in the design of every long-span bridge [3].

1.1.2: Bridge aerodynamic analysis methodology

There are three main options for performing the bridge aerodynamic analysis; the theoretical development and the formulation of the aeroelastic investigation, the experimental procedure involving wind tunnel tests for verifying the critical flutter wind speed and the numerical simulations performed for simplified finite element models of long-span bridges subjected to static, dynamic and self-exited motion conditions in order to simulate the flutter instability of the structure.

Aerodynamic principles will be used in the theoretical analysis, mainly employed for developing different kinds of mathematical models for wind loadings, and then by combining these with the basic theory of structural dynamics, solutions for the wind-induced vibrations and the structural stability problems will be determined. Theoretical methods play a critical role in wind engineering.

Wind tunnel experiments represent an irreplaceable verification method in the aerodynamic study of long-span bridges and they are commonly accepted as a procedure to test the

aerodynamic characteristics of a bridge. Open or closed circuit wind tunnel facilities can simulate the atmospheric boundary layer and can reproduce a natural wind pressure environment induced to the investigated structure or model of a structure placed in the wind tunnel; based on the response of the model used in the experiment, the response of the real structure is predicted.

Along with the development of information technology and popularization of the computer, the numerical simulation procedure has developed rapidly. This method relies on computer capacities and the available structural software which combines with the finite element theory, and according to numerical calculation performed on the given structure attempt to achieve the critical responses of the long-span bridge structures and to deliver solutions for engineering problems and optimum structural design. Currently there is a number of engineering software, such as ABAQUS, ANASYS, SAP, etc. [4] and these can simplify the complicated structural problems involving high number of degrees of freedom and complex loading histories which can be employed. All of these software are conveniently and widely used in structural design, response analysis and load simulation.

1.2: Background of wind effect on bridges

Physically, wind is flow of air, or is considered as the motion of the air with respect to the surface of the earth. [5] The fundamental cause of air motion is the differences in solar radiation from the sun towards the earth surface. This produces differences in the air temperature and the air pressure at the same height, thus, the air is forced to flow and to generate the wind.

Wind load is the force induced by the wind acting on a structure; this kind of applied load is

caused by the interaction between the wind and the structure itself. When the random variation of the wind speed pass through the bridge deck, a specific distribution will be generated by the atmospheric pressure around the bridge deck surface, and this distribution is continuously changing. Consequently, the randomness and the uncertainty of the wind load could lead to some unexpected motion and random vibrations of a long-span bridge.

Bridge aerodynamic engineering is a very complicated subject, which consists of structural engineering and wind engineering. The target of the wind engineering of a bridge is to determine the static and dynamic response under all possible scenarios of wind loading, and to provide solutions for the design and construction of the bridge structure, especially for long-span flexible bridges like suspension bridges and cable-stayed bridges.

When wind loading approaches the bridge structure, the produced oscillations of the bridge depend on the magnitude and direction of the wind speed; in addition, the motion of the structure is also determined by the dimensions, the cross-section of the structural elements and the properties of the construction materials used for the bridge. The aerodynamic response of long-span bridges exposed to high-intensity wind speeds can be generally classified as two types. The first one is determined for the bridge structure under the mean wind loading, when for critical stage; a self-excited vibration of the structure will be generated by the energy absorbed from the wind flow. For instance, the classic flutter aerodynamic instability, which is coupling phenomena between the torsional and the vertical bending vibrations, might occur for certain bridge decks of streamlined shapes. As for some no-streamlined shapes of the deck cross-sections, the separated-flow torsional flutter could be produced, therefore employing aerodynamic countermeasures, such as fairings, wind shields, etc. it is always recommended, regardless of the bridge deck shape. In general for high wind speeds galloping vibrations, as defined by the Den Hartog criterion

[6] would occur before the bridge reaches the flutter instability. A second type of oscillation response is the forced vibration of the bridge structure which is produced by the fluctuating component of the wind loading, through its random properties. This kind of random vibration response [5] is called buffeting aerodynamic response. The excessive buffeting response can lead to local fatigue of deck-cables and deck-towers connections and could endanger the traffic safety if local damage of these connections would occur.

The aim of the wind resistant design of long-span bridges is to avoid the occurrence of dangerous oscillations, in other words, the critical wind speed for which aerodynamic instability phenomena, such as flutter and buffeting, could occur should be greater than the design wind speed determined for the bridge structural design; at the same time, the amplitude of any potential vibrations of the bridge deck should be controlled so that in should be within the acceptable range, by employing dampers or other passive or active countermeasures.

1.3: Introduction to cable-stayed bridge

1.3.1: cable-stayed bridge

As a kind of cable-stayed system, cable-stayed bridge has a relatively greater crossover capability than other ordinary bridges. A cable-stayed bridge is composed of the tower, the cables and girder. Box-shaped pre-stressed concrete section is most frequently used in cable-stayed bridge.

Cable-stayed bridge belongs to the composite structure system, as the beam and girder are supported by stayed-cables fix on the tower. The stayed-cables are anchored in the girder

directly and under a great pressure. The horizontal force of the cable leads to girder pressured; hence, the girder and the tower are under compression, this is the main difference between cable-stayed bridge and suspension bridge. Because the girder of the cable-stayed bridge is directly connected to the tower by pre-tensioned cables, the bending stiffness and the torsional stiffness of the main girder increase, so, it is better resulting in dynamic characteristics, than the suspension bridge.

The maximum value of the internal force and deformation of the structure with the closest connection to the natural frequency of vibration and mode of vibration, are intrinsic dynamic characteristics of the vibration system. In a dynamic calculation and analysis of the structure, we often need to calculate the natural frequency of vibration or the period first.

The vibration of cable-stayed bridge is simple harmonic vibration either on vertical or lateral, so, when solving this kind of problem, the bridge should be divided into a number of units or elements, and then it is contribute to further analysis.

1.3.2: Stonecutters Cable-Stayed Bridge

The current study has been developed to investigate the aerodynamic performance of the already constructed Stonecutters Cable-stayed Bridge which has a total length of 1,596 m with a main span of 1,018 m. The geometrical details of the dimensions of the bridge and the cross-sections of the bridge decks are represented in Figure 1.1 and Figure 1.2 [7]. The Stonecutters Bridge was the second longest cable-stayed bridge in the world at the time of its completion in 2008, and was the first major bridge with a twin-box girder superstructure. The concrete side spans are composed of four smaller spans of 69.25 m, 70 m, 70 m and 79.75 m, respectively. The Stonecutters Bridge spans the Rambler Channel in Hong Kong, connecting Nam Wan Kok, Tsing Yi Island and Stonecutters Island and was opened to

traffic on 20th December, 2009. The most notable feature of this bridge is the slender twin-box deck girder, with two main box decks for the vehicular traffic, connected between them every 18 m with separated stabilizing beams, thus forming the main span of the bridge deck. Such twin-deck configuration increases the complexity of the numerical modeling and finite element analysis required for the structural verification of the bridge response to dynamic loadings.

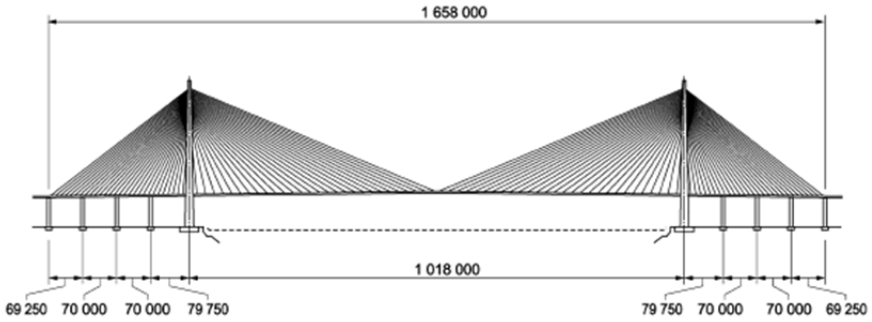

Figure 1.1: Side view of the Stonecutter Bridge. [7]

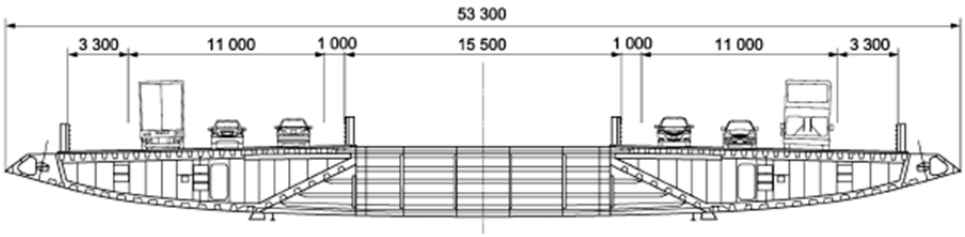

Figure 1.2: Cross-section of the bridge deck. [7]

The overall deck is 53.3 m wide and only 3.91 m deep, composed of two trapezoidal steel boxes with curved bottom panels, 19.5 m wide. The boxes are joined by heavy cross-beams spaced longitudinally at 18.0 m center to center providing a 14.3 m gap between the boxes [8].

The towers of the bridge are 300 m tall and they were built with a tapered circular cross-section. The towers were designed as a reinforced concrete structure up to 175 m and as a steel concrete composite from 175 m to 293 m. The tower section and dimension details are shown in the Figure 1.3 [9].

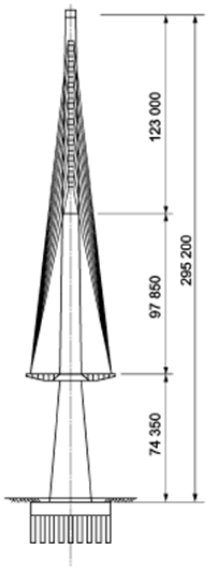

Figure 1.3 Tower cross-section details. [9]

Bridges with long spans and twin-deck configurations, like the Stonecutters Bridge will be subjected to severe wind-induced vibrations mostly due to the extreme weather conditions such as typhoons and considering the fact that the bridge structure must safely withstand earthquake loading as well, dynamic analysis becomes one of the most important elements of the design procedure. The Stonecutters Bridge has a twin-girder deck with a wide clear separation of 14.3 m between the two longitudinal girders; this kind of design of the deck is very attractive from the aerodynamic performance point of view and numerous studies have concentrated on investigating the wind-induced problem related to this kind of deck as it will be presented in detail in Chapter 2, however the most pertinent studies for the current research will be briefly mentioned in this section. Larsen, et al, (2007) [10] has examined

the vertical vortex shedding excitation of a twin girder bridge deck with the intention to unveil the details of the excitation mechanisms and to investigate the soffit mounted guide vanes, as a means for aerodynamic response mitigation measures. It is concluded that vortex excitation of twin girders are likely to be stronger than the vortex excitation of singular girder decks. Sato, et al (2000) [11] studied a combined 1-box and 2-box girder sections and from the multi-mode flutter analysis performed on a suspension bridge having a main span of 2,500 m they found out that the flutter onset velocity for the 2-box (twin box) and the 1-box (mono box) combined girders can be notably higher than that in the mono box combined girder. Kobayashi, et al (2005) [12] found that in general a slot at the center of a girder, geometry which is very similar to the twin-box deck configuration, would be effective in improving aerodynamic stability, while Matsumoto, et al (2004) [13] looked at the flutter characteristics of long span bridges with separated two box girders from the point of view of unsteady pressure distribution on bridge deck surface during heaving/torsional vibration related to the aerodynamic derivatives. And found that the flutter instability of H-shaped girders with side-ratios B/D, which is smaller than 10, is almost characterized only by the flutter derivative A_2^*. In addition, by comparing the results, the similarity of flutter characterized of H-shaped girders and rectangular girders has been demonstrated by suitably changing their side-ratios, such as 5, 8 and 12.5 for H-shaped corresponding to 10, 15 and 20 for rectangular girders.

Compared to an I-beam shaped bridge deck, the advantage of using a box deck girder is due to the fact that the later can better resist torsional vibrations. Having multiple vertical webs, the box deck girder can also carry more loads than an I-beam of equal height would withstand, hence it is widely used in Super Long-Span Bridges (1,000 m and more).

1.4: Study motivation

The static and dynamic wind loading always played a significant role in the structural design of bridge structures. Numerous experimental and numerical studies have been performed for investigating the aerodynamic instability of long-span bridges of mono bridge decks, and several experimental investigations were reported for the aerodynamic response of the twin-box deck girders bridges subjected to wind loading simulated by the aid of wind tunnel facilities. However, numerical models of twin-box bridge decks are still in an incipient stage and complex aerodynamic phenomena such as flutter instability is difficult to simulate. Moreover, in spite of the pass through experimental verifications [14], some of the constructed twin-box bridges were monitored and unexpected wind-induced vibrations have been reported [15] and adequate explanations were not found. In this regard, the aim of the current research is to clarify the static and aerodynamic instability effects of a long-span cable-stayed bridge with a twin-deck configuration and its performance and response under the effect of the wind load.

The Stonecutters Cable-stayed Bridge was selected in this research for clarifying the flutter aerodynamic instability for such long-span twin-box deck bridges. Initially, a complete detailed finite element model was created by the aid of ABAQUS, structural software, which is widely used software for finite element analysis. Several bridge properties and aerodynamic characteristics are computed using the finite element model, such as natural frequency, natural vibration mode, eigenvalue, etc.

To represent the simplified response to wind loading, the motion of the dynamic structural system was expressed by the equation of motion along three different directions: along-wind direction or drag, across-wind direction or lift and torsional direction around the

horizontal axis. The static wind loading and the self-excited loading were incorporated in the static and the aerodynamic analysis respectively. The static wind load was calculated from the mean wind equations, thus representing the static component of the wind flow. For the case of estimating the aerodynamic instability of the Stonecutters Bridge, the Scanlan's self-excited formulas [16] were employed to calculate the fluctuation of the wind flow, and it is generally conceded that Scanlan's formulation is one of the most popular methods to simulate the flutter dynamic load for the finite element of a bridge model. Whether it is mean wind loading or self-excited loading formulas, both of them are numerical ways which increase the level of complexity for the wind loading, which in practical cases is equivalent to a simple concentrate load on the model. Always the structural response of the model will be verified for the three different directions: horizontal force, vertical force and torsional moment. This kind of transformation is the most effective and convenient method to simulate the wind load in aerodynamic investigations. The critical flutter wind velocity and the critical flutter frequencies were determined at the end of this study. At the same time, the response of the bridge under different wind speeds will be presented as a comparative parametrical study.

1.5 Study objectives

The main target of this thesis is to determine the flutter aerodynamic instability of the Stonecutters Bridge by numerical investigations. In order to achieve this objective, several steps were necessary to be performed, following an established sequence:

- Initially, a 3D finite element model of the Stonecutters Cable-stayed Bridge was developed using ABAQUS software. The bridge model was built following the geometrical and the structural characteristics of the real bridge structure, and finally

the model was validated by comparing the obtained natural frequencies with the natural frequencies and modes reported in the literature for the Stonecutters Bridge monitoring data.

- Once the finite element model of the bridge was proven to have a validated response, the static mean wind load and the static lift, drag and torsional responses were determined. The maximum registered static deflections for the three directions were necessary for the self-excited aerodynamic loading equations which were applied to the structure for determining the flutter instability. Also a parametric study was performed employing wind speeds of 35 m/s, 70 m/s, 105 m/s, 141 m/s, 176 m/s and 211 m/s, for identifying the critical loading stages for the bridge. These specific wind speeds were selected based on the Hui's wind tunnel test in 2006 [17].

- In order to estimate the structural response of the Stonecutters bridge to wind loading, a time history analysis was performed by employing the three components of the wind loading, the drag, lift and moment, which were calculated based on the real wind speed records obtained from the anemometer installed by the SUNLab team at the solar panels research site existent on the flat roof of the Mann Parking Building in the University of Ottawa campus. The wind speed record was magnified by a factor of 5 to represent the loading applicable to the bridge site. Dynamic response of the bridge model at several locations were reported and discussed.

- The Scanlan's theoretical formulation for the bridge flutter was employed for calculating the self-excited loadings along the three directions, the drag, the lift and the torsion, and by incorporating the flutter derivatives reported by the experimental studies performed for the Stonecutters Bridge by Michael C.H. Hui [18]. The maximum static displacements which were determined above for the bridge model

were also employed in the same formulation, in order to adapt the numerical model to the finite element model of the Stonecutters Bridge. Flutter vibrations frequencies and mode shapes were identified and the coupling between the torsional and vertical vibration modes, thus clarifying the occurrence of the coupled flutter phenomena.

- Finally the main objective of this research project is to determine the critical wind speed for the Stonecutters Bridge FE model, based on the natural frequencies and the dynamic response obtained under flutter conditions. By discussing these critical wind speeds in regard to the design wind speeds for bridges of mono box deck girder, the efficiency and the better aerodynamic performance of twin-box deck girders was underlined.

1.6 Thesis layout

The thesis starts by presenting the background knowledge of the aerodynamic instability and the general wind effect on bridges in Chapter 2, where also some detailed theoretical formulations were presented to provide the basic understanding of the mean wind load calculations and the aerodynamic analysis. Chapter 3 described the assumptions and the details used for the finite element model of the Stonecutters Bridge, which was created in ABAQUS software. Several structural elements of the model were described in detail. For the bridge FE model, the element type, the material property and cross-section geometry were depicted and the rigid body connections and boundary conditions are discussed. A brief introduction to the static and the dynamic analyses were also provided in this chapter and the analysis steps for the natural frequencies and eigenvalues were discussed. The wind loadings determined for the Stonecutters Bridge model were described, and in particular some details regarding the mean wind load and self-excited load simulating were provided.

Chapter 4 discussed the results of the structural analysis. Due to the finite element model itself, the static and the dynamic responses of the bridge deck at certain locations were described, including the natural frequency of the bridge, the vibration modes and the mass participation factors influencing each vibration mode. As for the dynamic response of the bridge under the wind load, the vibration response of the bridge at mid-span and some other specific locations were mentioned. The figure of the displacement and the torsional angle varying with time and with the wind speed were also discussed.

In Chapter 5, the main conclusions were summarized from the analysis and the results, including the verification of the critical flutter wind speed and the flutter vibration frequencies. The critical speed and frequencies discussed here were calculated by the Fast Fourier Transform, which, in general, converts time domain signals into frequency domain signals. This transformation was achieved through the use of the MATLAB work software.

Chapter 2 Literature Review

2.1 Introduction

As mentioned in Chapter 1, the effect of wind on bridges is a very complex phenomenon, which depends on the characteristics of wind, the dynamic performance of the structure and the interaction between the structure and wind. The basic characteristics of natural wind were introduced in the previous section. Because of the effect of turbulence flow at the atmospheric surface layer, velocity, direction and spatial distribution are non-steady and random. Hence, non-streamlined bridge decks were suffered from this kind of non-steady wind speed, after which vortex and flow separation phenomena will occur and a series of complicated aerodynamic loads will be generated. This acting load will lead to bridge vibration, and the vibrating bridge will continue to influence the flow field at the same time. This interaction deepens the complexity of the problem.

A cable-stayed bridge is another suspension structure system in addition to the suspension bridge. The main components of a cable-stayed bridge are the stay cables, main girder and towers. The arrangement of stay cables and towers can be designed in many ways to meet the demand of transportation, cost, etc. As a result of effective stay cables, lateral bending and torsional deformation of the bridge are mutually coupled. The slender and flexible features of the structure itself make the dynamic characteristics of cable-stayed bridges more complicated than other bridge structures.

2.2 Criteria for bridge design

Both the static and dynamic responses of a bridge under wind loading should be considered in the design of super long-span cable support bridges. The design of a cable-stayed bridge is often governed by aero-elastic instability. To ensure the structure's safety and avoid failure due to flutter instability, the calculation and analysis of the critical velocity for the onset of flutter instability should be performed in the cable-stayed bridge design. Therefore, to understand the response of the long-span cable-stayed bridge under wind loading, this chapter focuses on and reviews research related to bridge aerodynamic problems, and this basic knowledge will be explained in the following section.

2.3 Bridge aerodynamic finite element theory

Aerodynamic theory originates from the aerospace field, which is widely used in aircraft design. When bridge design first began, designers considered the wind as a simple lateral static load. After the failure of the Tacoma Narrows Suspension Bridge in Washington in 1940, aerodynamic theory was involved in structural engineering, especially in bridge engineering. People began to realize that frequency and other dynamic phenomena other than fundamental factors should be considered in bridge design.

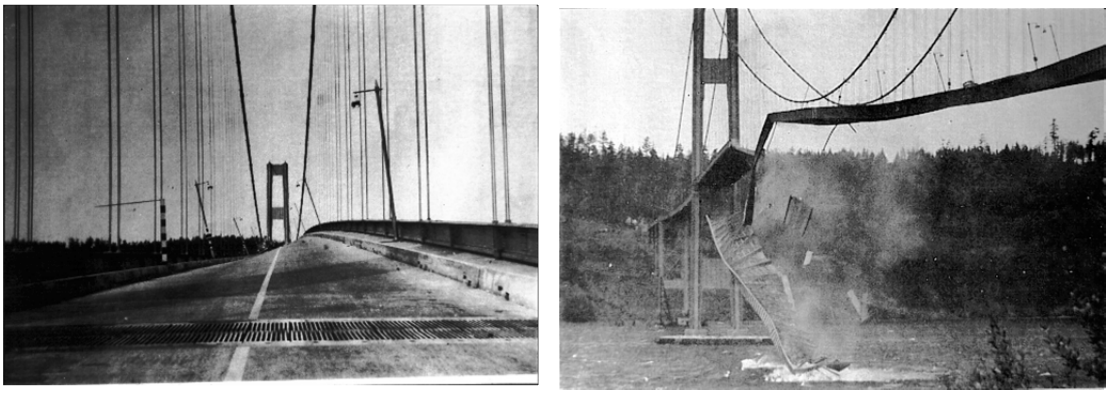

Figure 2.1: Tacoma Narrows Suspension Bridge collapse in 1940. [19]

As early as 1948, Dr. Friedrich Bleich (F. Bleich, 1948) [1] introduced the “Flutter” theory in the investigation of critical wind velocity. The study gives the critical wind for a section consisting of a thin plan plate, which was based on Theodorsen’s thin plate theory (T. Theodorsen, 1935) [2]. The flutter velocity is easily calculated, as reported by Bleich.

However, the bridge will never have pure plane plate cross-section like that. Therefore, follow-up studies continually improved the analysis method for bridge aerodynamic problems, and provided various kinds of equations for different situations.

2.3.1 Equations of motion

When a bridge is under wind loading, the reaction on the bridge deck could be separated into three parts, along with different directions: horizontal, vertical and torsional reactions. Therefore, the bridge structure should follow the aerodynamic formula for the analysis. In addition, the problem of a bridge under wind loading can attribute to dynamic motion; hence, the motion equation will be the basic theory for all calculations and analysis, and it is also the working principle of the finite element program.

From Newton's second law, the governing motion equation for a structure under the external force is defined as follows:

$$M\ddot{X} + C\dot{X} + KX = F \quad (2.1)$$

Where, M: Structure mass matrix;

C: Structural damping matrix;

K: Structural stiffness matrix;

$\ddot{X}$, $\dot{X}$ and X: Nodal displacement, velocity and acceleration vector, respectively.

F: External loading on the mass.

This equation can be rewritten in the form,

$$\ddot{X} + 2\zeta\omega\dot{X} + \omega^2 X = \frac{F}{M} \quad (2.2)$$

Where,

$\omega = \sqrt{\frac{K}{M}}$, ω is the natural circular frequency,

$\zeta = \frac{C}{2M\omega}$, $2M\omega$ is the critical damping coefficient.

As mentioned above, when it comes to the problem of the bridge, wind loading will act in three different directions, and the reactions that are induced by wind will also be separated into three components: horizontal force, vertical force and bending moment. Therefore, the

motion equation will be further improved for this situation.

The equations of motion to the model along the three different directions are as follows:

$$m\ddot{z}+c_z\dot{z}+s_z z=L;\ \ m\ddot{y}+c_y\dot{y}+s_y y=D;\ \ I\ddot{a}+c_a\dot{a}+s_a a=M \quad (2.3)$$

Where,

z = Vertical deflection, positive upwards,

y = Horizontal deflection, positive in wind direction,

a = Torsional deflection, positive when windward edge of deck is above leeward edge,

m = Mass per unit length,

I = Moment of inertia per unit length,

c_z, c_y, c_a = Damping constants in bending and torsion,

s_z, s_y, s_a = Stiffness constants in bending and torsion,

L = Aerodynamic lift force per unit length,

D = Horizontal wind force per unit length,

M = Aerodynamic pitching moment per unit length.

For the purpose of recognizing the characteristics of wind effects on the bridge, a moderate

abstract analysis is needed. Generally, wind flow changes with time and space can be viewed separately into two parts to simplify the study, which are mean wind speed and fluctuation speed [2], as shown in Figure 2.2.

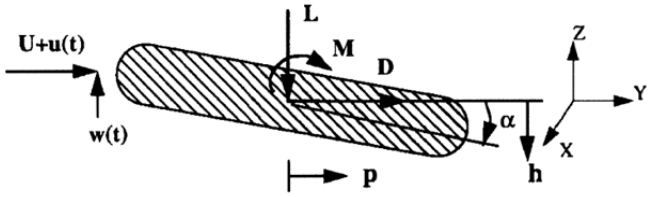

Figure 2.2: Reactions induced by wind. [20]

U represents the mean wind speed, which reflects static features of wind flow. The mean wind speed is assumed to be constant in the space and time domain. u(t) and w(t) are fluctuation wind speeds or turbulent wind speeds. This component of wind flow is a major source that creates aerodynamic instability.

In addition, the static and dynamic characteristics of wind speed will also occur in the loadings, which result in wind effects on the bridge. Hence, similarly, the external loading from wind on the mass can be divided into two components, which are mean wind loading and dynamic loading.

Consequently, the motion equation can also be further improved, as in the following:

$$M\ddot{X} + C\dot{X} + KX = F_m + F_d \quad (2.4)$$

Where, F_m: Mean wind loading, F_d: Dynamic wind loading.

For the three components from different directions, drag, lift force and torsional moment can also be expressed as,

$$L = L_m + L_d; \quad D = D_m + D_d; \quad M = M_m + M_d \quad (2.5)$$

2.3.2 Static effect of wind on bridges

Static wind load is the most basic wind effect considered when designing a bridge structure. For bridges, the static phenomena are not the critical states for the bridge design, and the behaviour is less critical to the dynamic effects.

Assume the bridge structure keeps still under steady wind flow, or in other words, the wind loading is not affected by bridge vibration. This kind of reaction, which is constant in time, is called the static effect of wind. The problems related to the static wind load can be explained by the mean wind force components like drag force, lift force and torsional moment, as mentioned in the previous section. Mean wind load equations are reported by Robert H. Scanlan (Scanlan, R. H. 1996) [21] and can be expressed as follows:

$$D_m = \frac{1}{2}\rho \bar{U}^2 C_D B L(\alpha); \quad L_m = \frac{1}{2}\rho \bar{U}^2 C_L B L(\alpha); \quad M_m = \frac{1}{2}\rho \bar{U}^2 C_M B^2 L(\alpha). \quad (2.6)$$

Where, ρ : Air density, 1.225 kg/m^3 in this thesis;

$\bar{U}$: wind velocity;

C_D, C_L, C_M : drag, lift and moment coefficients, respectively;

B, L: bridge deck width and bridge length.

α : The angle of attack of the wind.

In fluid dynamics, the static wind force coefficient is a dimensionless quantity used to quantify the drag, lift and torsion or resistance of an object in a fluid environment, such as air or water. It is used in the mean wind load equation, where a lower wind force coefficient indicates the bridge structure will have less aerodynamic drag, lift or torsion. The wind force coefficient is always associated with a particular surface area.[3]

From the mean wind load, the force coefficients are defined as follows:

$$C_D = \frac{2D_m}{\rho \bar{U}^2 BL(\alpha)};\ C_L = \frac{2L_m}{\rho \bar{U}^2 BL(\alpha)};\ C_M = \frac{2M_m}{\rho \bar{U}^2 B^2 L(\alpha)} \quad (2.7)$$

As it can be concluded from the coefficient equations, C_D, C_L, C_M are not constant but vary as a function of mean wind speed, size of cross-section, fluid density and attack angle of the wind. But for a certain body shape like the bridge deck, the force coefficients can often be treated as constant under a certain attack angle.

In bridge engineering, wind force coefficients are often tested in wind tunnel experiments. Diana and Fiammenghi (G. Diana and G. Fiammenghi, 2012) [22] indicated that the lift, drag and torsional moment coefficient are very important for bridge deck design optimization. They defined the static force coefficient through the sectional model of the bridge deck in the wind tunnel.

They also provided the force coefficients data from the Messina Suspension Bridge and Akashi-Kaikyo Suspension Bridge as follows, in Figure 2.3 and Figure 2.4.

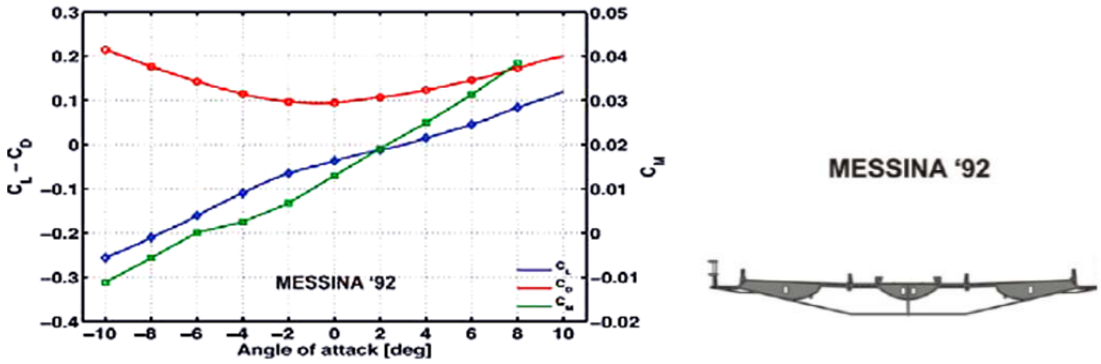

Figure 2.3: Wind force coefficients of Messina Suspension Bridge. [22]

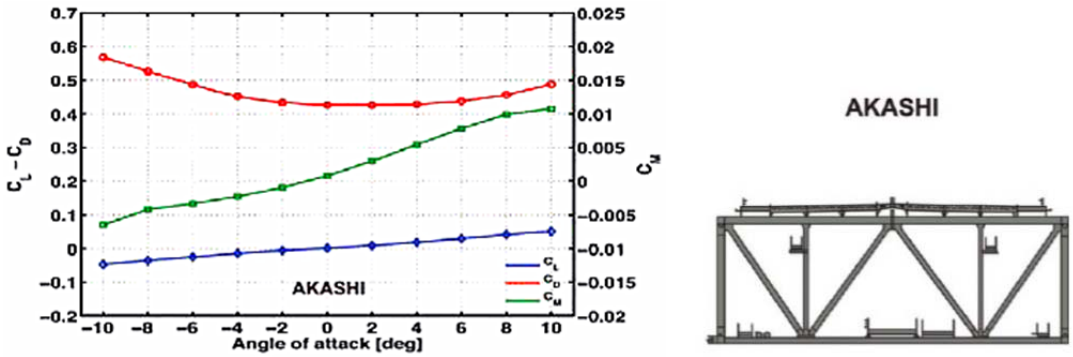

Figure 2.4: Wind force coefficients of Akashi-Kaikyo Suspension Bridge. [22]

In addition, the lift and moment coefficient slopes are very important for bridge stability and aerodynamic analysis and they must be positive with the increase of the attack angle to have an agreement with the convention sign of loading directions. Things are different for the drag coefficient. Generally, the value of the drag coefficient reaches a minimum value for 0 degree attack angle, but the change trend is not obvious.

Larsen et al, (Larsen et al, 2012) [10] provided the wind load coefficients of the Stonecutters Cable-stayed Bridge obtained in smooth wind flow at the attack angle of wind incidence α varying between -5 degrees and +5 degrees. Three different Reynold's numbers are also involved in the test.

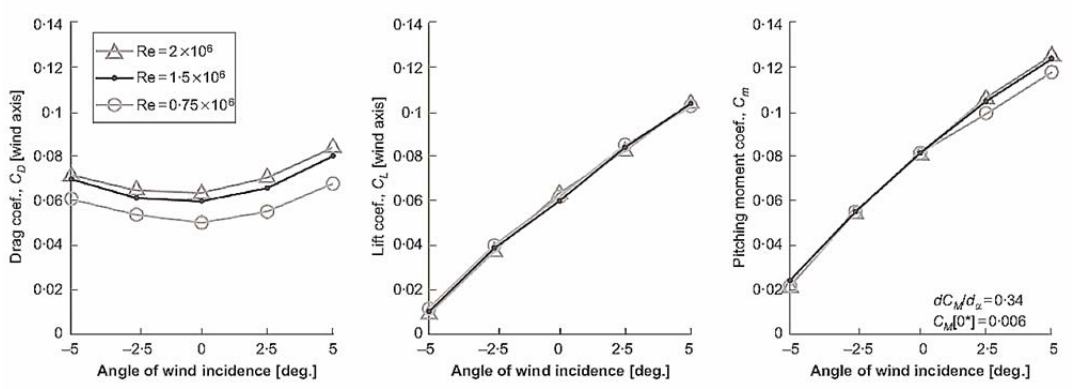

Figure 2.5: Variation of wind load coefficients for three Reynold's Number of Stonecutters Bridge. [10]

As shown above in Figure 2.5, the slope of drag, lift and pitching moment coefficients show similar changing characteristics to the Messina Suspension Bridge and Akashi-Kaikyo Bridge reported by G. Diana and G. Fiammenghi [22].

It is noted that lift and torsional moment coefficients are virtually unaffected by the Reynold's Number, but the drag force coefficient changes according to the value of R_e. [10] However, in bridge structures, most non-streamlined cross-sections have obvious edges except the circular cross-section, hence, the separation position of air flow is fixed, and it can be assumed that force coefficients do not vary with kinematic viscosity and the characteristic length scale of the object. Consequently, the effect from the Reynold's number can be ignored.

Larose et al, (2006) [23] noted that in the conclusion of their report for the sectional model experiments of the Stonecutters Bridge. They collected the data from different wind velocities to estimate the force coefficient variation. Their results are summarized in Table 2.1 below.

Table 2.1: Wind force and moment coefficients of Stonecutters Bridge from force balance measurements. [23]

Wind incidence	15 m/s (R_e =1.05e+06)			25 m/s (R_e =1.75e+06)			33 m/s (R_e =2.30e+06)		
	C_D	C_L	C_M	C_D	C_L	C_M	C_D	C_L	C_M
-5°	0.077	-0.347	-0.018	0.081	-0.351	-0.017	0.081	-0.372	-0.018
-2.5°	0.073	-0.209	-0.002	0.074	-0.214	-0.002	0.073	-0.219	-0.001
0°	0.065	-0.073	0.012	0.067	-0.074	0.013	0.067	-0.079	0.014
2.5°	0.068	0.040	0.026	0.069	0.040	0.027	0.070	0.046	0.028
5°	0.075	0.129	0.030	0.083	0.144	0.034	0.084	0.141	0.035

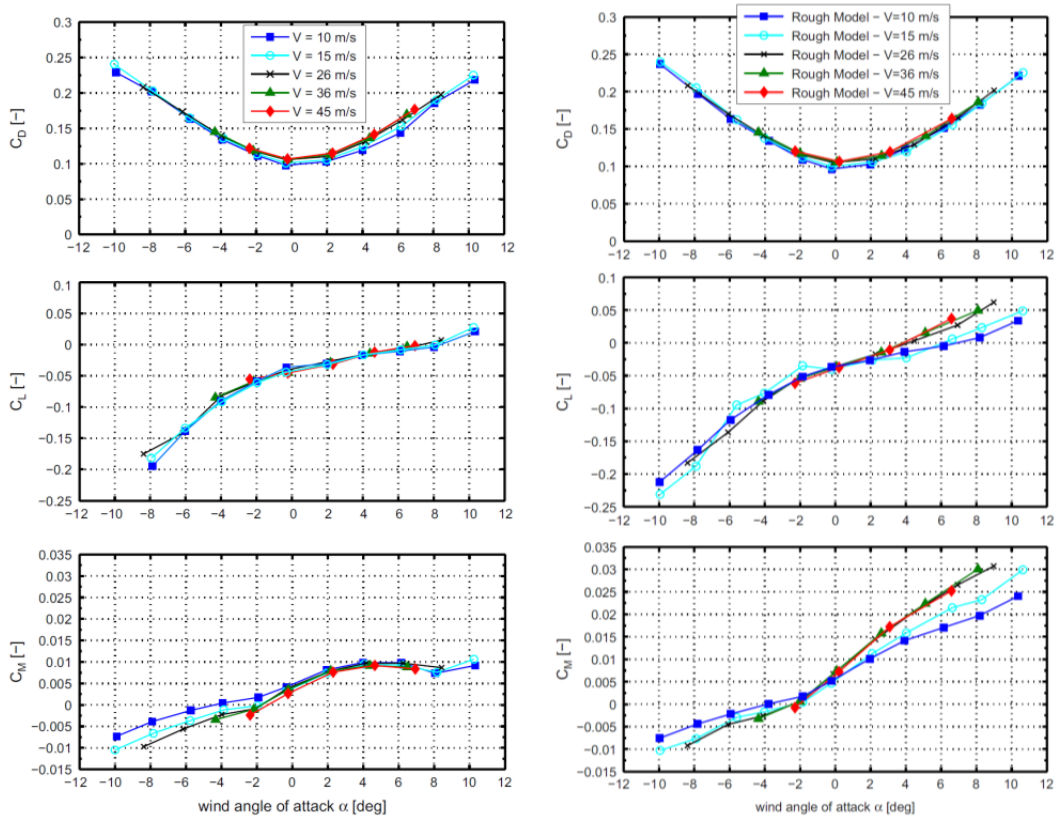

(a) (b)

Figure 2.6: Wind load coefficients of Stonecutters Bridge under different wind velocities. [22]

Various graphics as shown in Figure 2.6 have been used for a more detailed and direct display of the coefficient data. Changes in the curve in the figure show that wind load

coefficients are not affected by wind velocity.

Consequently, by summarizing the results above, if the calculation of static wind analysis involves the mean wind load and wind load coefficients, they are unaffected by wind velocity and Reynold's Number. C_D, C_L and C_M can be regarded as constant values when in a certain attack angle.

2.3.3 Dynamic behaviour of wind

Aerodynamics is the subject concerned with the study of phenomena of aerodynamic loads and how structural responses interact. When a bridge structure is subjected to wind flow, it may deflect suddenly or vibrate in the wind flow. The aerodynamic response of the bridge can generally be classified as two types.

The first is when the bridge is under wind loading, which is a self-excited vibration of the structure generated by absorbed energy from the wind flow. For instance, a classic flutter, which is a torsion coupled with a vertical bending vibration response, possibly occurs on the streamlined bridge deck. As for the no-streamlined shape of cross-sections, separated-flow torsional flutter would be produced. In addition, galloping and vortex-induced vibration may also be produced on the bridge.

Another kind of oscillation response is forced vibration. Forced vibration commonly comes with fluctuating wind loading, which has random properties. This kind of random vibration response is called buffeting. Excessive buffeting response can lead to local fatigue of connection and supporter, endangering traffic safety.

Fundamental knowledge of the dynamic behaviour of a bridge will be introduced first. As

mentioned above, the vibration response of the cable-stayed bridge caused by wind loading can be generally classified as these types:

1. Vortex shedding

2. Galloping

3. Buffeting

4. Flutter

Unlike the static behaviour, the dynamic response of the bridge structure is more critical and thus is very important to be considered in the structural design. The fundamental knowledge of different types of dynamic responses under wind loading is required to understand the wind effect on bridges and will be explained in the following section.

Vortex shedding:

It is well known that, an object with a certain mass and stiffness has its own natural frequency, which is defined as the square root of stiffness over mass. When one object interfaces with another object that is vibrating at the same natural frequency, resonance will occur. The phenomenon is very common in nature. Also, this is the basic mechanism of vortex shedding.

Simiu and Scanlan (Simiu and Scanlan, 1996) [6] indicated that, when wind flows through a bridge deck at a particular speed, the airflow will be separated by the structure and around the bridge body, this procedure generates a shear force on both sides of the structure separately; they interact with each other and then generate a vortex, which is subject to

regular periodicity. The vortex was showed in different times on both sides, which means air pressure will be different, and as the upper and down flow move to the low pressure region alternatively, then unstable vibration is created.

The extent of the vortex shedding depends on the Reynolds number (R_e) and Strouhal number (S_t), [24], which are defined as,

$$R_e = \frac{\rho U D}{\mu}, \quad S_t = \frac{N_s D}{U} \qquad (2.9)$$

Where, ρ = wind density;

U = wind velocity;

D = diameter;

μ = viscosity;

N_s = frequency of vortex cycle shedding.

Hence, frequency of vortex shedding can be determined from the transformation equation as follows:

$$N_s = \frac{S_t U}{D} \qquad (2.10)$$

Due to the bridge structure, vortex shedding always occurs under low wind speed. The cross-section of the bridge can be adjusted to avoid this unstable phenomenon, or install fairings on both sides of the deck section. In addition, a mechanical damper can also be

involved in the structure design to decrease the amplitude if the bridge structure or geometrical characteristics are not allowed to change.

Galloping:

Galloping is the vibration of a structure in the perpendicular direction to the mean wind direction. It occurs due to the aerodynamic forces that are induced by the small transverse motions of the structure. The aerodynamic self-excited forces act in the direction of the transverse motion resulting in negative damping, which increases the amplitude of the transverse motion until it settles down to a limited cycle. The galloping of a structure occurs above a certain critical wind speed is usually called the "onset galloping wind speed." [25] [26]

Galloping usually occurs in pylons of suspension and cable-stayed bridges; generally, the deck of the bridge will not be affected by galloping, and the other elements that we should consider are cable, hanger or truss welding, etc. These kinds of elements will be affected by galloping. [27] [8]

The prediction of the galloping amplitude has relied, so far, on curve fittings of the aerodynamic transverse force function that are obtained using wind tunnel experiments.

Buffeting:

Buffeting is defined as the wind-induced vibration in wind turbulence that is generated by unsteady fluctuating forces as origin of the random ones due to wind fluctuations. Buffeting of a structure is caused by velocity fluctuations in the flow, which inherently exist in natural wind. The effect of unsteady loading worsens as the flexibility of the structure increases, and thus it is of concern in the design of long-span bridges. Buffeting usually does not cause

divergent amplitudes in the structure; however, it can cause fatigue of the structure from repeated along-wind oscillations, large deflections of the structure during erection, traffic discomfort due to motion, as well as some concern for the safety of high-speed traffic due to the movements of the deck. [28]

The purpose of buffeting analysis is the prediction or estimation of the total buffeting response of structures (displacements, sectional forces: shear force, bending and torsional moments). Buffeting response prediction is a major concern (besides aero-elastic instability known as flutter) in the wind resistance design and evaluation of wind-induced vibrations for long-span bridges.

Flutter and buffeting responses are extremely important topics in the design of long-span bridges. Actually, flutter and buffeting are not completely independent. In any wind speed, bridges will be affected by buffeting load and self-excited load. In low-speed wind, the self-excited load is small and does not play a predominant role in the reaction of the structure, so buffeting is obvious in the oscillation of the bridge. But when the wind speed increases to a certain value, the self-excited load will diffuse gradually and then control the movement of the bridge. This is the process by which flutter happens.

Flutter:

Flutter has been determined to be one of the most dangerous aero-elastic structures in civil engineering, especially after the disaster of the Tacoma Narrow Bridge. The term *flutter* has been used variously to describe different types of wind-induced behaviour.

Flutter is caused by a small amplitude vibration of the bridge itself, which bridge absorbs energy from flow field. When the wind speed reaches a certain value, the amplitude of the

structure will rise rapidly, and can cause structural damage to bridges, and this value of wind velocity is the flutter critical wind velocity. [29] When flutter occurs, the oscillatory motions regarding all degrees of freedom in the structure couple to create a single frequency called the flutter frequency.

Flutter effects on the structure of bridges are generally divided into two types:

1. Single-degree-of-freedom-flutter.

2. Classical flutter.

Once self-excited vibration occurs, it will lead to damage of the whole structure. Therefore, flutter is one of the oscillation modes that must be strictly avoided whether in aerospace or in civil engineering. The flutter critical wind velocity is closely related to geometric shapes of the bridge section; therefore, a good way to avoid or decrease flutter behaviour is an appropriate selection in bridge design.

Due to the importance of flutter response, Th. Theodorson (T. Theodorsen, 1935) [2] studied the aerodynamics of wind effects on the thin plane plate from the Theodorsen theory developed in 1935. He used the potential theory to obtain the expression of functions for unsteady wind loads on the vibrating plane plate. In 1938, the study was repeated by Th. Von Karman with similar results.

The unsteady wind load acting on an ideal flat plate in the uniform wind flow field can be defined as follows:

$$L = -2\pi\rho b v^2 \left(C(k)\left[\alpha + \frac{\dot{h}}{v}\right] + \left[1 + C(k)\right]\frac{b}{2}\frac{\dot{\alpha}}{v} \right)$$

$$M = \pi\rho b^2 v^2 \left(C(k)\left[\alpha + \frac{\dot{h}}{v}\right] + \left[1 - C(k)\right]\frac{b}{2}\frac{\dot{\alpha}}{v} \right) \quad (2.11)$$

Where, ρ : Air density;

b: Half width of the plane plate, the width of bridge is $B = 2b$;

v: Wind velocity;

h and α are vertical displacement and torsional angle of cross-section, respectively;

$k = \frac{\omega \cdot b}{v}$, which is reduced frequency; ω is circular frequency;

$C(k)$: Theodorson function, which can be expressed as $C(k) = F(k) + iG(k)$. Or it also can be defined in the R. T. Jones format,

$$C(k) = 1 - \frac{0.165}{1 - \frac{0.0455}{k}\cdot i} - \frac{0.335}{1 - \frac{0.3}{k}\cdot i}; \quad (2.12)$$

$$F(k) = 1 - \frac{0.165}{1 - \left(\frac{0.0455}{k}\right)^2} - \frac{0.335}{1 + \left(\frac{0.3}{k}\right)^2}; \quad (2.12)$$

$$G(k) = -\frac{\frac{0.165 \times 0.0455}{k}}{1+\left(\frac{0.0455}{k}\right)^2} - \frac{\frac{0.335 \times 0.3}{k}}{1+\left(\frac{0.3}{k}\right)^2}. \quad (2.12)$$

Dr. Friedrich Bleich (F. Bleich, 1948) [1] was the first to use Theodorson's theory in flutter analysis of the suspension bridge. He indicated that the decks on truss and stiffening girder in the suspension bridge structure are close to a flat plate. And due to the wind load on the Vierendeel, truss is negligible. Therefore, Bleich improved the wind load equation reported by Theodorson as follows:

$$\ddot{p}_1 + \omega_b^2(1+ig_b)p_1 + \frac{sbv^2}{mb^2}\left(f_1\left[q_1 D + \frac{b}{v}\dot{p}_1\right] + f_2\frac{b}{2v}\dot{q}_1 D\right) = 0$$

$$\ddot{q}_1 + \omega_a^2(1+ig_a)q_1 - \frac{sbv^2}{2mr^2}\left(f_1\left[q_1 + \frac{b}{v}D\cdot\dot{p}_1\right] - f_3\frac{b}{2v}\dot{q}_1\right) = 0 \quad (2.13)$$

Where,

ω_b, ω_a are bending natural frequency and torsional natural frequency, respectively.

$g_b = \frac{\theta_b}{\pi} = 2\zeta_b$, $g_a = \frac{\theta_a}{\pi} = 2\zeta_a$ are the complex damping coefficients of bending and torsion.

$f_1 = C(k)$, $f_2 = 1 + C(k)$, $f_2 = 1 - C(k)$ and $s = 2\pi\rho b$.

When uniform wind flow passes by a non-streamlined vibrating cross-section, air flow will be separated by the edge of the windward side, thus the flow condition around the bridge body is very complicated. Hence, the unsteady wind load on the non-streamlined body

cannot be perfectly defined using this potential theory. In 1971, R. H. Scanlan (R. H. Scanlan and J. J. Tomko, 1971) [16] indicated that, although the aerodynamic coefficients similar to Theodorson's format cannot be derived by basic principles of hydromechanics, a specially designed wind tunnel test can be used to determine the unsteady wind load under the small amplitude vibration.

For the convenience of mathematical analysis, Scanlan improves the aerodynamic wind load equation for flutter analysis, which is still in use today. The self-excited and lateral forces and self-excited moment acting on the bridge deck per unit length are expressed in terms of Scanlan's format as follows:

$$L_{se}(t) = \frac{1}{2}\rho\bar{U}^2(2B)\left(KH_1^*\frac{\dot{h}}{\bar{U}} + KH_2^*\frac{B\dot{\alpha}}{\bar{U}} + K^2H_3^*\alpha + K^2H_4^*\frac{h}{B} + KH_5^*\frac{\dot{p}}{\bar{U}} + K^2H_6^*\frac{p}{B}\right)$$

$$D_{se}(t) = \frac{1}{2}\rho\bar{U}^2(2B)\left(KP_1^*\frac{\dot{p}}{\bar{U}} + KP_2^*\frac{B\dot{\alpha}}{\bar{U}} + K^2P_3^*\alpha + K^2P_4^*\frac{p}{B} + KP_5^*\frac{\dot{h}}{\bar{U}} + K^2P_6^*\frac{h}{B}\right)$$

$$M_{se}(t) = \frac{1}{2}\rho\bar{U}^2(2B^2)\left(KA_1^*\frac{\dot{h}}{\bar{U}} + KA_2^*\frac{B\dot{\alpha}}{\bar{U}} + K^2A_3^*\alpha + K^2A_4^*\frac{h}{B} + KA_5^*\frac{\dot{p}}{\bar{U}} + K^2A_6^*\frac{p}{B}\right) \quad (2.14)$$

Where, ρ is the air density;

$\bar{U}$ is the mean wind velocity;

B is the bridge deck width;

$K = \omega B / \bar{U}$ is the reduced frequency;

ω is the circular frequency of vibration;

h, p and α are the vertical, lateral and torsional displacements of the bridge deck, respectively; the over-dot denotes the partial differentiation with respect to time t;

H_i^*, P_i^*, A_i^* $(i = 1 \sim 6)$ are the non-dimensional flutter derivatives.

The problem of how to experimentally obtain H_i^*, A_i^* and other flutter derivatives should be a concern. Three methods have been employed since 1966. Ukeguchi et al, (1966) [30] provided methods for driving the bridge deck model through prescribed sinusoidal motions, after which aerodynamic forces are measured directly. In France, fluctuating pressures over the deck model were measured during forced oscillation by H. Loiseau and E. Szechenyi (1975) [31]. However, the most economical and convenient method related to required laboratory equipment is developed by R. H. Scanlan and J. J. Tomko (1971) [16]. The free oscillation of the spring-mounted model is utilized with applied system identification techniques, for known motions under wind, to identify H_i^* and A_i^*.

The formulas of flutter derivatives reported by Scanlan are as follows:

$$H_1^* = \frac{mH_1}{\rho B^2 \omega}, \quad H_2^* = \frac{mH_2}{\rho B^3 \omega}, \quad H_3^* = \frac{mH_3}{\rho B^3 \omega^2},$$

$$A_1^* = \frac{IA_1}{\rho B^3 \omega}, \quad A_2^* = \frac{IA_2}{\rho B^4 \omega}, \quad A_3^* = \frac{IA_3}{\rho B^4 \omega^2}. \qquad (2.15)$$

Where,

m and I are the section mass and mass moment of inertia per unit span of the test model,

ρ is the air density of the test,

B is the deck width,

ω is the radian frequency of the structural oscillation of the test.

Some examples of representative flutter derivatives are also presented; Figure 2.7 shows several different types of bridge cross-sections as a comparison.

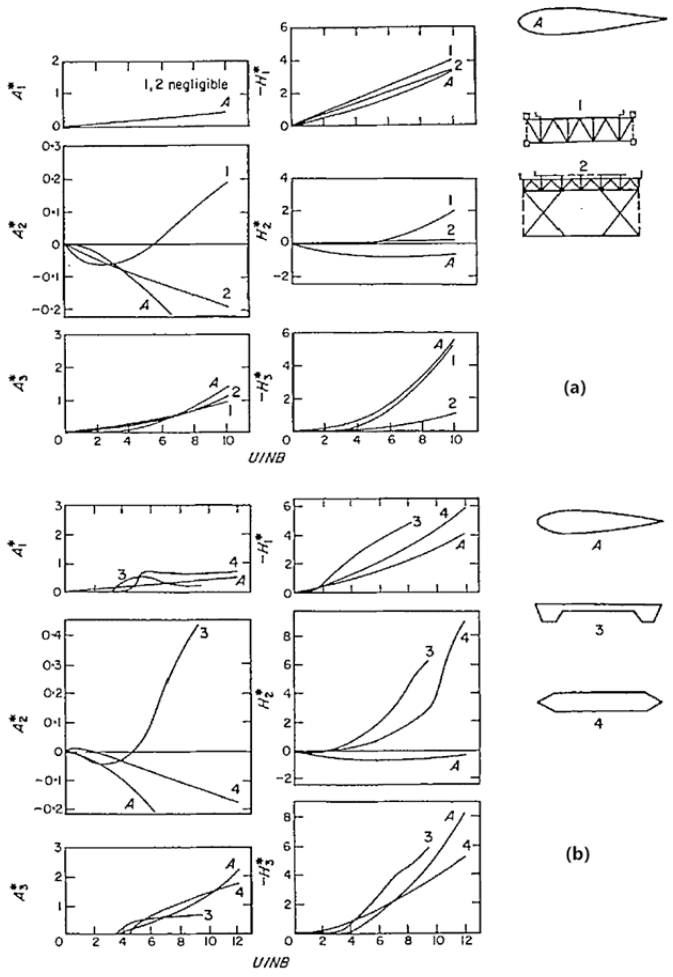

Figure 2.7: Examples of representative flutter derivatives. (a) A, thin airfoil; 1, trussed deck with instability tendencies; 2, stable truss deck. (b) A, thin airfoil; 3, unstable bluff box deck; 4, stable streamlined box deck. [16]

From Figure 2.7, the obvious differences between regular bridge deck and thin airfoil cross-section can be observed. The main difference is concentrated on A_2^*, which is a term of torsional air damping related to the torsional angle α. The value of A_2^* for the thin airfoil section decreases with wind velocity. In other words, the higher the wind velocity, the bigger the damping of torsional vibration generated by wind flow. On the contrary, due to the non-streamlined cross-section, the value of A_2^* will increase in wind velocity from negative to positive, which means the air damping transforms from positive damping to negative damping. And that is also the major reason for torsional flutter vibration.

Since the flutter derivatives related to the lateral motion of the bridge deck and the flutter derivatives H_5^*, H_6^*, A_5^* and A_6^* are not available, they are calculated based on the quasi-steady theory in terms of the aerodynamic coefficients as follows. [18] The aerodynamic parameters and the flutter derivatives mentioned above are assumed to be uniform along the bridge deck in the study.

$$P_1^* = -\frac{1}{K}C_D,\ P_2^* = -\frac{1}{2K}C_D',\ P_3^* = -\frac{1}{2K^2}C_D'$$

$$P_5^* = -\frac{1}{2K}C_D',\ H_5^* = \frac{1}{K}C_L,\ A_5^* = -\frac{1}{K}C_M$$

$$P_4^* = P_6^* = H_6^* = A_6^* = 0 \qquad (2.16)$$

2.3 Main methodology of bridge aerodynamic analysis

Wind disaster has the most widespread influence among natural disasters, and is also one of the most dangerous natural disasters that jeopardize people's lives and wealth. With close

cooperation between bridge engineers and aerodynamicists, the subject of wind engineering has been established. Bridge wind engineering concentrates on the static response and dynamic response of bridge structures under various possible wind conditions, and then provides solutions for the new bridge structure design and construction. Long-span and flexibility bridges such as suspension bridge, cable-stayed bridge and some flexibility elements in rigid frame bridge (e.g., Suspenders in arch bridge), etc., have to go through the analysis of wind engineering analysis and study. According to the research content, there are three main research approaches for the study: theoretical analysis, wind tunnel experiment and field observation, and numerical simulation.

2.3.1 Wind tunnel experiment studies

When the wind-induced vibration responses of the bridge are required, some theoretical analysis methods and wind tunnel experiments that have already been established are often used. But, for a complicated cross-section, it is a big challenge to solve the aerodynamic problem and some wind-induced issues by theoretical methods. After continuous development of experimental equipment and the laboratory environment, more and more people start to use the wind tunnel. The major purpose of the wind tunnel test is to provide references for wind resistance design of long-span bridges, so it is also one of the most effective tools and the most reliable method to analyze the wind-induced vibration of a bridge.

The wind tunnel experiment is one of the most important and irreplaceable methods in aerodynamic studies. A wind tunnel is a tool used in aerodynamic research to study the effects of air moving through solid objects. Wind tunnel does not mean a hole; it is a closed annular duct that can generate flow, and consists of a tubular passage with the object under

test mounted in the middle. It can simulate the real wind environment and the structures in the tunnel, and according to the response of the model in the experiment, can analyze and determine the reaction of the real structure.

Figure 2.8: Wind tunnel. [32]

For complex environment conditions, the shape and the cross-section of the structure will be also complicated; while it is more difficult for other approaches, it is easier to achieve the research objectives by using the wind tunnel experiment, which only needs to simplify the conditions. There are many types of wind tunnels. In the past, tunnels used in the study of bridge aerodynamics include low speed aeronautic wind tunnels, but at present, an atmospheric boundary layer wind tunnel that is specifically targeted at structural wind engineering has been widely used. The atmospheric boundary layer wind tunnel has a long test section that can simulate natural wind properties within the atmospheric boundary layer. The area of the test section ranges from an approximate few square metres to tens of square metres, and the test wind speed varies from a very low value (even 1~2 m/s) to tens of metres per second.

Classification of wind tunnel tests for bridges

According to its own characteristics and applications, the model of the bridge has two

different types, which are an entire bridge model and section model; hence, the wind tunnel experiment can be divided into the full bridge aeroelastic model test and the sectional model test.

Full bridge aeroelastic model testing

The full model is a reduced-scale geometric facsimile of the entire prototype bridge that includes all structural elements, the towers, the suspension cables, the road deck, etc. It is very necessary for dynamic studies. [33] The model of the aeroelastic full bridge can simulate the aerodynamic configuration of the real bridge, and the stiffness, mass, damping, frequency and other dynamic characteristics of the structure can also be simulated. The scale ratio for a long-span bridge may be very small; for example, the model of a 3,000 ft. (915 m) long bridge would have to be constructed at a scale ratio of about 1:400 if it were to be tested in an 8 ft. (2.44 m) wide wind tunnel test section. [33]

Sectional model testing

The wind effects of the bridge structure meet the strip theory, approximately. So, the wind-induced reaction of the bridge structure can be studied by the sectional model test. The expression “sectional model” is derived from the aeronautical engineer’s practice, which measures the two-dimensional or sectional properties of airfoils in wind tunnels by using constant section models. [33]

The sectional model is relatively easy to manufacture because it is comprised of elements instead of a full model, so it is low cost and small experimental space is used. In addition, it is easy to simulate the structure with details (e.g., handrail, maintaining roadway and the other accessory structures); rather than the complete bridge model, the aerodynamic

characteristics of the bridge deck can be studied by constructing a model that represents a short, mid-span section of the deck, and one that can be built more quickly and can be quickly modified for examining corrective configuration changes. [33]

Many studies investigated the flutter, buffeting and other wind-induced responses using the wind tunnel experiment.

Yozo Fujino (Y. Fujino, 2002) [34] summarized the preliminary study of girder aerodynamics of Trans-Tokyo Bay Crossing Bridge in Japan using the wind tunnel test. The bridge that the author studied is part of the bridge portion, the total length of which is 4,384 m. This part of the structure is from P3 to P13 in Figure 2.9. The overall length is 1,630 m, and the longest spans are 240 m between piers P6, P7 and P8.

Since the girder has varying depths, two models with different depths were chosen by Yozo Fujino, at points of mid-span (L/2) and L/6 span, which has 6.0 m and 7.63 m girder depth, respectively. At point of span, the centre has the minimum depth and the point at L/6 was selected because response characteristics at this girder depth were thought to be representative.

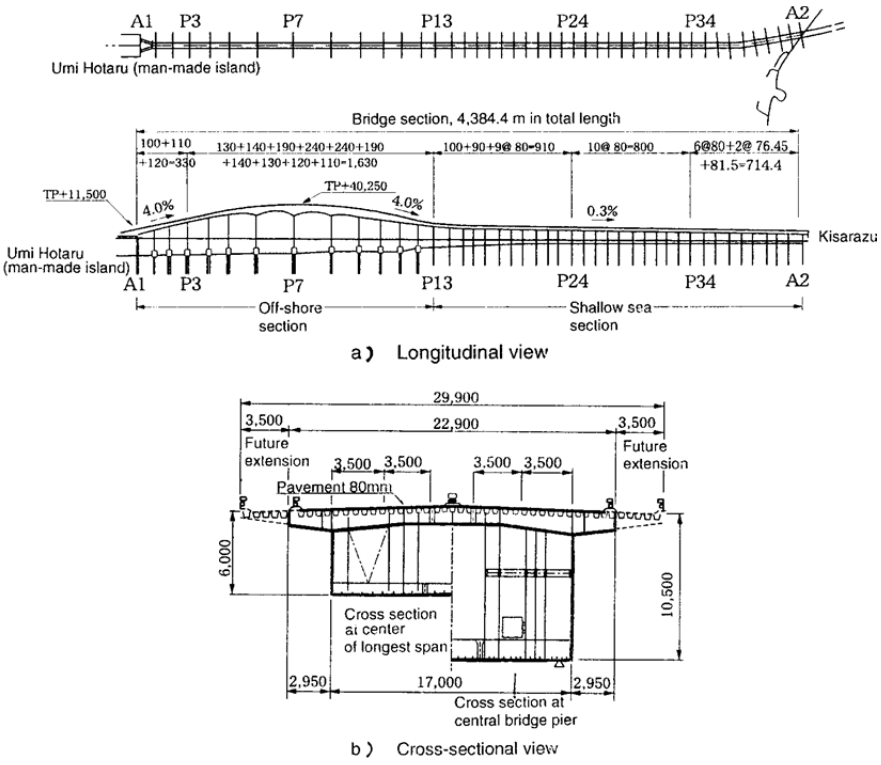

Figure 2.9 (a) (b): Outline of bridge structure for Trans-Tokyo Bay Crossing Bridge. [34]

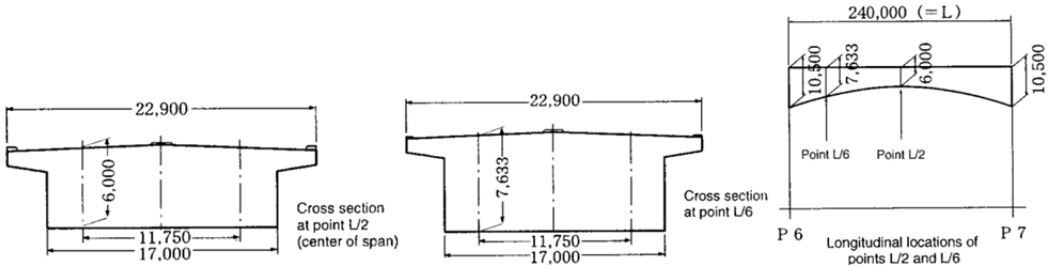

Figure 2.10: Cross sections of partial models used for two-dimensional wind tunnel tests (as-built design). [34]

The wind tunnel tests on the as-built sectional models without aerodynamic measures are summarized below and in Figure 2.11.

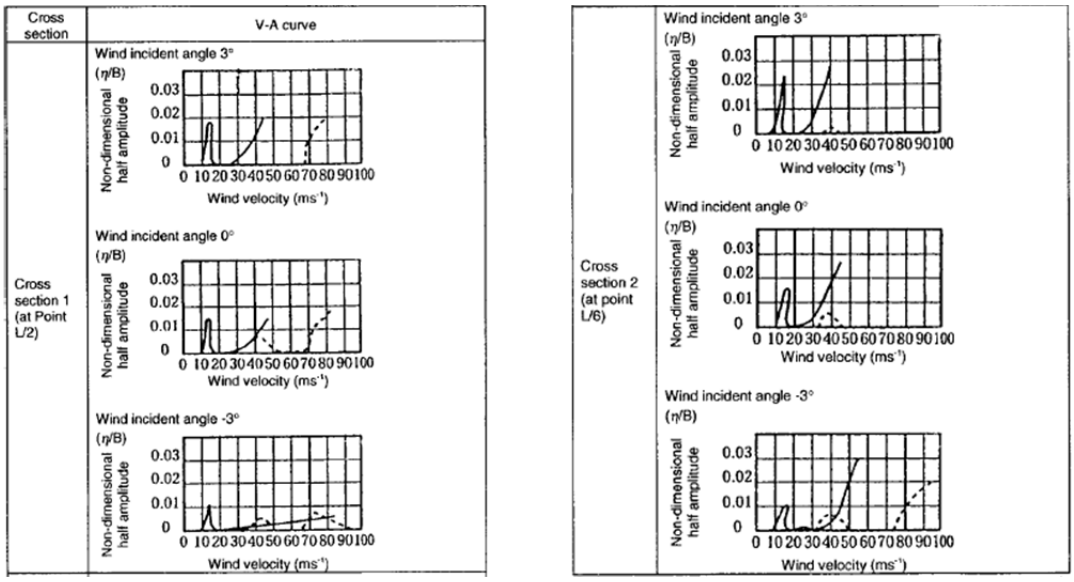

Notes: 1) On a scale of 1:30, as-built design, without aerodynamic control measures. 2) η is the deflection, B is the bridge width (=22.9m). 3) Torsional vibrations are shown in dotted curves.

Figure 2.11: Results of wind tunnel tests on two-dimensional models in uniform flow (Solid curve: Bending; Dotted curve: Torsional). [34]

Some conclusions can be summarized from the experiment:

1. Vortex-induced vibrations began to occur, for both the L/2 and L/6 models, when wind velocity exceeds about 10 m/s with the maximum amplitude measured at V=15~17 m/s.

2. Galloping began to occur gradually at wind velocities higher than about 30 m/s at point L/2, and at wind velocities higher than 25~30 m/s at the L/6 model.

3. Vortex-induced torsional vibrations occurred at V=35~40 m/s at both L/2 and L/6 models.

Thus, vortex-induced vibration and galloping occurred below the design wind velocity of U_d=67.7 m/s. In an attempt to control these vibrations, a series of wind tunnel tests were implemented to verify the effects of the aerodynamic devices such as a fairing, double flaps,

a skirt and their combinations.

2.3.2 Numerical simulation (finite element method)

In bridge structural design, especially long-span bridges, it is a great challenge at every stage: design, construction and completion, because too many complicated conditions have to be considered, like the weather, time, cost and the properties of the structure itself. Among the external factors to be considered, wind load becomes the prime concern for the design of the bridges. In the modern world, with the progress of computer science and technology, the computer modelling of wind-induced effects on a bridge by using the numerical model method is becoming more and more popular. The benefits of computer modelling are as follows:

1. It is not affected by landform, physiognomy and size of structure.

2. It can be set at any value of wind speed and any direction of wind, so the effect of simulation is fairly real.

3. The results of the analysis can be showed directly.

Sutong Bridge is a cable-stayed bridge; the total length of the bridge is 8,206 m and consists of 1,088 m main span and another 6 support spans and side spans arranged on both sides of the bridge symmetrically (100+100+300+1088+300+100+100) m. A side view of the bridge is shown in Figure 2.12. The tower is 306 m in height and connects with the deck by 272 stayed cables. According to weather reports, yearly maximum average wind speeds at the bridge location is $U_{10} = 34 m/s$.

X. Zhu (X. Zhu, 2011) [35] modelled the Sutong cable-stayed bridge, and studied the response of static wind effects and structural dynamic characteristics.

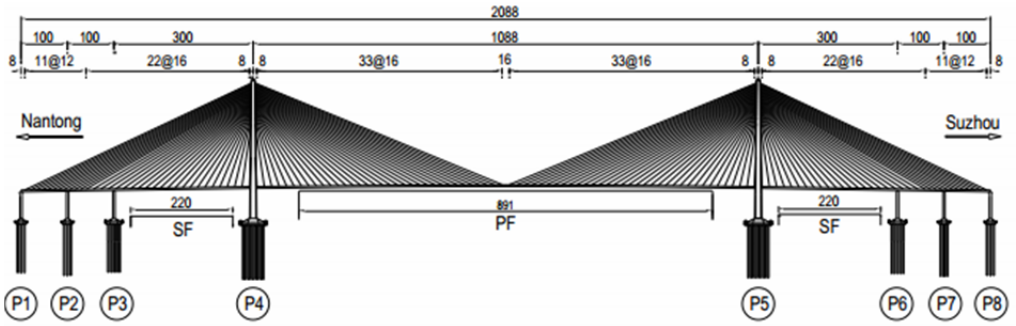

Figure 2.12: Span arrangement of Sutong Bridge (unit: m) [35]

Presently, three different kinds of models of main girder are widely applied: fishy bone model, double-girder model and triple-girder model, respectively.

The fishy bone model applies to the box girder which has a bigger torsional stiffness, and the stiffness and mass of the bridge are concentrated on the node in the middle. This kind of model has good accuracy on stiffness and mass of main girder modelling rather than cross girder. The main girder stiffness and mass will be in equal shear to each girder when using the double-girder model, but have low accuracy on lateral and torsional stiffness. The triple-girder model consists of a centre girder and two side girders; this kind of model has good mechanical behaviour, but also has too many elements in the model that can bring about more calculations.

The finite element model of the Sutong Bridge is shown in Figure 2.13. The bridge is modelled by ANSYS software, and there are 863 nodes and 1,271 elements in total. Three basic types of elements were used for modelling the different structural members: the main girder, towers and piers use BEAM4 elements; and all cables are modelled by LINK10

elements. The connections between cable and tower, cable and girder use a rigid arm connection without any mass. The self-weight of the bridge and other weights are inputted by the density of the girder, and the mass moment of inertia will be modelled by MASS21 elements.

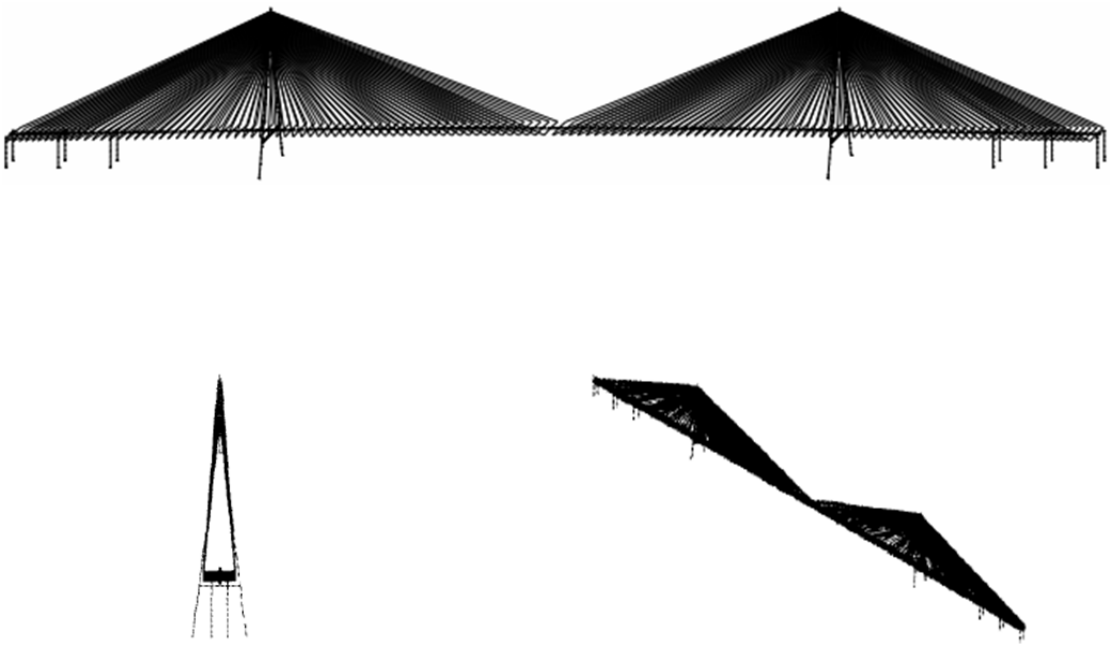

Figure 2.13: Finite element model of Sutong Bridge. [35]

Figure 2.14: shows the displacement variation of the node on the main girder at mid-span along with different wind velocities. From the figure, the relationship between displacement and wind velocity can be observed and change in shape to that of a parabola. That means the motion of the bridge structure in the elastic state has good static wind stability. When wind speed increases to 100 m/s, the angle of the twist becomes 1°, which can have some effects on the stability of the bridge.

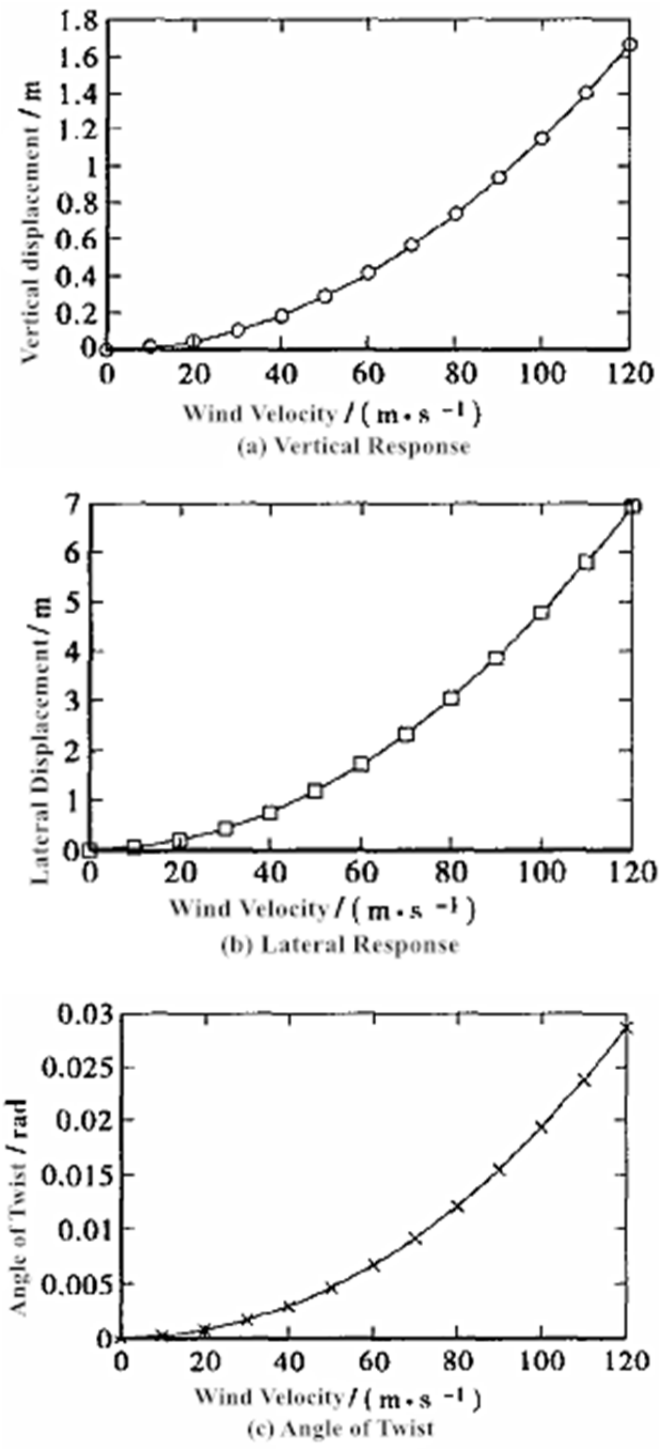

Figure 2.14 (a) (b) (c): Displacement of the node of main girder at mid-span along with the wind speed. [35]

The mode analysis is the base of the earthquake response and wind-induced vibration analyses. Table 2.2 below shows the frequency and mode shape characteristics in the previous 15 modes.

From the table above, the first shape of the vibration mode is a horizontal mode, which is good for anti-seismic.

Table 2.2: Frequency and mode shape characteristics in previous 15 modes. [35]

Mode	Frequency/Hz		Mode shape	Mode	Frequency/Hz		Mode shape
	Completion stage	Static wind effect considered			Completion stage	Static wind effect considered	
1	0.0630	0.0643	H	9	0.4420	0.4413	2nd SH/T
2	0.0970	0.0973	SH	10	0.4458	0.4474	H-tower
3	0.1735	0.1730	SV	11	0.4492	0.4492	H-tower
4	0.2116	0.2120	AV	12	0.4524	0.4563	3rd AV
5	0.2684	0.2694	AH	13	0.4812	0.4809	2nd AH
6	0.2996	0.3016	2nd SV	14	0.4888	0.4890	T
7	0.3610	0.3652	2nd AV	15	0.4892	0.4927	4th SV
8	0.4030	0.4071	3rd SV				

Note: H-Horizontal; V-Vertical; T-Torsional; A-Asymmetry; S-Symmetry.

In addition, a study of static wind response effects on the structural dynamic characteristics has been established. First, make static calculations when the wind speed at the surface of the bridge deck is 100 m/s. On this basis, structural internal forces should also be considered. From the results in Table 2.2, the deformation, displacement and internal force have little effect on the parameters of the structural mode.

For the modelling on stay cables, the non-linear characteristics due to cable sag should be considered. As the cable represents a flexible member with virtually no resistance to applied moments, several simplified methods can be used to account for the cable nonlinearities

associated with the sag. The idea of replacing the cable by a truss member with equivalent cable stiffness has been found to be widely accepted. In 1965, a method reported by Ernst [36] provides a simple and effective way to simulate the equivalent stiffness in the cable. The formula for the equivalent modulus is shown below:

$$E_{eq}^{truss} = \frac{E^{cable}}{1 + \frac{(\rho_c g L_x)^2}{12\sigma^3} \cdot E^{cable}} \qquad (2.17)$$

Where, E_{eq}^{truss} : Equivalent truss element modulus;

E^{cable} : the actual cable modulus;

ρ_c : the cable material density;

g : the acceleration due to gravity;

L_x : the horizontal projected length of the cable;

σ : the cable pre-stress.

Although Ernst's method improves the efficiency of cable modelling work, this procedure is limited to extracting the response of the long-span bridge structure only. The natural frequencies and vibration mode shapes cannot be determined. But that is still a very common method in a long bridge structure when the deck girders are only concentrated.

For the wind load's effect on the bridge, T. H. Odden and H. Skyvulstad (2012) [37] presented a method to simulate the static wind load on the finite element model. The Sogne Suspension Bridge in Norway is selected in their analysis, and ABAQUS software was used

to build the model.

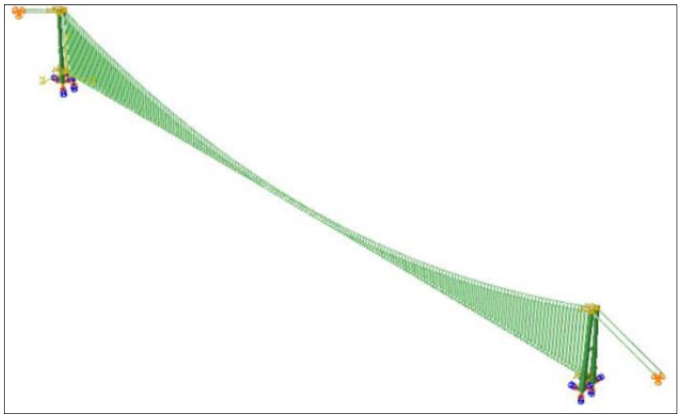

Figure 2.15: ABAQUS model of the Sogne Bridge. [37]

To calculate the static response of the bridge models under the mean wind load, the wind forces are applied to the models in ABAQUS as shown in Figure 2.16. It is assumed that the entire span of the bridge is subjected to the wind load. The drag and lift loads on the girder are applied as concentrated loads to the mass centre of the girder for every 20 m. The bending moment is applied as a concentrated moment in the middle of the girder every 20 m. The drag load on the cables is applied as concentrated forces where the hangers are fixed to the cables. [37]

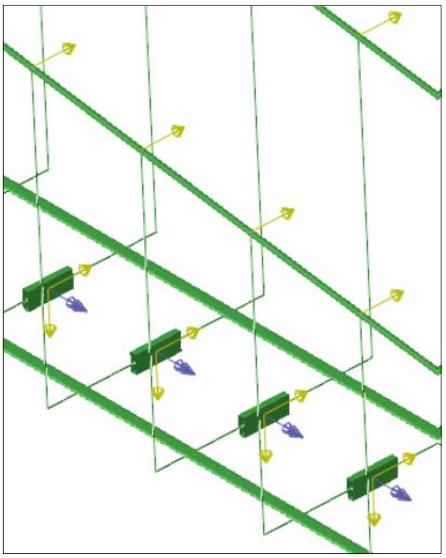

Figure 2.16: Static wind forces applied as concentrated forces in ABAQUS. [37]

The value of the static load applied on the model is calculated according to the mean wind load equation as given in the previous section 2.3.2 (Eq. 2.6). And they found that the variance increases with increasing mean wind speed as expected. Figure 2.17 shows horizontal variance at mid-span with mean wind velocities between 5 and 30 m/s.

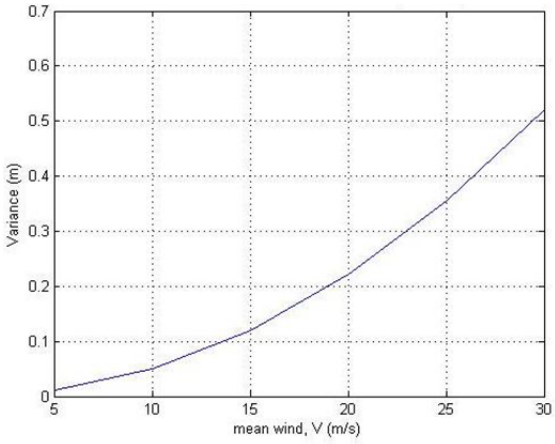

Figure 2.17: Plot of horizontal variance vs. mean wind velocity at mid-span. [37]

The horizontal displacement starts at a very low level and the value changes to about 0.5 m

at 30 m/s mean wind speed. They also mentioned that in wind engineering, the range of wind speed from 0 m/s to 30 m/s is considered a low speed, and vortex shedding usually makes the variances at low mean wind velocities bigger.

Øiseth, et al. [38] did a finite element analysis on the Hardanger Suspension Bridge. The horizontal, vertical and torsional buffeting response at the mid-span of the beam at a mean wind velocity of 40 m/s is shown in Figure 2.18.

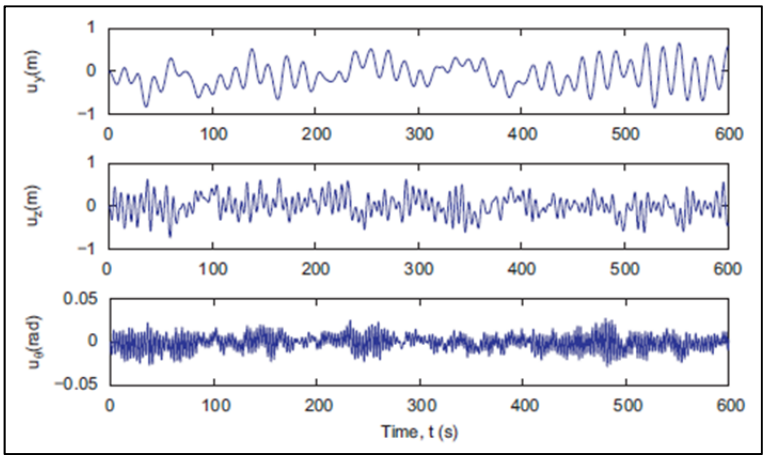

Figure 2.18: Wind-induced dynamic response at the mid-span of the beam. The mean wind velocity is 40 m/s. [38]

As can be seen from the figure, the response is clearly narrow banded but with a significant background.

The spectral densities estimated as the mean value of the spectral density of 20 time series of the horizontal, vertical and torsional response at the mid-span at a mean wind velocity of 40 m/s are shown in Figure 2.19 together with the multi-mode frequency domain results. [38]

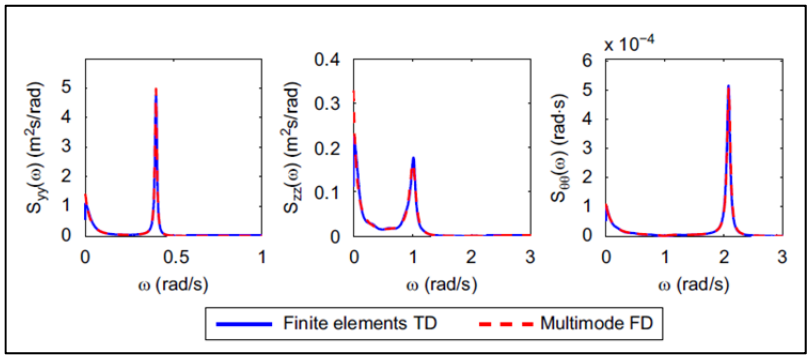

Figure 2.19: Spectral densities of the response components at a mean wind velocity of 40 m/s. [38]

The frequency ranges where the spectral densities are significantly different from zero have been displayed in the figure. As can be seen from the results, the spectral density corresponds very well to the spectral density obtained in the frequency domain in the entire frequency range for all response components. The figure confirms that the response is narrow banded and dominated by one natural frequency in each direction. [38]

Chapter 3 Bridge Finite Element Modelling

3.1 Finite element method

The finite element method (FEM) is a numerical technique for representing and simulating structural systems. The geometry is replaced with a set of elements, consisting of nodes with a finite number of degrees of freedom. These nodes form a grid called the mesh. Certain material and structural properties are assigned to the mesh, which define how the structure will react to certain loading conditions.

The finite element method is widely used in civil engineering, especially in Structure Engineering. The applications of the finite element method include stress analysis, vibration analysis, impact and crash analysis, etc. The finite element method provides a convenient and ideal way to simulate the structure. Complicated structures or complex engineering problems can be simplified using the finite element model, and at the same time, boundary conditions, support conditions and other complicated structure factors can also be considered, which is one of the most important advantages of the finite element method. Furthermore, in some cases, the finite element method could replace some complex experiments in the laboratory, thus the schedule of design will be sped up and development costs will be decreased.

The ABAQUS finite element analysis software was used to analyze the Stonecutters Cable-stayed Bridge. ABAQUS is a finite element modelling program designed for modelling a variety of material behaviour in both static and dynamic situations. The program has an extensive material behaviour library that allows for the use of data obtained from the testing laboratory to be directly inputted into the model definition. The advantage

of ABAQUS is in process optimization, material comparisons and general forming analysis. These can reduce time, effort and costs, and also makes the structural design more efficient and accurate. However, powerful functions need a stronger device for support. After the job is submitted, the computer runs out of memory, especially when modelling a very complicated structure. In addition, ABAQUS is not unit aware, so all dimension calculations must be done outside the software program, and all units of data inputted in the software must remain consistent. The most commonly used SI international system in ABAQUS is shown in Table 3.1.

Table 3.1 System of units in ABAQUS [39]

	Length	Force	Mass	Time	ME	Energy	Density	Acceleration
SI (m)	m	N	Kg	s	Pa	J	Kg/m^3	m/s^2
SI (mm)	mm	N	t	s	MPa	mJ	t/mm^3	mm/s^2

In this thesis and the ABAQUS modelling program, the SI (m) units system is selected to finish all calculations outside the software system and properties definition in modelling.

3.2.1 Scope of the finite element analysis

The main target of using ABAQUS software in this thesis is building a 3D finite element model of the Stonecutters Cable-stayed Bridge. Initially, the bridge model was built to determine the static and dynamic characteristics of the real bridge structure, like vibration mode shape and natural frequency. Secondly, the vibration response of the bridge under both the mean wind load and self-excited aerodynamic load was tested. Here, the powerful functions of ABAQUS are revealed. The post-processing system of the program will provide full detailed information about the bridge under wind load. It is very convenient to collect data from the structure.

The OEC method (one element cable method) will be used in building the main bridge model. In order to achieve the target, the process of modelling work was divided into the following parts.

1. Build the OEC finite element model for the Stonecutters Cable-stayed Bridge.

2. Different analysis steps were created, including static analysis, frequency estimation, mean wind loading test and self-excited loading (flutter) analysis.

3. Run the job and get the results.

3.3 Stonecutters Cable-stayed Bridge FE Model

3.3.1 Overview

The finite element model of Stonecutters Cable-stayed Bridge was developed with three main structural parts, which are the bridge deck and cross girder system, pylons and piers, and stay cable system. Figure 3.1(a)(b)(c) shows an ABAQUS model of the Stonecutters Cable-stayed Bridge.

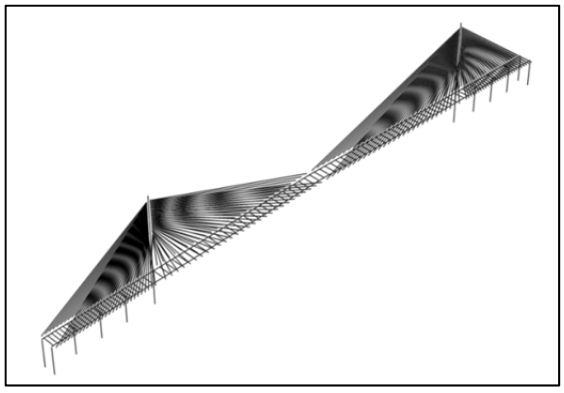

Figure 3.1(a): ABAQUS model of Stonecutters Cable-stayed Bridge, general view.

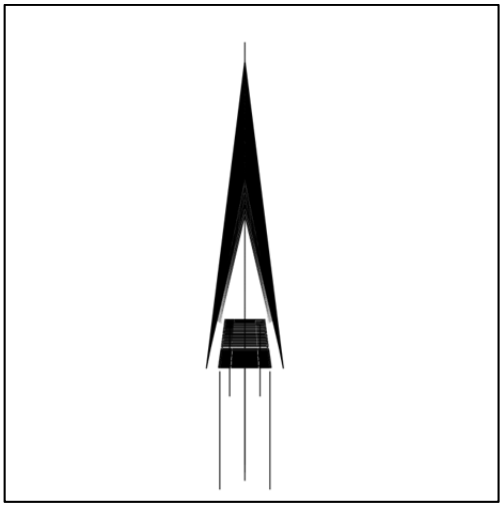

Figure 3.1(b): ABAQUS model of Stonecutters Cable-stayed Bridge, side view.

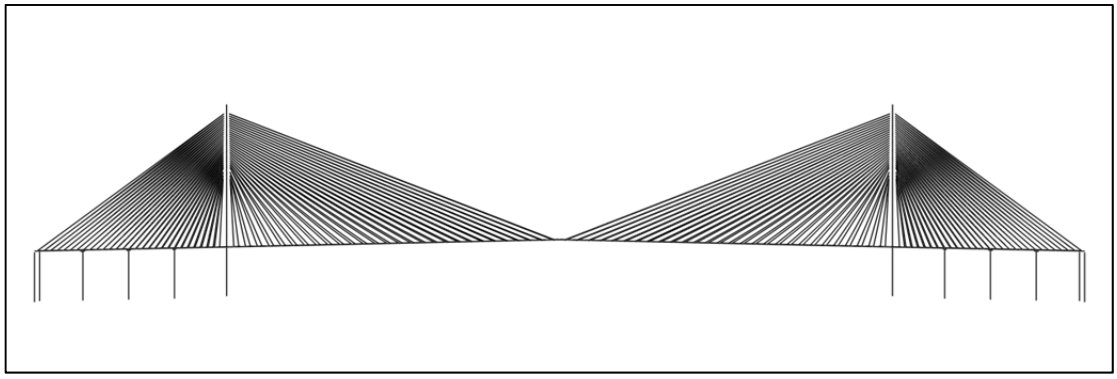

Figure 3.1(c): ABAQUS model of Stonecutters Cable-stayed Bridge, front view.

The geometry of the main bridge components are as follows: the total length of the bridge: 1,596 m; main span: 1,018 m; elevation of the top tower: 298 m; elevation of centreline road at mid-span: 78.3 m; full width of girder: 53.3 m; width of each traffic lane: 15.3 m; cable arrangement at side-span: 10 m interval; cable arrangement at centre-span: 18 m interval.

The overall geometric dimensions described above were preserved in the FE model of the bridge, however, a number of assumptions must be made in terms of the bridge geometry,

such as the mass center, the shear center of the bridge deck, the connections between cable ends and tower, etc, in order to simulate the actual structural resistance and response of the real bridge, but with smaller number of degrees of freedom. These geometric features are directly associated with the structural behaviour. Consideration must include not only the global coordinates of the bridge, but also the local geometric characteristics of every single element. Some section properties and material details are collected from reports and papers on the Stonecutters Cable-stayed Bridge, which have been published by other researchers. But during the initial work on the model, it was found that the data from literature are not sufficient enough. Therefore, some shell models were built to determine additional geometric properties of the bridge's elements. Most of the structural characteristics were used as recommended by Ayman, (2012) [40].

The structure of cable-stayed bridges is related to the geometric nonlinear problem; this kind of nonlinearity is generated by large deflection, interaction between bending moment and axial force, etc., hence, in order to carry all the characteristic parts of the bridge, a different modelling method and element type was selected to meet the requirements. Modelling details will be discussed in the following section.

A cable-stayed bridge is a complicated structural system. Every individual element and member makes a different effort. Therefore, in the Stonecutters Cable-stayed Bridge FE model, three different types of elements were used in the structure: 3D elastic beam elements (B31), 3D truss elements (T3D3) and rigid elements (RB3D2).

3.3.2 Element types

ABAQUS has an extensive element library to provide a powerful set of tools for solving many different engineering problems. Each element in ABAQUS has a unique name, such

as T2D2, S4R, C3D8I or C3D8R, which presents the degree of freedom, numbers of nodes and other definitions of element types. Therefore, in this section, some basic element types of the Stonecutters Cable-stayed Bridge will be introduced.

B31 beam element:

ABAQUS offers a wide range of beam elements, including "Euler-Bernoulli" and "Timoshenko" type beams with solid, thin-walled closed and thin-walled open sections. In this thesis, Timoshenko (B31) beams were used for bridge decks, cross girders, towers and piers. This kind of element is used most in the model.

A B31 beam is an element for stress/displacement analysis with two nodes and six degrees of freedom at each end. ABAQUS assumes the transverse shear behaviour of B31 beams is linear elastic with a fixed modulus, and thus independent of the response of the beam section to axial stretch and bending. For most beam sections, ABAQUS will calculate the transverse shear stiffness values required in the element formulation. But due to an irregular shape of the cross-section-like bridge deck and cross girder in the model, the properties of the section cannot be defined simply in the model. Here, a cross-section profile named "Generalized Profile" was used in these components with complicated cross-section properties.

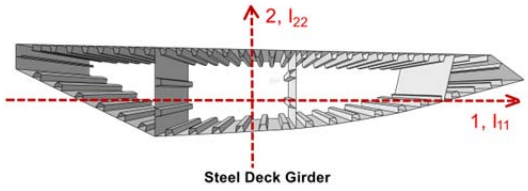

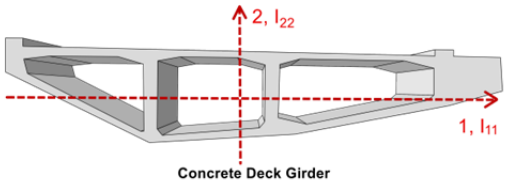

Area (m^2)	1.05	Area (m^2)	19.27
I_{11} (m^4)	1.42	I_{11} (m^4)	20.68
I_{12} (m^4)	3.96	I_{12} (m^4)	60.69
I_{22} (m^4)	31.32	I_{22} (m^4)	609.64
J (m^4)	3.96	J (m^4)	60.69
Warping constant (m^6)	15.78	Warping constant (m^6)	228.87

Figure 3.2: Cross-section profile of deck girder.

The cross-section profiles of the deck girder needed in the "Generalized Profile" setting are summarized in Figure 3.2; ABAQUS allows the user to create a section with certain geometric quantities and material properties.

However, the material properties are still defined through the "Section" module that will include the generalized profile, which has already been created. In addition, it is important to notice that sections can still have a linear or nonlinear response with a "Generalized Profile." "Generalized" nonlinear section behaviour can be defined by specifying the area, A; moments of inertia, I_{11} for bending about the 1-axis of the section, I_{22} for bending about the 2-axis of the section and I_{12} for cross-bending; and torsional rigidity, J. These values are used only to calculate the transverse shear stiffness; and if needed, the area is used to compute the mass density of the element [39]. Hence, the B31 beam element with a "Generalized Profile" has good behaviour on extracting the linear and nonlinear response of the structure.

T3D3 truss element:

Truss elements are used in two and three dimensions to model slender, line-like structures that support loading only along the axis or the centreline of the element. No moments or forces perpendicular to the centreline are supported.

The T3D3 truss element, which is a three-node element, was used primarily for modelling the stay cables. The three-node truss element available in ABAQUS/Standard is often useful for modelling curved reinforcing cables in structures, such as pre-stressed tendons in reinforced concrete or long slender pipelines used in the offshore industry. [39] Truss elements have no initial stiffness to resist loading perpendicular to their axis, hence, the truss element can transmit axial load only. If a stress-free line of trusses is loaded perpendicular to its axis in ABAQUS/Standard, numerical singularities and lack of convergence can result. After the first iteration in a large-displacement implicit analysis, stiffness perpendicular to the initial line of the elements develops, sometimes allowing an analysis to overcome numerical problems. In some cases, loading the truss elements along their axis first or including initial tensile stress can overcome these numerical singularities. [39]

RB3D2 rigid element:

The RB3D2 element is a two-node rigid beam that can simulate the very stiff members of the structure. Rigid elements are often used in ABAQUS/Standard analysis. They can also be used as rigid links between nodes on deformable bodies. In the Stonecutters Cable-stayed Bridge, because the bridge deck has an irregular and complicated cross-section, the shear centre and mass centre of the deck are not in the same position as shown in Figure 3.3 and Figure 3.4.

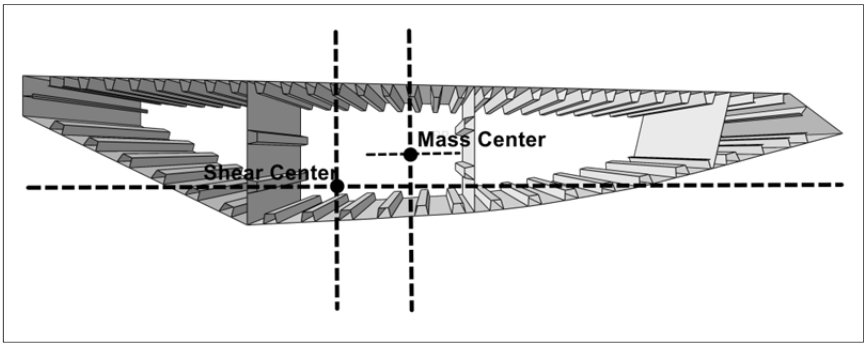

Figure 3.3: Cross-section of steel deck shell model.

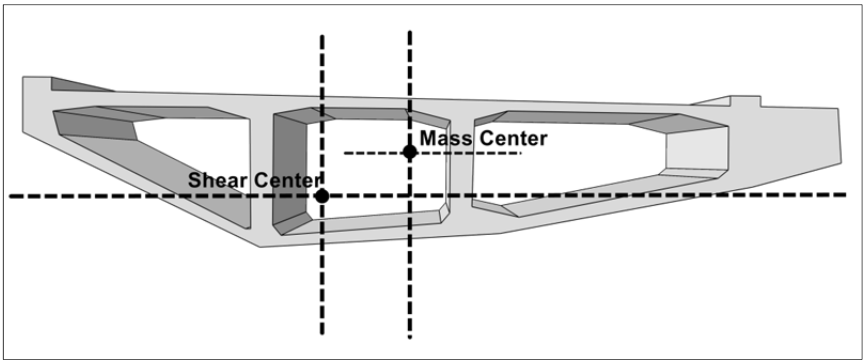

Figure 3.4: Cross-section of concrete deck shell model.

Therefore, in the model, the RB3D2 rigid elements are used to define the rigid connector that connects the mass and shear centre of the deck girder. Figure 3.5 shows the arrangement of RB3D2 between the shear centre and mass centre of the bridge deck.

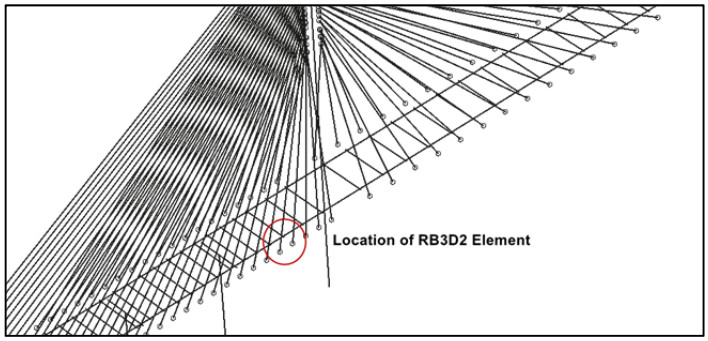

Figure 3.5 (a): Arrangement of RB3D2 between shear centre and mass centre of bridge deck.

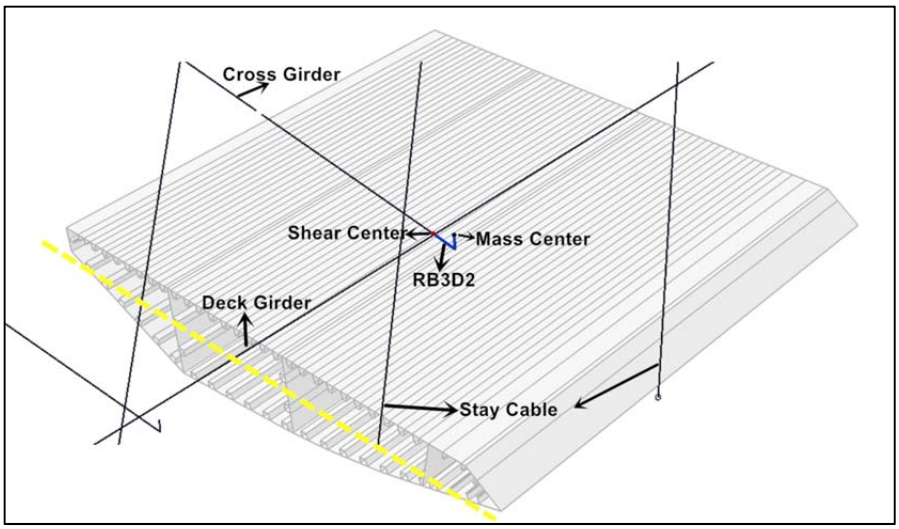

Figure 3.5 (b): Arrangement of RB3D2 between shear centre and mass centre of bridge deck.

The main advantage of rigid elements is high-efficiency calculations. The motion of the rigid body element is completely presented by six degrees of freedom at the reference point, and the properties must be assigned when creating a rigid element.

MPC beam constraints:

In ABAQUS, constraints are not the same as connections; rather, constraints partially or fully eliminate degrees of freedom of a group of nodes and couple their motion to the motion of a master node (or nodes). The MPC type beam provides a rigid beam between two nodes to constrain the displacement and rotation at the first node to the displacement and rotation at the second node, corresponding to the presence of a rigid beam between the two nodes. In other words, in an MPC beam, slave nodes will follow the movements of the degree of freedom of master nodes. Therefore, in the Stonecutters Cable-stayed Bridge model, the MPC beam has a very good effect when replacing the complicated anchor box structure in the upper tower and edge of the bridge deck. It is a very good connector

between the cables and deck-tower system.

Due to the cable sets anchored to the upper tower's section, the MPC beam was chosen to be the connection between the stay cables and tower.

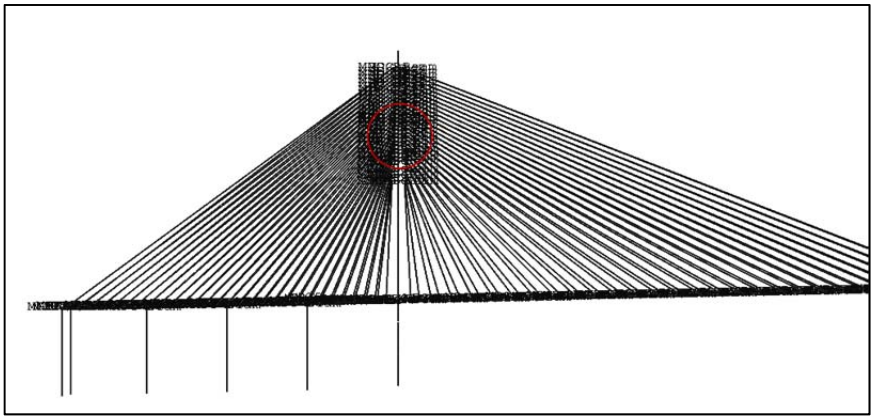

Figure 3.6: Arrangement of stay cable.

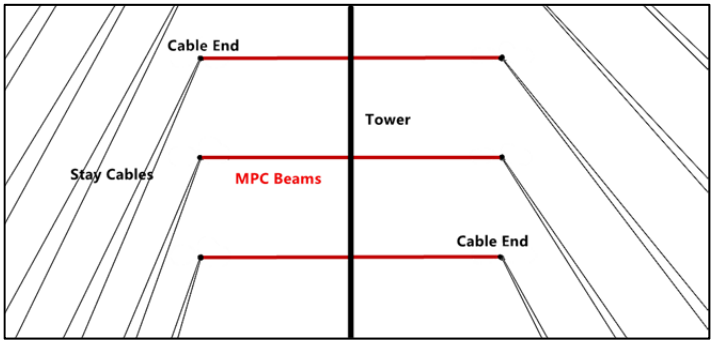

Figure 3.7: MPC (Multiple Point Constraints) beam between cables and tower.

As shown above in Figure 3.6 and Figure 3.7, the locations of all cable ends actually formed the surface of the concrete tower. Moreover, stay cables are connected directly to the tower centre.

For the other side of the stay cables, the cables should anchor to the deck in the real bridge.

In the FE Model, MPC beams were used to traverse the longitudinal axis deck span from the spine element to the cable locations. Then, the real offset of the cables of the bridge relative to the spine will be represented. Finally, the cables are connected to the outer edges of the MPC beam as shown in Figure 3.8.

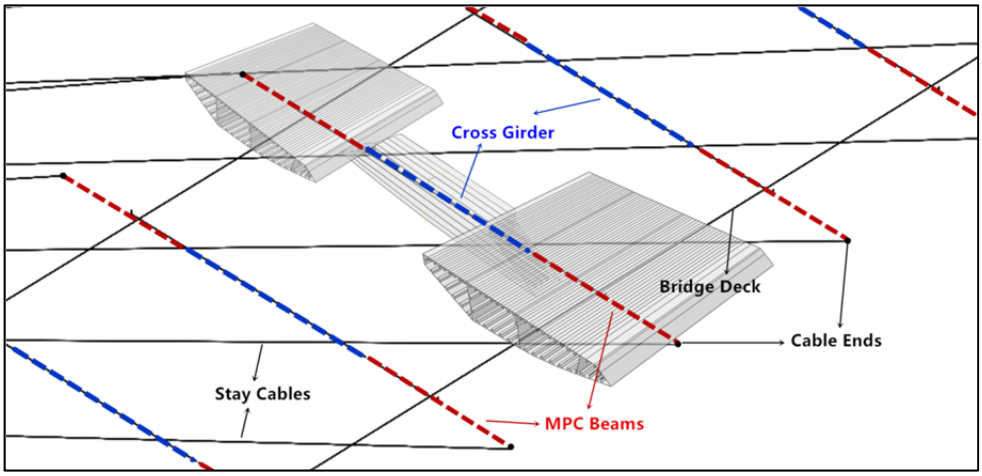

Figure 3.8: MPC (Multiple Point Constraints) beam between cables and bridge deck.

The advantages of this arrangement are discussed below:

Stay cables have an accurate response coupled with bridge towers and decks. The vibration responses of the cable ends will follow the movement of the tower and bridge deck. Otherwise, the pre-tension load applied on the cables will be delivered directly to the main structure.

MPC beams simplify the complicated connections between stay cables and the main bridge structure. It can greatly improve the efficiency of the simulation with the same accuracy.

3.3.3 Material and geometric properties

The basic materials used in the Stonecutters Cable-stayed Bridge are structural steel, reinforced concrete and high-strength steel (steel grade S420 M/ML). The material properties used in the finite element model are shown in Table 3.2.

Table 3.2: Material properties in finite element model.

Material	**Members**	**Mass Density** (kg/m^3)	**Young's Modulus** (GPa)	**Poisson's Ratio**
Reinforced Concrete	Towers, Piers, Back-span, Side Cross Girders	2400	60	0.2
Steel/S420	Centre Deck, Cross Girders	7850	205	0.3
Cable Steel	Stay Cables	7800	200	0.28

As mentioned above, some section properties and material details were collected from reports and papers on the Stonecutters Cable-stayed Bridge that have been published by other researchers. But during the initial work on the model, it was found that these data from literature are not sufficient enough. Therefore, some shell models were built to determine additional geometric properties of the bridge elements. All these important mass and geometric properties are summarized in Table 3.3, Table 3.4, Table 3.5 and Table 3.6.

Table 3.3: Mass properties of the Stonecutters Bridge steel deck cross-section.

Moments of Inertia about the Mass Centre ($kg \cdot m^2$)	I_{xx}	5.81 e+006
	I_{yy}	1.16 e+007
	I_{zz}	6.32 e+006
	I_{xy}	3.59 e+004
	I_{yz}	-0.114
	I_{zx}	1.51
Other	Total Mass (kg)	204883.28
	Mass Centre (m)	16.73, -1.46, 9.00

Table 3.4: Mass properties of the Stonecutters Bridge concrete deck cross-section.

Moments of Inertia about the Mass Centre ($kg \cdot m^2$)	I_{xx}	3.891 e+006
	I_{yy}	1.16 e+007
	I_{zz}	1.36 e+006
	I_{xy}	-1.46 e+004
	I_{yz}	0
	I_{zx}	-7.45 e-009
Other	Total Mass (kg)	412241.13
	Mass Centre (m)	-26.75, -3.20, 5.00

Table 3.5: Geometric properties of the Stonecutters Bridge steel deck cross-section.

Stonecutter's Steel deck geometric properties	
Cross-Sectional Area (m^2)	1.05
Moment of Inertia about Centroid AL X-axis (m^4)	1.42
Moment of Inertia about Centroid AL Y-axis (m^4)	31.32
Torsional Moment of Inertia (St. Venant) (m^4)	3.96
Warping Constant (m^6)	15.78

Table 3.6: Geometric properties of the Stonecutters Bridge concrete deck cross-section.

Stonecutter's Concrete deck geometric properties	
Cross-Sectional Area (m^2)	19.27
Moment of Inertia about Centroid AL X-axis (m^4)	20.68
Moment of Inertia about Centroid AL Y-axis (m^4)	609.64
Torsional Moment of Inertia (St. Venant) (m^4)	60.69
Warping Constant (m^6)	N/A

It is important to note that the warping constant of the concrete deck was not used in the modelling because it has a closed cross-section and is considered very well stiffened.

The Stonecutters Bridge cables are composed of 7-mm galvanized wires with the largest cable having a total of 451 wires. [41] Each of the cables is required to sustain at least half of an 18-metre length deck segment. The configuration properties are summarized in the Appendix A (Fig. A1), which includes the length, inclination angle, area of section, etc.

After the calculation using Ernst's equation as mentioned earlier in Section 2.3.2 (Eq. 2.17), the equivalent modulus and pre-tension forces in the cable truss are also summarized in the Appendix A (Fig. A2).

3.3.4 Boundary conditions

The boundary conditions (BC) of the bridge piers and towers are usually considered as fixed supports in the analysis models (Hu et al., 2006) [42]. In the present analysis, two towers, six piers and four side-piers at the ground were all considered fixed conditions. Here, a fixed condition means no translational and no rotational motions in all directions.

Due to the concrete back-span on both sides of the bridge, the same boundary conditions as towers and piers were selected.

The boundary conditions used in the FE model are as shown in Figure 3.9.

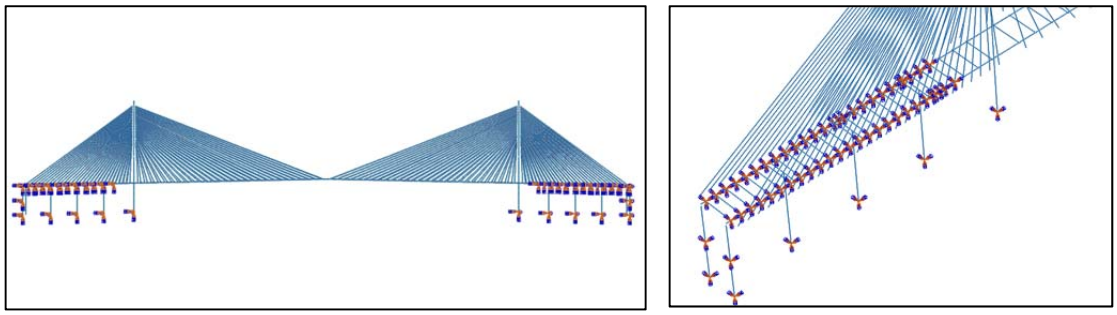

Figure 3.9: Boundary conditions of Stonecutters Cable-stayed Bridge model.

It should be noted that the reason for employing fixed boundary conditions for both the displacement and the rotation at side-span are as follows:

Figure 3.10: Concrete back-span and piers of Stonecutters Cable-stayed Bridge. [43]

Firstly, in this thesis, studies are more concentrated on the response of the steel deck girder, which crosses the sea channel in the middle.

Secondly, the two back-spans are located at the ground of Tsing Yi Island and Stonecutters Island; the ends of the bridge extend to the highway on both sides. Then, very solid foundations are provided for the bridge piers. On the other hand, the interval of the cable ends and concrete cross girders is more intensive than the steel span. Hence, they have a very small response in terms of being affected by wind load and can be ignored.

In addition, the reinforced concrete was used for the material of the back-span, which can provide stiffer properties than steel.

3.3.5 Analysis steps

For the analysis, the model was run in various stages. The stages are as follows:

1. Initial step with constraints, boundary conditions and pre-tension forces in cables.

2. Dead load of bridge defined in general static analysis.

3. Eigen-frequency and mode-shape analysis.

4. Static response of the bridge model due to the mean wind velocity.

5. Flutter response of the bridge model due to the self-excited dynamic loading.

All ABAQUS analysis steps automatically include an initial step where initial conditions can be defined. In the Stonecutters Bridge FE model, the pre-tension forces of the cables were defined through the initial conditions keyword in the input file, which is a code file auto-created when the model is running. Each cable was assigned an initial pre-tension force (Table A2 in Appendix A), and the deck was positioned and restrained in its equilibrium configuration.

Dead loads play an important role in the final stiffness of the bridge (and thus a major role in the final natural frequency and vibration modes of the bridge). To include the geometric stiffness when calculating the natural frequencies of the bridge, the first step accounts for the self-weight of the structure. Non-linear geometry is switched on in this step. In ABAQUS, a static analysis step named “Static, General” is used as the first step. To include the self-weight of the bridge, a “gravity load” must be defined in the general static step with a 9.81 m/s^2 acceleration value as the load component. In addition, the pre-tension forces are defined for every individual cable in the first analysis step.

The frequencies of the Eigen modes of a cable-stayed bridge are important when the dynamic response is studied. Therefore, in the second step, the first 30 natural frequencies and the corresponding vibration modes are calculated. The subspace method was used in the frequency analysis. The advantage of the subspace method is in its ability to achieve rapid

convergence to the eigenvectors in full space.

To calculate the static and dynamic response of the bridge models due to the mean wind loading and self-excited loading, General Dynamic and Modal Dynamic analysis steps in ABAQUS were used. In the model, the mean wind forces and self-excited forces were applied to the bridge directly. It was assumed that the entire span of the bridge is subjected to the wind load.

3.4 Eigen-frequency and mode-shape analysis

3.4.1: Structure eigenvalues extraction

In the mathematical field, the motion equation of a free vibration body is actually the Eigen-equation. The eigenvalues can be determined from the Eigen-equation, which can represent natural frequencies and vibration modes. Therefore, the eigenvalues extraction plays a very important role in vibration problems.

The eigenvalue is based on an un-damped free vibration system, which is a system without affection by damping. Hence, in the motion equation, the term with damping can be ignored.

$$M\ddot{X} + KX = 0 \qquad (3.1)$$

The eigenvalues and vibration modes of the structure represent the vibration characteristics and frequency features under free vibration situations. Often, in general practical problems, a conclusion can be made after the first several vibration modes are considered. But the dynamics of structures always come with a broader set of problems. Due to the complicated

finite element model with hundreds of degrees of freedom, dozens of vibration modes or more should be considered to finish the analysis. For different demands, ABAQUS provides several methods to solve the problem: the Lanczos method, Subspace method and AMS method.

3.4.2 Frequency step in ABAQUS

After the initial step and general static analysis with self-weight, the frequency analysis can be run as the eigenvalue extractor. In the frequency analysis, the subspace method was used. The advantage of the subspace method is in its ability to achieve rapid convergence to the eigenvectors in full space.

For the subspace iteration procedure, specifying the number of eigenvalues required is the only thing needed; ABAQUS/Standard chooses a suitable number of vectors for the iteration. If the subspace iteration technique is requested, the maximum frequency of interest can also be specified; ABAQUS/Standard extracts eigenvalues until either the requested number of eigenvalues has been extracted or the last frequency extracted exceeds the maximum frequency of interest. [39]

During the analysis, 30 eigenvalues were requested. In bridge engineering, the natural frequency and vibration mode are very important for dynamic analysis, especially the first ten modes, which will include the lateral vibration, vertical vibration, torsional vibration and some coupled vibration modes. For the Stonecutters Cable-stayed Bridge in the thesis, the first 30 vibration modes and natural frequencies are enough for the following mean wind load analysis and flutter analysis.

3.5 Static wind load analysis

For the static wind load analysis, and to calculate the static response of the bridge models due to the mean wind velocity, the wind forces were applied to the bridge decks in ABAQUS directly.

3.5.1 Mean wind load

The static wind load is calculated from the mean wind speed acting on the structure. This load consists of three components, which are given in Section 2.3.2, (Eq. 2.6):

$$D_m = \frac{1}{2}\rho \bar{U}^2 C_D BL(\alpha);$$

$$L_m = \frac{1}{2}\rho \bar{U}^2 C_L BL(\alpha); \qquad (3.2)$$

$$M_m = \frac{1}{2}\rho \bar{U}^2 C_M B^2 L(\alpha).$$

Some property coefficients of the Stonecutters Cable-stayed Bridge used in this thesis are summarized in Table 3.7 as follows:

Table 3.7: Property factors in the mean wind load equations.

Air Density ρ (kg/m^3)	1.29
Wind Velocity $\bar{U}$ (m/s)	Specific values from 35 to 211
Bridge Deck Width B (m)	53.3
Bridge Length L (m)	1596
Attack Angle α (deg.)	0

It should be mentioned that the range of the wind velocity chosen depends on the data that

have been published. As mentioned in the previous chapter, some coefficients are typically found in wind tunnel experiments, and they are selected to finish the calculation. Hence, in order to better complete the analysis, some specific values for wind velocity were used in the calculation. They are 35 m/s, 70 m/s, 105 m/s, 141 m/s, 176 m/s and 211 m/s.

Due to the wind force coefficients, the data reported by Michael C. H. Hui (M. C. H. Hui, 2013) [44] was used in the mean wind load calculation. The drag, lift and moment coefficients are summarized in Table 3.8. The unit of the rate of change of the force coefficient is per radian.

Table 3.8: Wind force coefficients for the deck of Stonecutters Bridge. [44]

Angle (deg.)	C_D	C_L	C_M	C_D'	C_L'	C_M'
-5	0.083	-0.29	-0.049	-0.322	2.123	0.575
-3	0.074	-0.212	-0.029	-0.179	2.317	0.558
0	0.07	-0.155	-0.018	0.0688	2.5097	0.5386
3	0.073	0.021	0.029	0.13	1.884	0.556
5	0.079	0.079	0.048	-0.192	1.401	0.572

Based on the given conditions, coefficients and factors, the mean wind load in three different directions can be determined using mean wind load equations. The results vary with specific wind velocities and are summarized in Table 3.9.

Table 3.9: Mean wind loads with wind velocity.

Load / Wind Velocity (m/s)	D_m / total (KN)	D_m / node (KN)	L_m / total (KN)	L_m / node (KN)	M_m / total ($KN{\cdot}m$)	M_m / node ($KN{\cdot}m$)
35	2390.9	43.5	-5294.1	-96.3	-32768.8	-595.8
70	9563.5	173.9	-21176.4	-385.0	-131075.0	-2383.2
105	21517.9	391.2	-47646.9	-866.3	-294918.8	-5362.2
141	38254.1	695.5	-84705.6	-1540.1	-524300.1	-9532.7
176	59772.1	1086.8	-132352.4	-2406.4	-819218.8	-14894.9
211	86071.7	1564.9	-190587.5	-3465.2	-1179675.1	-21448.6

3.5.2 Mean wind loads in ABAQUS

As shown in Figure 3.11 and Figure 3.12, when the mean wind loading comes to the finite element model, the drag and lift loads on the girder are applied as concentrated forces to the node at mass centre of the steel girder and concrete girder for every 10 m and 18 m. For the models with two box girders, the loads are applied on both sides in order to have symmetry. The torsional moment load is also applied as a concentrated moment at the mass centre.

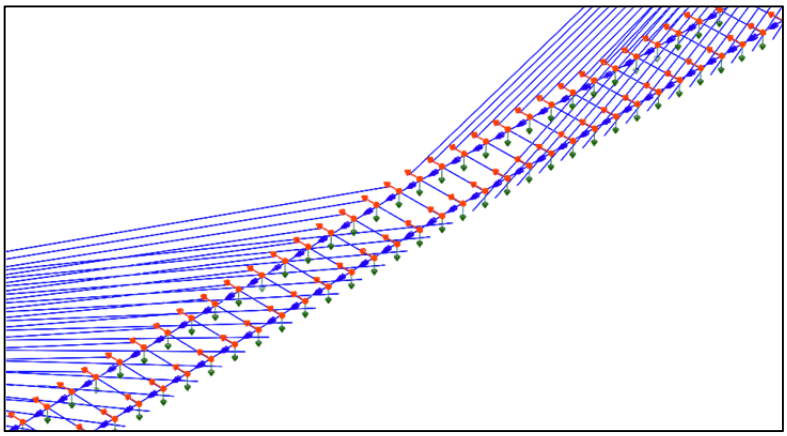

Figure 3.11: Static wind forces applied to the model in ABAQUS.

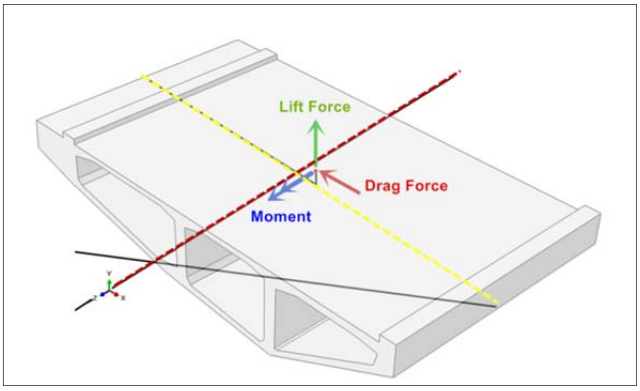

Figure 3.12: Static wind forces applied as concentrated forces in ABAQUS.

3.5.3 Dynamic, Implicit analysis step

When doing research for some responses to nonlinear problems, the motion equations must be solved by the direct integration method. In the ABAQUS/Standard program, an implicit analysis system was activated to accomplish the series of tasks. In the running procedure, the dynamic equilibrium equation with mass, damping and stiffness matrix was created for every individual node.

In this thesis, the "Dynamic, Implicit" analysis step in ABAQUS was created for static wind load analysis. The direct-integration dynamic procedure provided in ABAQUS/Standard uses the implicit operator for integration of the equations of motion. Implicit uses Newton-Raphson iterations to enforce equilibrium. The implicit procedure is effective when the analysis can be performed in relatively few time (load) increments. In an implicit dynamic analysis, the integration operator matrix must be inverted and a set of nonlinear equilibrium equations must be solved at each time increment. This type of analysis tends to be more accurate and can take somewhat bigger increment steps.

In the static wind load analysis, the vibration response at the mid-span of the bridge is

studied, which includes the horizontal, vertical displacement and torsional angle. The total time domain of the bridge under the mean wind load is set to 60 seconds, and the increment size depends on the complexity of the problem. The more complex the problem, the smaller the time increment. Through uninterrupted attempts and calculations, every case studied has a different suitable time increment size. For instance, the increment size for a bridge at 105 m/s mean wind loads is 0.1 s, which means there will be 10 data outputs per second.

It is should be mentioned that it is important to select a suitable time increment size for the analysis. On the one hand, the value of the time increment is too big to converge and finish the analysis. On the other hand, if the increment size is too small, that can increase the time cost of the calculation in ABAQUS software. Hence, after several repeated attempts, the sizes of the time increments for different mean wind load are summarized in Table 3.10 as follows:

Table 3.10: Sizes of time increment for different mean wind loads.

Wind Velocity (m/s)	Time Increment Size (s)	Time Domain (s)
35	0.1	60
70	0.1	60
105	0.1	60
141	0.05	60
176	0.05	60
211	0.05	60

After the cases are completed, the response of the bridge along with three different directions can be obtained from ABAQUS. ABAQUS has a very strong post-processing program for users to collect the data, plot X-Y figure and generate the animation of the structure's motion and deflection. ABAQUS can also generate a result file named "OBD" automatically for users to check the analysis results directly.

In this thesis, the data associated with the vibration response at mid-span were collected, which includes horizontal, vertical displacement and torsional angle. These data are used for extracting the static characteristics of the bridge under the mean wind load; in addition, they are also used for further flutter analysis. Besides the vibration response at mid-span, the deformation of the entire bridge and other relevant data were also collected.

3.5 Flutter analysis

To calculate the dynamic response of the bridge models due to self-excited loading, the "Modal Dynamic" analysis steps in ABAQUS were used. In the model, the self-excited forces were applied to the bridge deck directly.

3.5.1 Self-excited wind loads

The flutter dynamic wind load is calculated from the self-excited load equations. The self-excited vertical and lateral forces and self-excited moment acting on the bridge deck per unit length are expressed in terms of Scanlan's format as given in Section 2.3.3, (Eq. 2.14).

$$L_{se}(t) = \frac{1}{2}\rho\bar{U}^2(2B)\left(KH_1^*\frac{\dot{h}}{\bar{U}} + KH_2^*\frac{B\dot{\alpha}}{\bar{U}} + K^2H_3^*\alpha + K^2H_4^*\frac{h}{B} + KH_5^*\frac{\dot{p}}{\bar{U}} + K^2H_6^*\frac{p}{B}\right);$$

$$D_{se}(t) = \frac{1}{2}\rho\bar{U}^2(2B)\left(KP_1^*\frac{\dot{p}}{\bar{U}} + KP_2^*\frac{B\dot{\alpha}}{\bar{U}} + K^2P_3^*\alpha + K^2P_4^*\frac{p}{B} + KP_5^*\frac{\dot{h}}{\bar{U}} + K^2P_6^*\frac{h}{B}\right); \quad (3.3)$$

$$M_{se}(t) = \frac{1}{2}\rho\bar{U}^2(2B^2)\left(KA_1^*\frac{\dot{h}}{\bar{U}} + KA_2^*\frac{B\dot{\alpha}}{\bar{U}} + K^2A_3^*\alpha + K^2A_4^*\frac{h}{B} + KA_5^*\frac{\dot{p}}{\bar{U}} + K^2A_6^*\frac{p}{B}\right).$$

Due to the values of some basic property coefficients, air density, wind velocity, bridge width and length are the same as the value given in Table 3.7. In fact, these factors are constant because they are properties of the structure and environment.

For the most important coefficients, namely the non-dimensional flutter derivatives, H_i^*, A_i^* $(i = 1 \sim 4)$ in flutter analysis, the data for the Stonecutters Cable-stayed Bridge published by Michael C. H. Hui (Hui, 2013) [44] were used in the self-excited loads calculation in this thesis. The flutter derivatives of the Stonecutters Bridge deck without traffic were obtained from the section model tests in a wind tunnel. Only the flutter derivatives H_i^* and A_i^* $(i = 1 \sim 4)$ are available, and they are listed in Table 3.11 and plotted in Figure 3.13.

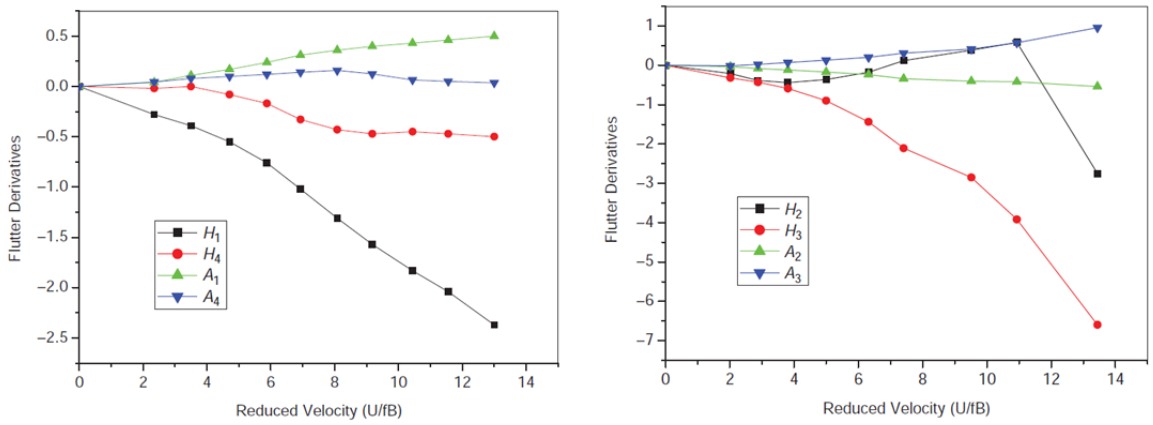

Figure 3.13: Flutter derivatives H_i^* and A_i^* $(i = 1 \sim 4)$ of Stonecutters Bridge deck without traffic. [44]

Table 3.11: Flutter derivatives for Stonecutters Bridge. [44]

U/fB	H_1^*	H_2^*	H_3^*	H_4^*	A_1^*	A_2^*	A_3^*	A_4^*
0	0.00	0.00	0.00	0.00	0.00	0.00	0.00	0.00
2	−0.41	−0.10	−0.21	0.37	0.12	−0.13	−0.02	0.01
4	−0.57	−0.10	−0.34	0.63	0.35	−0.22	0.10	0.16
6	−0.88	0.00	−0.83	0.40	0.51	−0.28	0.23	0.13
8	−1.33	0.17	−1.59	0.48	0.57	−0.37	0.41	0.06
10	−1.54	0.05	−2.89	0.65	0.72	−0.50	0.61	0.01
12	−2.17	−0.16	−4.13	−0.36	0.64	−0.61	0.96	−0.10
14	−1.84	−0.06	−4.55	1.16	0.92	−0.54	1.26	0.01
16	−2.46	0.09	−6.24	0.82	1.38	−0.75	1.24	0.21

As mentioned in the previous chapter, the flutter derivatives related to the lateral motion of the bridge deck P_i^* $(i = 1 \sim 6)$ and the flutter derivatives H_5^*, H_6^*, A_5^* and A_6^* are not available from the wind tunnel experiment; rather, they are calculated based on the quasi-steady theory in terms of the aerodynamic coefficients as given in Section 2.3.3, (Eq. 2.16). The aerodynamic parameters and the flutter derivatives mentioned above are assumed to be uniform along the bridge deck in the study.

$$P_1^* = -\frac{1}{K}C_D,\quad P_2^* = -\frac{1}{2K}C_D',\quad P_3^* = -\frac{1}{2K^2}C_D'$$

$$P_5^* = -\frac{1}{2K}C_D',\quad H_5^* = \frac{1}{K}C_L,\quad A_5^* = -\frac{1}{K}C_M$$

$$P_4^* = P_6^* = H_6^* = A_6^* = 0 \quad (3.4)$$

These additional values of flutter derivatives are summarized in Table 3.12 as follows.

Based on the variation of the vertical, lateral and torsional displacements of the bridge deck (h, p, α) their partial differentiation with respect to time t is determined ($\dot{h}$, $\dot{p}$, $\dot{\alpha}$) and these are used in the self-excited equations. The h, p, α data are obtained from the results of the

analysis under the mean wind load. After the static wind load analysis from the previous section, the response data of the bridge can be obtained from the ABAQUS results file.

Table 3.12: Flutter derivatives for Stonecutters Bridge. [44]

U/fB	H_5^*	H_6^*	A_5^*	A_6^*	P_1^*
0.00	0.00	0.00	0.00	0.00	0.00
2.00	-0.12	0.00	0.01	0.00	-0.05
4.00	-0.23	0.00	0.03	0.00	-0.10
6.00	-0.35	0.00	0.04	0.00	-0.16
8.00	-0.46	0.00	0.05	0.00	-0.21
10.00	-0.58	0.00	0.07	0.00	-0.26
12.00	-0.69	0.00	0.08	0.00	-0.31
14.00	-0.81	0.00	0.09	0.00	-0.36
16.00	-0.92	0.00	0.11	0.00	-0.42
U/fB	P_2^*	P_3^*	P_4^*	P_5^*	P_6^*
0.00	0.00	0.00	0.00	0.00	0.00
2.00	-0.01	0.02	0.00	0.03	0.00
4.00	-0.01	0.08	0.00	0.05	0.00
6.00	-0.02	0.17	0.00	0.08	0.00
8.00	-0.03	0.30	0.00	0.10	0.00
10.00	-0.03	0.47	0.00	0.13	0.00
12.00	-0.04	0.68	0.00	0.15	0.00
14.00	-0.04	0.93	0.00	0.18	0.00
16.00	-0.05	1.21	0.00	0.20	0.00

The time domain is created under the mean wind load analysis, and different time increment sizes are used during the calculation. Hence, the responses obtained from the static wind load analysis are a series of values that vary with time. For instance, the total time domain under the 35 m/s mean wind load is 60 seconds, and the size of increment is 0.1 seconds. So, the number of values from the response is 600 in total.

After substituting all the data and coefficients into the self-excited formulas created by Scanlan, the dynamic loads under different wind velocities can be obtained.

3.5.2 Self-excited loads in ABAQUS

The method of loading for flutter analysis is the same as the static wind load analysis. The mass centers of the bridge deck girder were applied to the self-excited dynamic wind load. But the difference between the static and dynamic analysis is the load definition in the software.

In contrast, the dynamic loadings are no longer constant like the mean wind loadings. They are changing in every time increment. ABAQUS provides a program named "Amplitude" to define these kinds of changing loads. An amplitude curve allows arbitrary time (or frequency) variations of load, displacement and other prescribed variables to be given throughout a step (using step time) or throughout the analysis (using total time); it also can be defined as a mathematical function (such as a sinusoidal variation), as a series of values at points in time (such as a digitized acceleration-time record from an earthquake), etc. [39]

The "Amplitude" program provides several different types of amplitude curves. The "Tabular" definition method was selected in this thesis to define the amplitude curve as a table of values at convenient points on the time scale. ABAQUS interpolates linearly between these values [39]. Table 3.13 shows an example of the partial load amplitudes at 35 m/s wind velocity.

Table 3.13: Load amplitudes at 35 m/s wind velocity (1-1.5 s).

Time (s)	Lateral Load (N/m)	Vertical Load (N/m)	Moment (N•m/m)
1	-57.7755	101.8004	-1149.1
1.1	-69.3511	111.1299	-22775.6
1.2	-78.2903	120.5964	-50433.8
1.3	-77.3112	126.8052	-76290
1.4	-65.0916	130.3263	-98646.1
1.5	-40.2937	130.544	-117347

3.6 Fast Fourier Transform and MATLAB program

3.6.1 Fast Fourier Transform (FFT)

A fast Fourier transform (FFT) is an algorithm to compute the discrete Fourier transform (DFT). Fourier analysis converts from the time domain (or space) to the frequency domain (or wavenumber) and vice versa; an FFT rapidly computes such transformations by factorizing the DFT matrix into a product of sparse factors. [45] As a result, fast Fourier transforms are widely used for many applications in engineering, science and mathematics.

A common use of Fourier transforms is to find the frequency components of a signal buried in a noisy time domain signal. As mentioned above, all the cases of analysis and calculation in this thesis are based on the time domain. Hence, the FFT program is an effective tool to extract the vibration frequency under different wind velocities. Moreover it is of crucial importance for determining the critical flutter velocity and flutter frequency.

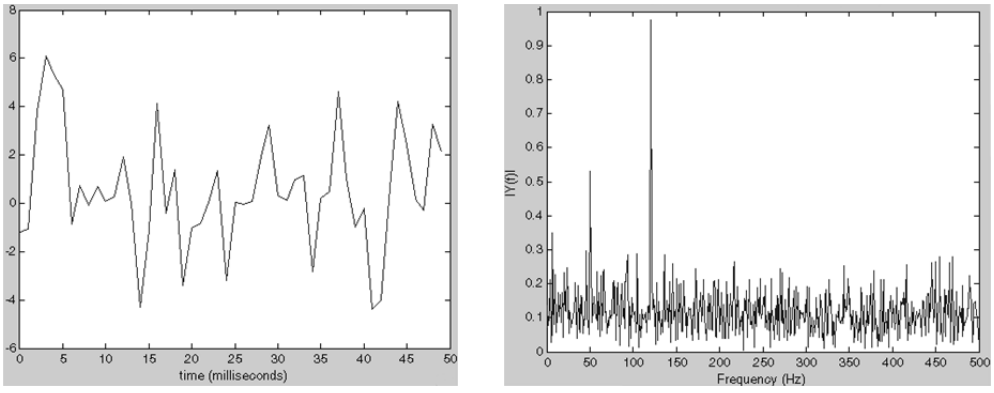

Figure 3.14: An example FFT analysis converts from time domain to frequency domain.

Figure 3.14 shows an example of how FFT converts time to frequency. Due to the voice in

the original data in the time domain, it is difficult to identify the frequency components. After converting to the frequency domain, the dominant frequencies can be clearly observed from the peak values. In the bridge aerodynamic studies, this value of frequency is the main vibration frequency of a specific motion situation.

In the Stonecutters Cable-stayed Bridge flutter analysis, the FFT program was used for extracting the flutter frequency of vertical and torsional response under the different wind velocities. And then according to the variation of frequency, the critical flutter wind velocity and flutter frequency can be determined.

The FFT calculations performed in this thesis were carried out in MATLAB. The codes in the program are shown in Appendix C.

3.7 Loading from natural wind data

In order to realistically estimate the structural response of the Stonecutters Bridge to an wind-induced loading, during a realistic windstorm event, a time history analysis was performed by employing the three components of the wind loading, the drag and lift loadings together with the torsional moment, which were calculated based on the real wind speed records obtained from the anemometer installed by the SUNLab team at the solar panels research site located on the flat roof of the Mann Parking Building in the University of Ottawa campus (Fig. 3.15) [46] [47]. The wind velocity and the wind direction for February 2014 are shown in Figure 3.16.

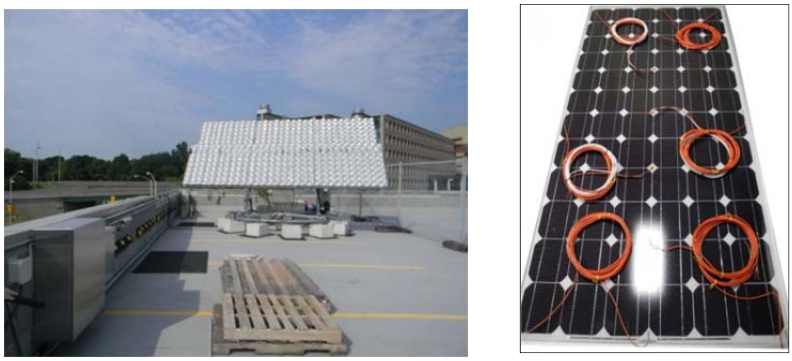

Figure 3.15: Solar panel research site and sensors on the panel. [46][47]

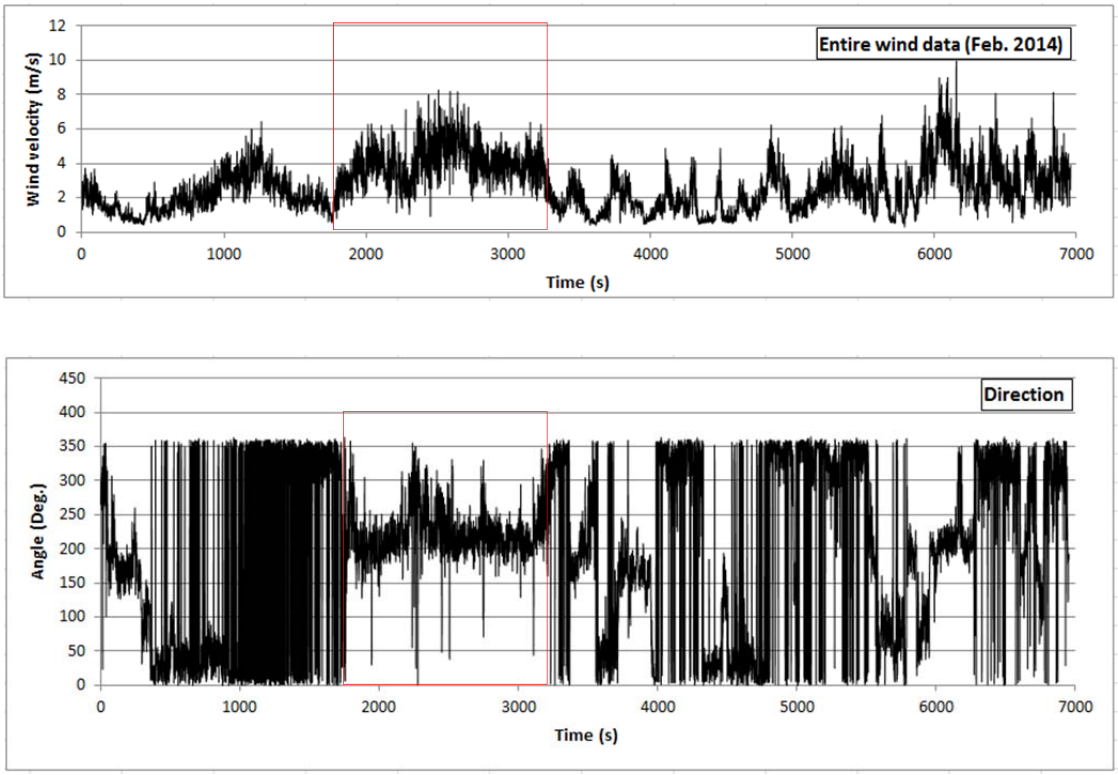

Figure 3.16: Wind speed and direction record from anemometer. [47]

However, such a large time domain wind data cannot be employed successfully in ABAQUS due to hardware and software capacity limitations. A trial analysis run for almost 4 days and it failed due to RAM limitations and then it crashed the computer. Therefore, an

interval of 1,500 seconds of wind record (represented in the red block in Fig. 3.16) was selected for the natural dynamic wind analysis. The wind velocity and the wind direction for the selected 1,500 seconds time domain are summarized in the Figure 3.17 below.

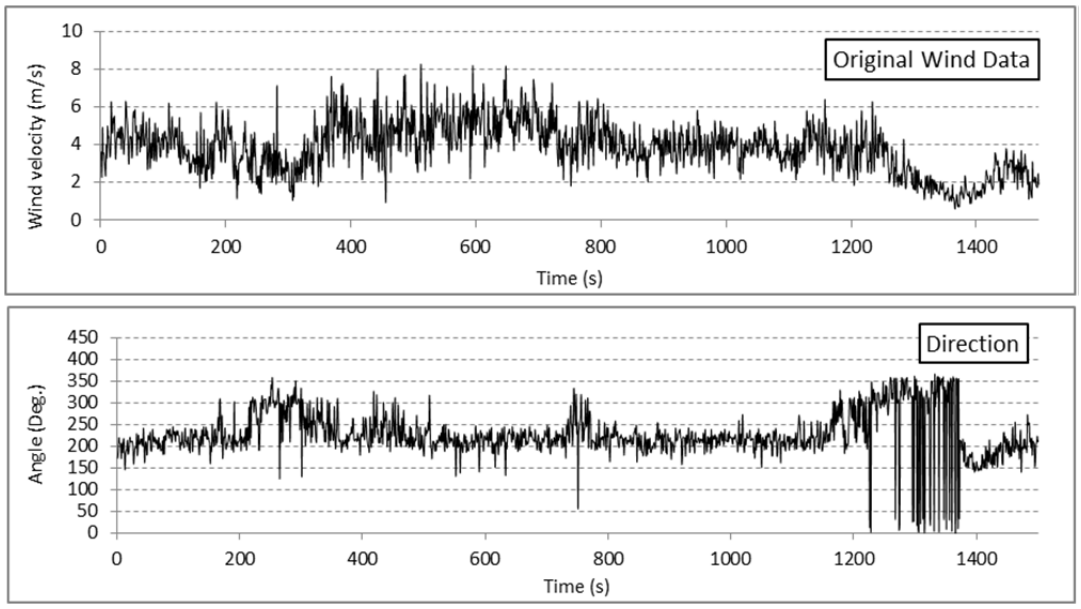

Figure 3.17: Selected wind speed and direction data.

From the wind speed record, the maximum wind speed in the 1,500 s wind data history was 8.14 m/s. The wind speed record was magnified by a factor of 5.0 to represent the most critical wind loading applicable at the bridge site. The calculated wind speed data is shown in Figure 3.18 below. After the amplification, the maximum wind speed became 40.72 m/s, which is close to the natural wind environment at the bridge site for an extreme windstorm event. Dynamic response of the bridge model at several locations were reported and discussed in the following Chapter.

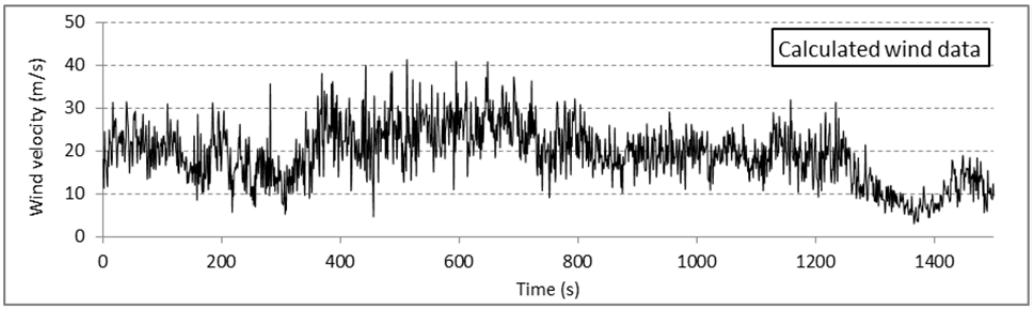

Figure 3.18: Calculated wind speed data.

The natural wind loads were calculated using the queasy-steady mean wind loads equations (Eq. 2.6) as mentioned in Section 2.3.2; the formulations (Eq. 2.6) were reproduced below for the convenience of the readers.

$$D_m = \frac{1}{2}\rho \bar{U}^2 C_D BL(\alpha);$$

$$L_m = \frac{1}{2}\rho \bar{U}^2 C_L BL(\alpha); \qquad (3.5)$$

$$M_m = \frac{1}{2}\rho \bar{U}^2 C_M B^2 L(\alpha).$$

The complete description of the horizontal and vertical wind loads along with the torsional moment, as obtained from the amplified natural wind data and Equations 3.5 were shown in the Appendix E (Fig. E1).

Chapter 4 Force Modeling and Structural Analysis of Twin-deck Cable-stayed Bridge

The FE model developed for the twin-decks Stonecutters Bridge provides a very good platform for investigating the static and dynamic structural responses of the bridge, under various wind loading scenarios, including the effect of flutter instability; thus the FE model can be used for predicting the critical wind speeds up to which such twin-deck bridge can be considered within the safe serviceability functioning conditions. However, before performing the structural analyses a validation of the FE model by verifying the deformed configuration of the bridge under the effect of its own weight and the maximum tension in the cables was done.

4.1 Static analysis with dead load and pre-tension forces

After performing the 'General, Static' analysis considering the dead load which is involved a 9.81 N/kg gravity acceleration on the entire bridge model, the initial conditions and the pre-tension force in the cables as recommended by the comprehensive study performed by Sabri, (2012) [40] . Part of the data is shown in the Table 4.1, and the entire table can be found in the Appendix A, Tables A1 and A2. The equilibrium configuration of the Stonecutters Bridge model is shown in Figure 4.1.

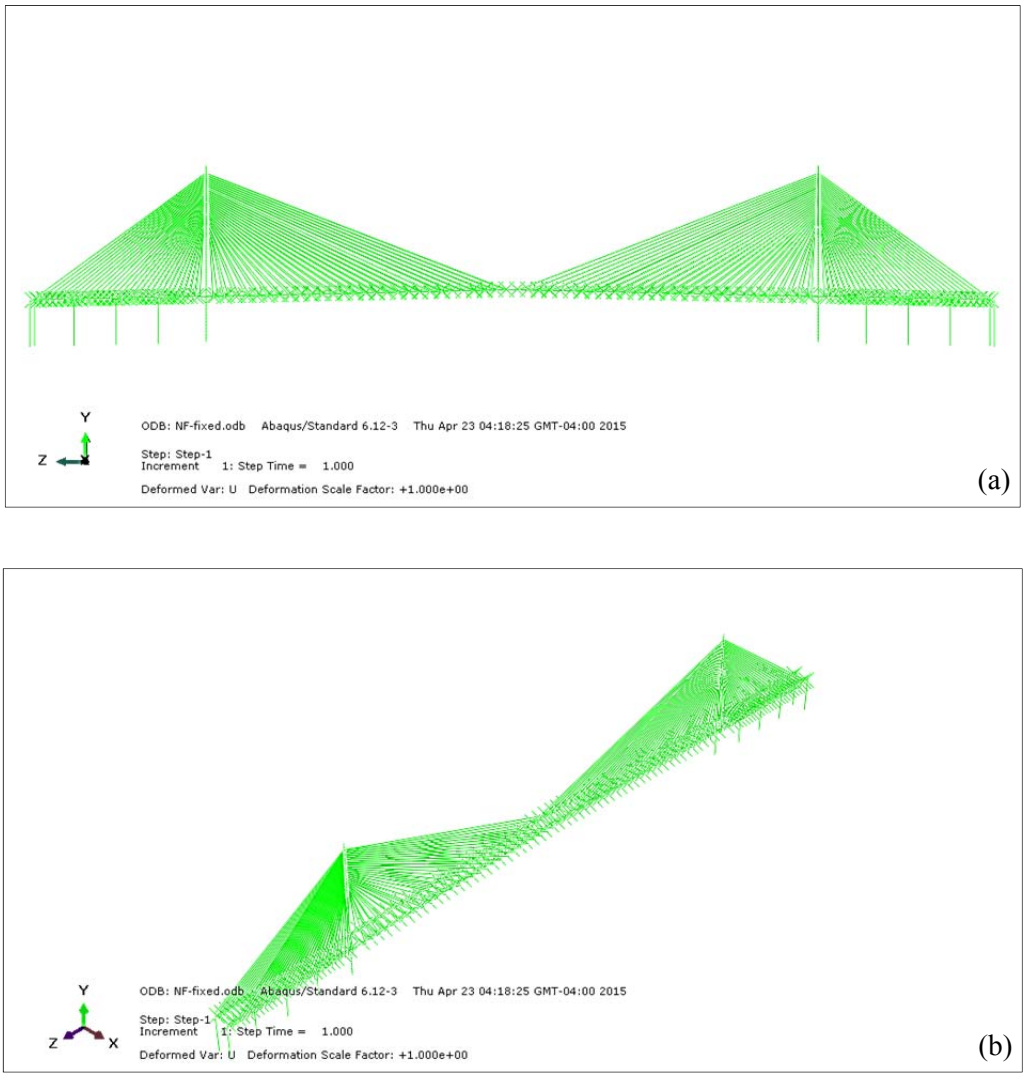

Figure 4.1: The equilibrium configuration of the Stonecutters Bridge FE model. (a) Front view (b) General view.

Table 4.1: Cable pre-tensioning pressure and force.

Cable #				**Tension Pressure in Cable (N/m^2)**	**Pre-Tension Force in Cable (N)**	**Tension Force (N)**
EL1	ER1	WL1	WR1	1770000000	51246621	5.12×10^7
EL2	ER2	WL2	WR2	1759380000	50939142	5.12×10^7
EL28	ER28	WL28	WR28	526482448.9	5264824	4.27×10^6
EL29	ER29	WL29	WR29	526482448.9	5264824	4.27×10^6

From Figure 4.1, the effect of the pre-tension force and the dead load induced by the self-weight of the structure cannot be clearly observed, especially for the main span between the two towers, but Figure 4.2, representing the internal force distribution gives more details. The cables situated near the base, in the immediate vicinity of the tower, have little or no deformations or axial force. However with the increase of the cable length and the distance from the base of the tower, the response of the cables and of the bridge deck becomes obviously higher especially for the region closer to the mid-span. The stresses developed in the cables under the effect of the dead load registered a maximum values of 5.12×10^7 N for the cables connecting the tip of the tower to the middle of the deck and side-span, while the minimum stress values registered were 4.27×10^6 N (Fig. 4.2).

Based on the stresses developed in the cables, the final axial tensions for each cable were determined. Table 4.1 also provides the axial tension comparison for the outer and inner 16 cables which have the maximum and minimum internal force, and very small differences could be noticed when compared with the pre-tension forces applied initially for each cable. Thus a first confirmation that the FE bridge model is adequately constructed can be ascertained. Because the aim of this research is to investigate the dynamic wind load effect on the bridge structure, then the natural frequencies (eigen-values) of the FE Stonecutters Bridge model developed should be verified against the actual data monitored for the Stonecutters Bridge and reported in the literature.

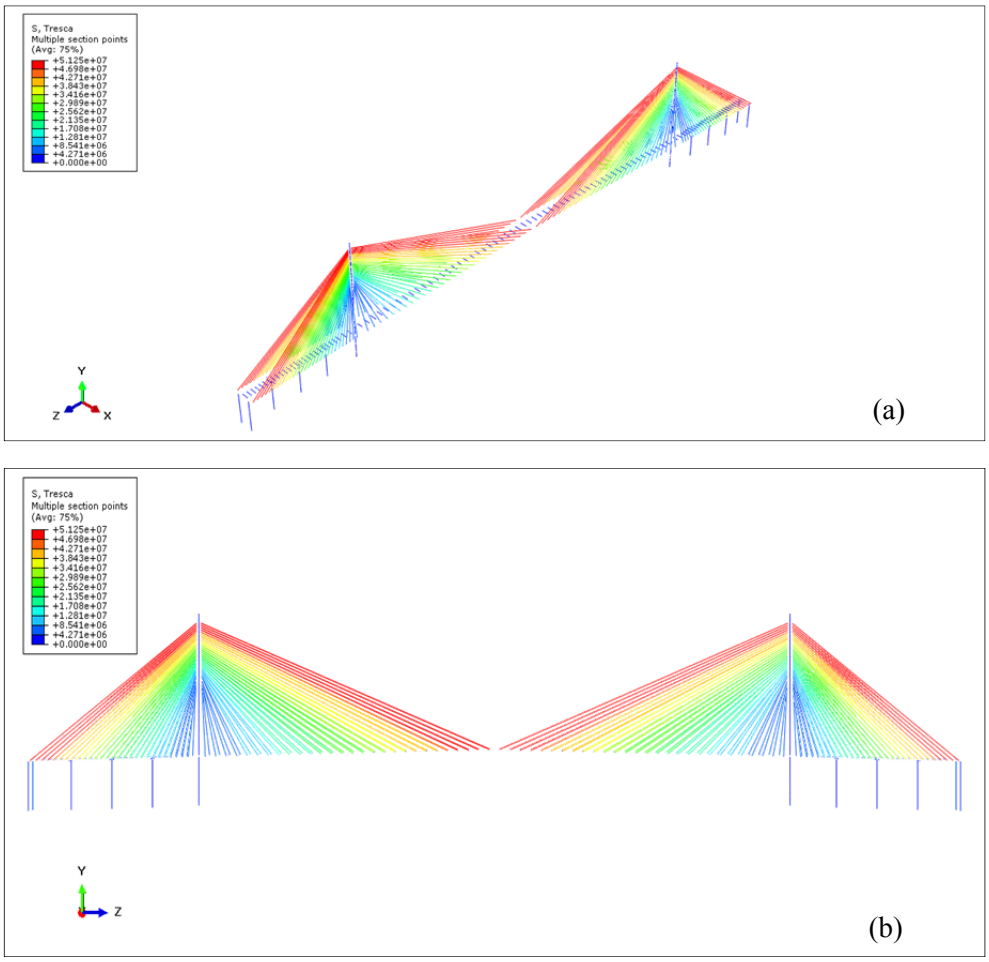

Figure 4.2: Stresses in cables under initial conditions. (a) General view. (b) Front view.

4.2 Eigen-frequencies and Eigen-modes

The long and slender deck spans encountered usually for the major cable-stayed bridges implies a higher degree of flexibility when compared to other bridge structures. The structural flexibility of the bridge deck can impact the overall structural stability in several ways, one important aspect being the large deformation of the bridge deck when subjected to dynamic loads. The dynamic behavior of the cable-stayed bridges caused by these flexible features represents the most significant factor in the bridge resistance design for

wind and seismic loadings.

4.2.1 Natural frequencies

The natural frequencies and the mode shapes of the bridge can be successfully employed for analyzing the dynamic characteristics of a flexible structure effectively. Hence, determining the frequencies (eigen-values) of the eigen-modes of a cable-stayed bridge is vital for the current study, which focuses on studying the dynamic response of the Stonecutters Cable-stayed Bridge model under different wind loading scenarios. Several vibration mode shapes were identified through the frequency analysis, which was performed following the static response of the bridge under the self-weight. The dominant horizontal, vertical and torsional vibration modes and also the coupling between them were reported for the bridge deck and for the tower.

The eigenvalues (frequencies) and the eigenvectors (vibration modes) were determined using the subspace method as described in chapter 3. The first 30 natural frequencies and the generalized masses for each vibration mode for the Stonecutters Bridge FE model are summarized in Table 4.2. Usually the first 5 to 10 vibration modes are considered to be the most important ones, because these vibration shapes can be excited easily, with the lowest energy input from the applied loading.

As it can be noticed from Table 4.2, the first 10 natural frequencies of the Stonecutters Bridge model were situated between 0.9 rad/sec and 3.65 rad/sec, however the generalized mass of the deck had a higher contribution towards the vibration modes 6, 10, 15 and 29, representing a higher involvement of the structural deck elements in these specific modes. Therefore, in order to clarify the type of the vibration mode and the response of the structure towards the dominant modes, the effective mass distribution and the participation

factors were analyzed.

Table 4.2: Natural frequencies and the generalized mass for Stonecutters Bridge FE Model.

Mode No.	Eigenvalue	Frequency		Generalized Mass
		Rad/sec	Cycles/sec	
1	0.82898	0.91048	0.14491	1.51e+07
2	1.1714	1.0823	0.17225	1.94e+07
3	1.4549	1.2062	0.19197	1.45e+07
4	2.5355	1.5923	0.25343	0.924e+07
5	2.5916	1.6098	0.25621	0.882e+07
6	4.1401	2.0347	0.32384	2.50e+07
7	5.0682	2.2513	0.3583	1.64e+07
8	5.9227	2.4337	0.38733	1.38e+07
9	7.086	2.662	0.42366	1.79e+07
10	13.331	3.6512	0.58111	2.20e+07
11	14.746	3.84	0.61116	1.91e+07
12	19.373	4.4015	0.70052	1.83e+07
13	23.696	4.8678	0.77474	1.92e+07
14	23.843	4.8829	0.77714	1.69e+07
15	28.695	5.3567	0.85255	2.14e+07
16	31.649	5.6257	0.89536	1.56e+07
17	33.777	5.8118	0.92498	1.49e+07
18	35.9	5.9917	0.95361	8.81e+06
19	37.873	6.1541	0.97945	1.04e+07
20	50.84	7.1302	1.1348	1.83e+07
21	59.101	7.6877	1.2235	8.22e+06
22	60.837	7.7998	1.2414	9.10e+06
23	78.835	8.8789	1.4131	1.72e+07
24	82.114	9.0617	1.4422	5.24e+06
25	84.038	9.1672	1.459	6.10e+06
26	96.89	9.8433	1.5666	1.56e+07
27	100.38	10.019	1.5946	1.50e+07
28	111.03	10.537	1.6771	1.66e+07
29	114.14	10.684	1.7004	2.20e+07
30	147.02	12.125	1.9298	1.38e+07

4.2.2 The effective mass distribution and the participation factors

The effective mass distributions are summarized in Table 4.3. The mass fraction expresses the mass participation in percentages for the specific vibration mode.

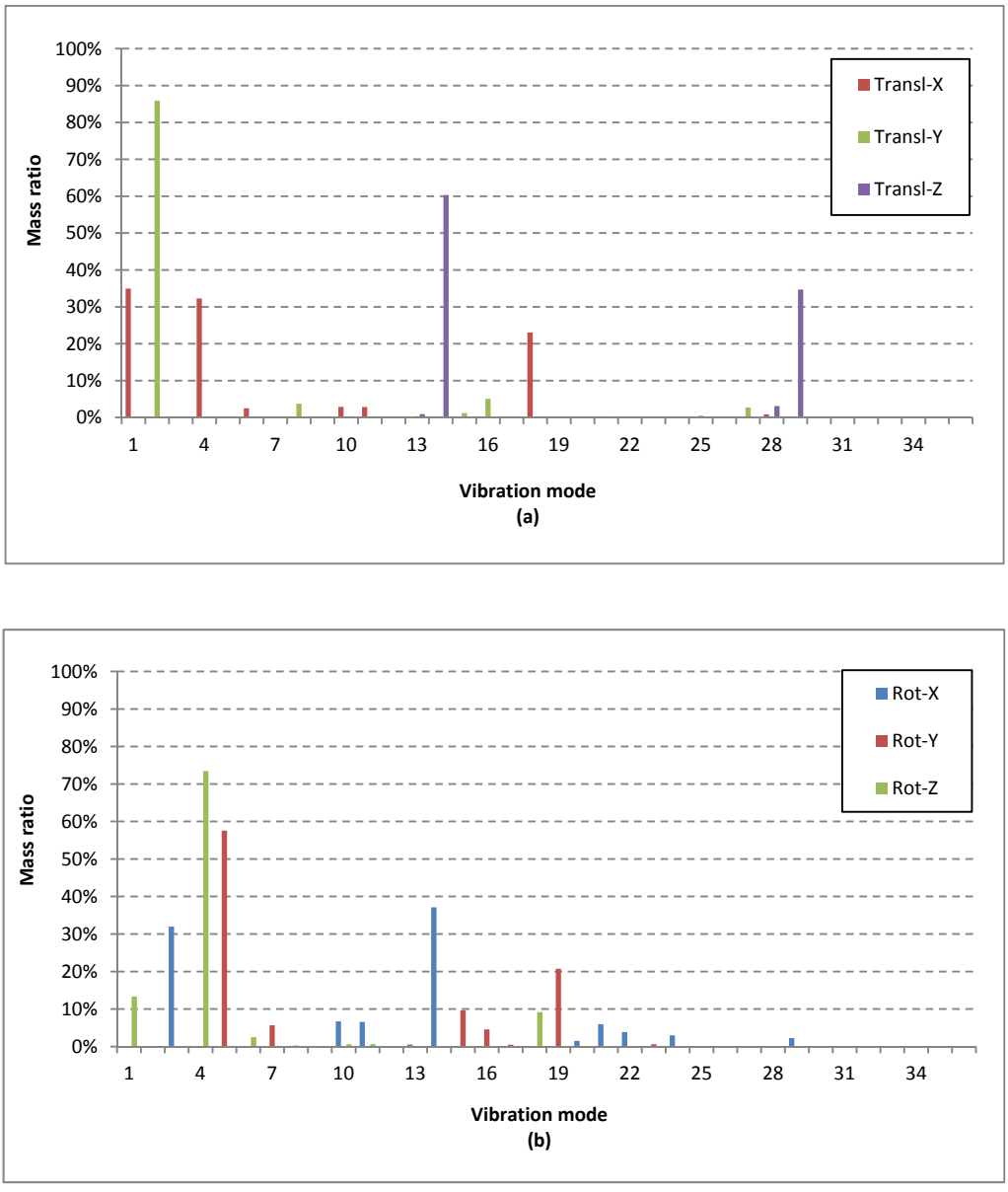

Figure 4.3: Effective mass ratio for the Stonecutters Bridge model. (a) Translations on X, Y, Z axes. (b) Rotations around X, Y, Z axes.

Table 4.3: Effective mass distribution for the Stonecutters Bridge model. (First 30 modes)

Mode No.	X-Component	Y-Component	Z-Component	X-Rotation	Y-Rotation	Z-Rotation
1	2.82E+07	1.79E-03	2.71E+02	5.33E+09	3.85E+05	2.28E+11
2	1.93E-01	2.63E+07	1.03E+00	1.81E+04	1.01E+09	2.43E+03
3	1.28E+05	1.97E+01	9.06E+04	1.14E+12	5.27E+03	1.24E+09
4	2.60E+07	1.51E-01	4.11E+00	3.29E+07	4.50E+09	1.25E+12
5	1.41E+04	3.86E+02	1.13E-01	3.57E+03	8.62E+12	6.76E+08
6	2.00E+06	2.53E-05	4.63E+02	9.07E+07	3.31E+06	4.28E+10
7	2.02E-02	1.77E+04	1.60E-01	7.57E+03	8.52E+11	2.73E+03
8	5.51E-03	1.14E+06	6.40E+00	3.67E+05	3.82E+10	2.43E+02
9	4.97E+00	3.39E+00	2.68E-04	1.01E+01	9.25E+09	2.21E+05
10	2.32E+06	8.49E-04	4.43E+03	2.41E+11	5.25E+04	1.03E+10
11	2.29E+06	5.82E-06	3.30E+04	2.35E+11	6.23E+04	1.09E+10
12	7.22E+04	4.25E-04	2.39E+04	3.97E+09	1.94E+02	1.41E+05
13	7.54E+01	1.14E+05	6.85E+05	1.98E+10	1.24E+10	5.08E+05
14	4.93E+03	1.45E+03	4.63E+07	1.33E+12	1.95E+08	3.23E+07
15	1.07E+00	3.66E+05	2.71E+01	5.79E+05	1.45E+12	5.70E+03
16	5.11E+00	1.55E+06	1.63E+02	3.37E+06	6.88E+11	3.49E+04
17	2.29E+02	3.62E+04	4.30E+00	1.23E+05	7.66E+10	1.74E+06
18	1.86E+07	1.44E-02	7.65E+03	8.50E+08	2.85E+06	1.56E+11
19	1.06E+01	1.36E+04	3.32E-03	2.89E+03	3.10E+12	9.62E+04
20	1.22E+04	1.01E-01	9.07E+04	5.44E+10	3.91E+04	4.76E+08

The participation factors are summarized in Table 4.4. The participation factors of a particular vibration mode demonstrate the importance of that specific mode. The vibration mode classification can be identified by observing the effective mass distribution and the participation factors for each vibration mode. The mass distribution and the participation factors aim at characterizing the vibration modes in terms of pure horizontal, vertical and torsional modes of vibration. As shown in Figure 4.3 and Figure 4.5, the effective mass and the participation factors along the three translational and rotational directions are represented. But normally for a bridge structure, only three of them are considered which are the translations in X and Y-axis, and the rotation in Z axis, because it is improbable for a

long span bridge to rotate in X and Y directions as shows in the Figure 4.4.

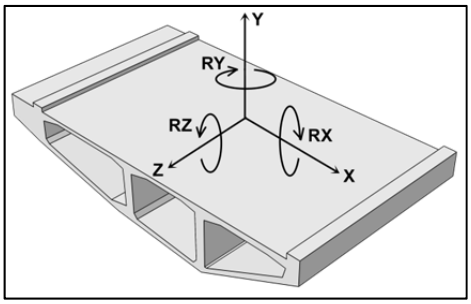

Figure 4.4: Translation and rotation axis system in ABAQUS.

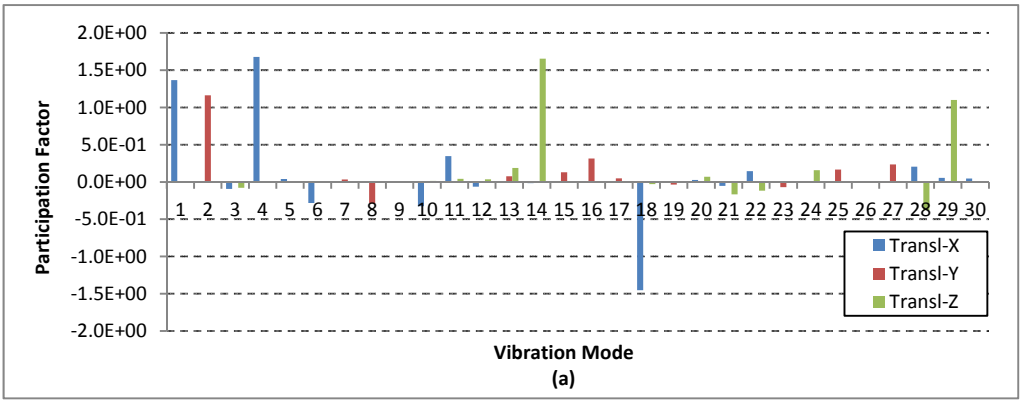

Figure 4.5 (a): Participation factors for the Stonecutters Bridge model. (translations on X, Y, Z axes.)

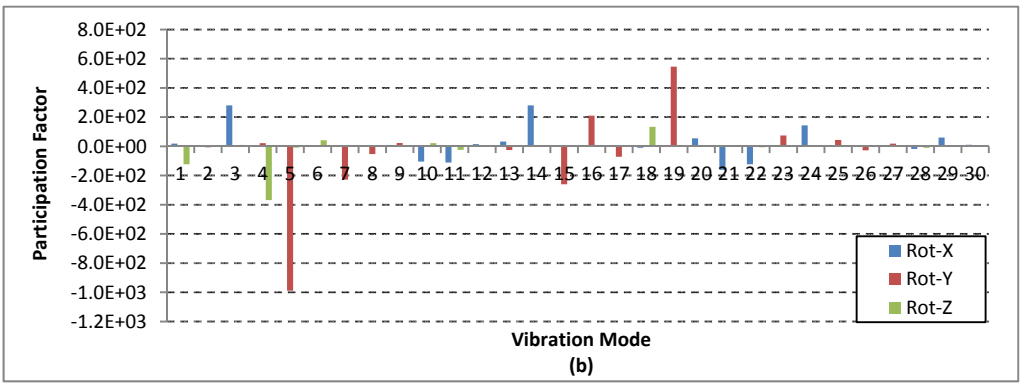

Figure 4.5 (b): Participation factors for the Stonecutters Bridge model. (rotations around X, Y, Z axes.)

Table 4.4: Participation factors for the Stonecutters Bridge model (First 20 modes).

Mode No.	X-Component	Y-Component	Z-Component	X-Rotation	Y-Rotation	Z-Rotation
1	1.37E+00	-1.09E-05	-4.24E-03	1.88E+01	-1.60E-01	-1.23E+02
2	9.98E-05	1.16E+00	2.31E-04	-3.06E-02	-7.22E+00	-1.12E-02
3	-9.37E-02	1.16E-03	-7.90E-02	2.81E+02	-1.90E-02	9.25E+00
4	1.68E+00	1.28E-04	-6.66E-04	1.89E+00	2.21E+01	-3.68E+02
5	4.00E-02	-6.61E-03	-1.13E-04	2.01E-02	-9.89E+02	-8.76E+00
6	-2.83E-01	1.01E-06	4.31E-03	1.91E+00	-3.64E-01	4.14E+01
7	-3.51E-05	3.29E-02	9.89E-05	2.15E-02	-2.28E+02	1.29E-02
8	-2.00E-05	-2.87E-01	-6.82E-04	-1.63E-01	-5.26E+01	4.20E-03
9	5.27E-04	-4.35E-04	-3.86E-06	-7.52E-04	2.27E+01	-1.11E-01
10	-3.24E-01	-6.20E-06	1.42E-02	-1.05E+02	4.88E-02	2.16E+01
11	3.46E-01	5.52E-07	4.16E-02	-1.11E+02	-5.71E-02	-2.39E+01
12	-6.29E-02	4.82E-06	3.62E-02	1.47E+01	-3.26E-03	-8.79E-02
13	-1.98E-03	7.70E-02	1.89E-01	3.21E+01	-2.54E+01	1.63E-01
14	-1.71E-02	-9.26E-03	1.65E+00	2.80E+02	3.39E+00	1.38E+00
15	-2.24E-04	1.31E-01	-1.13E-03	-1.64E-01	-2.60E+02	1.63E-02
16	5.73E-04	3.15E-01	-3.23E-03	-4.65E-01	2.10E+02	-4.73E-02
17	-3.91E-03	4.93E-02	-5.37E-04	-9.07E-02	-7.16E+01	3.41E-01
18	-1.45E+00	-4.04E-05	-2.95E-02	-9.82E+00	5.69E-01	1.33E+02
19	-1.01E-03	-3.61E-02	1.78E-05	-1.66E-02	5.45E+02	9.60E-02
20	2.59E-02	-7.44E-05	7.05E-02	5.46E+01	-4.63E-02	5.10E+00

In general, the participation factors are a measure of how much a vibration mode could participate in the dynamic structural response of the structure, excited with a dynamic loading on a given direction. Investigating the participation factors for each mode shows which vibration modes would participate in a certain direction [48].

In general, if the modal mass ratio contributing to a certain direction/rotation is not considerably high, then no vibration mode would develop, even if the participation factors might register a higher value for that specific direction/rotation. Figures 4.3 (a) and (b) show the modal effective mass distribution (normalized by the total mass for each directional mode) of the Stonecutters Bridge FE model. A high modal mass was noticed to

contribute in the same direction as indicated by the participation factors (Figures 4.5 (a) and (b)), for the global modes 1, 4 and 18, for which horizontal/torsional vibration modes and also for the global modes 5, 7 and 15, where a rotation around the vertical axis (Y-axis), resembling a horizontal vibration mode, similar actually with global modes 16 and 19. Pure vertical vibration modes were indicated by both mass contribution and participation factors for the translation on the vertical Y-axis, for the global modes 2, 8, 15 and 16. The global vibration modes 3, 10 and 11, on the other hand, are represented as asymmetric vertical modes in Figure 4.5 however the participation factors and the mass contribution indicate a rotation around the transversal X-axis, which resembles an asymmetric vertical mode; also they contain a translation along the longitudinal Z-axis, pointing to a coupling with the horizontal vibration mode. Similar discussion can be concluded for the global vibration modes 14, 21, 22 and 29, some of them with a dominant horizontal mode and others with the asymmetric vertical as dominant vibration mode.

The participation factors obtained from the first 30 modes of the finite element model of the Stonecutters Bridge model have shown pure horizontal, vertical or torsional dominant modes mostly, and they did not provide sufficient information regarding the deck-towers-cables coupled modal behavior. In other words, the detailed modal behavior cannot be determined only from these factors but the vibration mode visualization is also required.

4.2.3 Vibration mode shapes

Since the Stonecutters Cable-stayed Bridge is simulated as a complete 3D finite element model, all possible coupled vibration modes can be obtained and clearly observed from the mode shapes of the entire bridge. Thus the 3D FE model of the Stonecutters Cable-stayed

Bridge provides a full picture of the dynamic behavior and of the characteristics of the bridge. The first six vibration mode shapes are shown in the Figures 4.6 to 4.11. Therefore, a full detail modal behavior of Stonecutters Bridge can be observed from the first six vibration mode shapes; however more mode shapes (7^{th} to 11^{th}) are shown in the Appendix Figures B1 to B5.

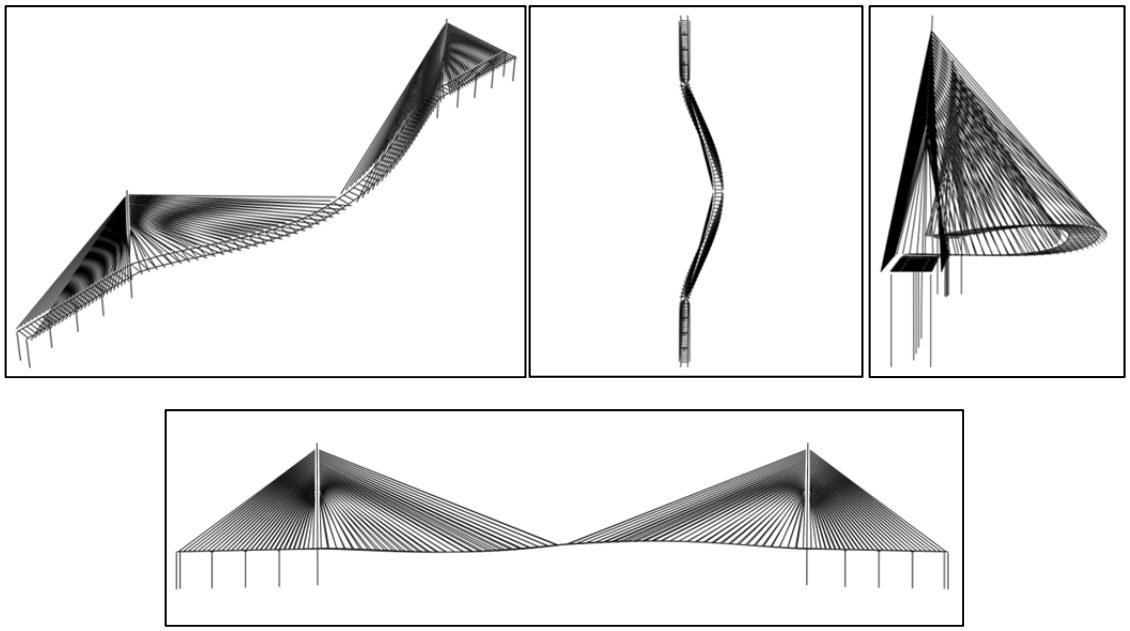

Figure 4.6: 1^{st} Mode shape (f=0.14491 Hz, horizontal deck, scale factor: 1.597e+02).

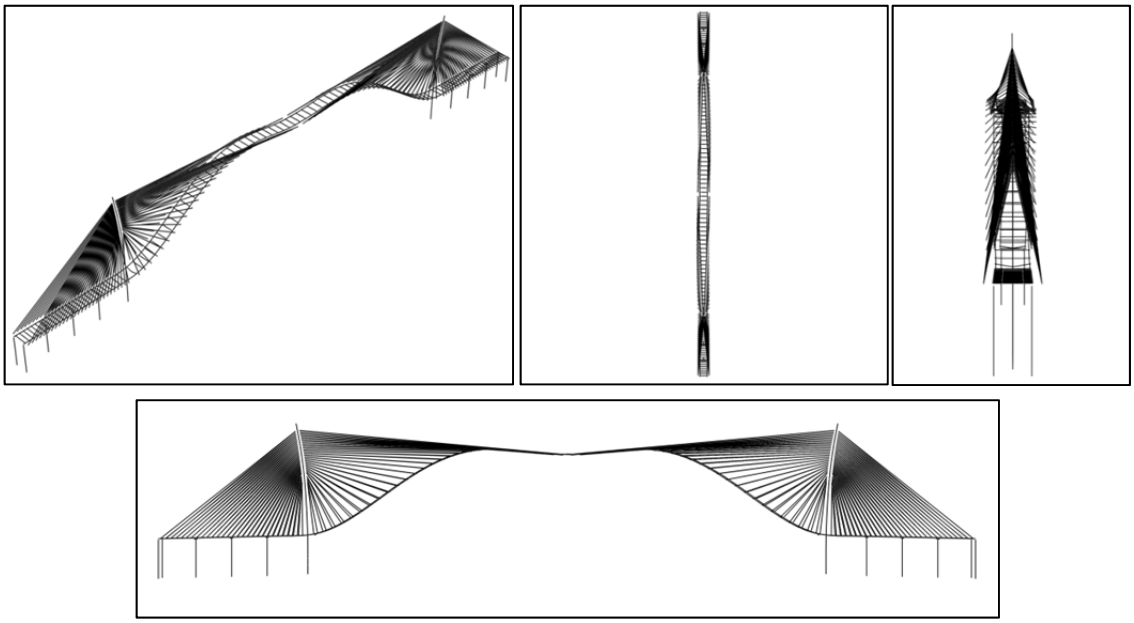

Figure 4.7: 2nd Mode shape (f=0.17225 Hz, vertical deck, scale factor: 1.597e+02).

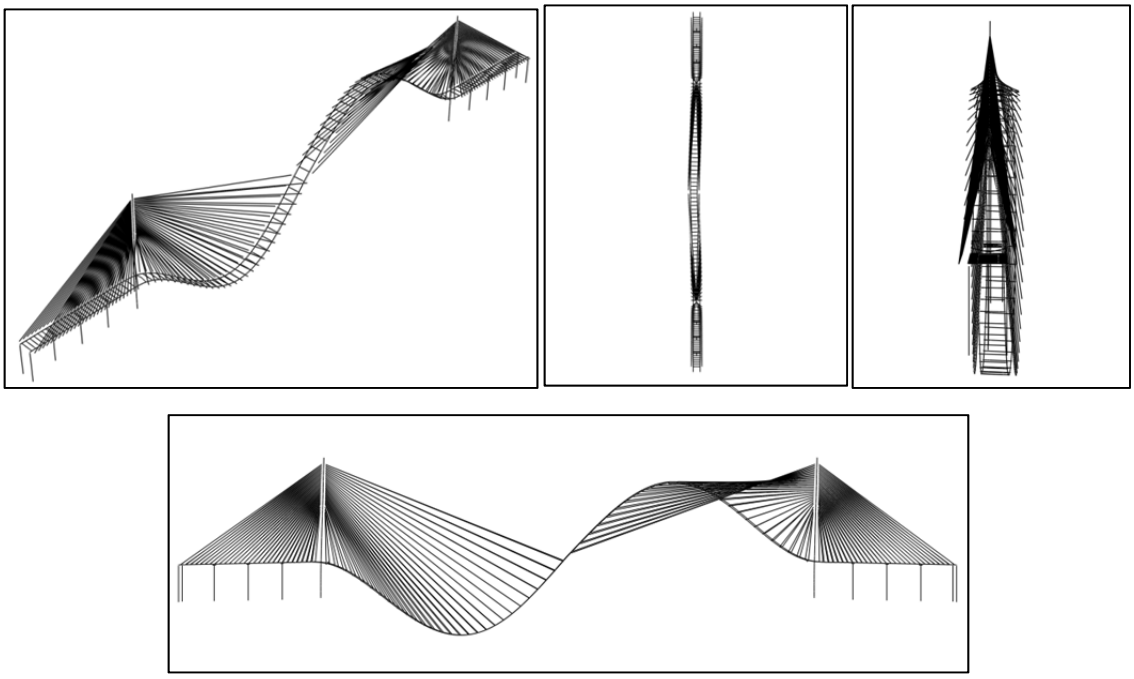

Figure 4.8: 3rd Mode shape (f=0.19197 Hz, 2nd vertical deck, scale factor: 1.594e+02).

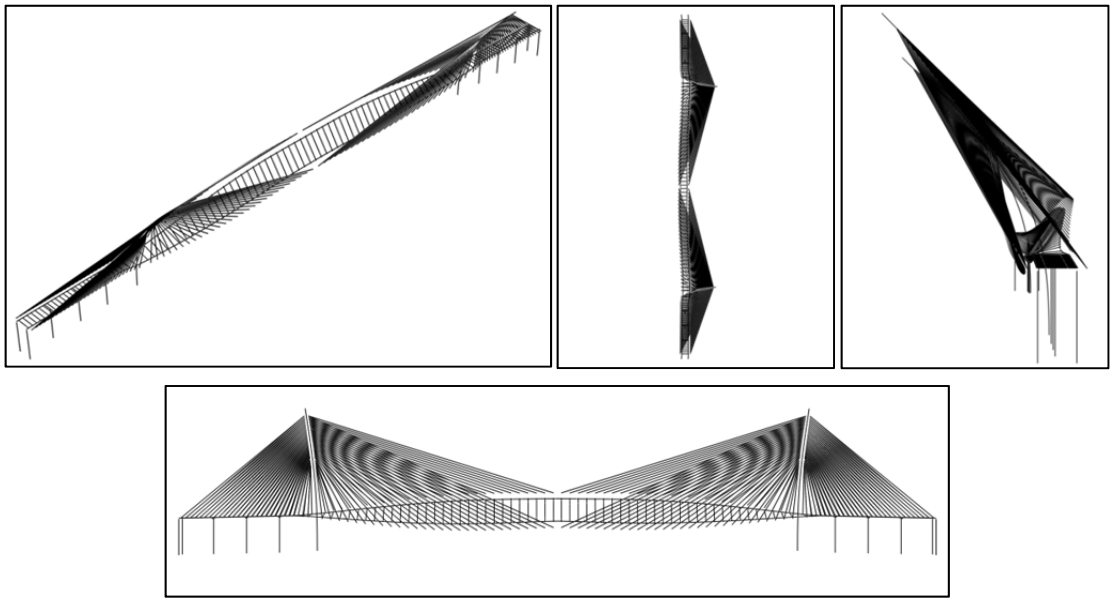

Figure 4.9: 4th Mode shape (f=0.25343 Hz, horizontal tower, scale factor: 1.597e+02).

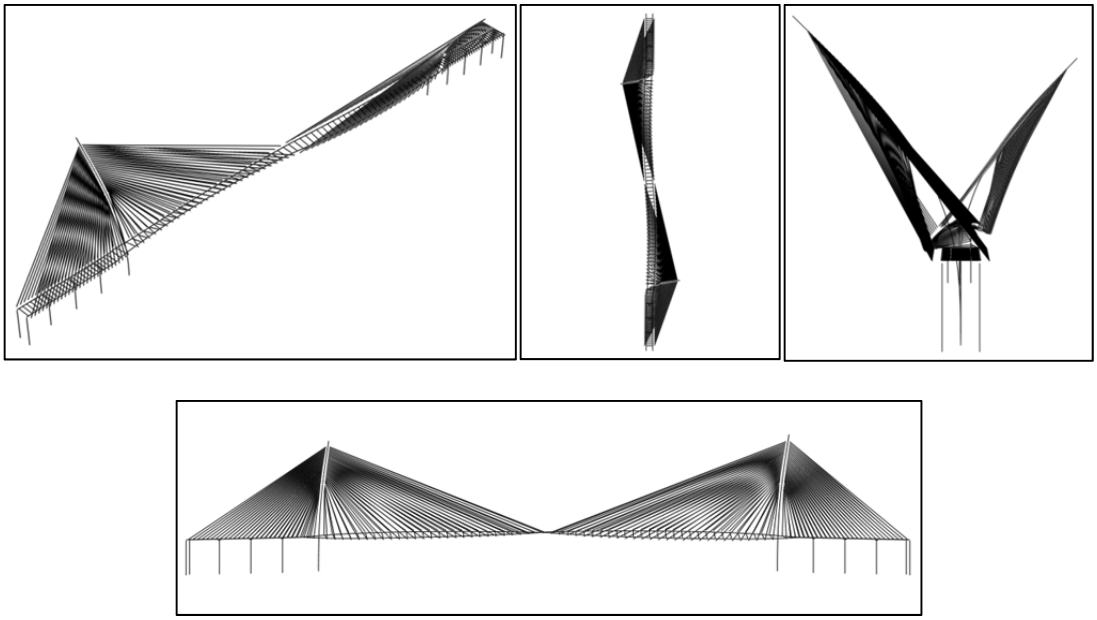

Figure 4.10: 5th Mode Shape (f=0.25621 Hz, asymmetry horizontal tower, scale factor: 1.597e+02).

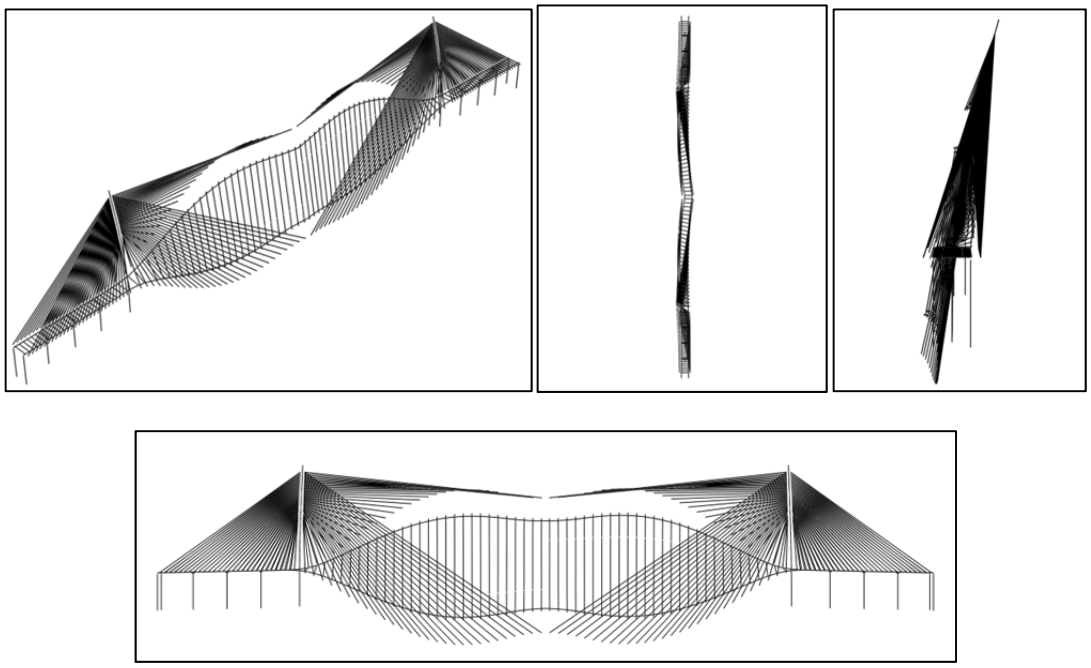

Figure 4.11: 6th Mode shape (f=0.32384 Hz, torsion deck, scale factor: 1.042e+02).

In order to better identify the type of the vibration, Figures 4.6 to 4.11include the isometric, the top, the lateral and the side views for each mode shape. The mode shapes and the coupling effect depicted in Figures 4.6 to 4.11 are described in detail in the following section, where they are also compared them with the results reported in the literature.

4.2.4 Natural frequency results and comparison

The major results from the modal analysis of the Stonecutters Cable-stayed Bridge FE model with single-truss-element cable model can be summarized as follows:

1. The first 30 natural frequencies of the Stonecutters Bridge FE model developed in the range of 0.14491 Hz to 1.9298 Hz, which is within the limits of the natural frequencies reported for other cable-stayed bridges [23] [22] [18] [44] .

2. The lowest natural frequency is 0.14491 Hz with the first horizontal vibration mode at bridge deck and the motion of the deck is symmetric along the main span (Fig. 4.6).

3. Following the first horizontal mode of the bridge deck, there are the symmetric and asymmetric vertical vibration modes (Figs. 4.7 and 4.8) dominated by the bridge deck. The first vertical mode is a symmetrical shape at a natural frequency of 0.17225 Hz (Fig. 4.7) and the second one is asymmetrical along the main span at a natural frequency of 0.19197 Hz (Fig. 4.8). The first two vertical modes and the natural frequencies are relatively close.

4. The fourth and fifth vibration modes are horizontal vibration modes dominated by the bridge towers bending modes (Figs.4.9 and 4.10). The two towers are in symmetric mode shape at the natural frequency of 0.25343 Hz, and then they move in asymmetric mode shapes at the natural frequency of 0.25621 Hz. The natural frequencies in these two horizontal modes characterizing the towers are relatively close and the motion of the towers always combines with the horizontal or vertical modes of the bridge deck girder.

5. The sixth mode (Fig. 4.11) comes with the first symmetric torsional mode shape of the bridge deck at the natural frequency of 0.32384 Hz. The first torsional mode is very important for the bridge dynamic analysis because most of the times, the collapse from flutter of a bridge under wind loading would happen when the coupling between the vertical motion and the torsional motion occurs. Thus, the value of the critical flutter frequency is close to the value at first torsional mode.

The design concept for the Stonecutters Cable-stayed Bridge was provided by the Highways Department in Hong Kong [17], however, until present, the monitoring data of the natural frequencies of this bridge have not been published by Highways Department or by the designers. In recent years, many people are devoting their research to clarify the static and

the dynamic characteristics of the Stonecutters Cable-stayed Bridge, based on numerical models they employed. Therefore, as a comparison, the data published by. Hui et al. (2006) [17] was selected. This is also the most comprehensive data on the Stonecutters Bridge widely accepted at present. Table 4.5 shows a comparison between the frequencies and the mode shapes obtained from the current research and those reported by Hui et al. (2006), [17].

Table 4.5: Comparison of natural frequencies and mode shapes (first 10 modes)

Data Published by Hui, et al. (2006) [17]			Data from current Stonecutters Bridge FE Model		
Mode No.	Frequency	Mode Shape	Mode No.	Frequency	Mode Shape
1	0.145	S-H-deck	1	0.14491	S-H-deck
2	0.19	A-H-tower	2	0.17225	S-V-deck
3	0.197	S-H-tower	3	0.19197	A-V-deck
4	0.201	S-V-deck	4	0.25343	S-H-tower
5	0.246	A-V-deck	5	0.25621	A-H-tower
6	0.302	A-V-deck	6	0.32384	S-T-deck
7	0.311	S-V-deck	7	0.3583	A-H-deck
8	0.361	A-H-deck	8	0.38733	S-V-deck
9	0.376	A-V-deck	9	0.42366	A-T-deck
10	0.422	S-V-deck	10	0.58111	A-T-V-deck
Note: S: Symmetry A: Asymmetry H: Horizontal V: Vertical T: Torsional					

From the Table 4.5, it was found that the first natural frequencies and the mode shapes of the FE model are almost the same as the data published by Hui et al, (2006) [17]. The first mode occurs at about 0.145 Hz natural frequency as a symmetric horizontal mode shape; this frequency range and the type of the mode shape also match most of the first vibration mode shapes reported for the cable-stayed bridge [18]. Also from Table 4.5, it can be concluded that for the first ten modes, there is no large difference between the two groups of data reporting natural frequency, except for the fourth and the tenth mode where the frequency obtained in the current study was slightly higher.

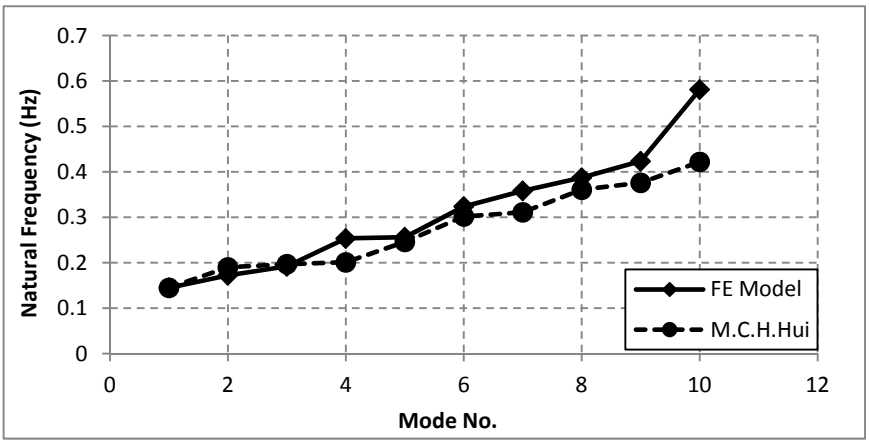

Figure 4.12: Difference between FE Model and data reported by Hui et al [17].

In order to observe clearly the variations of the natural frequencies for the two groups of data, these are also summarized in the Figure 4.12. The errors of the natural frequency between the FE Model and the data from Hui et al [17] are summarized in the Table 4.6. From Figure 4.12 and Table 4.6 it can be concluded that the biggest differences were of 26% and 37.7% for the vibration modes 4 and 10.

Table 4.6: Percentage difference of natural frequency between FE model and data published by Michael C. H. Hui, et al [17] (First 10 modes)

Mode No.	F1 (Hui, et al) [17]	F2 (FE Model)	Frequency Error (%)
1	0.145	0.14491	-0.06%
2	0.190	0.17225	-9.34%
3	0.197	0.19197	-2.55%
4	0.201	0.25343	26.08%
5	0.246	0.25621	4.15%
6	0.302	0.32384	7.23%
7	0.311	0.35830	15.21%
8	0.361	0.38733	7.29%
9	0.376	0.42366	12.68%
10	0.422	0.58111	37.70%
Note: Frequency Error (%) = (F2-F1)/F1			

Also, there were some differences regarding the types of the mode shapes for the higher modes, in particular. As shown in the Table 4.5 in the data published by Hui et al, (2006) [17], none of the first ten modes were reported as torsional vibration modes; actually the first pure torsional mode shape for the Stonecutters Bridge FE model appears as the mode 6 at 0.32384 Hz, in the current study.

Also Hui et al, (2006) [17], reported that the mode 2 and mode 3 are both tower modes coupled with horizontal deck modes, which occur before the vertical deformation of the bridge deck. However the order is switched between the vertical-deck and the horizontal-tower for the results obtained from the currently developed FE model, the tower deformation mode comes before the vertical motion of the deck starts to occur. The main differences may depend on the method of modeling, the element types employed and some of the properties of the bridge deck itself. However, overall the natural frequencies and mode shapes of Stonecutters Bridge FE model are considered to agree well with the FE model results reported by Hui et al, (2006) [17], but because both are numerical models, other references for the Stonecutters Bridge were also consulted for a better validation of the current FE model.

Table 4.7: Percentage difference of natural frequency between the FE model and the data published by Pappin and Kite. (First 4 modes)

Mode No.	F1 (Pappin and Kite) [49]	F2 (FE Model)	Frequency Error (%)
1	0.1429	0.14491	1.44%
2	0.1852	0.17225	-6.99%
3	0.1887	0.19197	1.74%
4	0.1961	0.25343	29.25%
Note: Frequency Error (%) = (F2-F1)/F1			

Table 4.7 shows the natural frequency of the first four modes reported by Pappin and Kite, (2008) [49] in their seismic study of the Stonecutters Cable-stayed Bridge employing a

three-dimensional finite element model as well; only the first four modes of vibration were detailed in this study, therefore comparison was made in Table 4.7 only for the reported modes and natural frequencies.

As mentioned above, the Stonecutters Bridge is a cable-stayed bridge with a twin-box girder, however considering similar dimensions of the main span, several bridges of single deck and multiple deck configurations were considered for the validation purpose. Thus the current results of the natural frequencies were also compared with the other cable-stayed bridges with different type of bridge decks and towers, in Table 4.8.

Table 4.8: Characteristics of different type of cable stayed bridges

Bridge Name	Deck	Tower	Length-main span (m)	Width (m)	Type
FE Model	twin	2	1018	53.3	cable-stayed
Jingsha Bridge [50]	single	2	300	27	cable-stayed
Songpu Bridge [51]	single	1	268+208	39.5	cable-stayed
Taizhou Bridge [52]	single	3	1080+1080	33	suspension
Sutong Bridge [35]	single	2	1088	41	cable-stayed
Messina Bridge [53]	triple	2	3300	52	suspension
Humen Bridge [54]	single	2	888	35.6	suspension

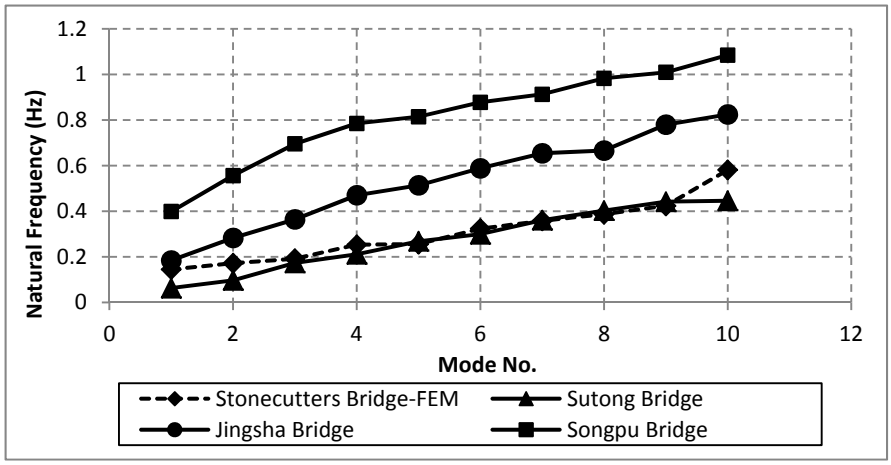

Figure 4.13: Natural frequencies for the Stonecutters FE model and for other cable-stayed bridges.

Figure 4.13 summarizes the natural frequencies of the Stonecutters Bridge FE model and of other cable-stayed bridges with different deck configuration properties. It was found that the Sutong Bridge has almost the same modal properties as the FE model of the Stonecutters Bridge, except for the shape of the bridge deck [35]; thus the natural frequencies indicated by the first 10 vibration modes for the Sutong Bridge are very close to the Stonecutters Bridge FE Model; For the case of Jingsha Cable-stayed Bridge [50] which has a much smaller main span of 300 m main span, the natural frequencies start at a similar values as the Stonecutters Bridge FE model, but these increase to higher values for the following modes; the major difference appears for the Songpu Bridge, which has also a smaller span, but it is designed with only one single tower [51]. From Figure 4.13, it can be clearly observed that, the natural frequencies of Songpu Bridge are much higher than those of the Stonecutters Bridge FE model.

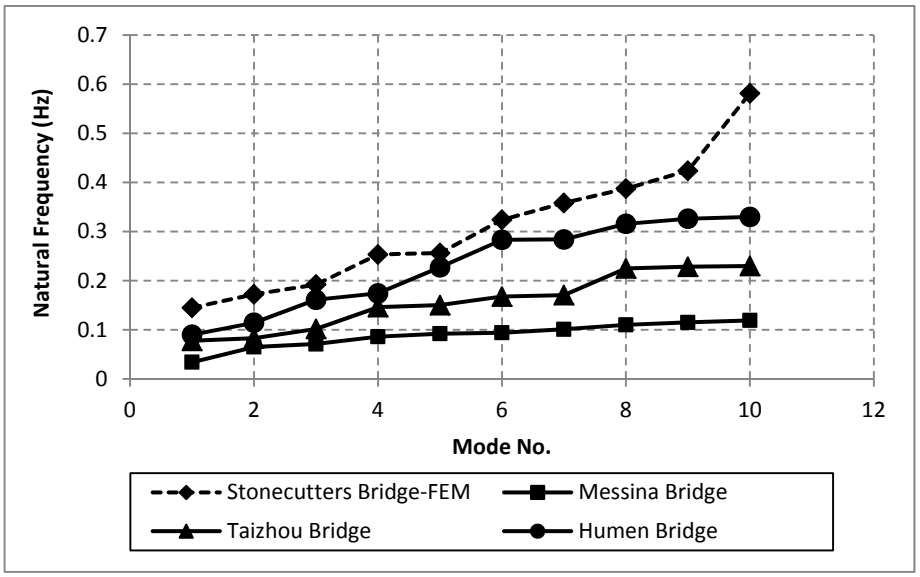

Figure 4.14: Natural frequencies for the Stonecutters FE model and for other suspension bridges.

Because both structures, the suspension bridges and the cable-stayed bridges, belong to the

same category of cable supported bridges, they all have similar dynamic characteristics. In Figure 4.14, the differences between the Stonecutters Cable-stayed Bridge FE model and other suspension bridges available in the literature are summarized.

Overall, the values of the natural frequencies for the cable-stayed bridge discussed above are smaller than the value of Stonecutters Bridge FE model, but still in the same range. The length of the main span of the Humen Bridge [54] is shorter than Stonecutters Bridge FE model, but other structural properties are similar, therefore from the Figure 4.14, it can be noticed that the natural frequencies of the Humen Bridge are closer to the Stonecutters Bridge FE model, but just below these. Things become different for bridges with very long main span. Taizhou Bridge [52] has two main spans of 1,080 m, but it is designed with three towers, therefore the bridge structure and the construction conditions are different. The Messina Bridge, which was vastly investigated, but was not yet constructed and is in designing stage, has a 3,300 m main span [53] with a triple-deck girder. The first 10 mode shapes of these two very long suspension bridges indicate lower natural frequencies than the ones obtained currently from the Stonecutters Bridge FE model as well, these increase more slowly with the mode number.

4.3 Bridge response under queasy-steady wind loading

The overall wind load analysis can be separated into two parts: ‘General, Static’ which involves a static wind load applied on the Stonecutters Bridge FE model, without time domain analysis and ‘Implicit, Dynamic’ which uses the 60 seconds time history of the same wind loading, but applied continuously on the Stonecutters Bridge FE model, for this time interval. These mean wind loads were calculated using the queasy-steady mean wind loads equations (Eq. 2.6) as mentioned in section 2.3.2 and the results were shown in the

Table 3.9 in Chapter 3. The queasy-steady wind loads formulations (Eq. 2.6) were reproduced below for the convenience of the readers.

$$D_m = \frac{1}{2}\rho \bar{U}^2 C_D BL(\alpha);$$

$$L_m = \frac{1}{2}\rho \bar{U}^2 C_L BL(\alpha); \qquad (4.1)$$

$$M_m = \frac{1}{2}\rho \bar{U}^2 C_M B^2 L(\alpha).$$

4.3.1 General, Static analysis

At the beginning of the analysis, a general static step was performed under the mean wind load without time history step. This was necessary for extracting the static response of the Stonecutters Bridge under the queasy-steady wind loading. Figure 4.15 reports the static deflection of the Stonecutters Bridge FE model main span under the action of the static mean wind forces for different mean wind speeds ranging from 35 m/s until very high values of 176 m/s and 211 m/s. These values were selected based on the results of wind tunnel experiments from Hui, et al. (2006) [17]

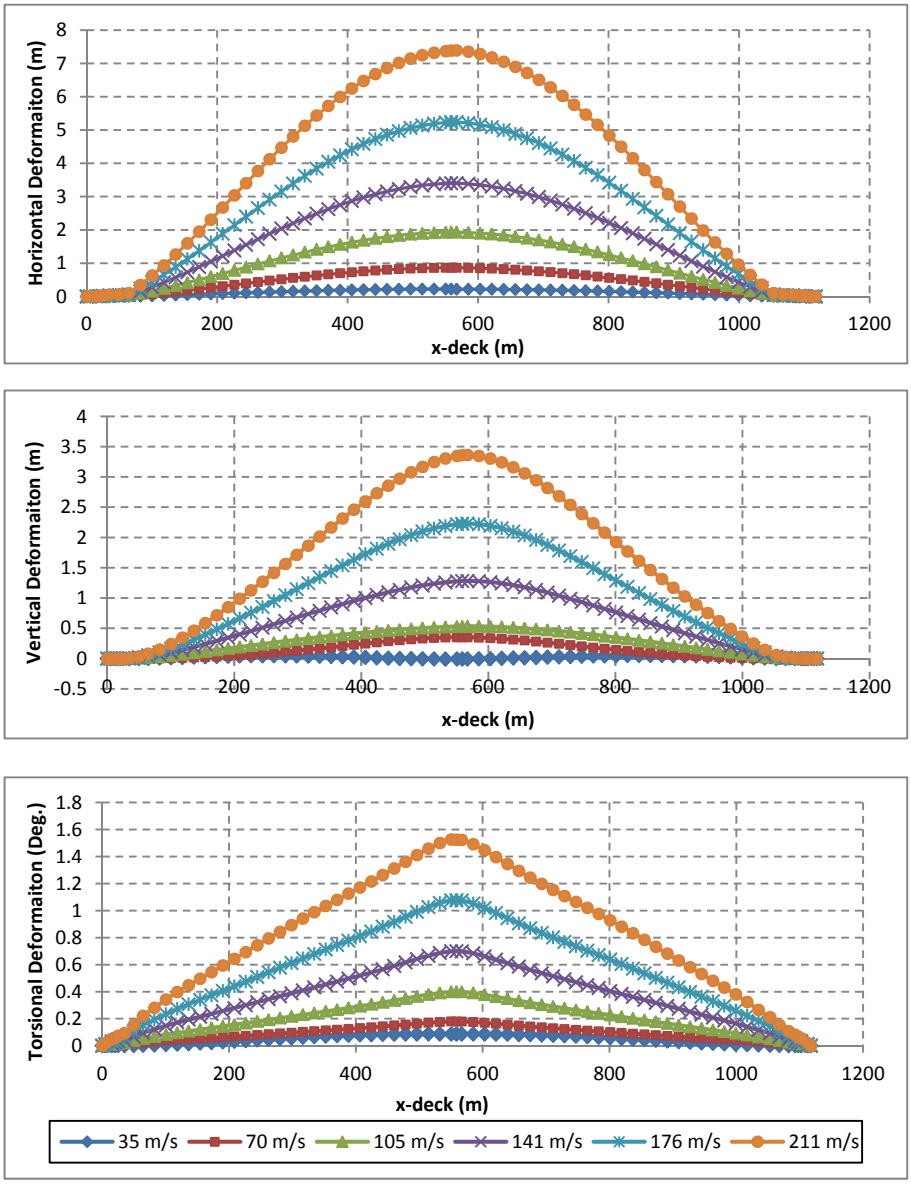

Figure 4.15: Static deformation of Stonecutters Bridge deck under different mean wind speeds.

As it can be noticed from Figure 4.15, the vertical, horizontal and torsional deformations registered the maximum values at the middle of the main span; when comparing with the results reported by Diana (Diana, et al. 2013) [22] in Figure 4.16 for the Messina Bridge, which has a triple deck and a 3,300 m span. It can be found that the overall evolution was similar, namely the horizontal, vertical and torsional deformations of the bridge deck

increased with the wind velocity, and the most critical position under the mean wind load was at the mid-span.

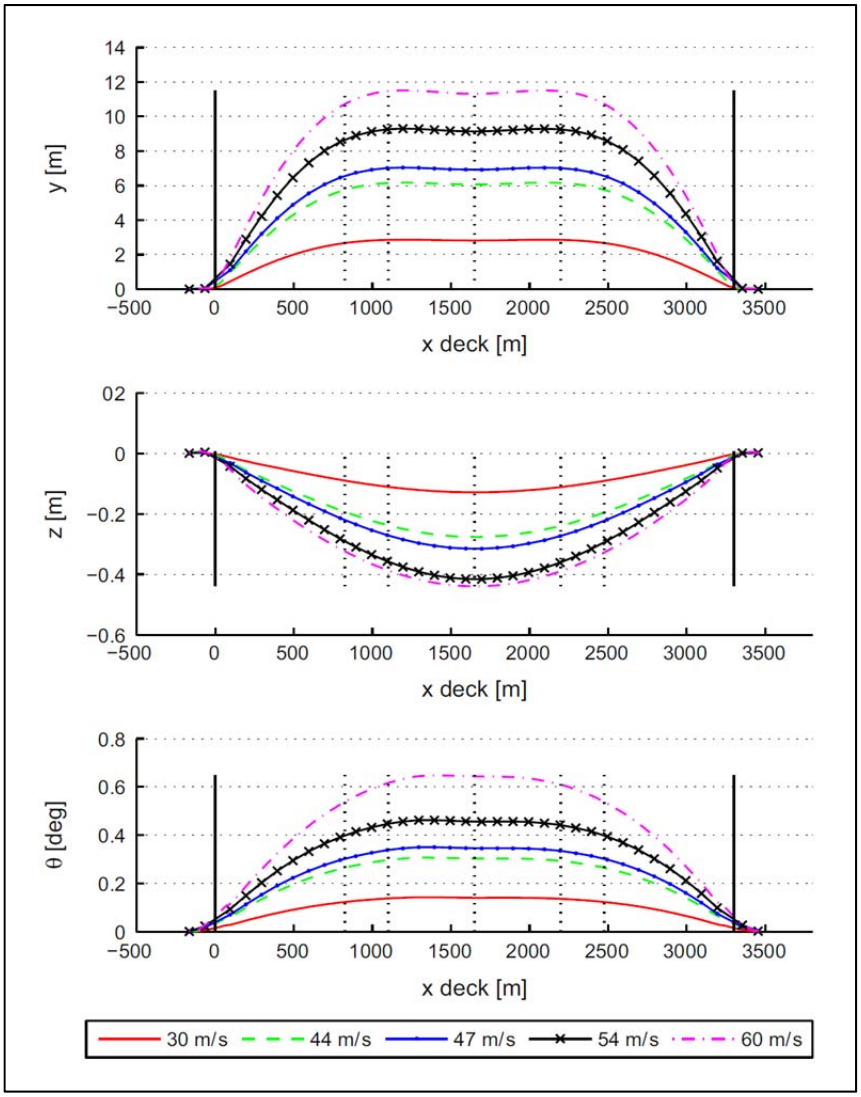

Figure 4.16: Static deformation of Messina Bridge under different mean wind speeds. (Diana, et al. 2013) [22]

Therefore the deformations at the mid-span under different mean wind speeds are summarized in Figure 4.17 as follows. The results of Messina Bridge are also summarized as a comparison.

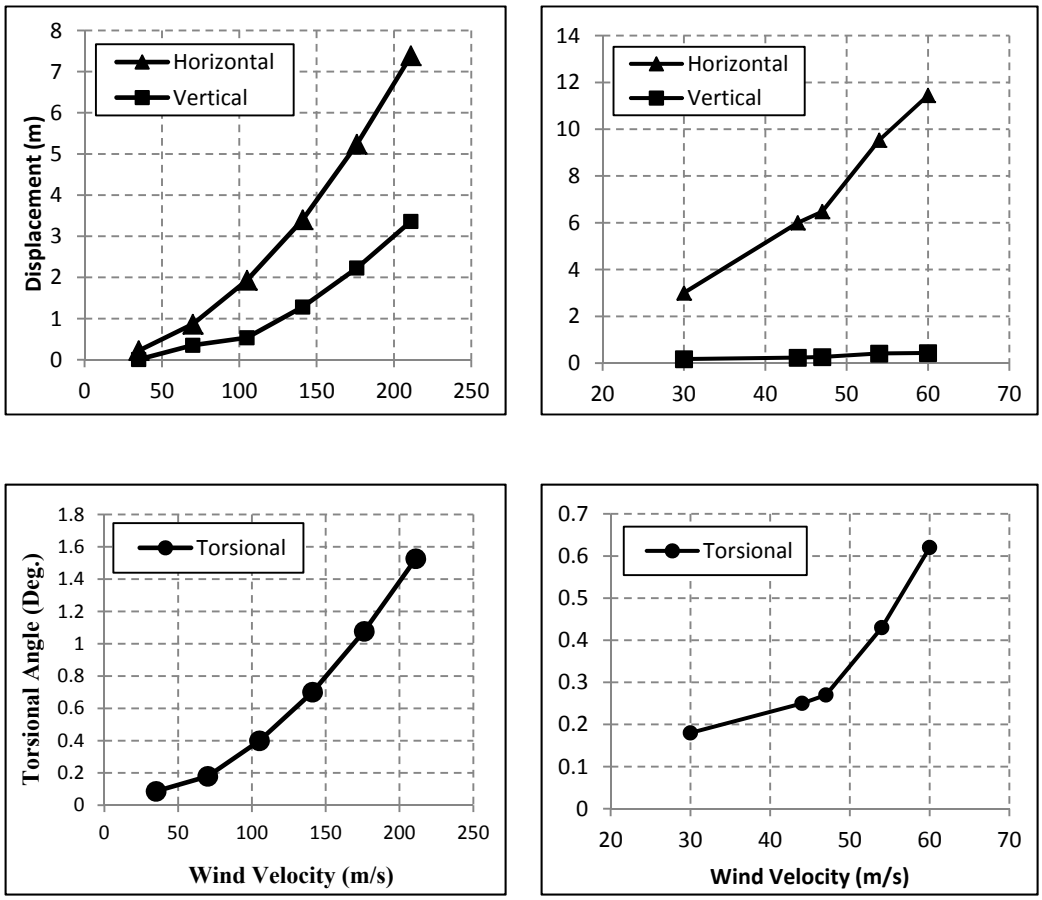

Figure 4.17: Deformations at mid-span under different mean wind speeds. Left: Stonecutters Bridge. Right: Messina Bridge.

It can be observed that all the deformations at mid-span along the three directions are increasing gradually with wind velocity. The maximum reported values, as expected are for 211 m/s wind velocity where the vertical displacement is 3.36 m, the horizontal displacement is 7.39 m and the torsional angle is 1.53 degrees. For the Messina Bridge, at the maximum wind speed of 60 m/s, the vertical, horizontal and torsional displacements were 0.43 m, 11.45 m and 0.62 degrees, respectively.

4.3.2 Implicit, Dynamic analysis

After the 'General, Static' step, an 'Implicit, Dynamic' step was performed by applying the mean wind loads as calculated by equation (4.1), however these loadings were applied continuously for a time history of 60 sec, thus a dynamic wind loading was created. This step was necessary for determining the displacement data which are needed in the self-excited loading formulas of Scanlan's method (Eq. 2.14). As given in section 2.3.3, the self-excited load formulas (Eq. 2.14) involve the data of vertical, lateral and torsional displacements of the bridge deck and their partial differentiation with respect to time. Those data are generally obtained from the wind tunnel experiment, however in the current research, the tests in the tunnel were simulated by numerical analysis in ABAQUS with an 'Implicit, Dynamic' step.

The vibration response at mid-span was selected for data extracting and further calculation, because, in terms of displacement, it was found that this is the most critical position of the entire main span. The displacement responses at mid-span under the lowest and highest wind loadings corresponding to the 35 m/s and 211 m/s mean wind speed are shown in the Figures 4.18 (a) and (b). The rest of the vibration responses determined for wind speeds of 70 m/s, 105 m/s, 141 m/s and 176 m/s are summarized in the Appendix C (Figs.C1 to C6) in spite of applying the same type of dynamic wind loading, but with a different magnitude, the responses at the mid-span differ in magnitude but in nature and period of the vibration, as it will be detailed later in this section.

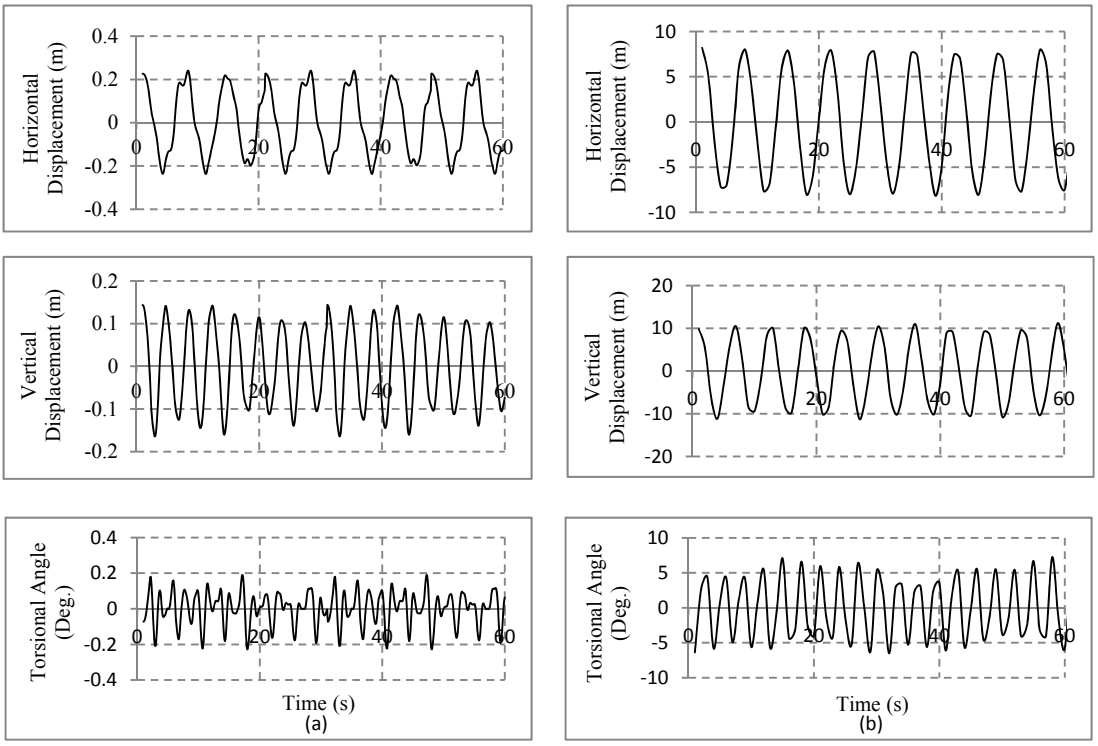

Figure 4.18: Vibration response at mid-span under mean wind load for (a)35 m/s. (b)211 m/s.

The average displacement at mid-span under all the wind mean speeds investigated are summarized in the Figure 4.19; these values are calculated from the average of the horizontal, vertical and torsional displacement peaks as presented in the response data of Figs. 4.18 (a) and (b) and Figs C1 to C6 in Appendix C.

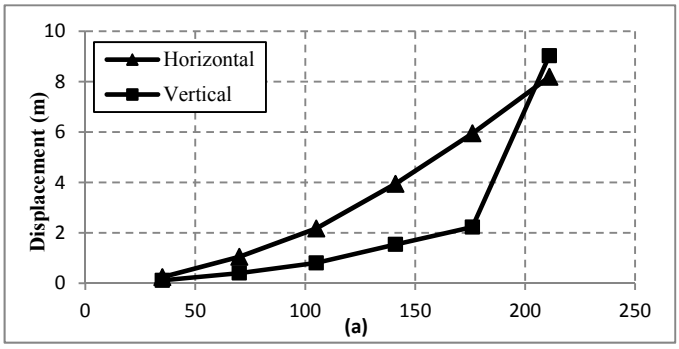

Figure 4.19 (a): Deformations at mid-span through the implicit, dynamic step. (horizontal and vertical)

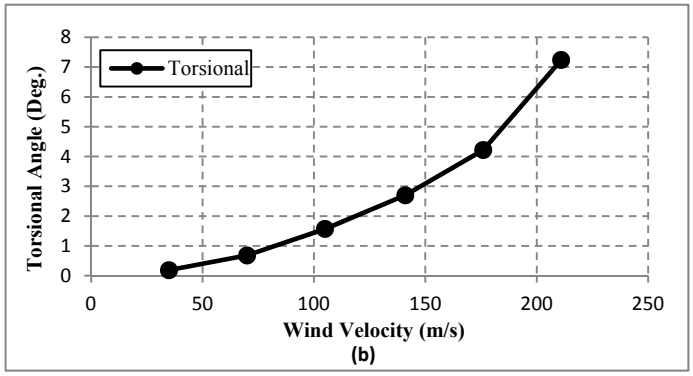

Figure 4.19 (b): Deformations at mid-span through the implicit, dynamic step. (torsional)

As expected, from Figure 4.19, it can be found that the average amplitude of vibrations increases gradually with the increase of the wind speed, especially the vertical response changed rapidly after 176 m/s wind velocity becoming even higher than horizontal displacement, thus reaching a value of 11.23 m at 211 m/s wind velocity. The horizontal displacement at 211 m/s wind velocity was 8.19 m and the torsional vibration was 7.24 degree. It should be mentioned that the 211 m/s is much beyond the maximum values registered for the extreme wind speeds in the Hong Kong region which were reported in [55].

In Figure 4.20, the results from the 'Implicit, Dynamic' analysis are compared with the results from the 'General, Static' step, and it could be noticed that the horizontal displacement has a similar evolution being slightly underestimated by the static analysis, however this remains the same therefore, the response in the horizontal direction dose not play a leading role in the vibration of the entire bridge deck The amplitudes of the vertical and torsional deformations however showed some obvious discrepancies between the static values and the time history .

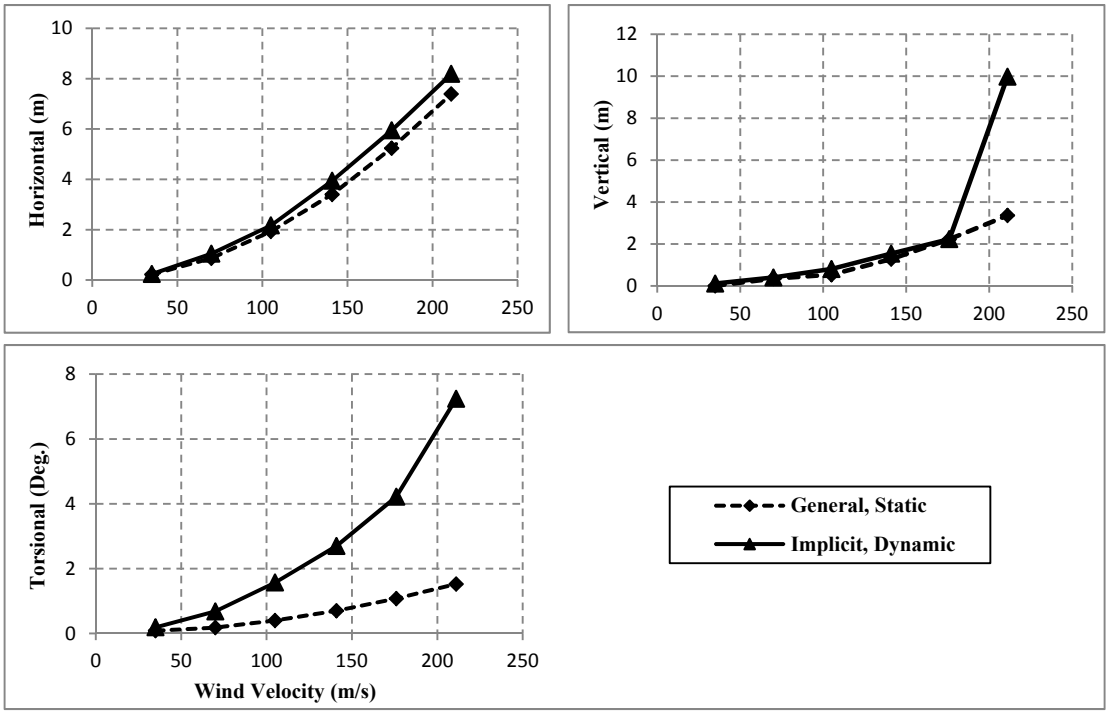

Figure 4.20: Difference of the responses at mid-span between 'General, Static' and 'Implicit, Dynamic'.

The vertical response for the 'Implicit, Dynamic' step, increase rapidly between 176 m/s and 211 m/s. The vibration frequency under the wind load at this moment may match the natural frequency for vertical mode, and then some coupling phenomenon could occur as it will be detailed in the sections below. The vibration modes coupling might represent the main reason that contributes to the sudden increase of the response, however in order to clarify the complex aerodynamic instabilities which might occur in this wind speed range, a further dynamic analysis employing the self-excited deck motion as part of the flutter analysis will be provided in the following sections.

Due to the torsional responses at mid-span, which are much larger than the values from the 'General, Static' step, especially for wind speeds of 100 m/s and higher, it could indicated that the torsional vibration mode may be the main shape of the vibration under such high

wind speeds, and could even lead to permanent damage of the bridge structure when reaching the critical wind velocity.

4.4 Flutter analysis

4.4.1 Flutter response at the mid-span of the bridge deck

The self-excited loads were calculated using the vertical, horizontal and torsional responses h, p and α respectively, obtained from the mean wind load static analysis and as per the Scanlan's self-excited loads formulas (Eq. 2.14), as presented in detail in Chapter 2. For the convenience of the readers, these formulations were recalled below (Eq. 4.2). By applying these self-excited lift and drag forces together with the torsional moment, along the vertical and horizontal bridge structural axes and as torsional motion around the horizontal axis, a complete simulation of the aerodynamic wind loading can be carried out.

$$L_{se}(t) = \frac{1}{2}\rho\bar{U}^2(2B)\left(KH_1^*\frac{\dot{h}}{\bar{U}} + KH_2^*\frac{B\dot{\alpha}}{\bar{U}} + K^2H_3^*\alpha + K^2H_4^*\frac{h}{B} + KH_5^*\frac{\dot{p}}{\bar{U}} + K^2H_6^*\frac{p}{B}\right)$$

$$D_{se}(t) = \frac{1}{2}\rho\bar{U}^2(2B)\left(KP_1^*\frac{\dot{p}}{\bar{U}} + KP_2^*\frac{B\dot{\alpha}}{\bar{U}} + K^2P_3^*\alpha + K^2P_4^*\frac{p}{B} + KP_5^*\frac{\dot{h}}{\bar{U}} + K^2P_6^*\frac{h}{B}\right) \quad (4.2)$$

$$M_{se}(t) = \frac{1}{2}\rho\bar{U}^2(2B^2)\left(KA_1^*\frac{\dot{h}}{\bar{U}} + KA_2^*\frac{B\dot{\alpha}}{\bar{U}} + K^2A_3^*\alpha + K^2A_4^*\frac{h}{B} + KA_5^*\frac{\dot{p}}{\bar{U}} + K^2A_6^*\frac{p}{B}\right)$$

Figure 4.21 shows the dynamic loads in horizontal, vertical and torsional directions applied on the Stonecutters Bridge deck under the 35 m/s wind velocity, determined as per the equation 4.2 above. The time history of the dynamic loadings determined for the wind

speeds of 70 m/s to 211 m/s can be found in the Appendix C (Figs.C4 to C6).

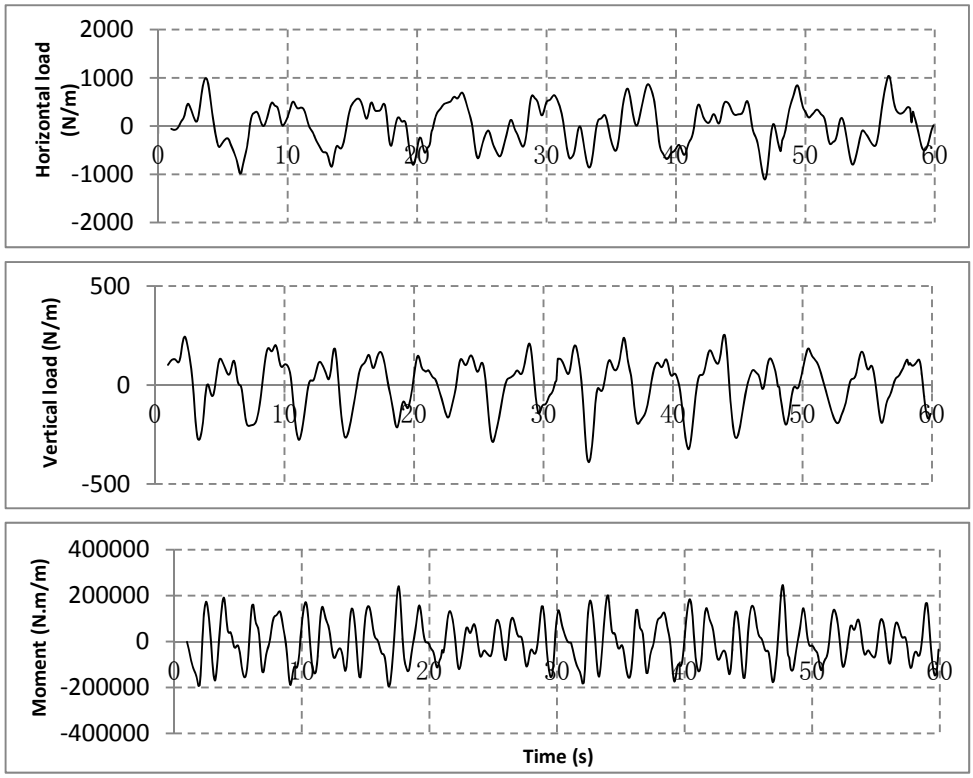

Figure 4.21: Dynamic loads applied on the Stonecutters Bridge deck. (35 m/s)

As the most critical point in terms of displacement is estimated to be the middle of the span, first the vertical and torsional responses at the mid-span of the Stonecutters Bridge FE model are determined under the dynamic wind loading and self-excited motion effect. The vibration responses for 35 m/s and 70 m/s wind speeds are shown in the Figures 4.22 (a) and (b) as follows. For both wind speeds, very low amplitudes of vertical and torsional vibrations could be noticed, moreover the diverging response, as the sudden increase of the vibration towards the end of the loading interval, was not noticed, therefore it can be concluded that no flutter aerodynamic instability would occur for the Stonecutters bridge FE model under 30 m/s and 70 m/s wind speeds.

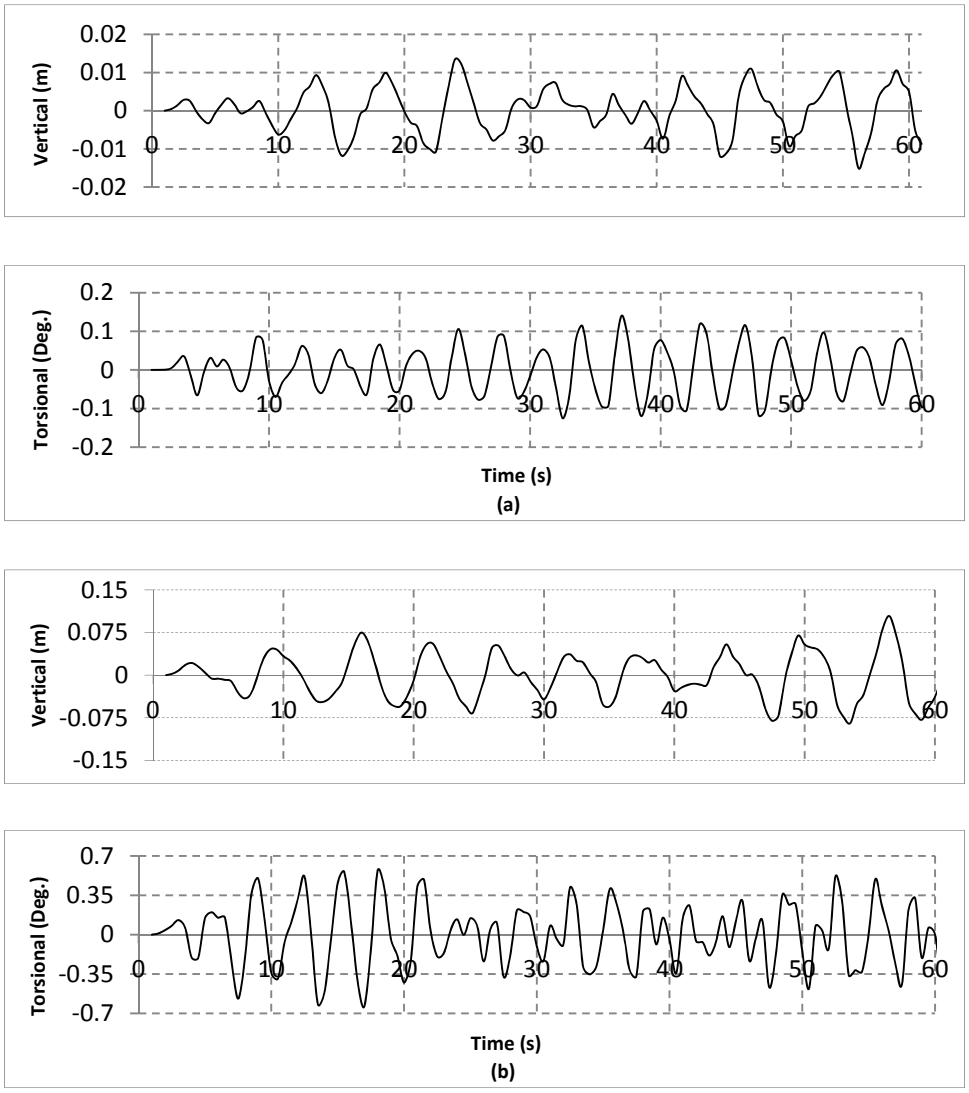

Figure 4.22: Flutter response at mid-span under self-excited loads for (a) 35 m/s. (b) 70 m/s.

Figure 4.23 shows the flutter responses for 141 m/s and 176 m/s wind velocity. It should be noted that the torsional response at mid span changes its characteristics from a small amplitude random response, which was noticed in Figures 4.22, to a high amplitude divergent response when the wind velocity increased above 100 m/s. Finally, the divergence phenomenon fully occurs between 141 m/s and 176 m/s when also the coupling of the vertical and torsional directions can be proved start to occur at this moment; hence it can be concluded that such divergent amplitude associated with the coupling between the vertical

and torsional responses represent a more concrete indication of the flutter instability occurrence.

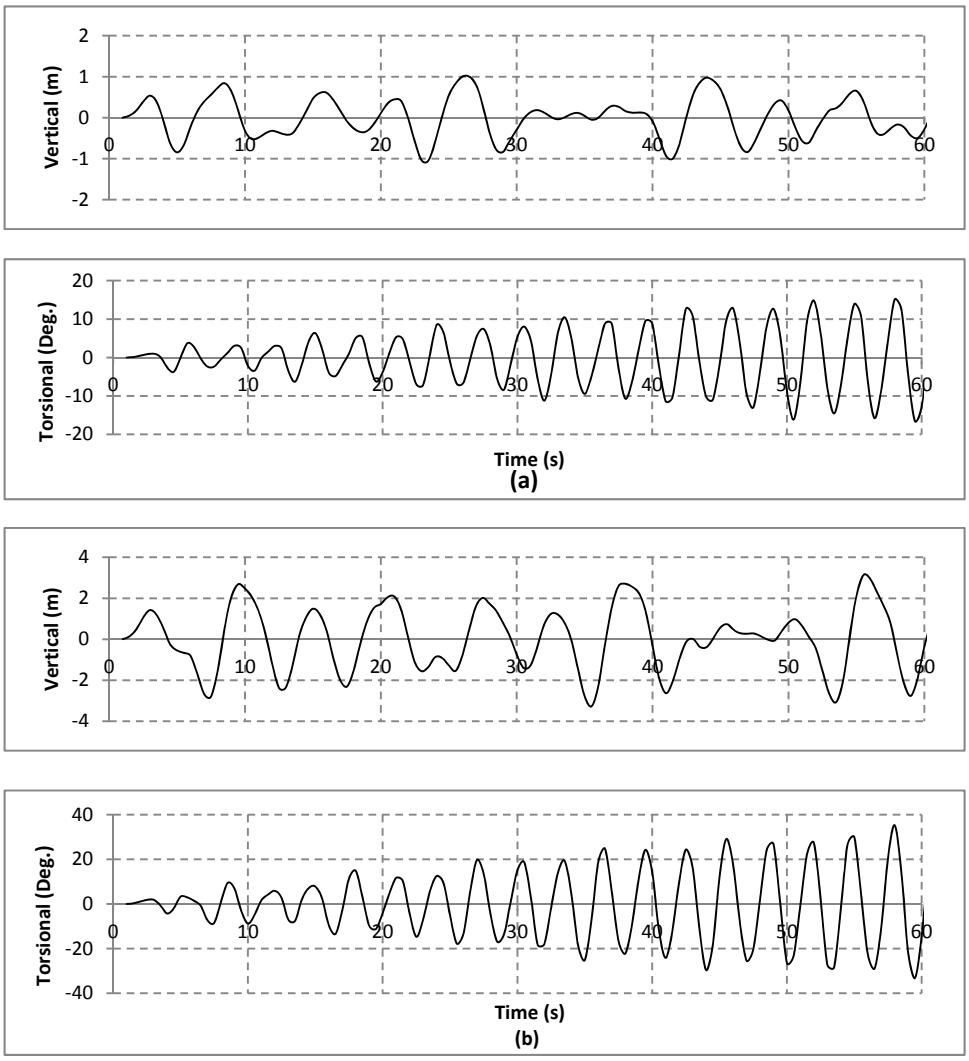

Figure 4.23: Flutter response at mid-span under self-excited loads. (a)141 m/s. (b)176 m/s.

A similar method as employed for the Figures 4.19 and 4.20 were used for averaging and summarizing the deformations at the mid-span under different dynamic wind speeds. The major peak values were selected to determine the mean value of the displacement for along the vertical and the torsional directions. Deformations at mid-span under different dynamic

wind speeds are shown in Figure 4.24.

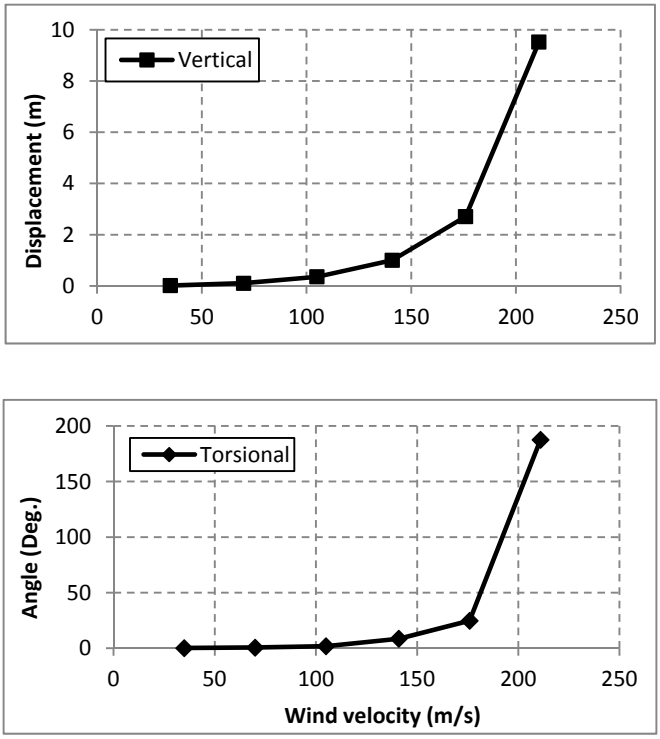

Figure 4.24: Deformations at mid-span under different flutter wind loads.

From the variation of the response at the mid-span, it could be found that the values for both vertical and torsional displacement increased with the wind velocity, registering high vertical response of 2.7 m and a torsional response of 24 degrees and changed rapidly from 176 m/s, and it can be considered as a critical wind speed. Above the 176 m/s, the vertical and torsional vibrations showed extreme magnitudes 9.5 m and 185 degrees which are not acceptable and clearly indicate the potential failure of the Stonecutters Bridge. Thus the results from the mean wind load analysis obtained in the previous section are re-confirmed by the flutter analysis.

4.4.2 Flutter response of deck girder near the tower

The most critical point of the bridge deck is considered to be at the mid-span location where the maximum static and dynamic displacements were reported above, however other points around the main deck were also investigated. The responses of the bridge deck in the vicinity of the tower were determined under the effect of the self-excited loads. The nodes where the response was estimated are located on the main steel deck, but in the Stonecutters Bridge FE model there are several constrains between the tower and the deck girder which simulate the hydraulic buffer connecting the tower with the deck girder. The properties of the hydraulic buffer connection around the tower were employed as recommended by Atsushi Kaji, et al. (2010) [7] as represented in the Figure 4.25 [7].

Figure 4.25: Hydraulic buffer connection between the tower and the girder deck [7]

The response of deck girder in the vicinity of the tower are affected by the flutter loads for very high wind velocity, but some of the kinetic energy absorbed from wind flow will be transferred to the tower in the same time. In addition, due to the foundation at the ground under the sea level, and due to the tension effects in the stay cables, the towers have more stiffness in vertical and torsional directions. Therefore, the response at deck girder in the vicinity of the tower is accepted to be different from the mid-span response. Thus the

response at the deck location in Stonecutters Bridge FE model as shown in Figure 4.26 was investigated under the flutter loadings conditions.

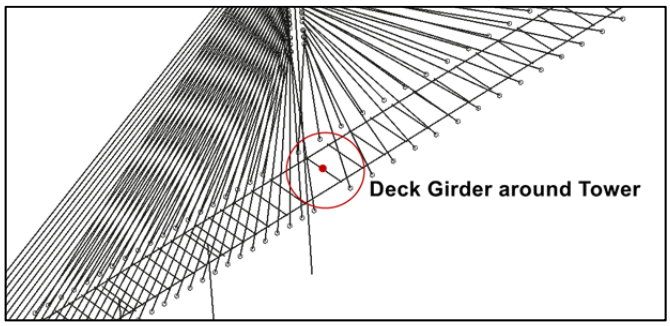

Figure 4.26: Location of the deck girder node in the vicinity of the tower in FE model.

The vertical and torsional responses of the deck girder near the tower for 35 m/s and 176 m/s are shown in the Figure 4.27. The responses for the other wind velocities are shown in the Appendix C (Figs. C13 to C18). For the lower wind speeds of 35 m/s, no major amplitudes could be noticed for the vertical and for the torsional vibrations while the motions are random in nature, but not diverging. For 176 m/s however the response raised in magnitude for both vertical and torsional vibrations, even though these are smaller than the magnitudes registered at the mid-span for the same wind speed. The divergent tendency towards the end of the loading period can be also noticed.

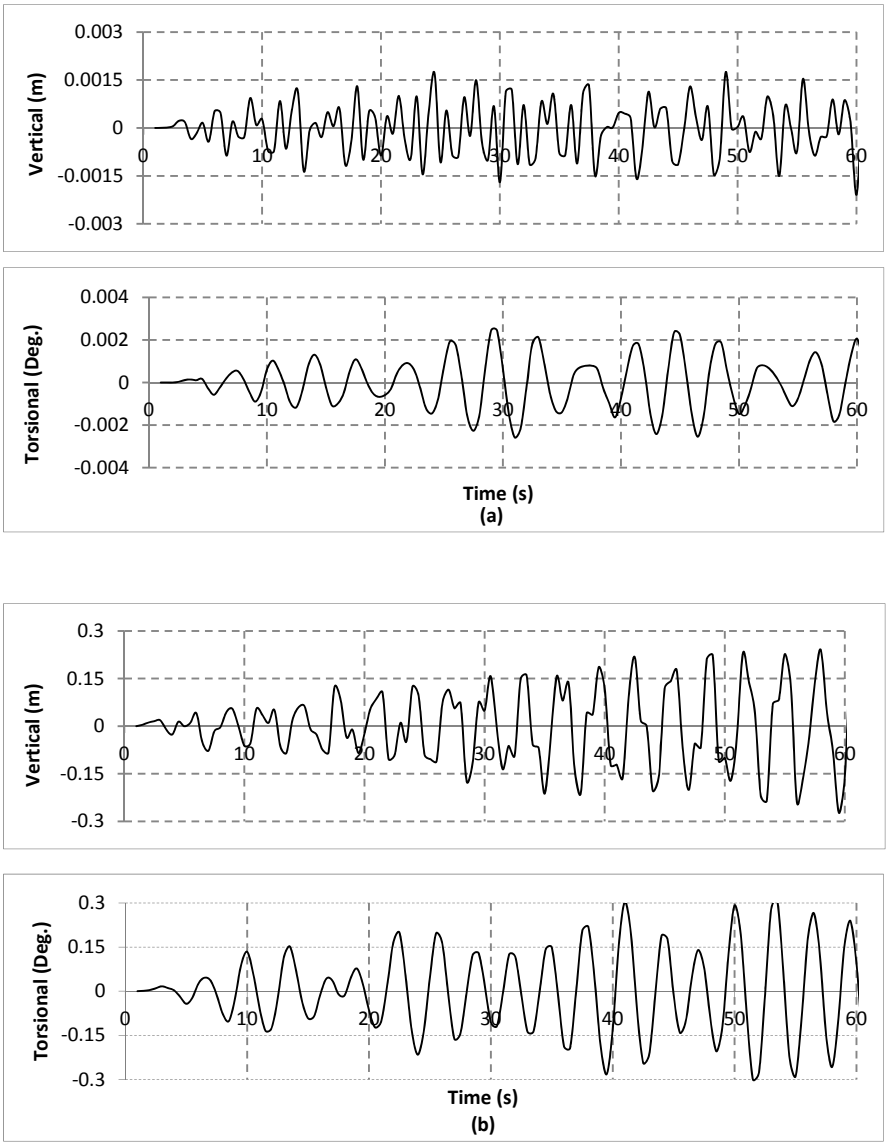

Figure 4.27: Vibration response at deck around tower under self-excited loads for (a) 35 m/s. (b) 176 m/s.

The mean value of the peak displacements along the vertical and torsional directions at different wind velocity are summarized in the Figure 4.28, and it could be found that the values of both vertical and torsional displacement increased and changed rapidly from 176 m/s, which is in good agreement with the vertical and torsional displacements reported for the mid-span location.

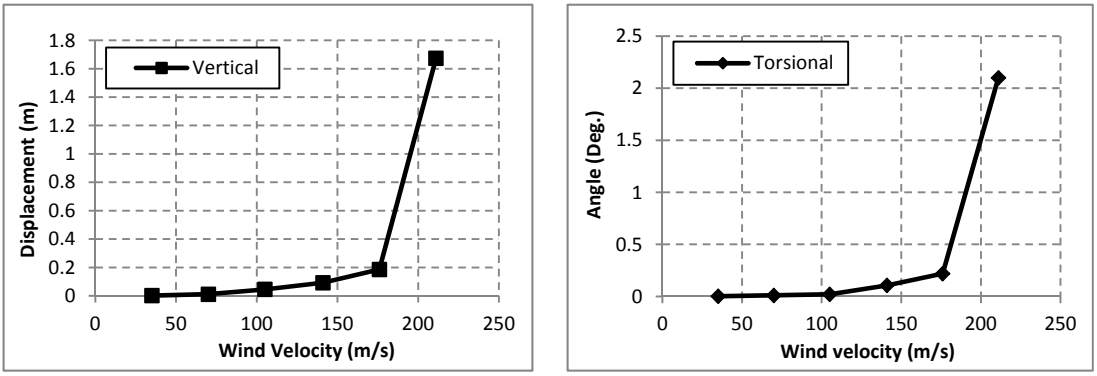

Figure 4.28: Deformations at deck around tower under different dynamic wind speeds.

Moreover, the vertical responses start at a very low level and the magnitude of vibration do not increase significantly even at a very high wind velocity. For wind speeds of 211 m/s, the vertical displacement is only about 1.7 m which is much smaller than the response at mid-span, while the torsional angle is very high, of up to 65 degrees, indicating a potential failure in torsion.

4.4.3 Flutter response of the concrete back-span deck girder

Besides the responses at mid-span and deck girder near the tower, the dynamic responses around for the connection between the main-span and the concrete back-span are also determined, which are unpredictable because of the effect of the initial conditions and the different structure properties of concrete back-span (Fig. 4.29 (a)) [7] The exact location of the node monitored in the FE model is represented in Figure 4.29 (b).

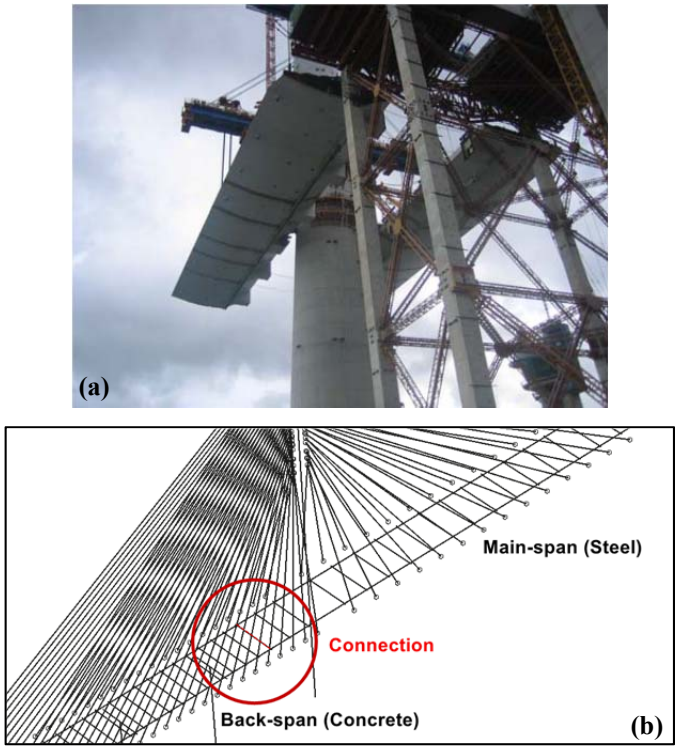

Figure 4.29: Connection between steel main span girder and concrete back-span. [7]

The vertical and torsional responses of deck girder near the span connection at 35 m/s and 70 m/s are shown in the Figure 4.30 as follows. The responses of other cases at different wind velocity are shown in the Appendix C (Figs. C25 to C30).

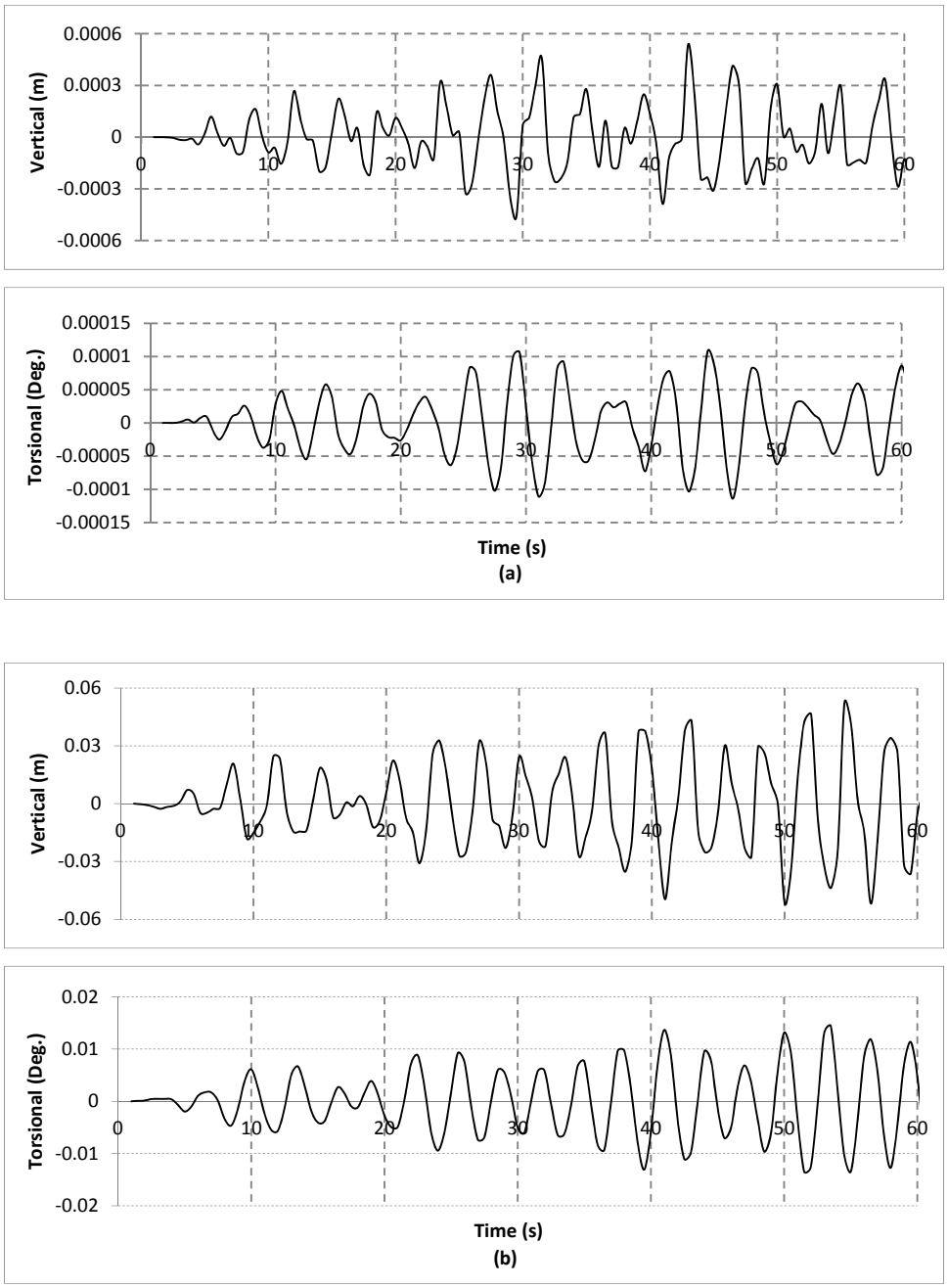

Figure 4.30: Vibration response at deck around span connection under self-excited loads for (a) 35 m/s. (b) 176 m/s.

The mean values of the displacements peaks for the vertical and torsional directions at different wind velocity summarized in the Figure 4.31 re-confirmed the critical wind speed

of 176 m/s beyond which both the vertical and the torsional displacements increases rapidly.

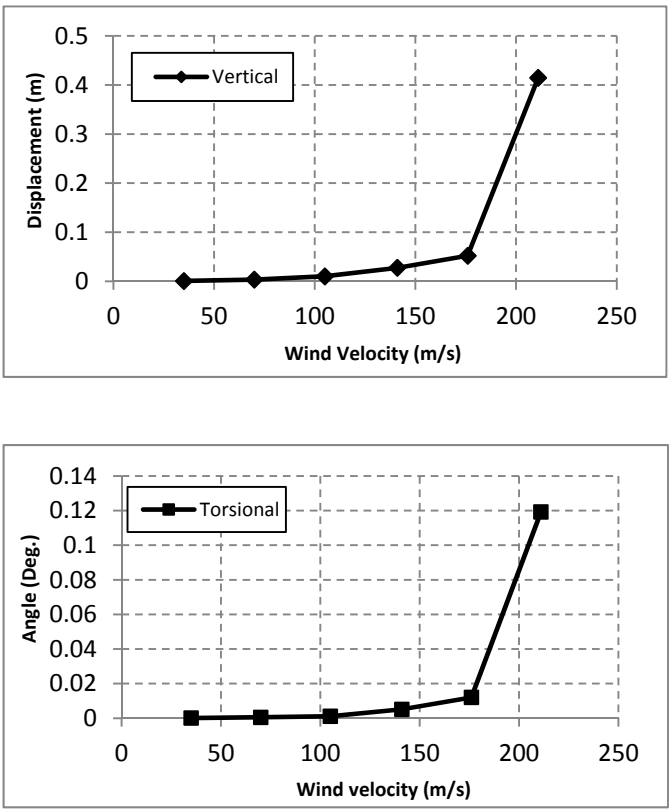

Figure 4.31: Deformations at span connection under different dynamic wind speeds.

The amplitudes of the vertical deformation for the span connection at a high wind velocity are very small, registering values of only 0.42 m at 211 m/s while the torsional angle at 211 m/s is only 0.12 degrees. Therefore it can be concluded that the flutter instability does not affect the concrete back-spans, which are simply supported.

4.4.4 Dynamic response of the tower-top under deck flutter conditions

The first bending frequencies of the towers of the Stonecutters Bridge model were reported to be very close to the first natural frequencies of the main span (Table 4.2) and thus the

responses of the top of the tower, under the effect of the self-excited loads are also determined. The vertical and the torsional responses of tower-top at 35 m/s and 176 m/s are shown in the Figure 4.32 as follows. The responses of other cases obtained for different wind velocity are summarized in the Appendix C (Figs. C19 to C24).

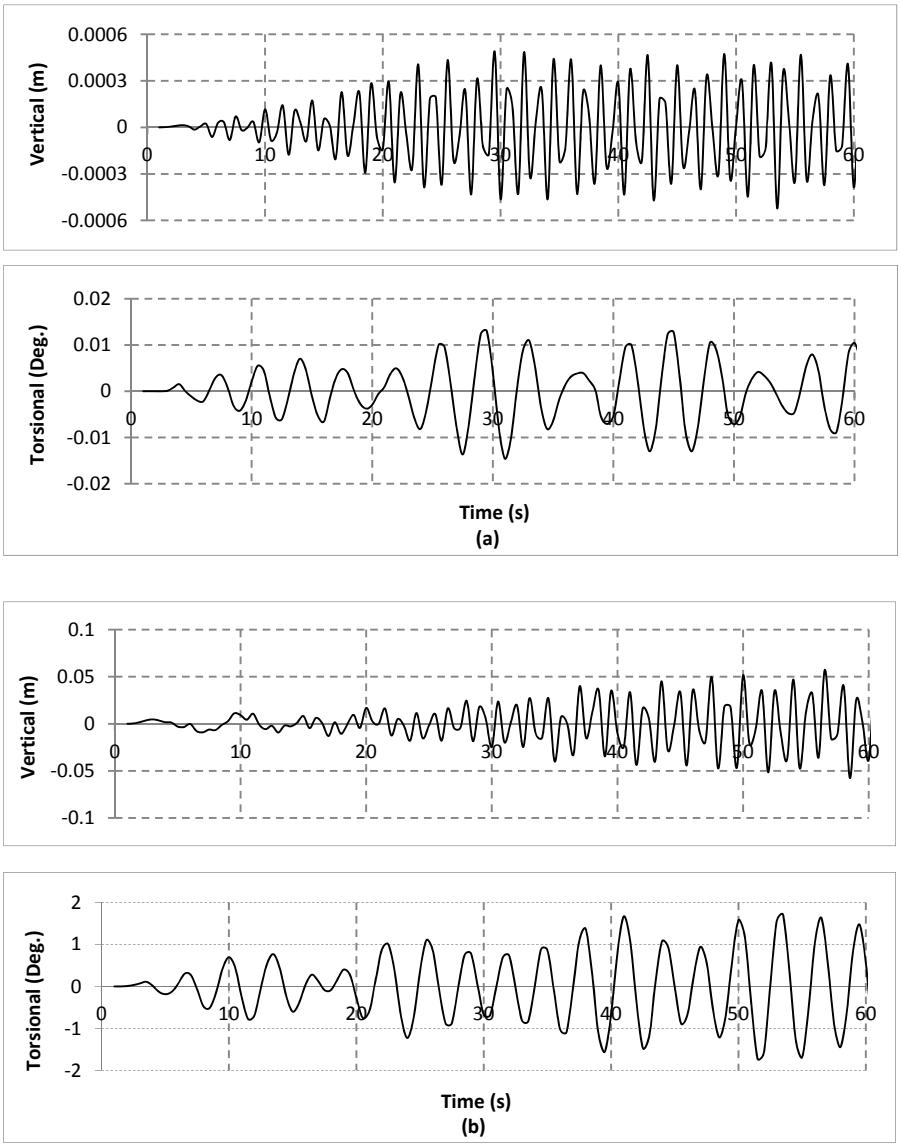

Figure 4.32: Vibration response at tower-top under self-excited loads. (a) 35 m/s. (b) 176 m/s.

The mean value of the several peak displacements along the vertical and torsional directions

at different wind velocity are summarized in the Figure 4.33 show that the values of the vertical displacement of the tower-top increased with the increase of the wind speed but it changed rapidly after 141 m/s, which is earlier than the critical flutter velocity of 176 m/s reported for the main deck. However the amplitudes of the vertical vibrations achieved at very high wind velocity are very small of only 0.043 m at 211 m/s.

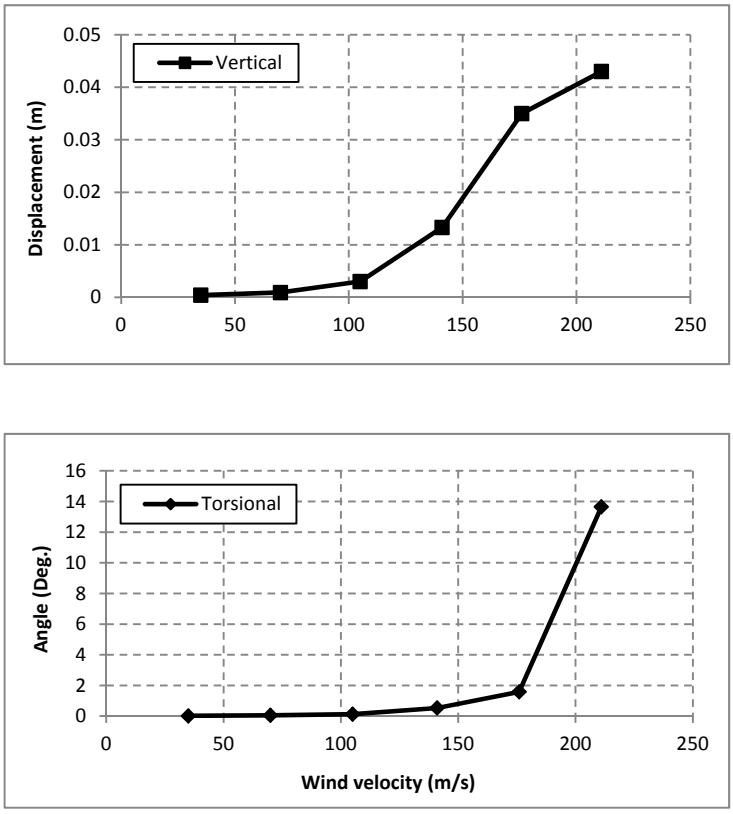

Figure 4.33: Deformations at top of tower under different dynamic wind speeds.

The angle representing deformation given by the torsional vibration is smoothly increasing before 176 m/s reaching very small values of only 1.58 degrees. Beyond 176 m/s however, the torsional amplitudes increased suddenly up to 13.65 degrees at 211 m/s. The evolution of torsional deformation curve indicates that the tower of the Stonecutters Bridge FE Model performs a swinging vibration mode in the horizontal direction.

4.4.5 Flutter response summary

In order to identify the main differences in the responses registered for the mid-span, near the tower, on the concrete span connection and at the tower-top, the vertical and torsional averaged amplitudes of vibrations under the effect of flutter conditions are summarized in Figure 4.34.

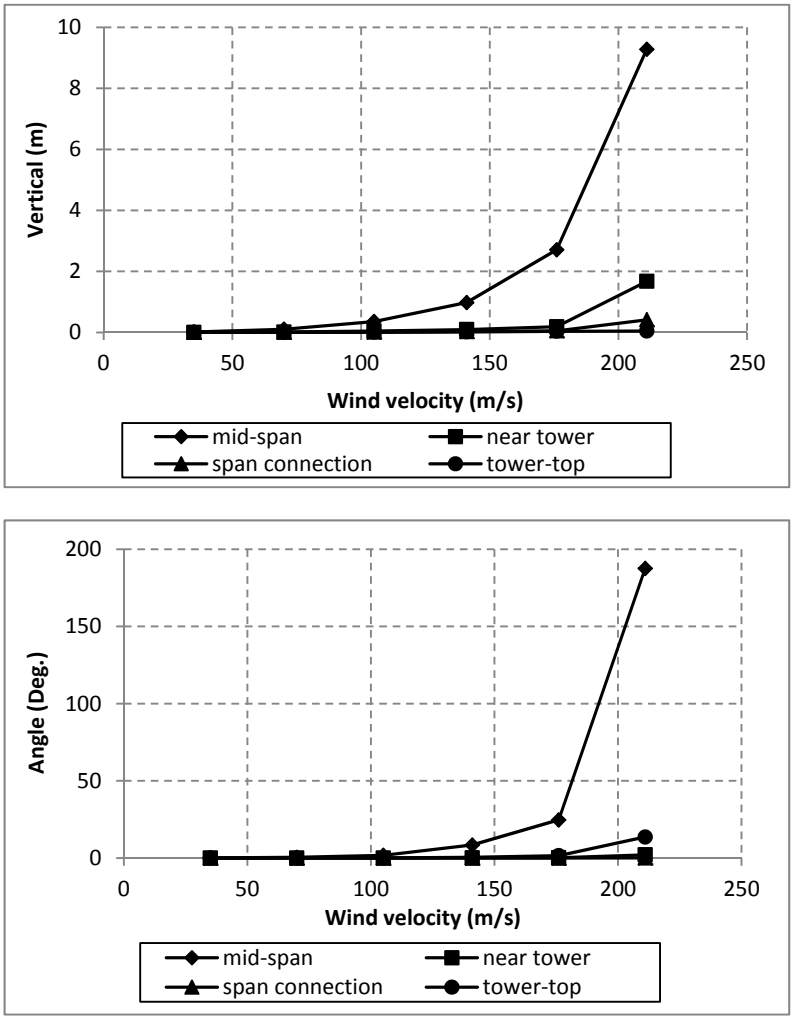

Figure 4.34: Response average for mid-span, near the tower concrete span connection and the tower-top.

As expected the evolution of the vertical and torsional responses for the four locations investigated curves are similar, however they differ in magnitude; they all start at a small value for smaller wind speeds and then increase rapidly after 176 m/s wind velocity. The girder structure at the mid-span is more prone to structural instability than the girder deck in the vicinity of the tower and for the other two positions on the concrete back-span and the top of the tower. The responses around the concrete span connection are smallest in the torsional direction because of the effect of the initial conditions and due to the high stiffness of the concrete simply supported back-span. The top of the tower has a higher torsional deformation than the span connection and girder near the tower, but this is much smaller than deformation at the mid-span. For the responses in the vertical direction could be observed that the Stonecutters Bridge FE model has good bending capacity for the tower-top, the back span and the girder near the tower, for the mid-span location.

4.5 Frequency analysis through Fast Fourier transform

4.5.1 Results from the FFT

In order to determine the flutter frequency and the critical wind velocity associated with this, the Fast Fourier Transform code of MATLAB was used for extracting the energy content from the structural vertical and torsional responses of the Stonecutters Bridge FE model. The MATLAB codes used for the FFT transform are shown in Appendix D. Figure 4.35 shows the results of the FFT calculation under the 35 m/s and 70 m/s. For the rest of the investigated cases the FFT frequency results are presented in Appendix D, Figure D1.

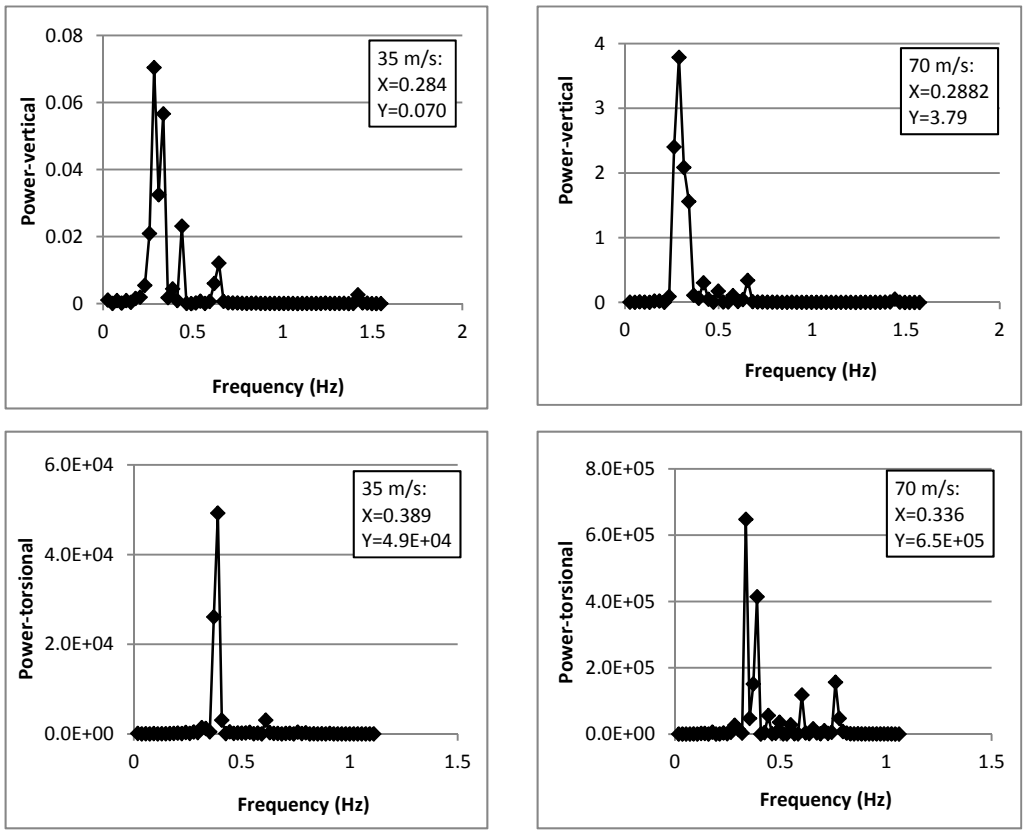

Figure 4.35: Results from FFT program. Left: 35 m/s. Right: 70 m/s.

The dominant frequency under different wind velocities can be observed clearly from the peak values of the FFT results (Fig. 4.35 and Appendix D). For instance, when the bridge is subjected to the dynamic wind loading corresponding to 35 m/s, it can be found that the dominant frequency of the vertical response at mid-span is 0.284 Hz, and for torsional response is 0.389 Hz. The vertical frequency is 0.288 Hz and the torsional frequency is 0.336 Hz for 70 m/s wind velocity.

4.5.2 Critical state extraction

By employing a similar FFT procedure, the dominant frequencies for all the cases

performed in vertical and torsional directions are determined and are summarized in Table 4.9 and Figure 4.36.

Table 4.9: Dominant frequencies from FFT analysis.

Wind Velocity (m/s)	Vertical Frequency (Hz)	Torsional Frequency (Hz)
35	0.2836	0.3888
70	0.2882	0.3360
105	0.2893	0.3159
141	0.2955	0.3002
176	0.2982	0.3020
211	0.2991	0.3089

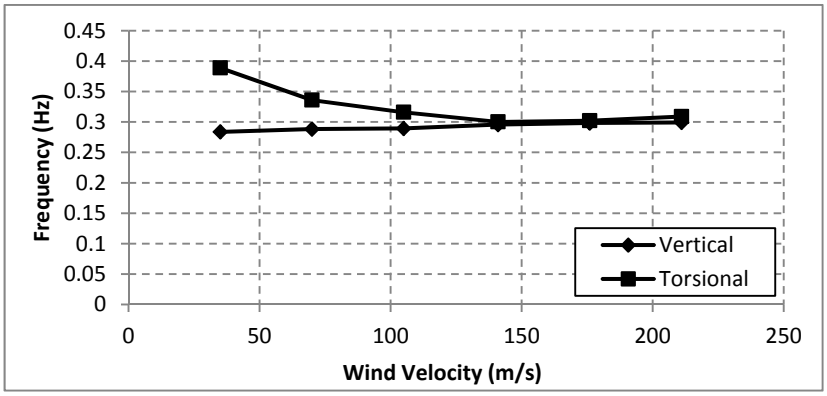

Figure 4.36: Variation of the dominant frequencies with the wind velocity.

From Figure 4.36, it can be found that the torsional dominant frequency starts at a high level under a lower wind speed and then decreases gradually with the increase of the wind speed changing from 0.3888 Hz to 0.3089 Hz. The vertical frequency however does not change significantly remaining around the value of 0.3 Hz for the entire wind speed interval of 35 m/s to 211 m/s.

The phenomenon of loss the stability due to aerodynamic phenomena occurs when the values of the vertical frequency and the torsional frequency become closer and finally

intersect. Because when these two frequencies approach the same value, the coupled vibration modes become apparent, and this can cause serious damage to the bridge structure. When these two curves intersect each other, the amplitude of the motion for the vibration mode shape indicated at that specific wind speed reaches the maximum value. Hence, the critical wind speed and flutter frequency can be estimated for this intersection point.

Therefore, from the results presented in the Figure 4.36, finally it can be concluded that the critical wind speed for the Stonecutters Cable-stayed Bridge is about 176 m/s and the flutter frequency at this point is 0.3 Hz. But before the critical state is reached, the bridge structure already registers high vertical and torsional motion amplitudes and it cannot be considered safe enough for traffic. Therefore, from the Figure 4.36, it can be assumed that the 141 m/s is the incipient onset flutter wind speed, and the vertical frequency at this point is 0.2995 Hz, while the torsional frequency is 0.3002 Hz. However these values need to be proved in the further calculation.

4.6 Results validation

Comparing with the data existing already in the literature from wind tunnel experiment, it can be seen that the critical wind speed and flutter frequency of Stonecutters Bridge FE model developed are very close to the data reported for similar models of the Stonecutters Bridge in wind tunnel, which are summarized in Table 4.10 as follows.

Table 4.10: Results comparing between Stonecutters FE model and other published data.

	Flutter Frequency (Hz)	Critical Wind Speed (m/s)
M. C. H. Hui, et al. (2006) [17]	0.331	230.4
W. Qiu and Z. Xu (2008) [56]	0.297	215.5
Stonecutters FE Model (current)	≈0.3	≈176

The critical wind speed predicted by the Stonecutters Bridge FE model is smaller than others but differences in the wind speed are of 13.2% and 7.2%, respectively. The flutter frequency is smaller than the result from Hui et al (2006) [17] and larger than value from W. Qiu and Z. Xu, (2008) [56]; the frequency errors are very small though namely -9.3% and 1.0%, respectively. The critical flutter wind speed for the Stonecutters Bridge FE model is smaller than the published data for the same bridge. because the FE model simulates the elementary structure without taking into account the wind shields and other wind countermeasures accessories, hence, the properties of the bridge deck are slightly different from the real bridge.

In 1976, an onset flutter critical wind speed formula was summarized by Van der Put [57] as follows, and it is well known by its simplicity and convenience.

$$U_{cr} = \left[1 + (\varepsilon - 0.5)\sqrt{\left(\frac{r}{b}\right) \cdot 0.72\mu}\right] \cdot \omega_h b \qquad (4.4)$$

Where, $\varepsilon = \frac{\omega_\alpha}{\omega_h} = \frac{f_\alpha}{f_h}$, ω_α and ω_h are the resonance frequencies of torsion and bending of the bridge deck in rad/s respectively; f_α and f_h are the cycle frequencies in *Hz*. And $\mu = \frac{m}{\pi \rho b^2}$, is the mass ratio in respect to the air properties;

$\frac{r}{b} = \frac{1}{b} \cdot \sqrt{\frac{I}{m}}$, is the ratio of the inertia radius to the half width of the bridge deck.

I: Moment of inertia per unit length;

m: Mass density of the bridge deck;

ρ : Air density;

Table 4.11: Parameters in Van der Put critical wind speed formula.

	m (kg/m)	$I\ (kg \cdot m^2/m)$	ρ (kg/m^3)	$f_\alpha\ (Hz)$	$f_h\ (Hz)$	ε
Stonecutters FE model	20,488.3	6.32 e+06	1.225	0.324	0.172	1.88
Stonecutters real bridge [7]	32,600	9.27 e+06	1.225	0.324	0.172	1.88

In order to apply the Van der Put formulation several structural properties of the bridge deck are required. Table 4.11 summarizes all the parameters of the Stonecutters FE model needed in the Eq. 4.4, in addition, the mass density and the moment of inertia of the real Stonecutters Bridge [7] are also shown. The mass density and the moment of inertia of the Stonecutters FE model are different from the real bridge data, because the FE model presents the elementary simplified structure of the deck without any deck pavement or other accessory elements, while the real data are from the completed Stonecutters Bridge structure.

Applying the Eq. 4.4 and considering the FE model parameters given in Table 4.11, critical flutter wind speed for the Stonecutters model was found to be U_{cr} =131.4 m/s; if the parameters of FE model are used in the same formula (Eq.4.4) but with the mass density and moment of inertia given for the real Stonecutters Bridge [7] then the critical flutter speed is U_{cr}=155.4 m/s.

In addition, the onset critical wind speed was mentioned by K. Qiu and Z. Sun (2011) [58] in their studies determined based on the simplified formula for estimating the critical flutter wind velocity. They reported that the onset critical wind speed of Stonecutters Cable-stayed Bridge is 140 m/s and also they provided a simplified formula of critical flutter wind velocity for a bridge with separated steel box girder:

$$U_{cr} \approx 76.9 \times \frac{B}{\sqrt{L}} \qquad (4.5)$$

Where, B is the width of the bridge deck and L is the length of the main span. For the Stonecutters Bridge, B=53.3 m, L=1018 m, hence, the onset flutter wind speed can be determined by the equation above (Eq. 4.5) as U_{cr}=128.5 m/s. The values of the onset and critical flutter speed obtained by different formulations are indicated on the frequency response graph obtained for the Stonecutters FE model (Figure 4.37). The fifth and the third dotted lines represents the flutter critical and onset wind speeds obtained through the flutter analysis, the fourth and the second dotted lines represent the critical flutter velocities obtained through the general formulation (Eq. 4.4) and the bridge structural properties represented in Table 4.11 and finally the first dotted line represents the onset flutter velocity determined based on Eq. 4.5 as a simplified formulation applicable to twin-deck bridges.

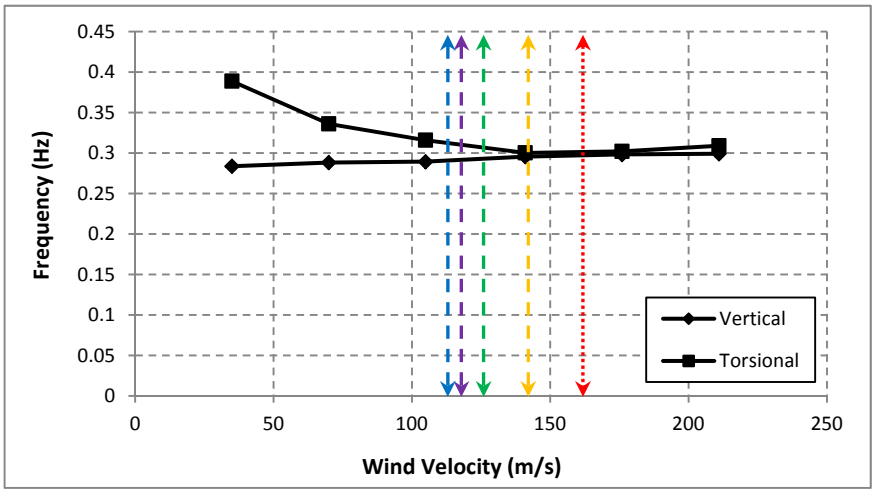

Figure 4.37: Summarized onset flutter wind speed and critical flutter wind speed.

The critical flutter wind speed and onset flutter wind speed are summarized in the Table 4.12 as below.

Table 4.12: Summarized onset flutter wind speed and critical flutter wind speed.

Onset flutter wind speed (m/s)		Critical flutter wind speed (m/s)	
FE model-Van der Put	131.4	Stonecutters FE model	176
Real bridge-Van der Put	155.4	M.C.H. Hui, et al. [17]	230.4
Published data [58]	140	W. Qiu and Z. Xu [56]	215.5
Simplified formula [Eq.4.5]	128.5		

In Hong Kong, the maximum wind speed for which the Stonecutters Bridge is designed to resist is 95 m/s, and this study proved that both the critical flutter wind speed and onset flutter wind speed determined based on the FE Model developed for the Stonecutters Bridge are larger than the requirement values. Moreover the wind speeds collected at two different sites in Hong Kong are summarized in Table 4.13 [55] and show that maximum wind speed registered for a return period of 200 years was 53 m/s which is much lower than the 142 m/s and 176 m/s as the flutter onset and critical wind velocities determined in this thesis. Hence, due to the bridge structure itself, it can be proved that Stonecutters Cable-stayed Bridge has a very good performance in aerodynamic stability and its separate twin-box steel girders are very good configuration for improving the capacity of resisting high wind speeds.

Table 4.13: Observation wind data in Hong Kong [55]

Location	Return Period (years)	Maximum Hourly Wind Speed	
		knots	m/s
Waglan	50	85	44
	100	94	48
	200	103	53
Hong Kong Observatory	50	80	41
	100	87	45
	200	95	50

4.7 Bridge response under natural wind data

The static, dynamic and flutter analyses describe very well the critical conditions and the maximum velocities for flutter instability, however these are still theoretical formulations, which do not take into account the turbulent nature of the wind speed. For determining the fluctuating wind effect on the response of the long-span bridges, usually the buffeting analysis is performed; however this is beyond the scope of the current thesis. Instead a measured natural wind speed data was employed for determining the wind loadings on lift, drag and torsional directions. These loadings were applied to the Stonecutters Bridge deck FE model and the responses at several locations along the main span were estimated. The responses for the top of the tower and the bridge deck near the connection with the tower were very small and were summarized in Appendix E, only the responses at one third (339.3 m) and at the half (509 m) locations along the main span of length 1,018 m were discussed below because these developed the highest response amplitudes.

4.7.1 Response of the bridge at mid-span under the wind data

The vibration responses at mid-span are extracted as shows in the Figure 4.38.

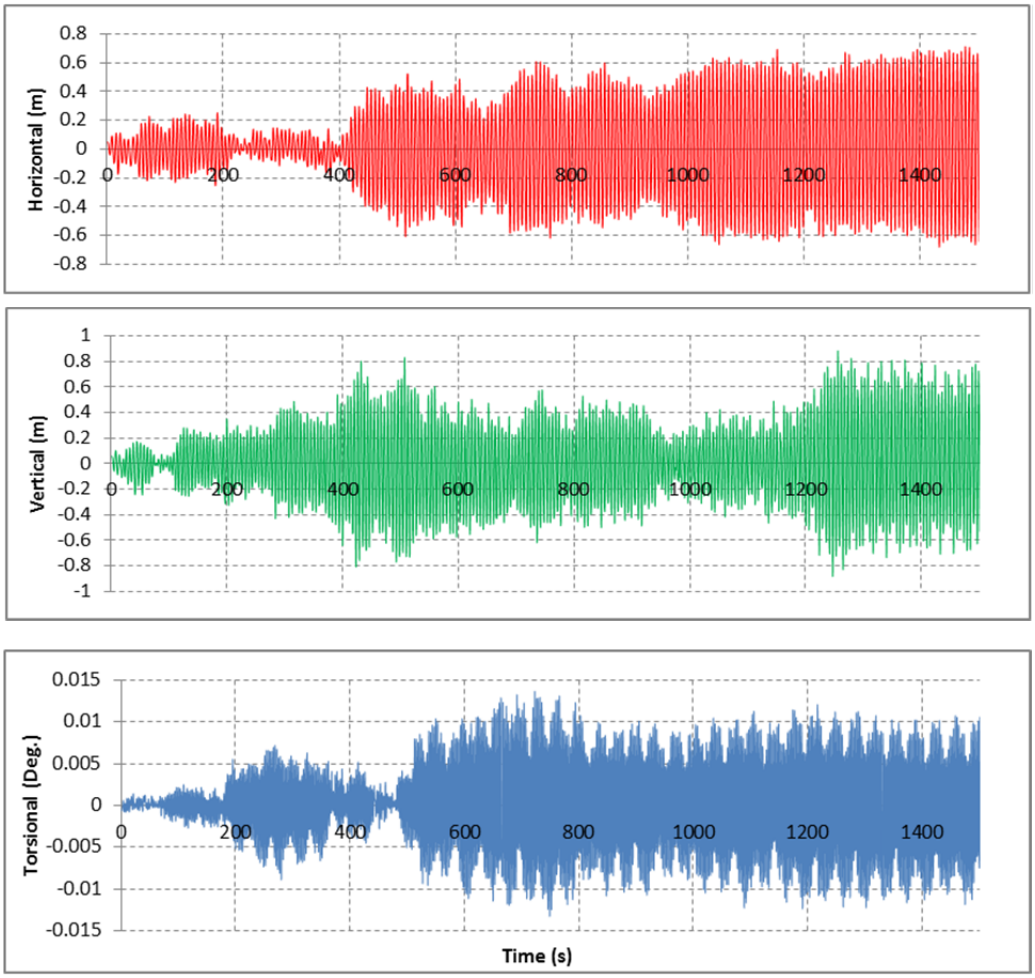

Figure 4.38: Bridges responses at mid-span under natural wind data.

The horizontal and torsional responses increased significantly with the increase of the wind speed, while for the vertical response attenuation was noticed during the loading interval, however this increased immediately after. The maximum horizontal displacement at mid-span is 0.710 m and the averaged amplitude of all peaks is 0.441 m. The maximum vertical displacement is 0.882 m while the average was recorded at around. The maximum torsional angle is 0.014 degrees, which was very close to the average torsional response of 0.010 degrees.

The horizontal, vertical and torsional vibration responses at one third location along the

main span (at 339.3 m) are shown in Figure 4.39. These responses registered smaller values then the response at the mid-span, but respected the same evolution, which is very important, because it proves that these respond together to the applied loading. The maximum horizontal displacement at 339.3 m of the main span is 0.578 m which is much higher than the average of the peaks which is 0.393 m. The maximum vertical displacement is 0.820 m, while the average of the peaks is 0.412 m. The maximum torsional response is 0.012 degrees and the average of peaks is 0.009 degrees.

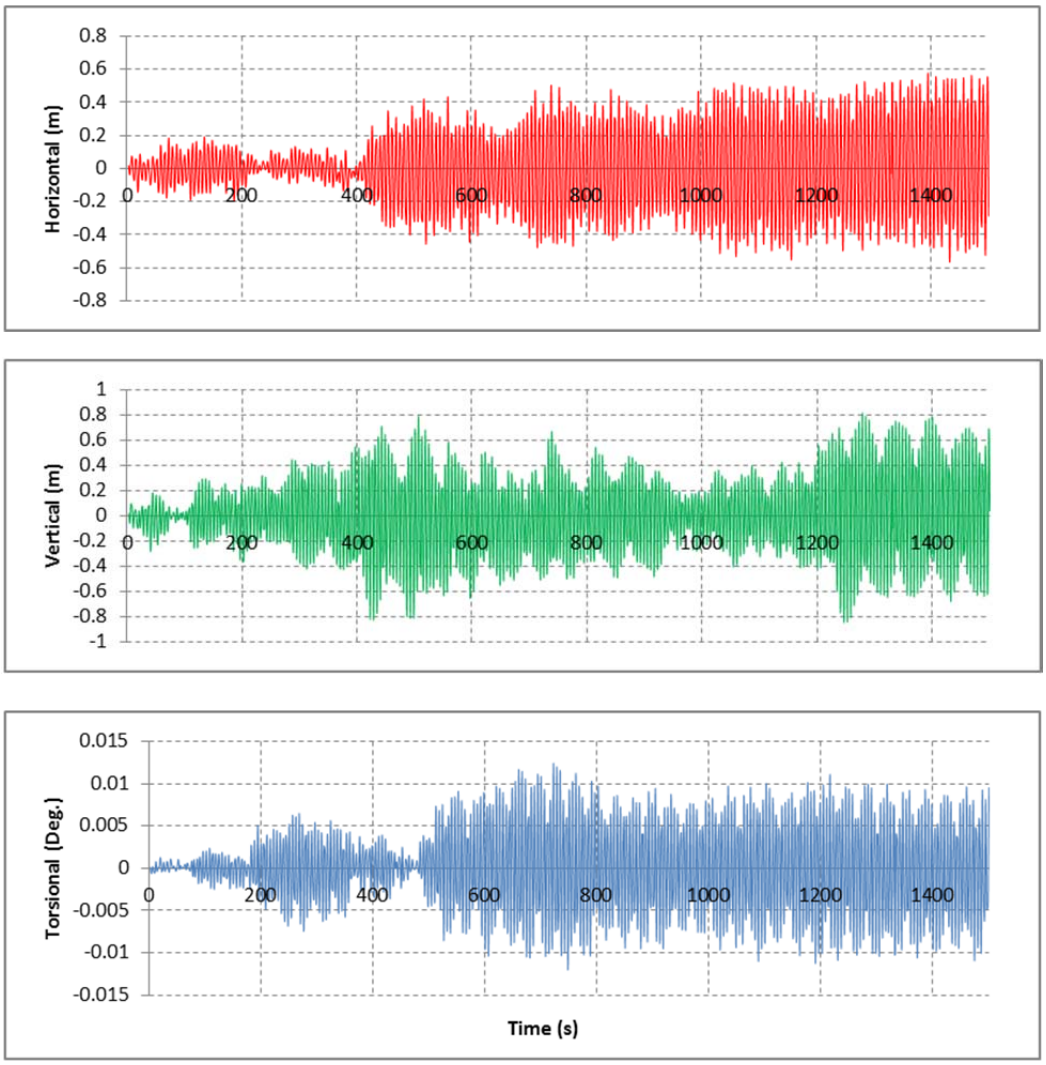

Figure 4.39: Bridge responses at 339.3 m point of the main span under natural wind data

4.7.2 Fast Fourier Transform of wind data response

The frequency analysis performed by the FFT, as previously described, indicated that the horizontal and the torsional responses, for both locations the mid-span and at one third location along the main span (339.3 m) were exited for the same frequency of 0.1451 Hz and 0.1731 Hz respectively, as it can be noticed in Figures 4.40 and 4.41, thus behaving as one single rigid body. The FFT calculation of the other positions of bridge can be found in the Appendix E (Figs. E6 to E9).

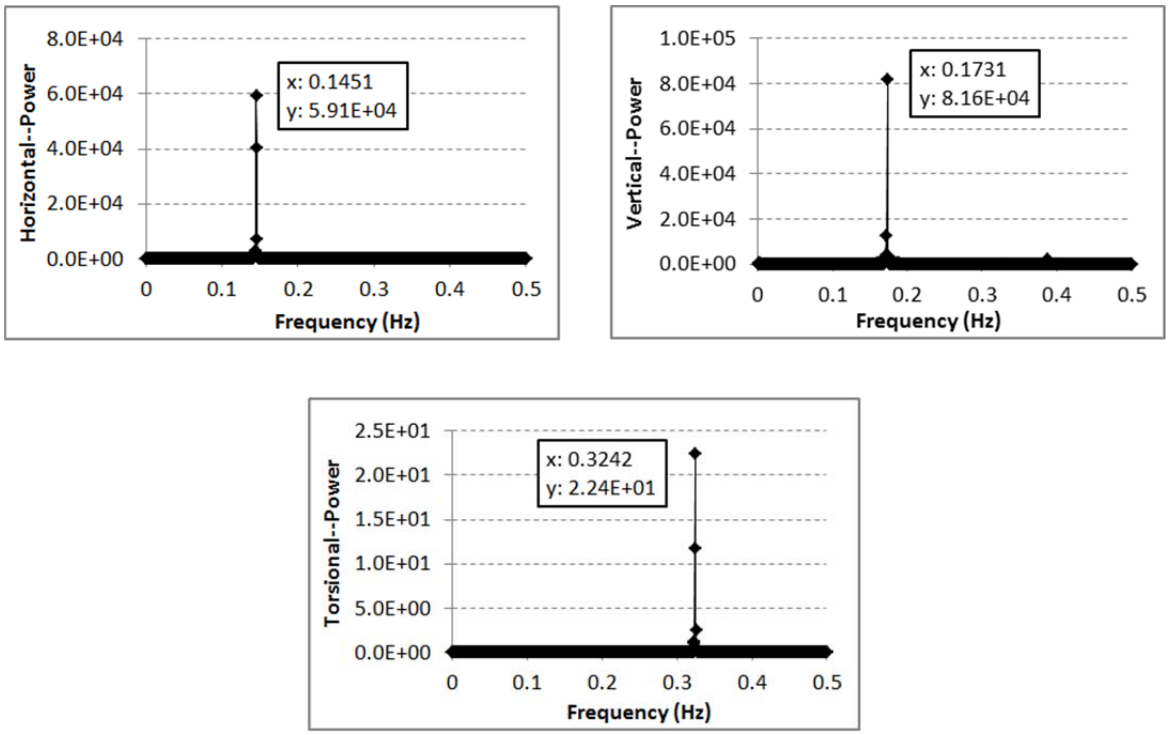

Figure 4.40: FFT of responses at mid-span.

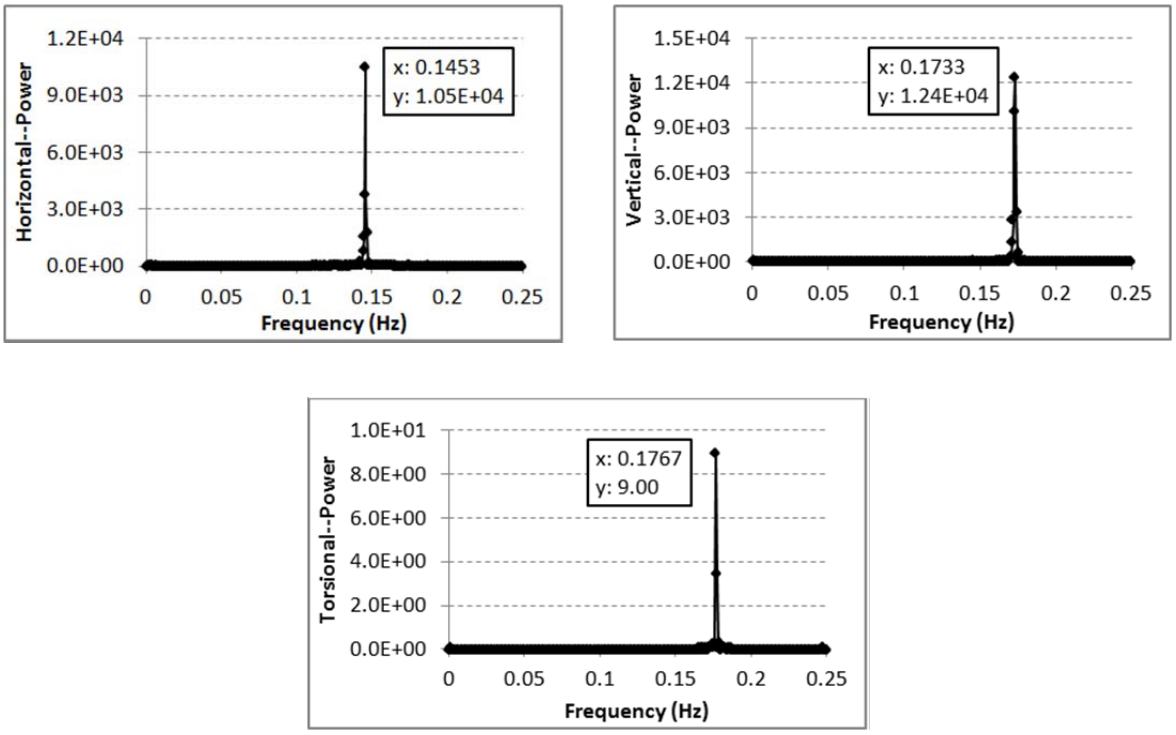

Figure 4.41: FFT of responses at 339.3 m point of the main span.

The torsional response however had a different frequency for the middle point (509 m) and the one third point (339.3 m) along the main span, of 0.3242 Hz and 0.1767 Hz respectively, indicating that the torsional stiffness of the middle deck is lower than the one at the one third deck location, due to the tower connection, thus the cycles of the torsional motion are much faster. Because the amplitudes of the rotational vibrations are very small for both investigated locations, therefore this difference in frequencies is not considered to have a significant effect on the critical response of the bridge.

Chapter 5 Conclusions

In this thesis, a complete 3D finite element model was developed for the Stonecutters Cable-stayed Bridge and it was used for extracting the static and dynamic characteristics along with the aerodynamic response of the Stonecutters Cable-stayed Bridge. By performing the eigenvalues analysis, the natural frequencies and the vibration mode shapes were determined; also the static response was estimated under the effect of the mean wind loadings, while the dynamic response at different locations along the bridge deck and at the top of the tower, under the effect of the self-excited flutter loading and under a natural wind data loading applied to the bridge and the following observations and conclusions could be formulated:

The Stonecutters Cable-stayed Bridge was designed with a separated twin-box steel girder, and based on the aerodynamic theory of bridge structures and due to development of bridge engineering in recent years, it was found that, bridges become more flexible with the increase of the main span length of the bridge. Therefore, the long-span bridges are predisposed to critical oscillations when subjected to wind. Thus, in order to improve the aerodynamic stability of the long-span bridge, twin-separated box girder configuration was adopted for the deck design. The results of the eigen-modes analysis the vibration mode shapes and the natural frequencies of the Stonecutters Bridge FE Model were found and these were in the same range of natural frequencies as reported for other long-span cable-stayed and suspension bridges. After collecting extensive data from other cable-stayed bridges, it could be observed that, in general, for such long-span bridges, the horizontal deformation always coincides with the first vibration mode shape. The torsional vibration modes appear quite late after the dominant vertical modes of vibration; these were observed in the sixth, seventh or even higher vibration modes. The range of natural frequencies

obtained for the Stonecutters Bridge FE model was between 0.1449 Hz to 1.9298 Hz and these values were in good agreement with the general values reported for the natural frequency of other cable-stayed bridges.

Due to the eigen-modes of the bridge, it was observed that usually one dominant mode is coupled with other modes; thus pure vibration modes along one direction are seldom encountered. The dominant mode shapes of the Stonecutters Cable-stayed Bridge in the lower frequency range are mainly the horizontal deck and the tower modes, but they still coupled with the torsional modes. Obvious coupled vibration shapes can be clearly observed in the higher modes. This reveals the fact that the cable-stayed bridge investigated is more flexible than the other type of bridges reported in the literature. Compared with the data published for the Stonecutters Bridge by other researchers, the results of the currently developed FE model were found to be very similar in terms of the vibration frequencies and as the overall order of the vibration mode shapes. Some differences appear for higher frequencies range, and these might be caused by different modelling method and assumptions, different elements selection or other properties of the structure itself; however, no significant influence in further calculation and analysis. Therefore, it is proves that the Stonecutters Bridge FE model is validated and the dynamic characteristics and other conditions can predict closely the response of the real Stonecutters Bridge to static and dynamic loadings.

From the mean wind load analysis, the deformations of the main span of Stonecutters Bridge for different wind speeds are obtained. The evolution of the displacement changed along the bridge span, diminishing towards the towers. Also it could be concluded that the deformation results were consistent with the deformations reported by other analyses for long-span cable-stayed and suspension bridges. The responses at the mid-span location

under a time history mean wind load, corresponding to the wind tunnel experimental procedure, were also investigated. From those response data, it could be predicted that the torsional vibration mode may be the main vibration mode shape excited by high wind speeds, and may be coupled with the vertical vibration at the same time. This kind of torsional-based, vertical supplemented mode shape can even lead to permanent damage of the bridge structure when reaching a critical wind velocity. The response data at mid-span were also prepared and used for the calculation of the self-excited loads calculation and for the dynamic flutter analysis.

From the dynamic analysis performed based on the assumptions of the time history mean wind load analysis at different wind speeds was concluded that the displacement at the mid-span increased rapidly after 176 m/s in both the vertical and torsional directions. According to the results of Fast Fourier Transform carried out for the displacement response history, it could be found that the value of torsional frequency starts at a high level for lower wind speeds and then decreases for high wind speeds. But the vertical frequency has an opposite evolution, slightly increasing with the increase of the wind speed. The flutter instability starts to occur when the frequencies in the two directions vertical and torsional become closer and finally couple. The critical flutter wind speed and the flutter frequency can be extracted when the dominant vertical and torsional frequency register the same value. At this frequency, the flutter phenomenon occurs, and the coupled vertical and torsional vibration mode reaches the maximum amplitude.

In this research, the critical flutter wind speed of the Stonecutters Bridge FE model was estimated at about 176 m/s, and the flutter frequency achieved at this speed is 0.30 Hz. Thus it was found that, the natural frequency of the first torsional mode shape is 0.32384 Hz, which is very close to the flutter frequency. It was also confirmed that the torsional mode

shape plays an important role in the flutter instability of the long-span bridges. After comparing with the published data for the Stonecutters Bridge, it was determined that the critical flutter wind speed and the flutter frequency of the FE model are realistically predicted and are feasible.

According to the observation from Figure 4.19, it can be assumed that 141 m/s is the onset critical flutter wind speed, because the vertical and torsional frequencies become very closer at that point, while the 176 m/s is the wind speed for which flutter instability is already achieved. After verifying the calculation of the onset flutter wind speed by employing several different methods and formulas it could be determined that wind speeds of 128.5 m/s and 131.4 m/s are the on-set and the critical velocity for flutter. Comparing with the published data 140 m/s and 155.4 m/s from Van der Put method using real properties of Stonecutters Cable-stayed Bridge, the results of Stonecutters Bridge FE model were found to be in a reasonable range.

Finally in this thesis, the critical flutter wind speed and the onset critical flutter wind speed for the Stonecutters Bridge FE model were smaller than the published data for the same bridge. Because the FE model simulates the elementary structure without wind shield and other wind resistance accessory, hence, the properties of bridge deck are slightly different from the real bridge.

Moreover, it should be mentioned that in the Hong Kong region, the maximum design wind speed for the Stonecutters Bridge is about 95 m/s, and both the critical flutter and the onset critical flutter wind speeds determined for the Stonecutters FE Model in the thesis are larger than the required values, therefore the bridge is considered to be safe. Hence, as per the aerodynamic analysis of the bridge structure itself, it can be proves that the Stonecutters Cable-stayed Bridge has a very good performance and aerodynamic stability. Therefore the

separate twin-box steel girder decks are found to be very good for improving the capacity of wind resistance design of long-span bridges.

Recommendations for future work

In this thesis, the finite element model of the Stonecutters Cable-stayed Bridge was developed using the ABAQUS CAE program, which is a finite element analysis software, with powerful and flexible functions. However for a super-long span bridge model or complex structure like the Stonecutters Bridge, this it is a fairly new methodology and little is known by researchers at present. This will have an influence on the modelling and on the structural analysis work because of the shortage of published materials and research. Hence, in the FE model of the Stonecutters Bridge, some methods of modelling are not accurate enough to present the features of the real bridge perfectly. However, the situation can be improved if more researchers involved in developing FE models of large structures by commercial software such as ABAQUS would make their studies available.

Also a main reason of delay in this project was the lack of technical information for the Stonecutters Bridge, which is impetuously required for developing an accurate FE model. The properties of the real completed bridge have not been published yet by the Hong Kong Highways Department and by the designers. Thus in the FE model developed, some properties released by other researchers involved in the pre-design stage of the Stonecutters Bridge (Larose, Hui, etc.) were employed, and some structural properties were calculated based on the mechanics and the extraction from ABAQUS analysis. Hence, this part of properties needs further investigation, such as mass center and shear center of bridge deck, moment inertia, etc.

For the mean wind loading and for the flutter analysis of the FE model in this thesis, only several cases of wind velocity were selected in the final wind loading calculation. Also the self-excited loadings formulation is based on the Scanlan's method, and as mentioned in the previous chapter, there is a strong link between the Scanlan's method and the wind tunnel experiments. Hence, for a finite element analysis performed without the wind tunnel tests, the data for these parameters are limited. Therefore, in order to obtain more data and to improve the accuracy of the analysis in future work, a complementary study involving a sectional bridge twin deck model or a full scale bridge model tested in the wind tunnel facility is recommended.

In order to improve the aerodynamic stability of long-span bridges, a twin-separated box girder configuration was designed for the Stonecutters Bridge. However the flow characteristics around the bridge deck became more complicated, due to the effects of the gap between the two separated box girders, and thus vortex-induced vibration might occur for lower wind speeds. Although the vortex-induced vibration is limited in amplitude of vibration and it does not cause the collapse for the bridge, it can result in large displacements and in discomfort for the drivers. In addition, the vortex-induced oscillations commonly occur in the low wind speed region; therefore the occurrence of vortex-induced vibration is high. Therefore, an additional analysis for verifying the response of the FE model to vortex-induced instability should be considered in order to identify the structural behavior of long-span bridge with twin box girder decks at low wind velocities.

Reference

[1] Bleich, Friedrich. “Dynamic Instability of Truss Stiff Suspension Bridge”. Proc. Am. Soc. Civil Engineering. 1948.

[2] T. Theodorsen. “General Theory of Aerodynamic Instability and the Mechanism of Flutter”. National Advisory Committee for Aeronautics (NACA), Washington, D. C., 1934, Technical Report No. 496, pp. 413-433, 1935.

[3] McCormick, Barnes W. “Aerodynamics, Aeronautics, and Flight Mechanics”. p. 24, John Wiley & Sons, Inc., New York, ISBN 0-471-03032-5, 1979.

[4] Zhenqing Chen. “Bridge Wind Engineering (Chinese Edition)”. China Communications Press Pub. Date: 2005-05-01 (1991). ISBN-10: 7114055277. ISBN-13: 978-7114055270.

[5] M. S. Troitsky. “Cable-Stayed Bridges: Theory & Design”. Published December 1st 1977 by Beekman Publishers. ISBN13: 9780846402312.

[6] E. Simiu and R.H. Scanlan. “Wind effects on Structures”. Wiley Interscience, New York, 3 edition, 1996.

[7] Atsushi Kaji, Taku Hirai, Rory O’Grady and Robin Sham. “An introduction to Stonecutters bridge, Hong Kong: Erection of the steel segments, hydraulic buffers and lateral bearings”. IABSE-JSCE Joint Conference on Advances in Bridge Engineering-II, August 8-10, 2010, Dhaka, Bangladesh. Amin, Okui, Bhuiyan (eds.) ISBN: 978-984-33-1893-0.

[8] Ito, M. and Nakamura, Y. “Aerodynamic Stability of Structures in Wind”. International Association for Bridge and Structural Engineering, S-20/82, 1982, pp. 33–56.

[9] Guido Morgenthal, Robin Sham and Brian West. “Engineering the Tower and Main Span Construction of Stonecutters Bridge”. Journal of Bridge Engineering ASCE. March/April 2010. DOI: 10.1061/(ASCE)BE.1943-5592.0000042.

[10] Allan Larsen, Ngai Yeung and Matt Carter. “Stonecutters Bridge, Hong Kong: wind tunnel tests and studies”. Bridge Engineering Volume 165 Issue BE2 June 2012.

[11] Sato, H., Kusuhara, S., Ogi, K., et al. (2000), “Aerodynamic Characteristics of a 2-box Girder Section Adaptable for a Super-Long Span Suspension Bridge”, J. Wind Eng. Ind. Aerodyn., 90(12-15), 2033-2043.

[12] Kobayashi H. and Phan, D. H. “Bridge Deck Flutter Control by Control Surfaces”. Proc, 6th Asia-Pacific Conf. on Wind Engineering, Seoul, Korea, 2005.

[13] M. Matsumoto and et al. “Flutter Characteristics of H-Shaped Cylinders with Various Side-Ratios and Similarity to Rectangular Cylinder Ones”. Proc. of the 5th International Colloquium on BBAA, Ottawa, 2004.

[14] F. Y. Xu, B. B. Li, C. S. Cai, F.ASCE and Z. Zhang. “Experimental Investigations on Aerostatic Characteristics of Bridge Decks under Various Conditions”. American Society of Civil Engineers. DOI: 10.1061/(ASCE)BE.1943- 5592.0000601. 2014.

[15] Yao-Jun Ge and Hai-Fan Xiang. “Bluff Body Aerodynamics Application in Challenging Bridge Span Length”. Department of Bridge Engineering State Key Laboratory for Disaster Reduction in Civil Engineering, Tongji University. BBAA VI International Colloquium on: Bluff Bodies Aerodynamics & Applications Milano, Italy, July, 20-24 2008.

[16] R. H. Scanlan and J. J. Tomko. “Airfoil and bridge deck flutter derivatives”. 1971 Journal of the engineering mechanics division, American society of mechanical engineers 97, 1717-1737, 1971.

[17] Hui, Michael C. H., Ding, Q. S. and Xu, Y.L. “Flutter Analysis of Stonecutters Bridge”. Hong Kong: Wind and Structures, 2006, Vol. 9. pp.125-146.

[18] Michael C. H. Hui and Q. S. Ding. “Flutter Analysis of Stonecutters Bridge”. Wind and Structures, Vol. 9, No. 2(2006) 125-146.

[19] From Wikipedia. http://en.wikipedia.org/wiki/Tacoma_Narrows_Bridge_(1940). “Tacoma Narrows Bridge (1940)”.

[20] Xinzhong Chen, Masaru Matsumoto and Ahsan Kareem. “Aerodynamic Coupling Effects on Flutter and Buffeting of Bridges”. Member, ASCE, Journal of Engineering Mechanics, January 2000.

[21] Scanlan, R. H. “Aerodynamics of Cable-supported Bridges”. Department of Civil Engineering, The Johns Hopkins University, Baltimore, MD 21218, USA. J. Construct.

Steel Res. Vol. 39, No. 1, pp. 51-68, 1996.

[22] G. Diana, G. Fiammenghi, M. Belloli, D. Rocchi. “Wind Tunnel Tests and Numerical Approach for Long Span Bridges: The Messina Bridge”. Dipartimento di Meccanica, Politecnica di Milano, Via La Mas, 1-Milano, Italy. J. Wind Eng. Ind. Aerodyn. 122 (2013) 38–49.

[23] G. L. Larose, M. G. Savage and A. Lafreniere. “Sectional Model Experiments for Verfication of the Aerodynamic Properties at High Reynolds Number of the Stonecutters Bridge, Hong Kong”. Highways Department, Hong Kong Special Administrative Region. LTR-AL-2006-0013.

[24] Strouhal, V. "Ueber eine besondere Art der Tonerregung", Annalen der Physik und Chemie, 3rd series, 5 (10): 216–251, 1878.

[25] Parkinson, G. V. and Smith, J. D. “The Square Prism as an Aeroelastic Non-linear Oscillator”. Quarterly Journal of Mechanics and Applied Mathematics 17(2), 1964, 225–239.

[26] Novak, M. “Aeroelastic Galloping of Prismatic Bodies”, ASCE, Journal of Engineering Mechanics Division 96, EMI, 1969, 115–142.

[27] Fujino, Y., Warnitchai, P., and Ito, M. “Suppression of Galloping of Bridge Tower Using Tuned Mass Damper”. Journal of the Faculty of Engineering, University of Tokyo, (B) 38(2), 1985, 49–73.

[28] Xiang Haifan. “Buffeting Response Analysis and Control of Long-Span Bridges”. International Association for Wind Engineering. Recent Advances in Wind Engineering. Wiley Eastern Limited, New Delhi, 295-319, 1994.

[29] Duc-Huynh Phan and Ngoc-Trung Nguyen. “Flutter and Buffeting Control of Long-span Suspension Bridge by Passive Flaps: Experiment and Numerical Simulation”. Int’l J. of Aeronautical & Space Sci. 14(1), 46 – 57 (2013).

[30] Ukeguchi N. Sakata H. and Nishitani H. “An Investigation of Aeroelastic Instability of Suspension Bridges”. Proceedings of the International Symposium on Suspension Bridges, Lisbon, pp. 273-284, 1966.

[31] Szechenyi, E. and Loiseau, H. “Mesures Aerodynamiques et Dynamiques sur le Pont

de Saint-Nazaire". Communication and General Reports for 6 and 7 June 1978, Association Francaise des Ponts et Charpentes.

[32] National Physical Laboratory. http://www.npl.co.uk/. Item#: 9953751.

[33] R. L. Wardlaw. "Sectional Versus Full Model Wind Tunnel Testing of Bridge Road Decks". Low Speed Aerodynamics Laboratory, National Aeronautical Establishment, Ottawa, Canada, Proc. Indian Acad. Sci. (Engg. Sci.) Vol. 3, Pt. 3, November 1980, pp. 177-198.

[34] Yozo Fujino, M.ASCE, and Yoshitaka Yoshida. "Wind-Induced Vibration and Control of Trans-Tokyo Bay Crossing Bridge". J. Struct. Eng. 2002.128:1012-1025.

[35] Xianyu Zhu. "Response of Static Wind and Effect of Dynamic Characteristics on Sutong Cable-stayed Bridge". China Railway 18th Co. Ltd., Tianjin, Hunan Communication Science and Technology, Vo1. 37 No. 1 Mar. 2011, 1008-844X(2011)01-0080-04.

[36] Ernst, H. J. "Der E-modul von Seilen unter Berücksichtigung des Durchhanges". Der Bauingenieur, Vol. 40, No. 2, 1965, pp. 52-55 (in German).

[37] T. H. Odden and H. Skyvulstad. "Wind-induced Dynamic Response and Aeroelastic Stability of a Suspension Bridge crossing Sognefjorden". Department of Structural Engineering. Faculty of Engineering Science and Technology. NTNU- Norwegian University of Science and Technology. 2012.

[38] Ole Øiseth, Anders Ronnquist, Ragnar Sigbjornsson. "Finite Element Formulation of the Self-Excited Forces for Time-Domain Assessment of Wind-Induced Dynamic Response and Flutter Stability Limit of Cable-Supported Bridges". Department of Structural Engineering, Norwegian University of Science and Technology, 7491 Trondheim, Norway. Finite Elements in Analysis and Design 50 (2012) 173–183.

[39] ABAQUS. Version 6.11 Documentation. [Online] ABAQUS Inc., Providence, RI., 2012.

[40] Ayman Sabri. "Finite Element Modeling of the Stonecutters Cable-Stayed Bridge". Department of Civil Engineering. University of Ottawa Ottawa, Canada. April 2013.

[41] Vejrum, T. "Danish Engineers behind the world's largest Cable Stayed Bridges: Sutong and Stonecutters Bridge". Norsk Staldag, Oslo : COWI, 2008.

[42] Hu J.D., Harik Issam E., Smith S.W., Campbell J. Gagel, J.E. and Graves R.C. “Baseline Modeling of the Owensboro Cable-stayed Bridge over the Ohio River”. Research Report KTC-06-04/FRT116-020-1F, College of Engineering, University of Kentucky. 2006.

[43] Danny Chung. “A Stonecutters Bridge Too Far”. http://www.construction-post.com/stonecutters-bridge/. Industry News, Slider. 21th Oct 2013.

[44] Michael C.H. Hui. “Full-bridge Aeroelastic Model Wind Tunnel Tests for the Stonecutters Bridge”. Civil Engineering and Development Department, Hong Kong Special Administrative Region, Civil Engineering and Development Building, 101 Princess Margaret Road, Hong Kong, People’s Republic of China. HKIE Transactions, Vol. 20, No. 2, 109 – 123, 2013.

[45] Charles Van Loan. “Computational Frameworks for the Fast Fourier Transform”. (SIAM, 1992)

[46] SUNLAB, University of Ottawa. http://apecs.site.uottawa.ca/.

[47] Shayan Mehranfar. “Finite Element Modelling and On-Site Measurements for Roof Mounted PV Solar Panels under High Wind Load”. Department of Civil Engineering, University of Ottawa, May 2014.

[48] A. Sabri, E. Dragomirescu and F. Feng. “Multiple Element Cable Modelling for Long-span Cable-stayed Bridges”. Civil Engineering Dep. University of Ottawa, Canada, 2014.

[49] Pappin, J. W. and Kite, S. “Seismic Design of Stonecutters Bridge, Hong Kong”. Beijing: The 14th World Conference on Earthquake Engineering, 2008.

[50] Zhuo Zhuang, Fan Zhang, et al. “Non-linear Finite Element Analysis and Practical in ABAQUS”. Science Press, Beijing. Mar. 2005, ISBN 7-03-015088-0.

[51] Zhe Liu. “Dynamic Characteristics Analysis of Single Pylon Cable-stayed Bridge”. Bridge and Tunnel Engineering, Northeast Forestry University. June, 2010.

[52] Changke Jiao, Aiqun Li and Hao Wang. “Analysis on Parameters of Dynamic Property of Triple-pylon Suspension Bridge”. Key Laboratory of Concrete and Prestressed Concrete Structure of Ministry of Education, Southeast University, Nanjing, Jiangsu, 210096, China.

Journal of Highway and Transportation Research and Development, Vol. 27 No. 4, Apr. 2010.

[53] Ahmed Riaz Khan. “Finite Element Modelling of Messina Bridge”. Eighteenth Postgraduate Student Conference on MSc Dissertations 2011-12. Department of Civil & Structural Engineering, University of Sheffield, 2012.

[54] Xugang Hua and Zhengqing Chen. “Full-mode Flutter Frequency Domain Analysis Method of Bridge Based on ANSYS”. Wind Engineering Experiment Research Center, Hunan University, Changsha 410082, Hunan, China. China Journal of Highway and Transport, Vol. 20 No. 5 Sep. 2007.

[55] “Structures Design Manual for Highways and Railways”. Third Edition. Highways Department, Government of the Hong Kong Special Administrative Region.

[56] Wenshan Qiu and Zhihao Xu. “Flutter Analysis of Stonecutters Cable-stayed Bridge”. Bridge the Eighteenth National Conference, Bridge the Eighteenth National Conference Proceed, 2008.

[57] Put, T.A.C.M. van der. “Rigidity of Structures against Aerodynamic Forces”. Ein Dienst der ETH-Bibliothek ETH Zürich, Rämistrasse 101, 8092 Zürich, Schweiz. IABSE publications, 36 (1976).

[58] Ke Qiu, Zuoyu Sun. “An Order Reduction Method of Bridge Flutter Equation and a Simplified Formula of Critical Flutter Wind Velocity”. Journal of Highway and Transportation Research and Development. Vol. 28, No.11, Nov. 2011. 1002-0268(2011)11-0105-0.

[59] Giorgio Diana and Giuseppe Fiammenghi. “Wind Tunnel Tests and Numerical Approach for Long Span Bridges: the Messina Bridge”. Dipartimento di Meccanica, Politecnica di Milano, Via La Mas, 1-Milano, Italy. BBAA7, Shanghai, China; Sep. 2-6, 2012.

[60] Bleich, McCullough, Rosecrans and Vincent. “The Math. Theory of Vibration in Suspension Bridges”. Department of Commerce. Bureau of Public Roads, Wash. D. C. 1950.

[61] Farquharson, F. B. “Model Verification of Publication”. Vol. 12, Zurich 1952.

Appendix A

Table A1: Configuration properties of Stonecutters Bridge stay cables.

Cable #				Length of cable (m)	Horizontal length (m)	Angle of inclination (rad)	Angle of Inclination (degrees)	d (m)	A (m^2)
EL1	ER1	WL1	WR1	533	509	0.301231	17.25929	0.192	0.028953
EL2	ER2	WL2	WR2	515.18	491.7	0.303074	17.36483	0.192	0.028953
EL3	ER3	WL3	WR3	497.37	473.7	0.30975	17.74739	0.192	0.028953
EL4	ER4	WL4	WR4	479.45	455.7	0.316071	18.10952	0.192	0.028953
EL5	ER5	WL5	WR5	461.7	437.7	0.323847	18.55508	0.181946	0.026
EL6	ER6	WL6	WR6	444	419.7	0.332374	19.04365	0.181946	0.026
EL7	ER7	WL7	WR7	426.2	401.7	0.340717	19.52166	0.181946	0.026
EL8	ER8	WL8	WR8	408.6	383.7	0.35091	20.10568	0.181946	0.026
EL9	ER9	WL9	WR9	391.1	365.7	0.362382	20.76297	0.174808	0.024
EL10	ER10	WL10	WR10	373.44	347.7	0.373453	21.39726	0.174808	0.024
EL11	ER11	WL11	WR11	356	329.7	0.386793	22.1616	0.174808	0.024
EL12	ER12	WL12	WR12	338.74	311.7	0.40227	23.04836	0.174808	0.024
EL13	ER13	WL13	WR13	321.39	293.7	0.418147	23.95805	0.169569	0.022583
EL14	ER14	WL14	WR14	304.3	275.7	0.437027	25.03983	0.169569	0.022583
EL15	ER15	WL15	WR15	287.37	257.7	0.458419	26.26547	0.169569	0.022583
EL16	ER16	WL16	WR16	270.48	239.7	0.481714	27.60016	0.169569	0.022583
EL17	ER17	WL17	WR17	253.92	221.7	0.509252	29.17796	0.159577	0.02
EL18	ER18	WL18	WR18	237.6	203.7	0.540749	30.98265	0.159577	0.02

EL19	ER19	WL19	WR19	221.49	185.7	0.576432	33.02713	0.159577	0.02
EL20	ER20	WL20	WR20	205.85	167.7	0.618635	35.44517	0.159577	0.02
EL21	ER21	WL21	WR21	190.7	149.7	0.668096	38.27908	0.143973	0.01628
EL22	ER22	WL22	WR22	176	131.7	0.725308	41.55706	0.143973	0.01628
EL23	ER23	WL23	WR23	162.2	113.7	0.794017	45.4938	0.143973	0.01628
EL24	ER24	WL24	WR24	149.3	95.7	0.875007	50.13422	0.143973	0.01628
EL25	ER25	WL25	WR25	137.7	77.7	0.971247	55.64838	0.112838	0.01
EL26	ER26	WL26	WR26	124.34	59.7	1.069988	61.30577	0.112838	0.01
EL27	ER27	WL27	WR27	114.4	41.7	1.197689	68.62254	0.112838	0.01
EL28	ER28	WL28	WR28	106.8	23.7	1.347023	77.17875	0.112838	0.01
EL29	ER29	WL29	WR29	107.4	19.7	1.386325	79.4306	0.112838	0.01
EL30	ER30	WL30	WR30	113.8	29.7	1.306755	74.87153	0.112838	0.01
EL31	ER31	WL31	WR31	121	39.7	1.236506	70.84656	0.112838	0.01
EL32	ER32	WL32	WR32	130.5	49.75	1.179674	67.59035	0.112838	0.01
EL33	ER33	WL33	WR33	137	59.75	1.119501	64.14269	0.143973	0.01628
EL34	ER34	WL34	WR34	144.3	69.75	1.066298	61.0944	0.143973	0.01628
EL35	ER35	WL35	WR35	151.8	79.75	1.017655	58.30736	0.143973	0.01628
EL36	ER36	WL36	WR36	159.8	89.75	0.97443	55.83074	0.143973	0.01628
EL37	ER37	WL37	WR37	168	99.75	0.935085	53.57643	0.159577	0.02
EL38	ER38	WL38	WR38	176.4	109.75	0.899291	51.52555	0.159577	0.02
EL39	ER39	WL39	WR39	185	119.75	0.866763	49.66186	0.159577	0.02
EL40	ER40	WL40	WR40	194	129.75	0.838183	48.02437	0.159577	0.02
EL41	ER41	WL41	WR41	203.1	139.75	0.81195	46.52131	0.169569	0.022583
EL42	ER42	WL42	WR42	212.4	149.75	0.78832	45.16741	0.169569	0.022583
EL43	ER43	WL43	WR43	221.7	159.75	0.766175	43.89858	0.169569	0.022583

EL44	ER44	WL44	WR44	231.2	169.75	0.74629	42.75926	0.169569	0.022583
EL45	ER45	WL45	WR45	240.8	179.75	0.728055	41.71447	0.174808	0.024
EL46	ER46	WL46	WR46	250.45	189.75	0.711112	40.74374	0.174808	0.024
EL47	ER47	WL47	WR47	260.2	199.75	0.695585	39.85411	0.174808	0.024
EL48	ER48	WL48	WR48	270	209.75	0.681146	39.02677	0.174808	0.024
EL49	ER49	WL49	WR49	279.88	219.75	0.667845	38.26471	0.181946	0.026
EL50	ER50	WL50	WR50	289.8	229.75	0.655426	37.55316	0.181946	0.026
EL51	ER51	WL51	WR51	299.84	239.75	0.644179	36.90873	0.181946	0.026
EL52	ER52	WL52	WR52	309.83	249.75	0.633286	36.28462	0.181946	0.026
EL53	ER53	WL53	WR53	319.86	259.75	0.623099	35.70093	0.192	0.028953
EL54	ER54	WL54	WR54	330.1	269.75	0.614301	35.19685	0.192	0.028953
EL55	ER55	WL55	WR55	340.2	279.75	0.605337	34.68325	0.192	0.028953
EL56	ER56	WL56	WR56	350.3	289.75	0.596782	34.19311	0.192	0.028953

Table A2: Cable pre-tensioning values and the calculated equivalent E values.

Cable #				Tension Pressure in Cable (N/m^2)	Tension Force on Cable (N)	Eeq (N/m^2)
EL1	ER1	WL1	WR1	1770000000	51246621	1.99081E+11
EL2	ER2	WL2	WR2	1759380000	50939142	1.99126E+11
EL3	ER3	WL3	WR3	1722433020	49869420	1.99136E+11
EL4	ER4	WL4	WR4	1689706793	48921901	1.99153E+11
EL5	ER5	WL5	WR5	1649153830	42878000	1.99159E+11
EL6	ER6	WL6	WR6	1607924984	41806050	1.99166E+11
EL7	ER7	WL7	WR7	1569334784	40802704	1.99178E+11
EL8	ER8	WL8	WR8	1525393410	39660229	1.99183E+11
EL9	ER9	WL9	WR9	1478106215	35474549	1.99185E+11
EL10	ER10	WL10	WR10	1433763028	34410313	1.99192E+11
EL11	ER11	WL11	WR11	1386448848	33274772	1.99197E+11
EL12	ER12	WL12	WR12	1330990894	31943781	1.99189E+11
EL13	ER13	WL13	WR13	1283075222	28975688	1.99196E+11
EL14	ER14	WL14	WR14	1231752213	27816660	1.99199E+11
EL15	ER15	WL15	WR15	1177555116	26592727	1.99199E+11
EL16	ER16	WL16	WR16	1124565136	25396054	1.99205E+11
EL17	ER17	WL17	WR17	1068336879	21366738	1.99206E+11
EL18	ER18	WL18	WR18	1011715024	20234300	1.99211E+11
EL19	ER19	WL19	WR19	951012122.8	19020242	1.99211E+11
EL20	ER20	WL20	WR20	893000383.3	17860008	1.99222E+11
EL21	ER21	WL21	WR21	835848358.8	13607611	1.99244E+11
EL22	ER22	WL22	WR22	777338973.7	12655078	1.99273E+11
EL23	ER23	WL23	WR23	722925245.5	11769223	1.99326E+11
EL24	ER24	WL24	WR24	671597553.1	10933608	1.99404E+11
EL25	ER25	WL25	WR25	623914126.8	6239141	1.9951E+11
EL26	ER26	WL26	WR26	586479279.2	5864793	1.99651E+11
EL27	ER27	WL27	WR27	551290522.4	5512905	1.99795E+11
EL28	ER28	WL28	WR28	526482448.9	5264824	1.99924E+11
EL29	ER29	WL29	WR29	526482448.9	5264824	1.99947E+11
EL30	ER30	WL30	WR30	551290522.4	5512905	1.99896E+11
EL31	ER31	WL31	WR31	586479279.2	5864793	1.99846E+11

EL32	ER32	WL32	WR32	623914126.8	6239141	1.99799E+11
EL33	ER33	WL33	WR33	671597553.1	10933608	1.99767E+11
EL34	ER34	WL34	WR34	722925245.5	11769223	1.99746E+11
EL35	ER35	WL35	WR35	777338973.7	12655078	1.99733E+11
EL36	ER36	WL36	WR36	835848358.8	13607611	1.99728E+11
EL37	ER37	WL37	WR37	893000383.3	17860008	1.99724E+11
EL38	ER38	WL38	WR38	951012122.8	19020242	1.99724E+11
EL39	ER39	WL39	WR39	1011715024	20234300	1.99727E+11
EL40	ER40	WL40	WR40	1068336879	21366738	1.99727E+11
EL41	ER41	WL41	WR41	1124565136	25396054	1.99729E+11
EL42	ER42	WL42	WR42	1177555116	26592727	1.99729E+11
EL43	ER43	WL43	WR43	1231752213	27816660	1.9973E+11
EL44	ER44	WL44	WR44	1283075222	28975688	1.99731E+11
EL45	ER45	WL45	WR45	1330990894	31943781	1.99729E+11
EL46	ER46	WL46	WR46	1386448848	33274772	1.99733E+11
EL47	ER47	WL47	WR47	1433763028	34410313	1.99733E+11
EL48	ER48	WL48	WR48	1478106215	35474549	1.99731E+11
EL49	ER49	WL49	WR49	1525393410	39660229	1.99731E+11
EL50	ER50	WL50	WR50	1569334784	40802704	1.9973E+11
EL51	ER51	WL51	WR51	1607924984	41806050	1.99727E+11
EL52	ER52	WL52	WR52	1649153830	42878000	1.99725E+11
EL53	ER53	WL53	WR53	1689706793	48921901	1.99724E+11
EL54	ER54	WL54	WR54	1722433020	49869420	1.99719E+11
EL55	ER55	WL55	WR55	1759380000	50939142	1.99716E+11
EL56	ER56	WL56	WR56	1770000000	51246621	1.99701E+11

Appendix B

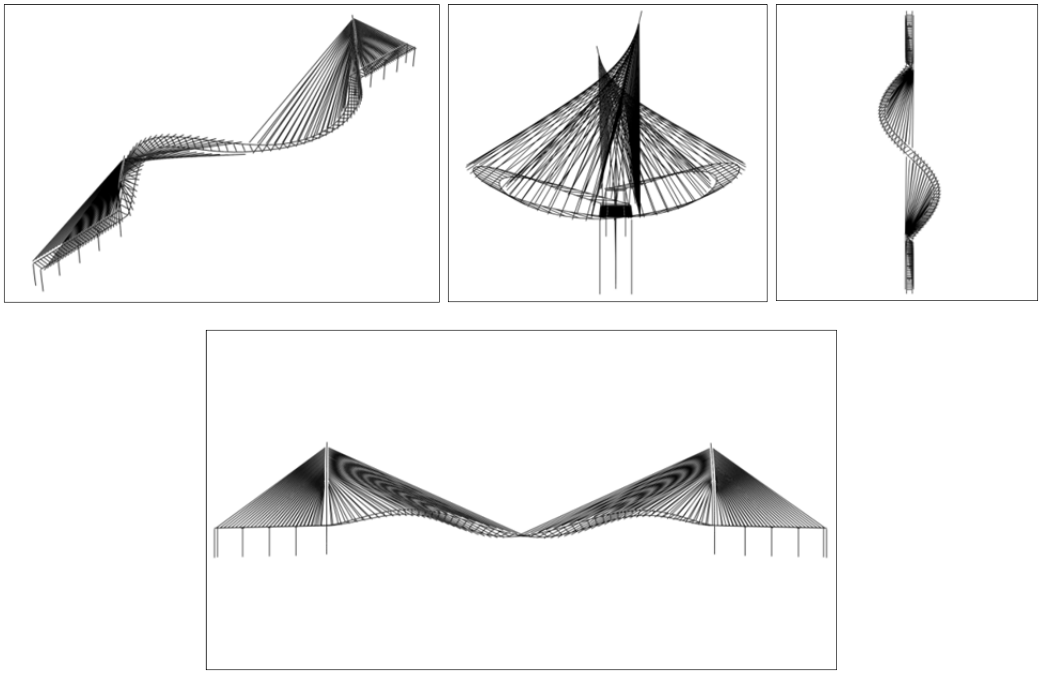

Figure B1: 7th Mode shape, f=0.3583 Hz, scale factor: 1.595e+02.

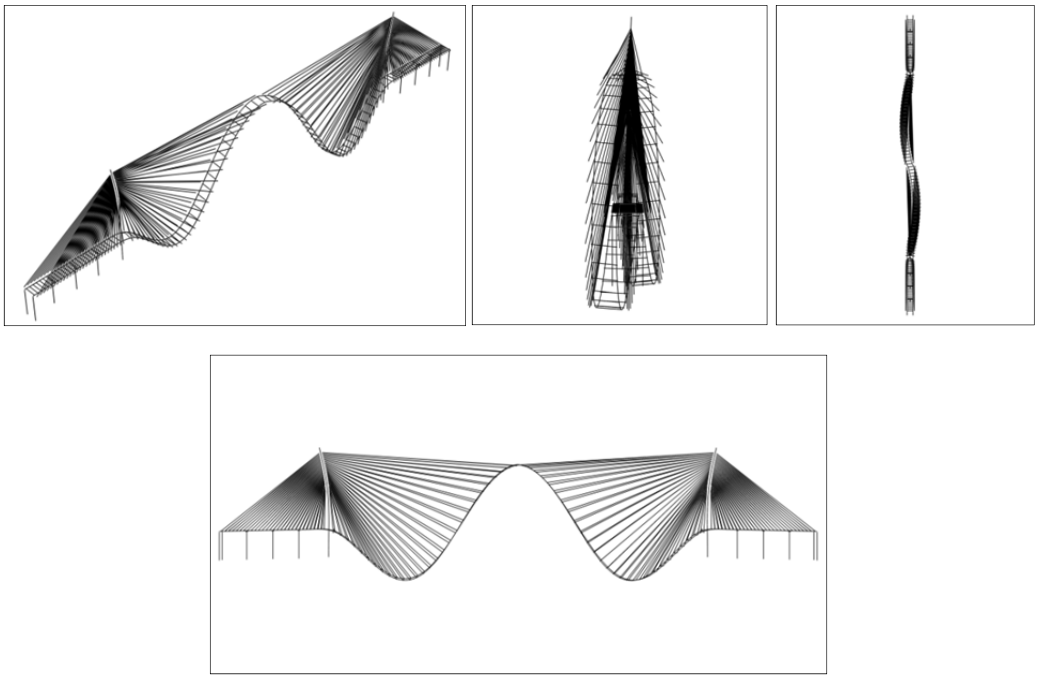

Figure B2: 8th Mode shape, f=0.3873 Hz, scale factor: 1.597e+02.

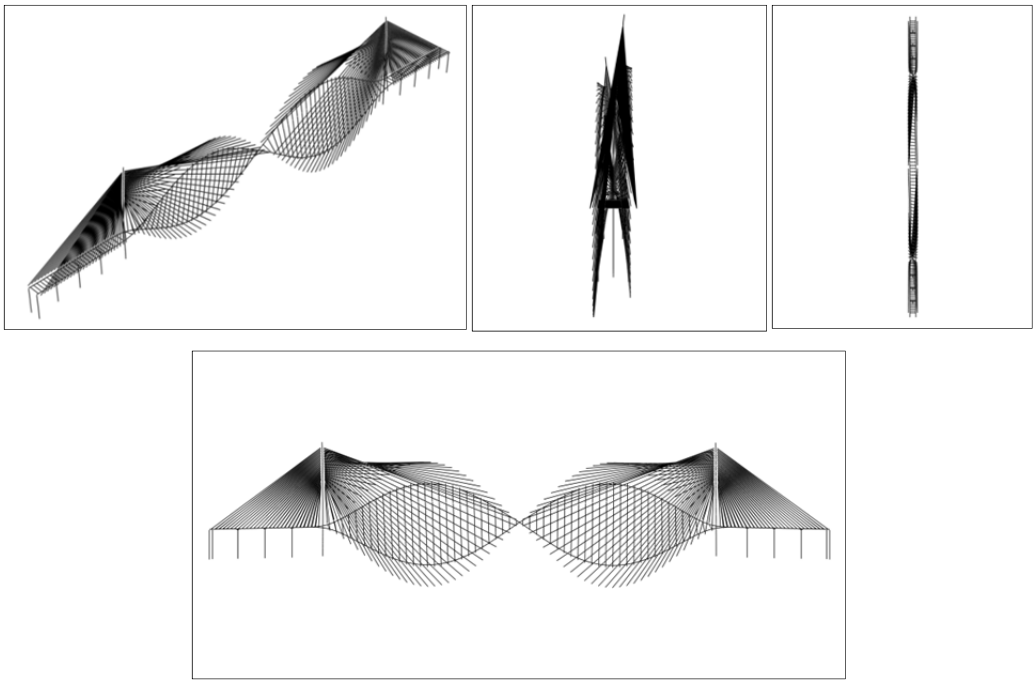

Figure B3: 9th Mode shape, f=0.4237 Hz, scale factor: 1.039e+02.

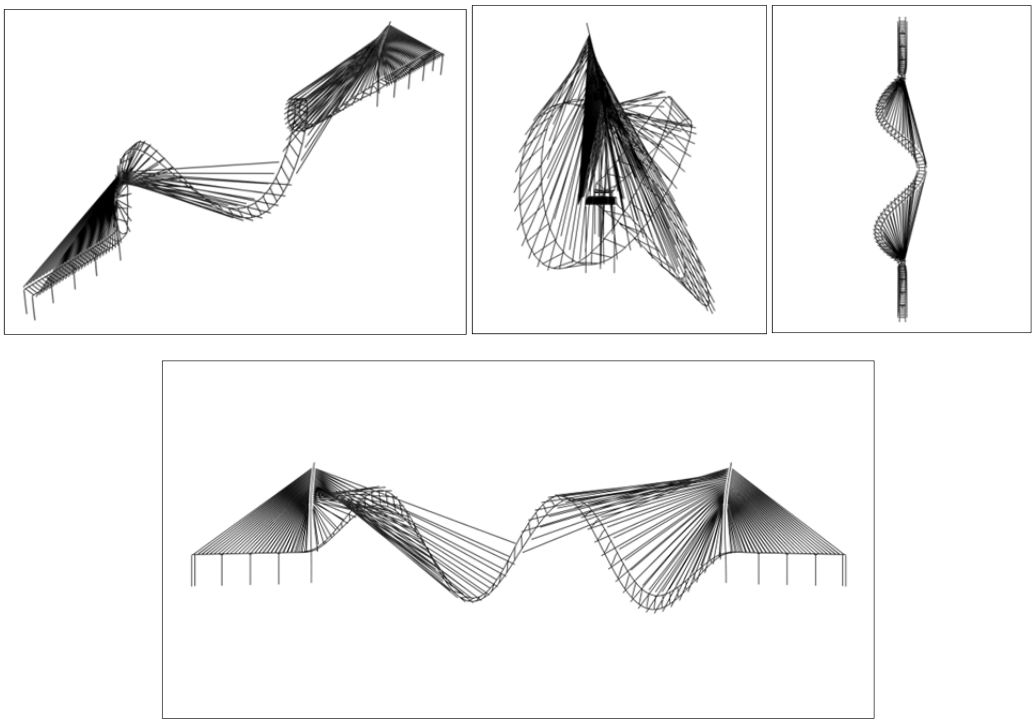

Figure B4: 10th Mode shape, f=0.5811 Hz, scale factor: 1.500e+02.

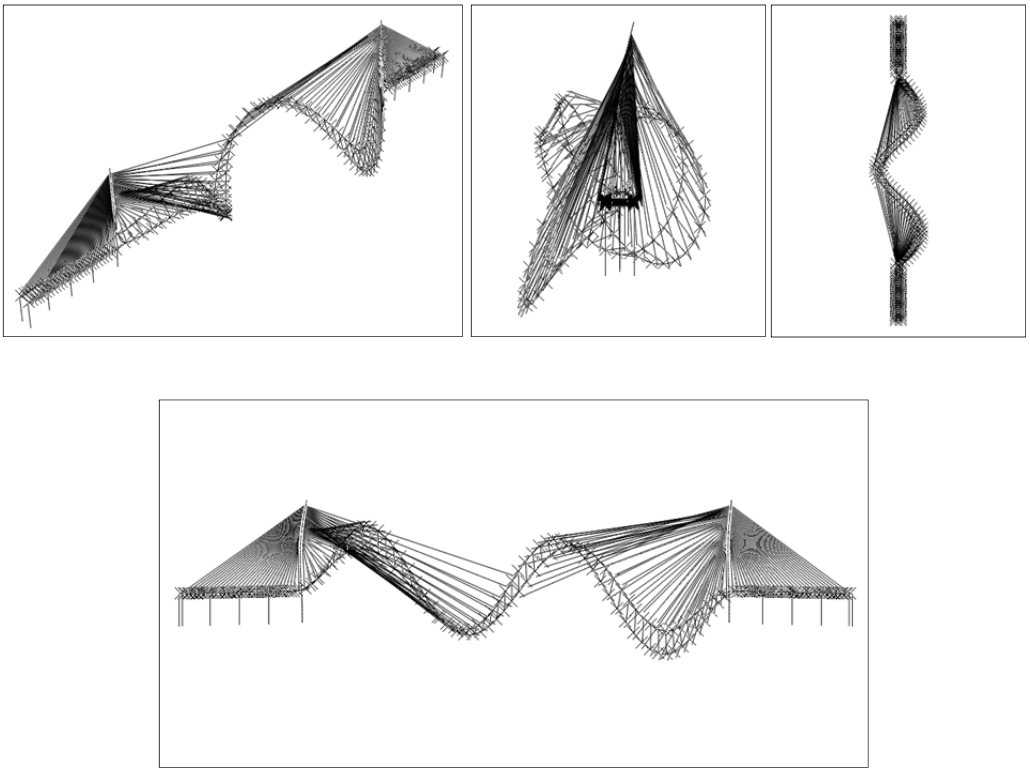

Figure B5: 11th Mode shape, f=0.6112 Hz, scale factor: 1.460e+02.

Appendix C

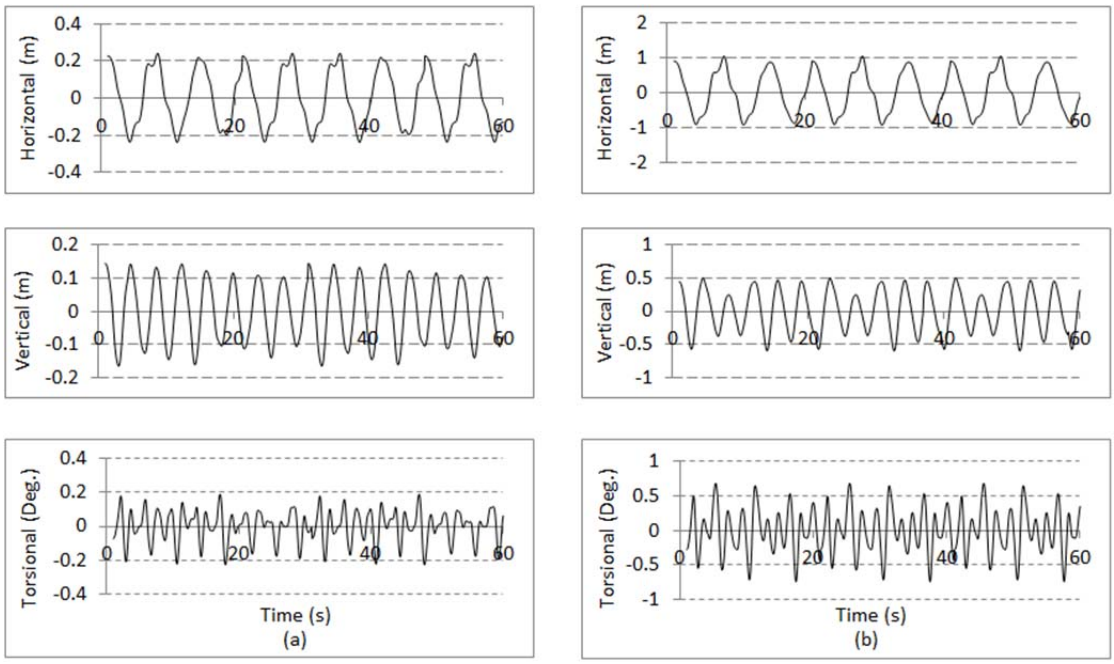

Figure C1: Responses of mid-span under mean wind loads. (a) 35 m/s. (b) 70 m/s.

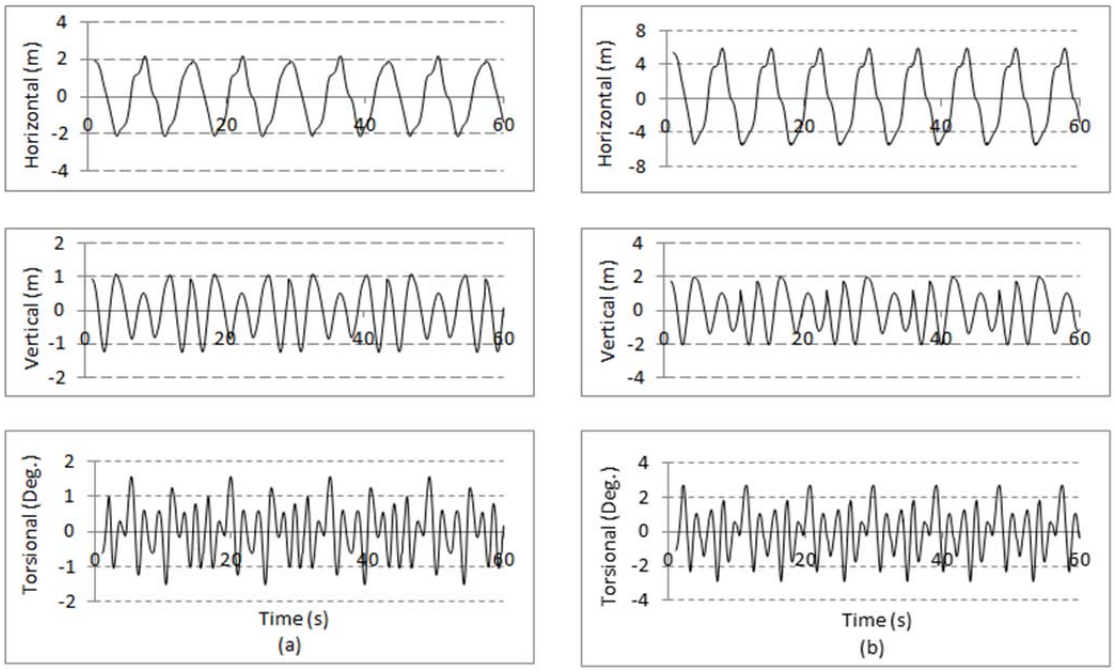

Figure C2: Responses of mid-span under mean wind loads. (a) 105 m/s. (b) 141 m/s.

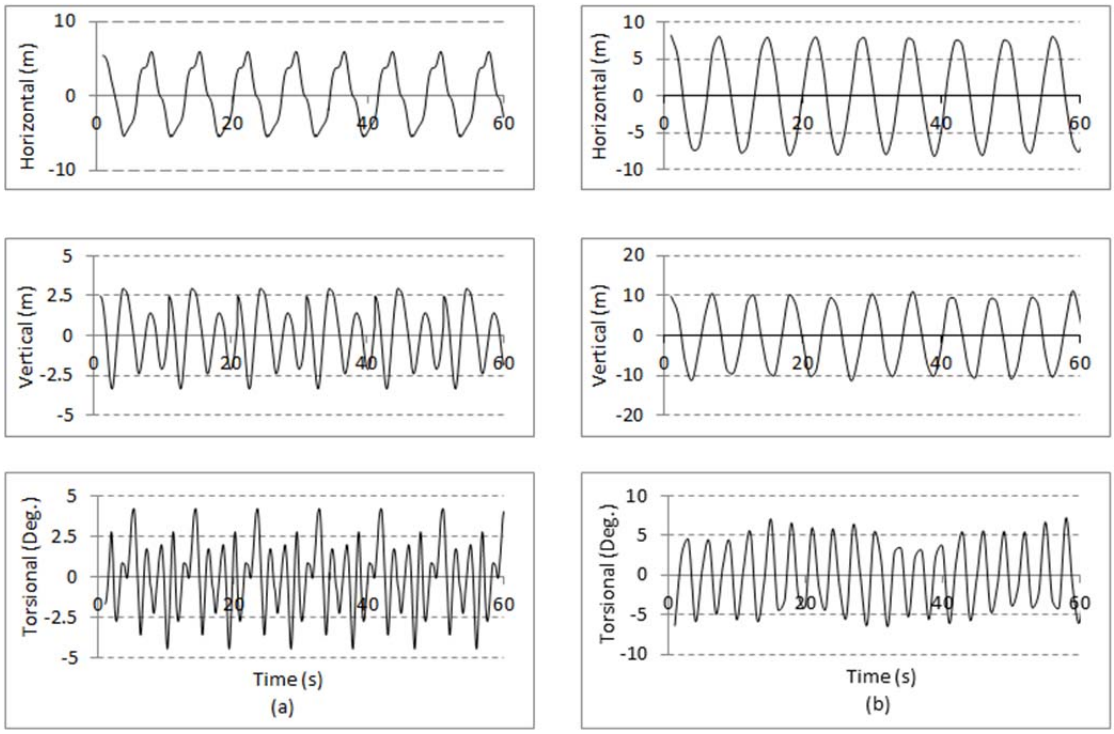

Figure C3: Responses of mid-span under mean wind loads. (a) 176 m/s. (b) 211 m/s.

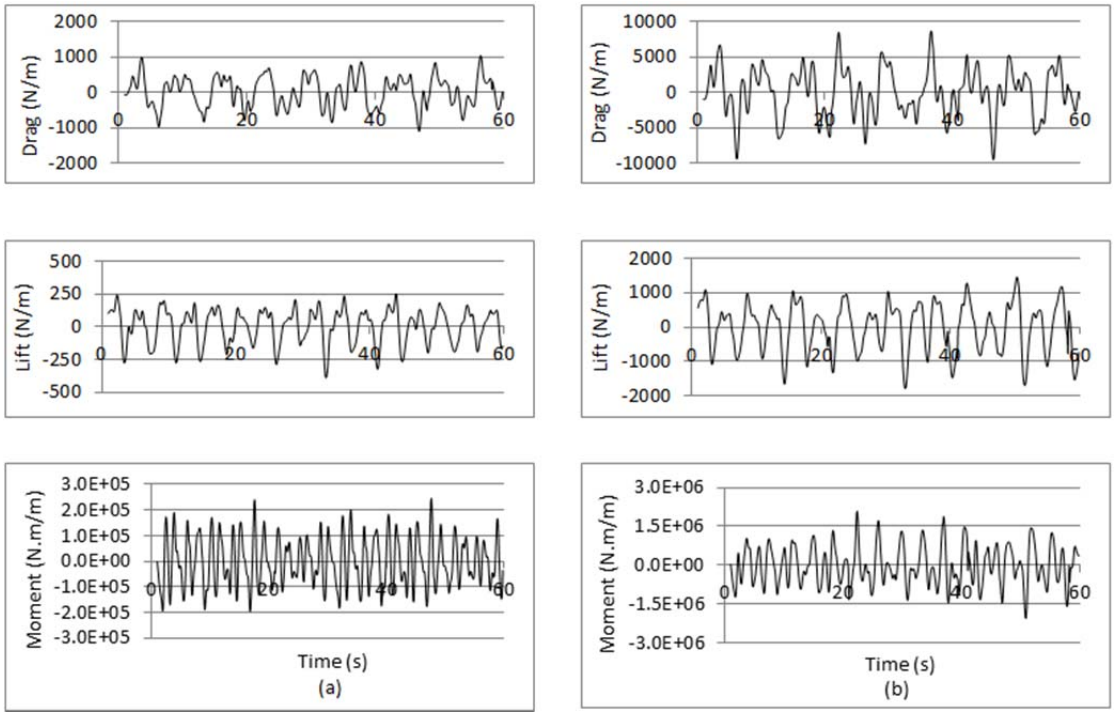

Figure C4: Flutter loads (Self-excited loads). (a) 35 m/s. (b) 70 m/s.

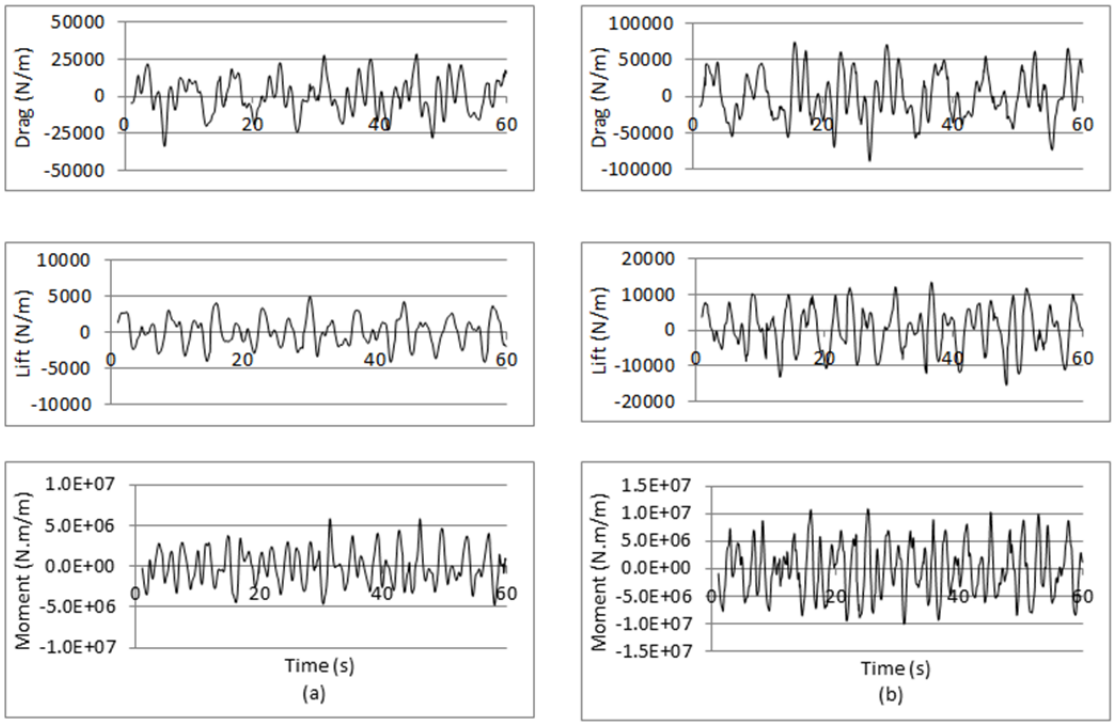

Figure C5: Flutter loads (Self-excited loads). (a) 105 m/s. (b) 141 m/s.

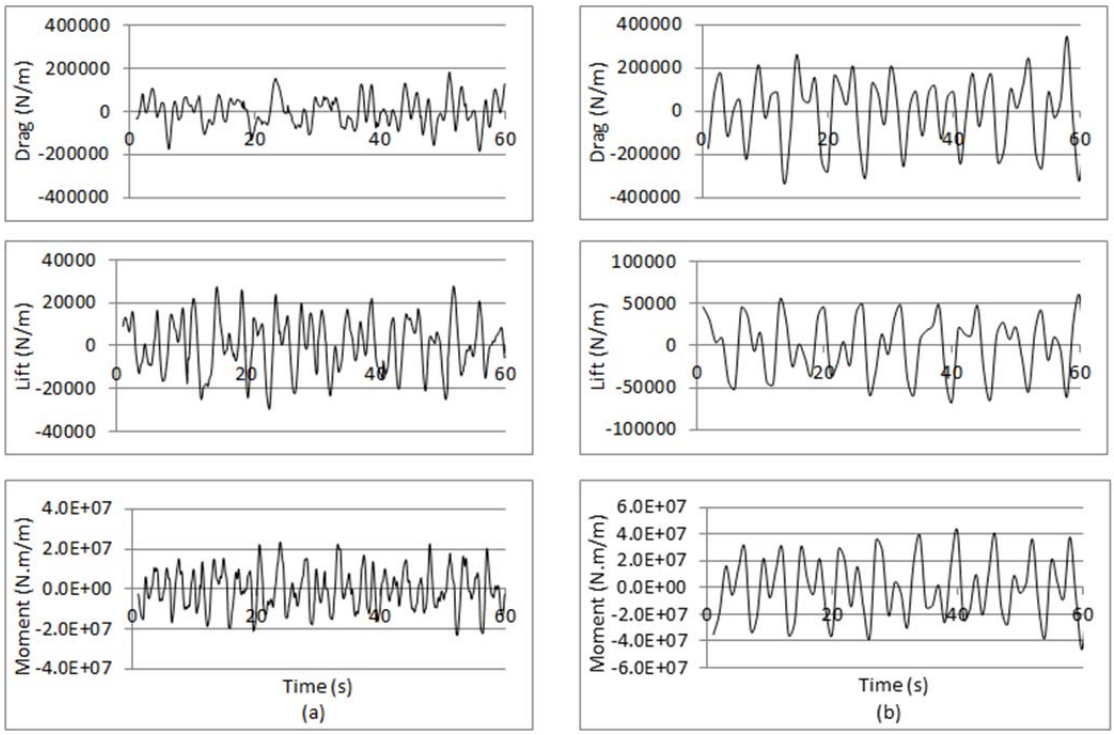

Figure C6: Flutter loads (Self-excited loads). (a) 176 m/s. (b) 211 m/s.

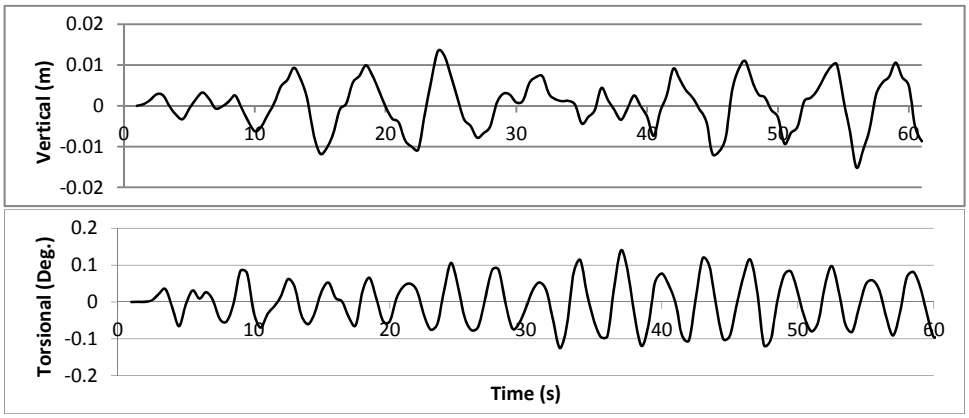

Figure C7: Flutter responses of mid-span at 35 m/s wind speed.

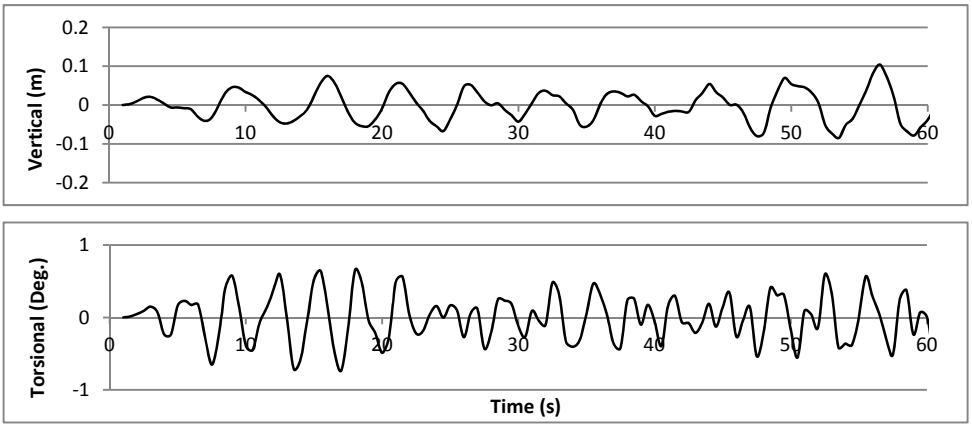

Figure C8: Flutter responses of mid-span at 70 m/s wind speed.

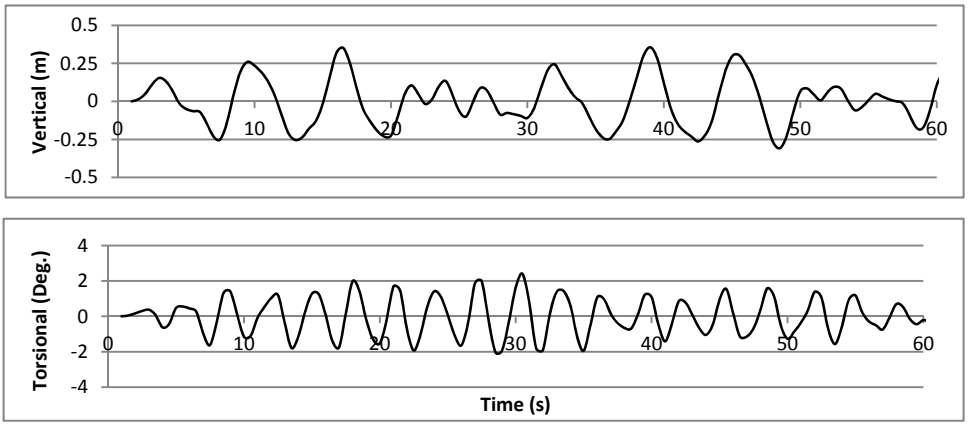

Figure C9: Flutter responses of mid-span at 105 m/s wind speed.

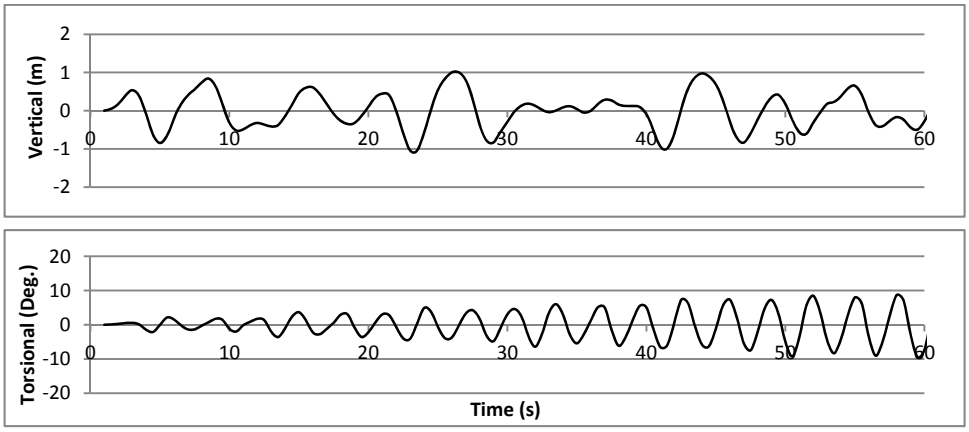

Figure C10: Flutter responses of mid-span at 141 m/s wind speed.

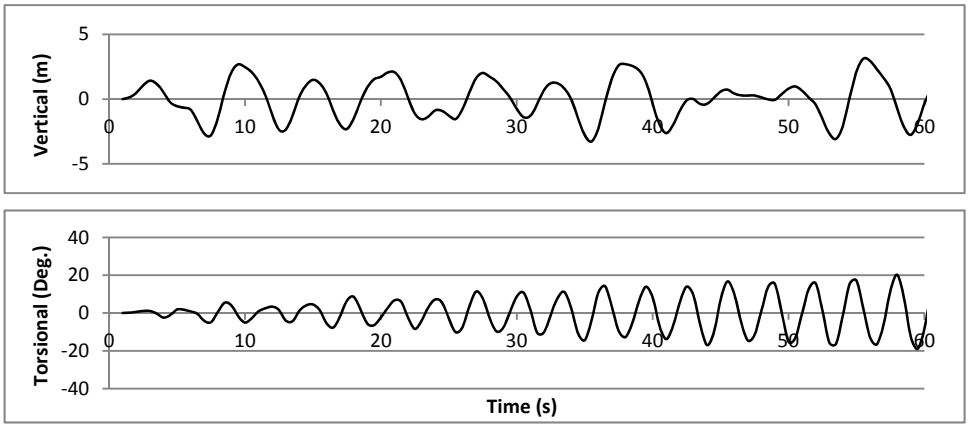

Figure C11: Flutter responses of mid-span at 176 m/s wind speed.

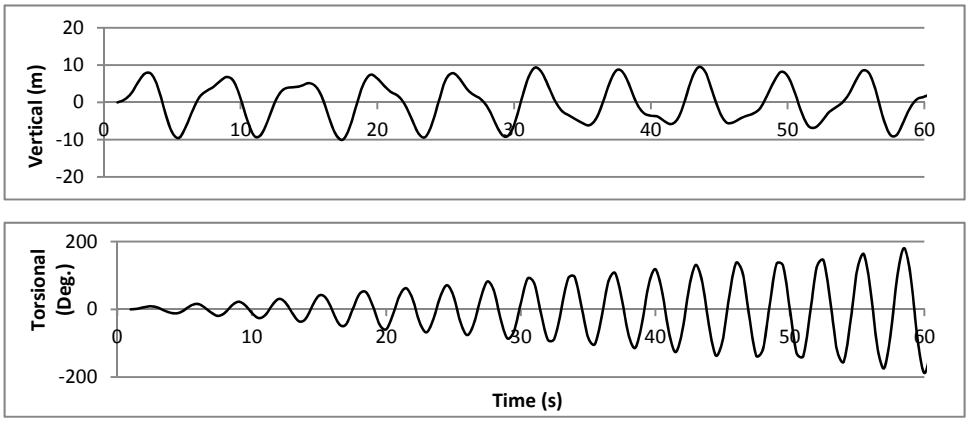

Figure C12: Flutter responses of mid-span at 211 m/s wind speed.

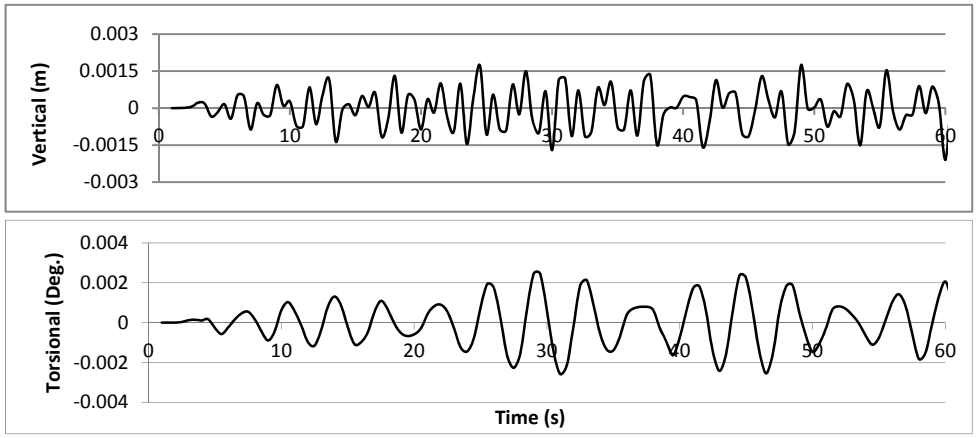

Figure C13: Flutter responses of deck girder around tower at 35 m/s wind speed.

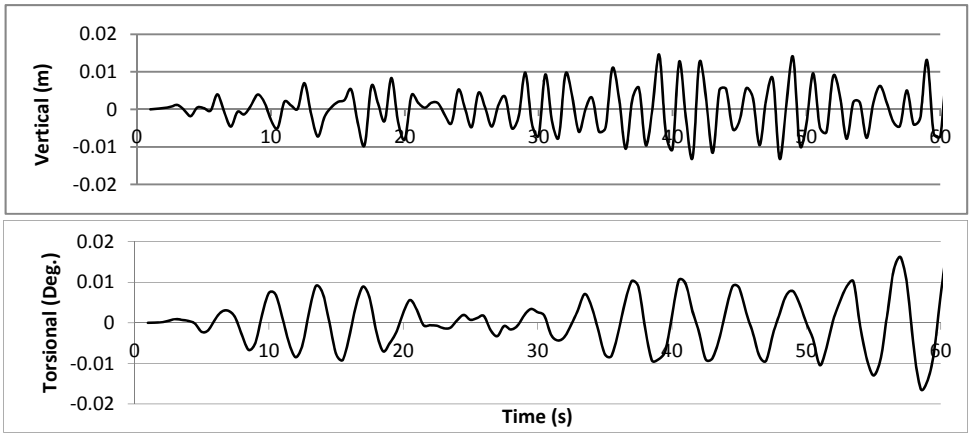

Figure C14: Flutter responses of deck girder around tower at 70 m/s wind speed.

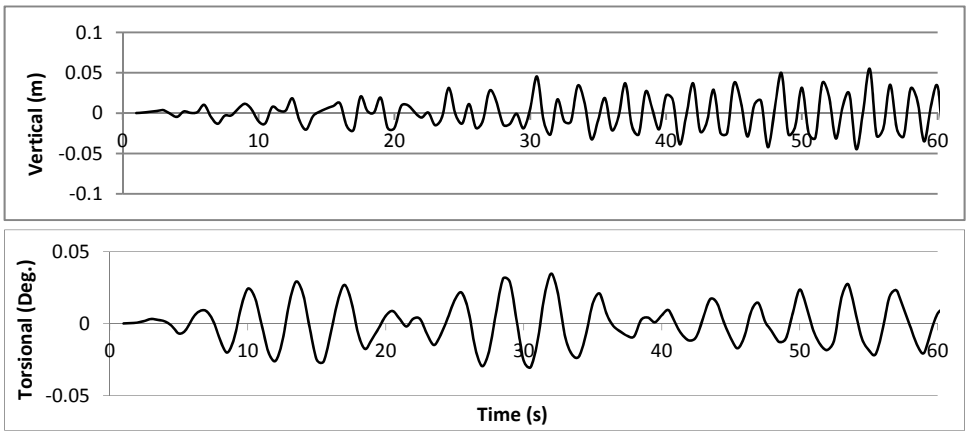

Figure C15: Flutter responses of deck girder around tower at 105 m/s wind speed.

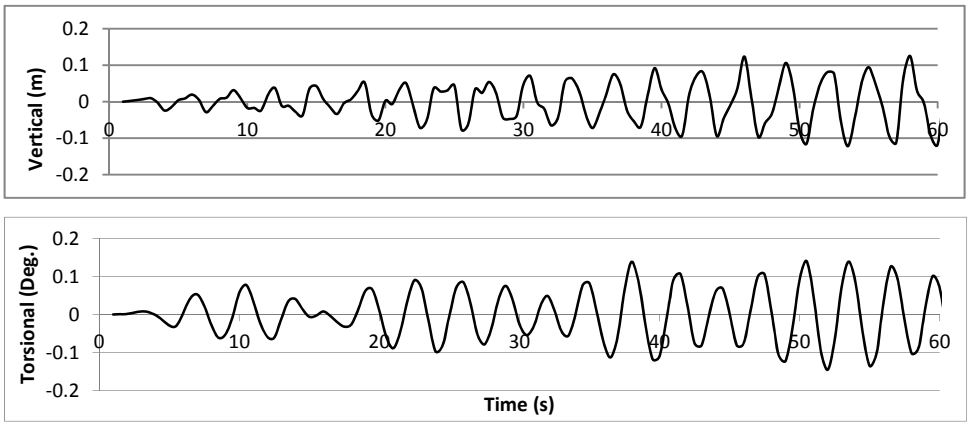

Figure C16: Flutter responses of deck girder around tower at 141 m/s wind speed.

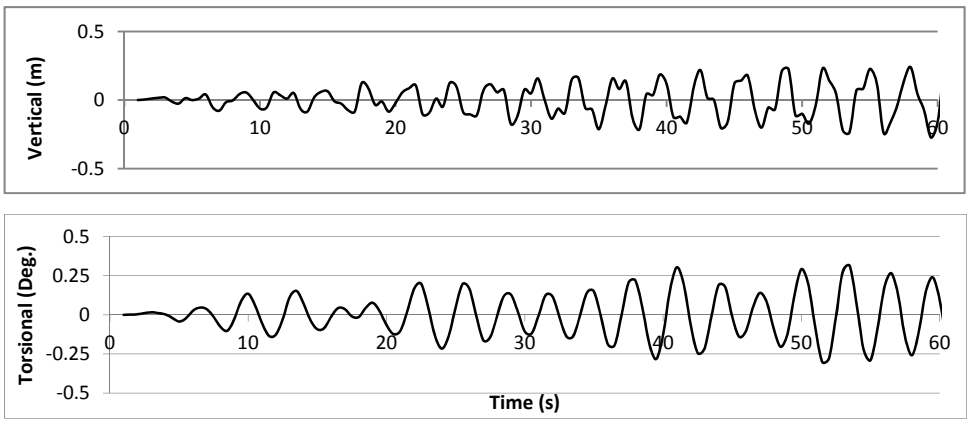

Figure C17: Flutter responses of deck girder around tower at 176 m/s wind speed.

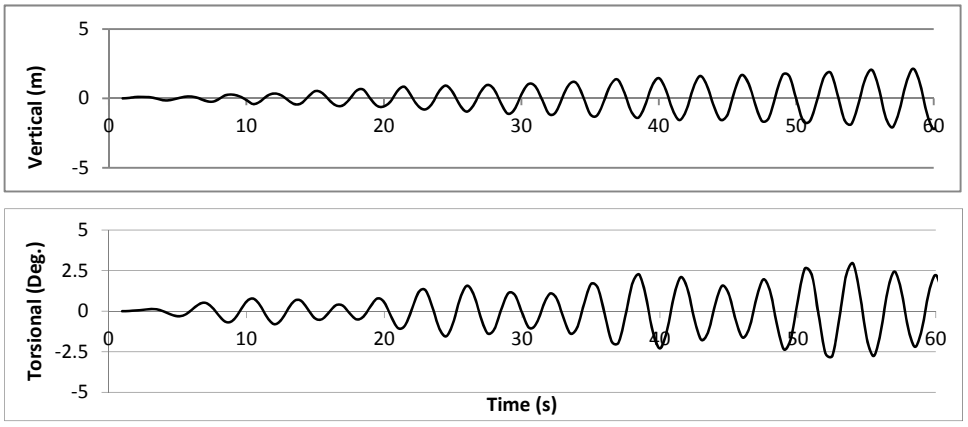

Figure C18: Flutter responses of deck girder around tower at 211 m/s wind speed.

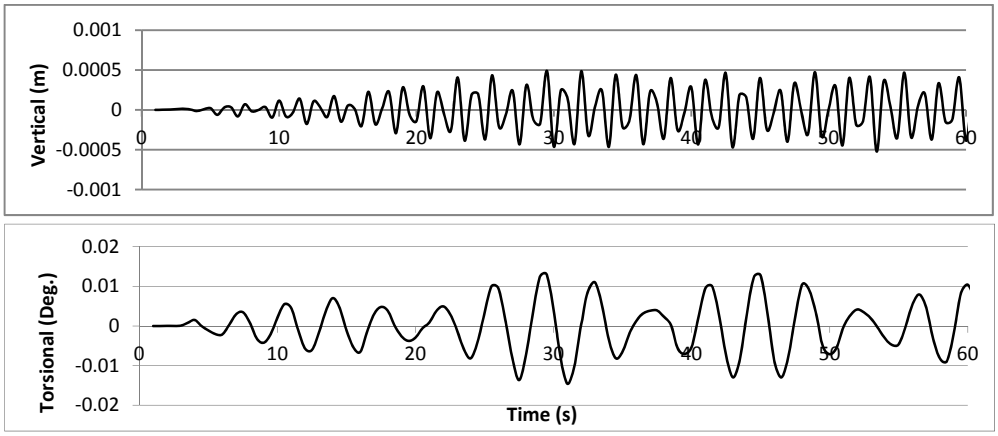

Figure C19: Flutter responses of tower-top at 35 m/s wind speed.

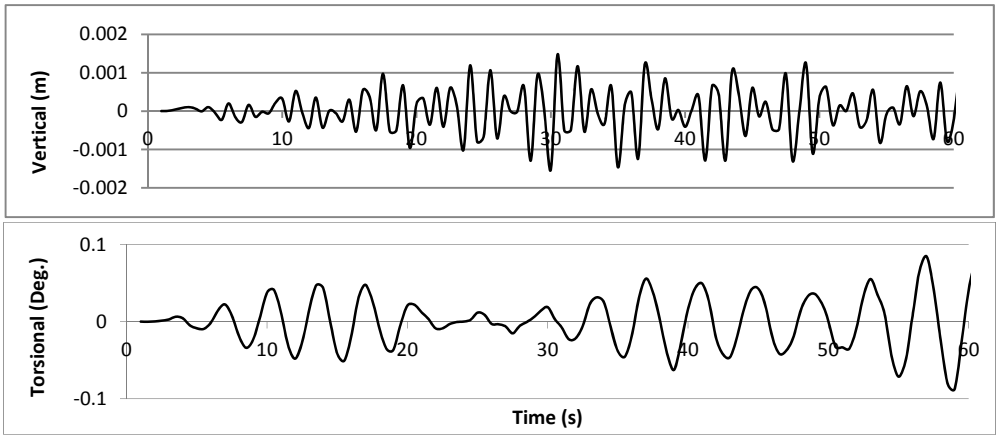

Figure C20: Flutter responses of tower-top at 70 m/s wind speed.

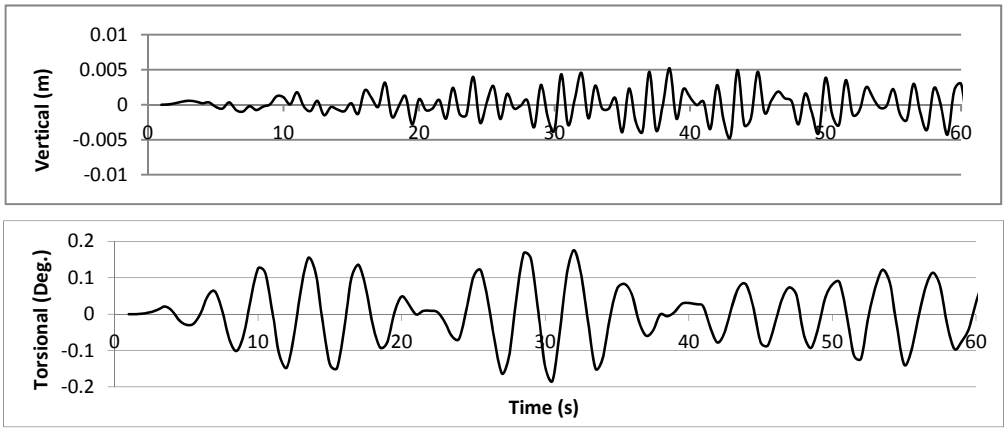

Figure C21: Flutter responses of tower-top at 105 m/s wind speed.

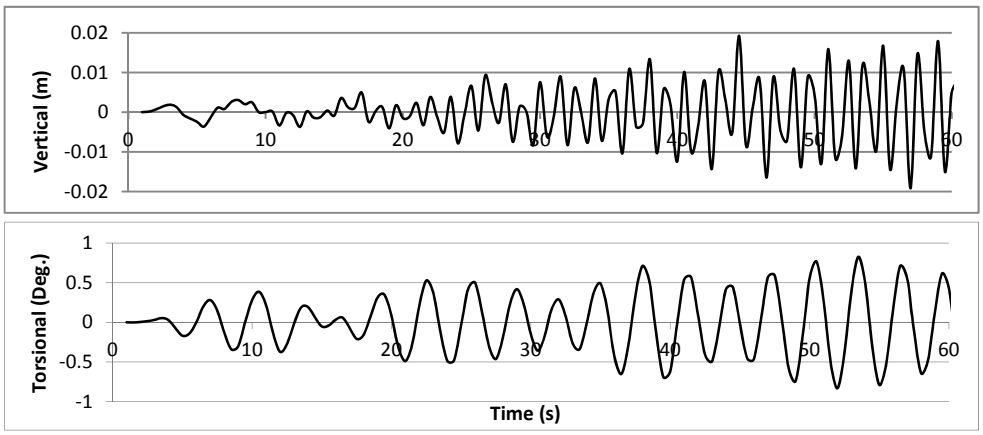

Figure C22: Flutter responses of tower-top at 141 m/s wind speed.

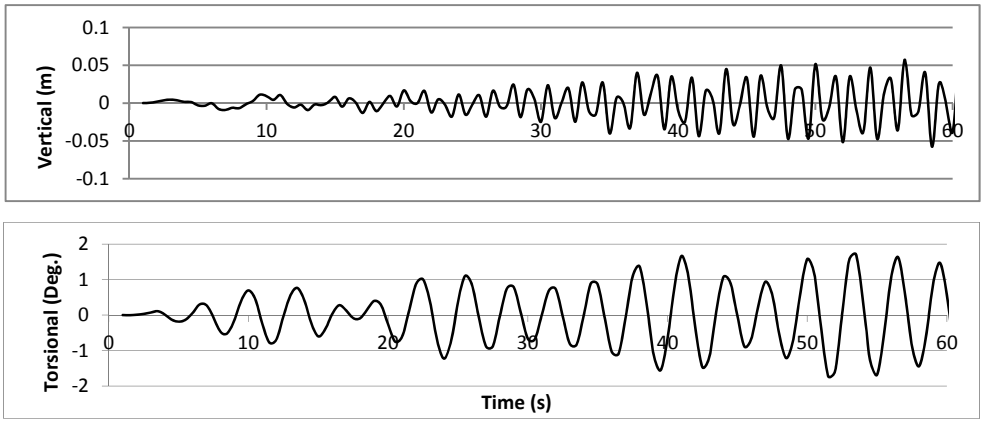

Figure C23: Flutter responses of tower-top at 176 m/s wind speed.

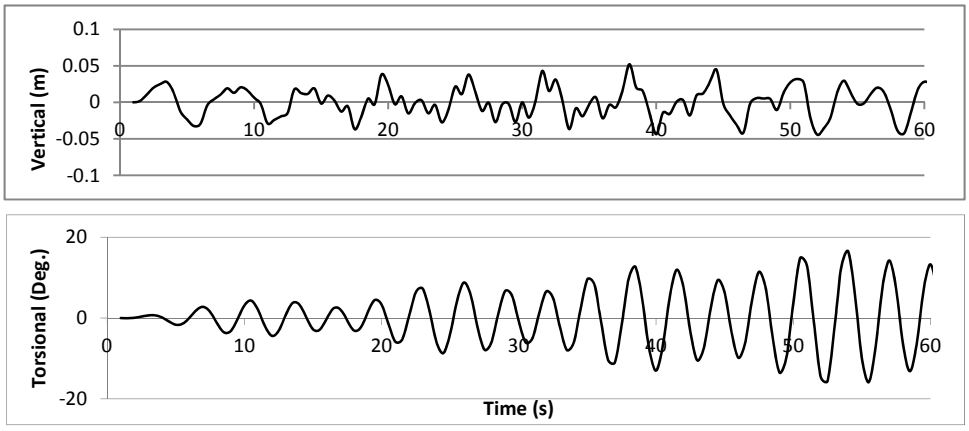

Figure C24: Flutter responses of tower-top at 211 m/s wind speed.

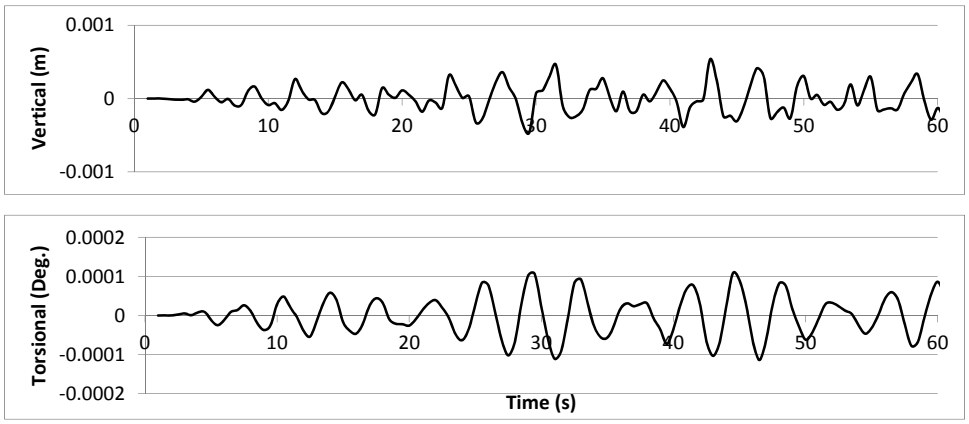

Figure C25: Flutter responses of span connection at 35 m/s wind speed.

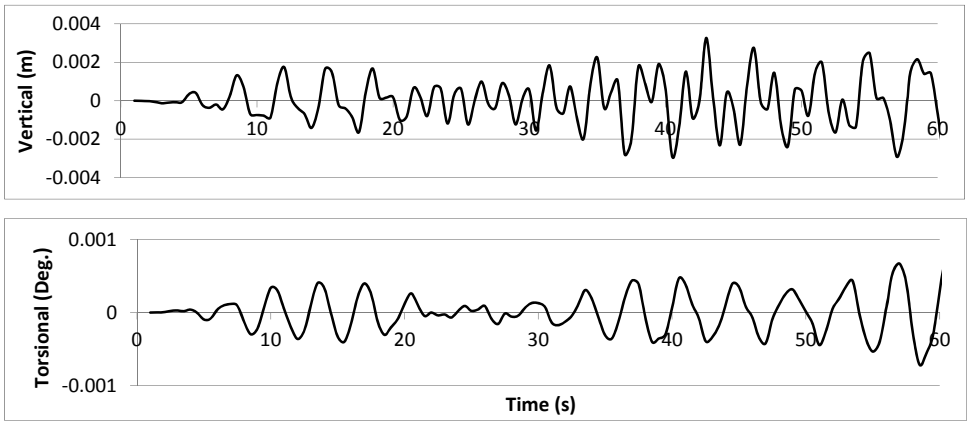

Figure C26: Flutter responses of span connection at 70 m/s wind speed.

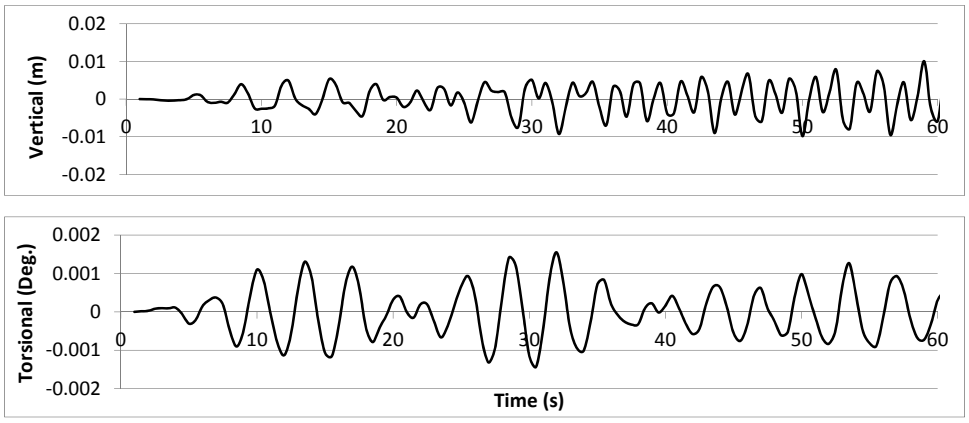

Figure C27: Flutter responses of span connection at 105 m/s wind speed.

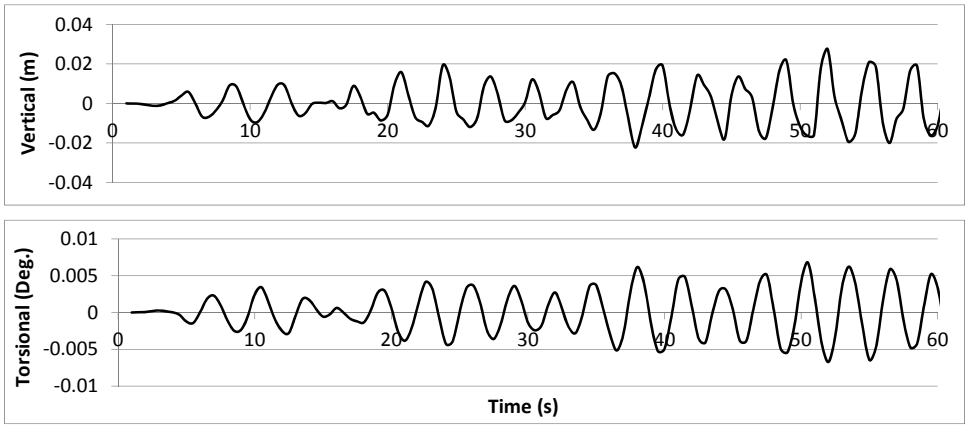

Figure C28: Flutter responses of span connection at 141 m/s wind speed.

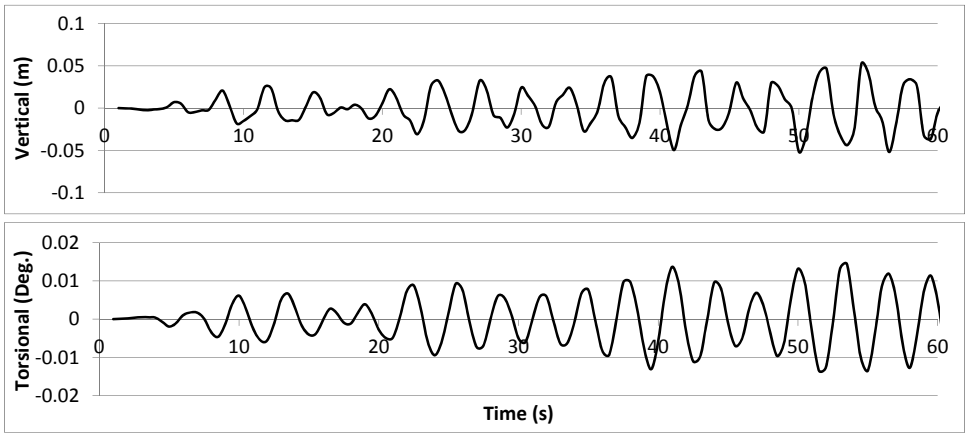

Figure C29: Flutter responses of span connection at 176 m/s wind speed.

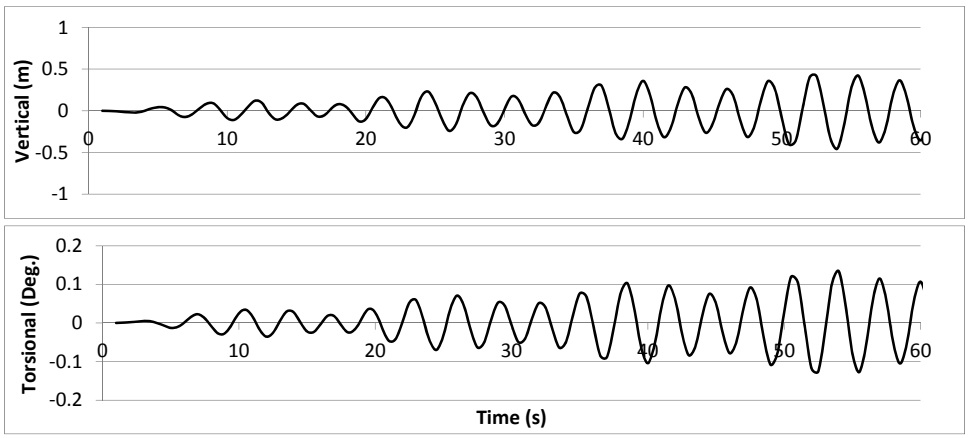

Figure C30: Flutter responses of span connection at 211 m/s wind speed.

Appendix D

Fast Fourier Transform MATLAB program:

```
x=load ('xxx.txt');            'xxx.txt' response data input file.

y=fft(x);

n=length(y);

power = abs(y(1:floor(n/2))).^2;

nyquist =1/2;

freq = (1:n/2)/(n/2)*nyquist;

plot(freq,power)

xlabel('Frequency (Hz)')

ylabel('Power')
```

Results of Fast Fourier Transform (flutter analysis):

(a). Vertical direction:

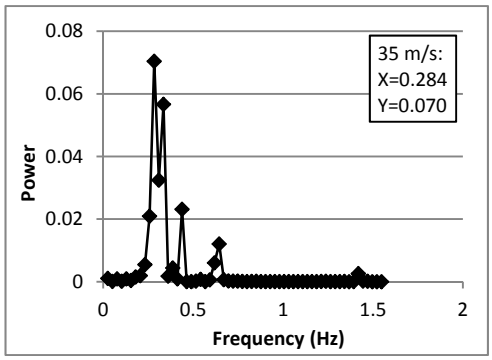

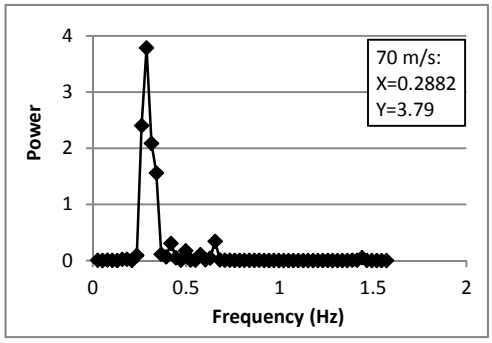

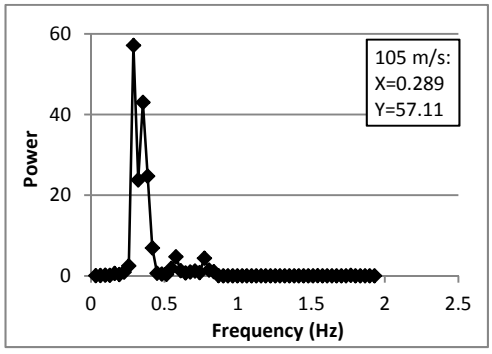

(b). Torsional direction:

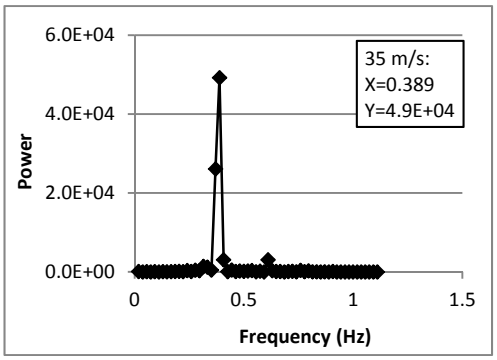

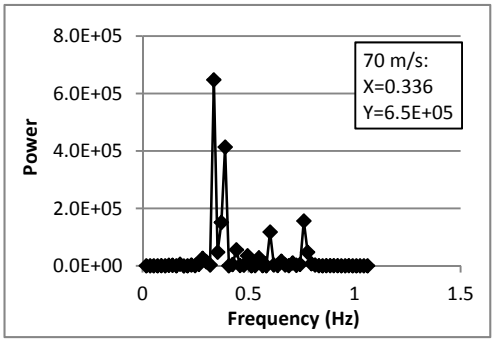

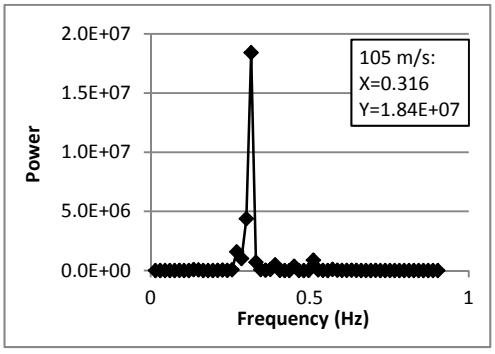

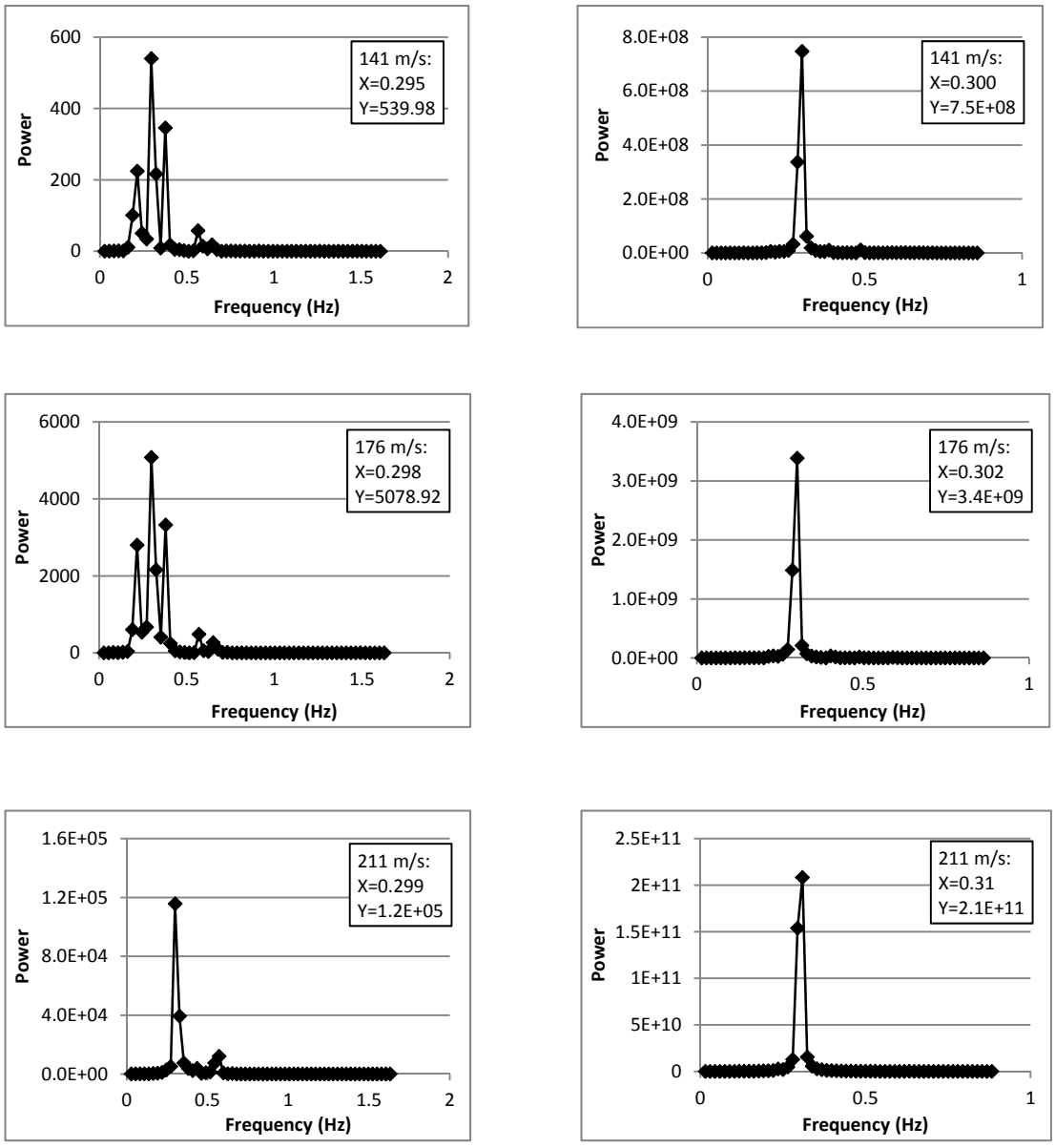

Figure D1: Results of Fast Fourier Transform (flutter analysis). (a) Vertical. (b) Torsional.

Appendix E

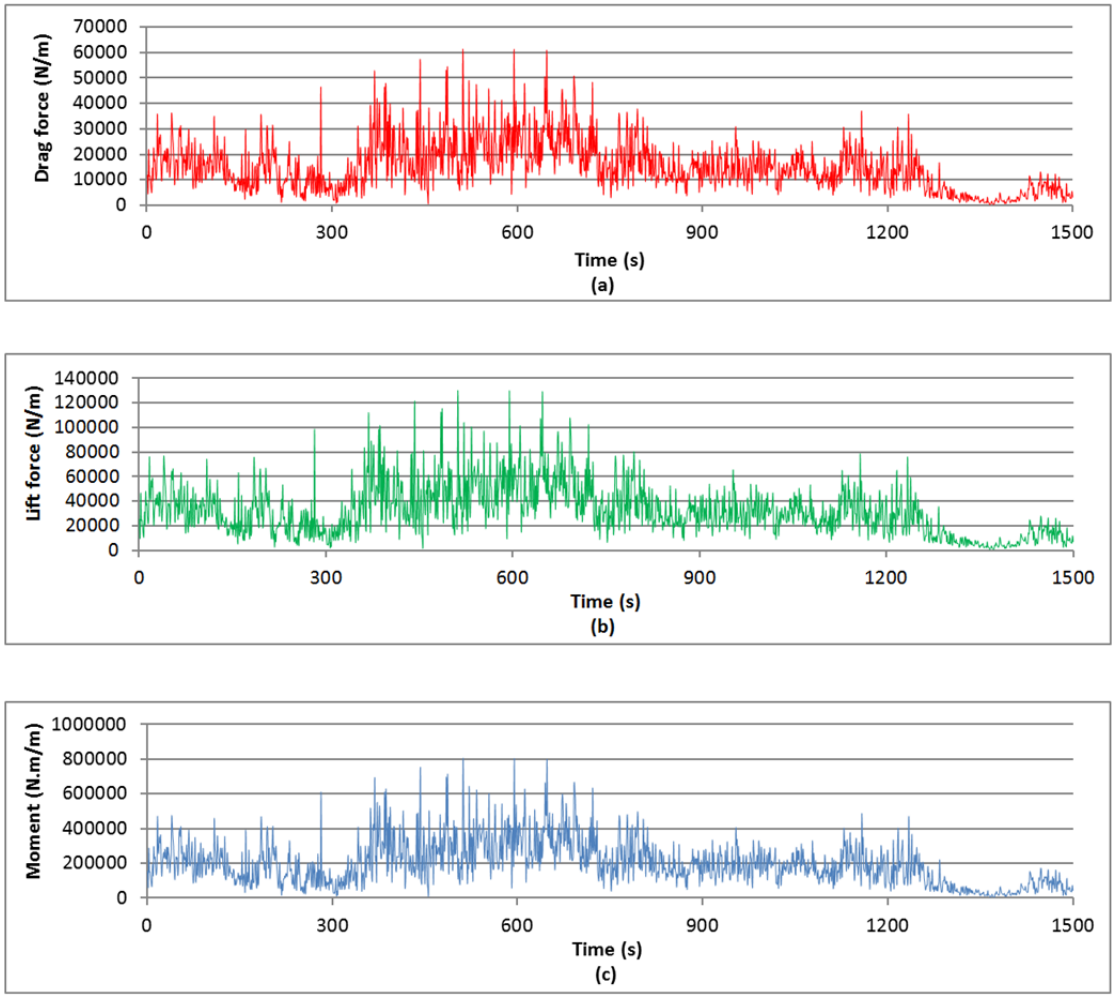

Figure E1: Dynamic wind loads from wind data. (a) Drag load. (b) Vertical load. (c) Torsional moment.

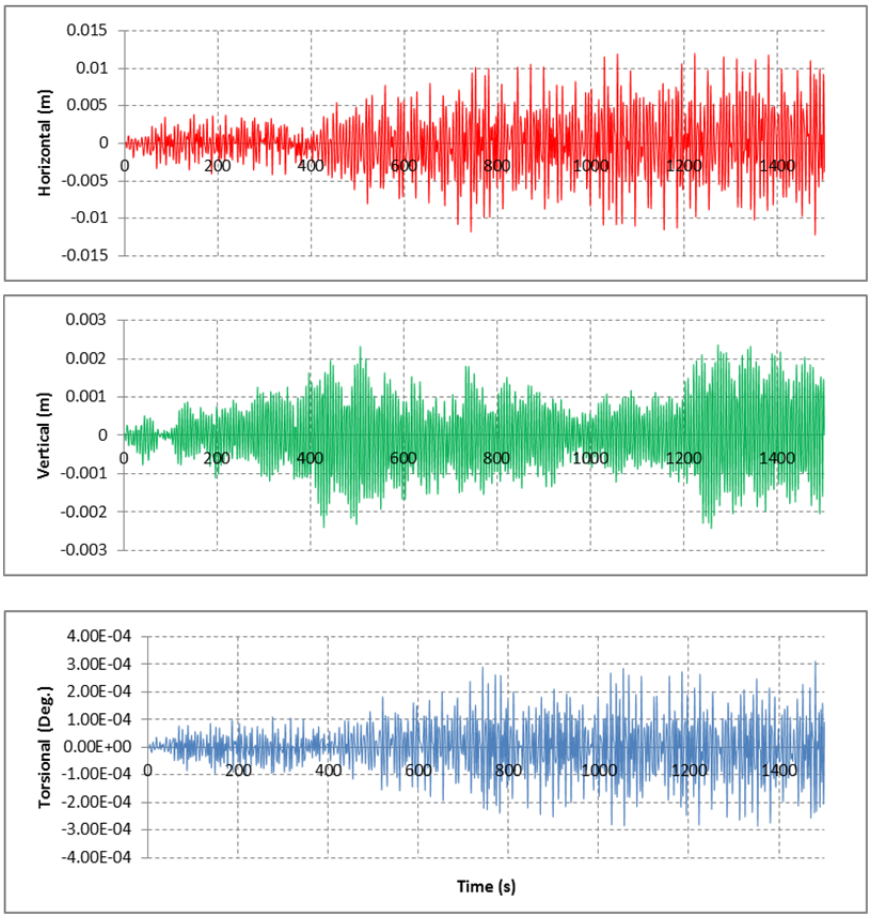

Figure E2: Bridge responses at deck girder round tower under natural wind data.

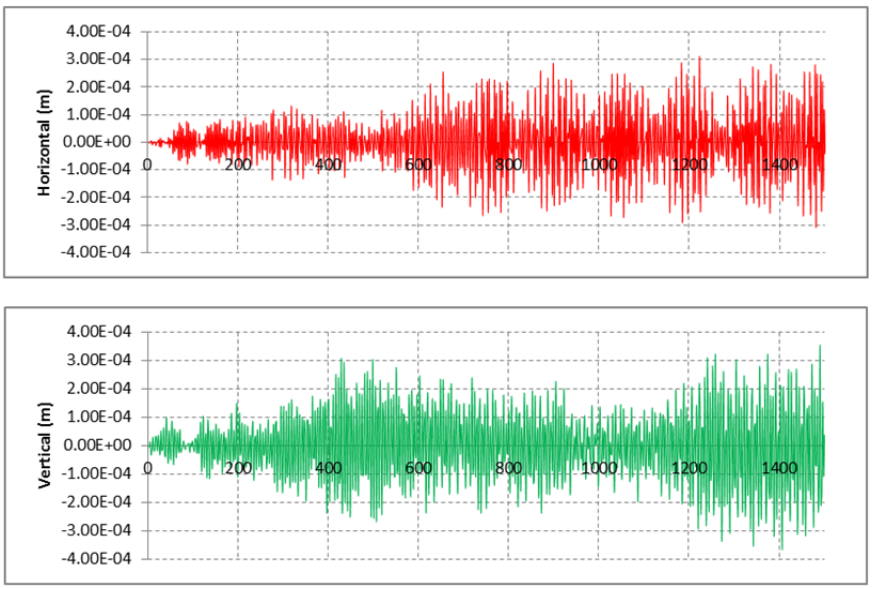

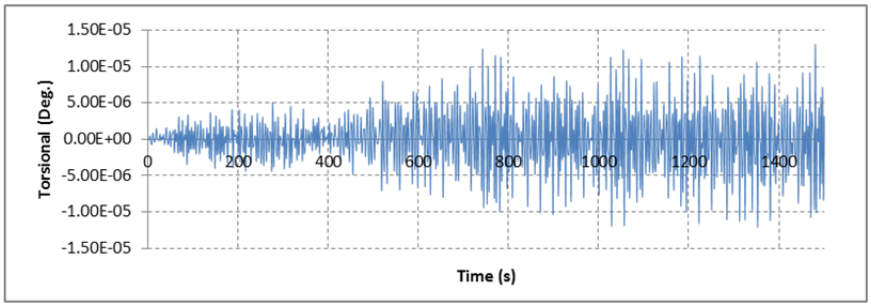

Figure E3: Bridge responses at span connection under natural wind data.

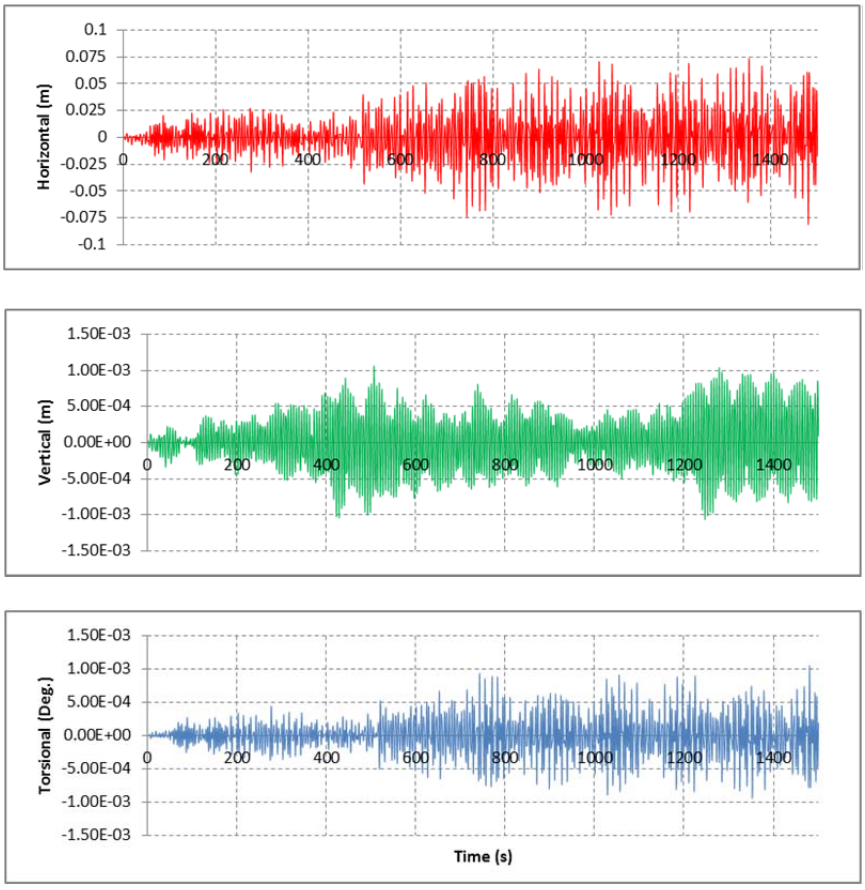

Figure E4: Bridge responses at mid-tower under natural wind data.

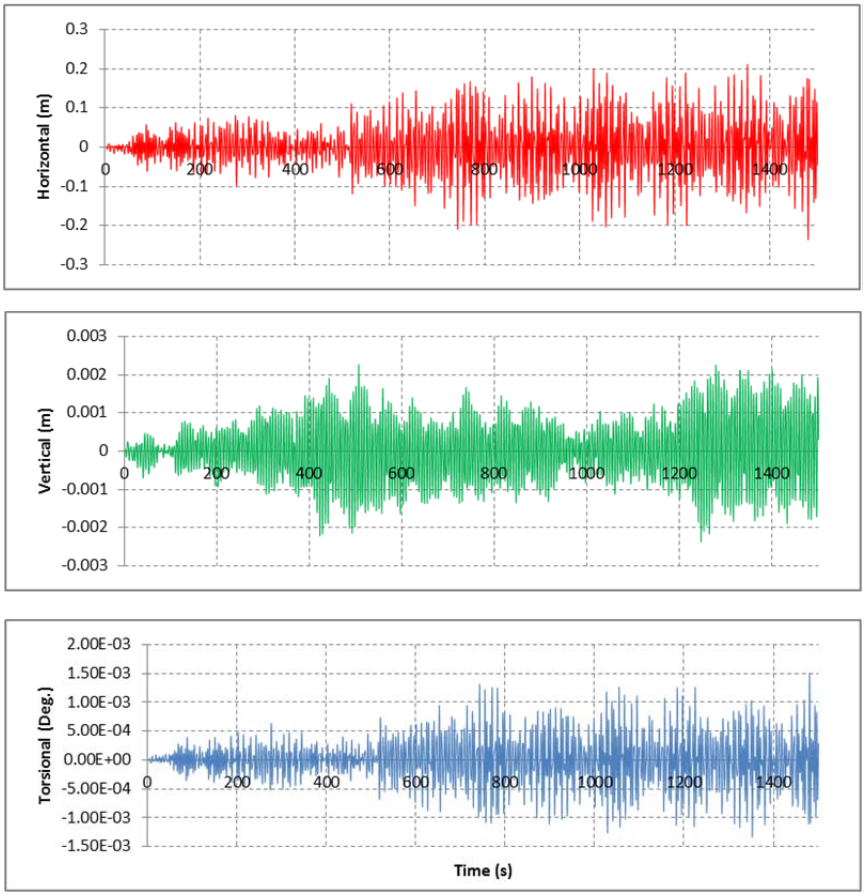

Figure E5: Bridge responses at top tower under natural wind data.

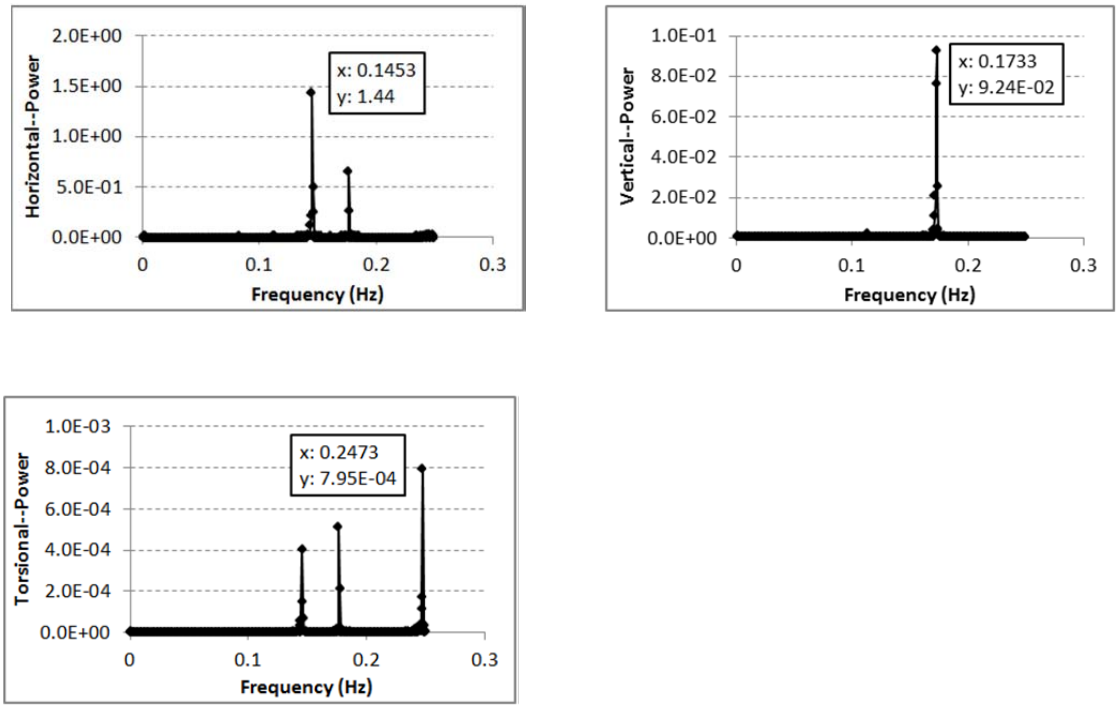

Figure E6: FFT calculation at deck girder around tower under natural wind data.

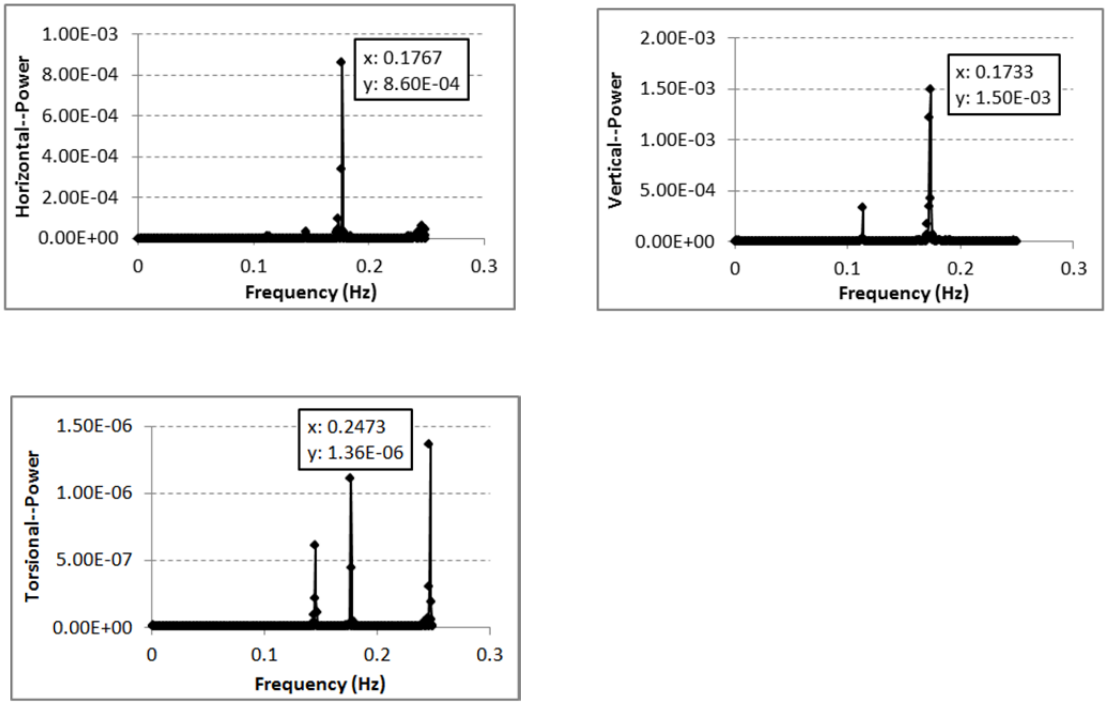

Figure E7: FFT calculation at span connection under natural wind data.

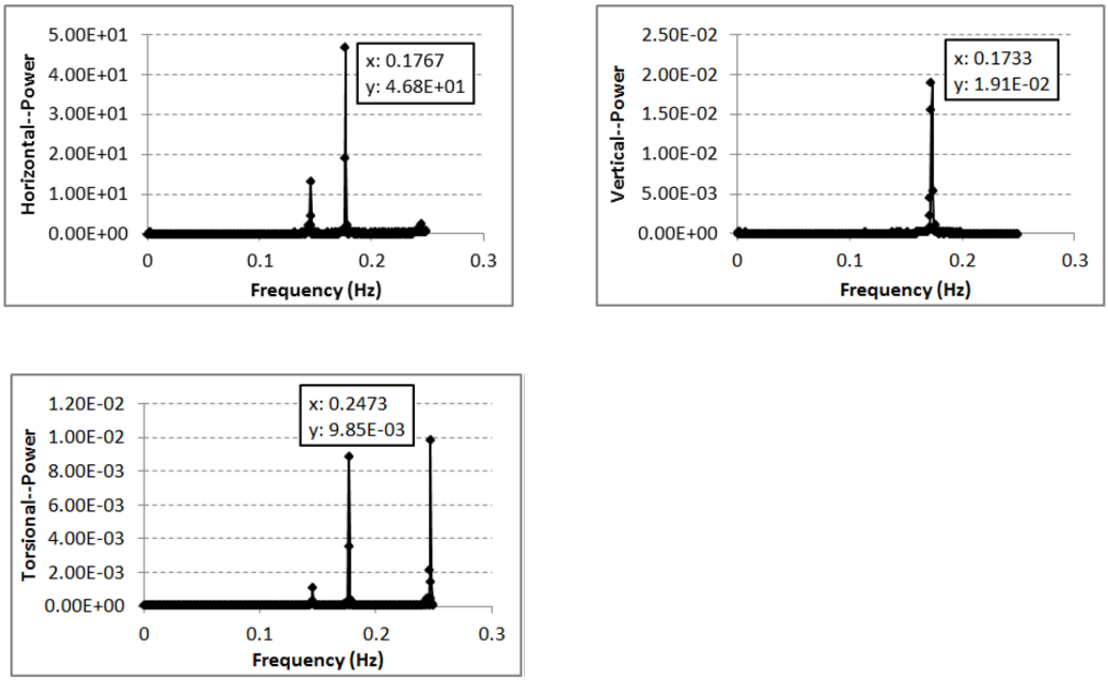

Figure E8: FFT calculation at mid-tower under natural wind data.

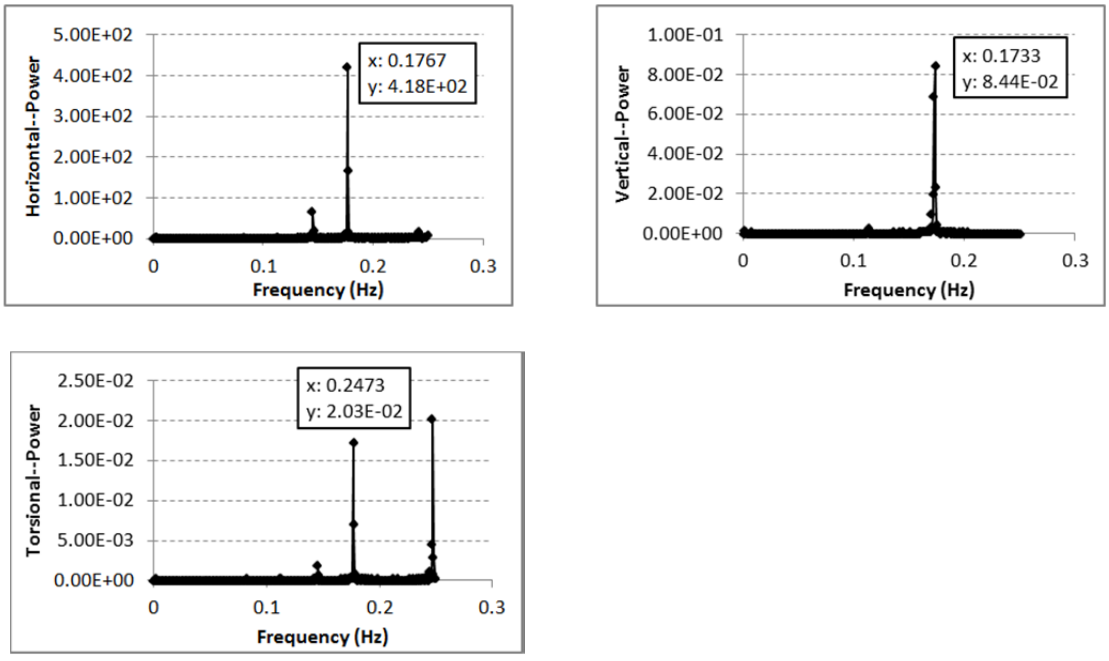

Figure E9: FFT calculation at top-tower under natural wind data.